# Parkinson's disease genes orchestrate mechanisms of mitochondrial quality control

Gian-Luca McLelland

Integrated Program in Neuroscience

McGill University, Montreal, Canada

August 2017

A thesis submitted to McGill University in partial fulfillment of the requirements of the degree of Doctor of Philosophy in the Faculty of Medicine (Neuroscience)

*C'est en forgeant qu'on devient forgeron*.

Unknown

*Courage, my friends; 'tis not too late to build a better world*.

Tommy Douglas

*Do, or do not. There is no try*.

Master Yoda, *The Empire Strikes Back*

TABLE of CONTENTS

## ABSTRACT

A functional mitochondrial network is cardinal to cellular fitness, and declines in mitochondrial function are linked to neurodegeneration, most notably the motor disorder Parkinson's disease. Two genes mutated in autosomal recessive juvenile parkinsonism, *PARKIN* and *PINK1*, work together to maintain mitochondrial health *in vivo*. Study over the past decade has revealed that *PARKIN* and *PINK1* constitute a molecular system that recognizes and destroys damaged mitochondria via the autophagy pathway, in a process known as mitophagy. By removing dysfunctional organelles from the reticulum via this quality control mechanism, the *PARKIN*/*PINK1* pathway protects the integrity of the mitochondrial network. The work comprised within this thesis delves into the mechanism of *PINK1*/*PARKIN* mitochondrial quality control. Firstly, it is shown that, in addition to mitophagy, *PARKIN* and *PINK1* function in a second quality control mechanism that oversees the removal of damaged mitochondrial components, preserving mitochondrial function in the absence of organellar destruction. Selected, damaged mitochondrial cargo are extracted from the organelle via a class of mitochondrial-derived vesicles (MDVs), which are shuttled to the lysosome for turnover in a manner involving classical membrane fusion factors. Secondly, the work here demonstrates that uncoupling of mitochondria from the endoplasmic reticulum via the destruction of a tethering factor represents an important step in the mitophagic cascade. Together, these findings have furthered our understanding regarding the cellular toolkit that maintains mitochondrial health, and how its deterioration can lead to neurodegenerative disease.

## RESUME

Un réseau mitochondrial fonctionnel est critique à la survie cellulaire, et les diminutions de la fonction des mitochondries sont liées à la neurodégénérescence, notamment la maladie de Parkinson. Deux gènes mutés dans le parkinsonisme juvénile autosomique récessif, *PARKIN* et *PINK1*, travaillent ensemble pour maintenir la santé mitochondriale *in vivo*. Au cours de la dernière décennie, des études ont révélé que *PARKIN* et *PINK1* constituent un système moléculaire qui reconnaît et détruit les mitochondries endommagées via l'autophagie; un processus appelé mitophagie. En éliminant les organites dysfonctionnels via ce mécanisme de contrôle de la qualité, *PARKIN* et *PINK1* protègent l'intégrité du réseau mitochondrial, ce qui est le sujet de cette thèse. Tout d'abord, il est démontré que, en plus de la mitophagie, *PARKIN* et *PINK1* fonctionnent dans un deuxième mécanisme de contrôle de la qualité qui surveille l'élimination des cargos mitochondriales endommagées, en préservant la fonction mitochondriale en l'absence de destruction organellaire. Les cargos sélectionnées et endommagées sont extraits de l'organite par une classe de vésicules dérivées de mitochondries (VDMs) qui sont transportées au lysosome d'une manière impliquant des facteurs classiques de fusion membranaire. Deuxièmement, le travail ici démontre que le désaccouplement entre les mitochondries et le réticulum endoplasmique par la destruction d'un facteur d'attachement représente une étape importante dans la cascade mitophagique. Ensemble, ces résultats ont favorisé notre compréhension de la trousse d'outils cellulaire qui maintient la santé mitochondriale et de la façon dont sa détérioration peut conduire à une maladie neurodégénérative.

ACKNOWLEDGMENTS

This thesis is dedicated to my grandfather Joseph McLelland and my *nonno* Gianni Ricciardelli, both of whom instilled in me the merits of one's curiosity, perseverance, hard work and – most importantly – sense of light-heartedness.

I would like to thank my family and friends for their unwavering love and support during my graduate studies. To my mom and dad in particular, thank you for grounding me when things got especially tough. And to Adèle, thank you for supporting and encouraging (and putting up with) my unbridled enthusiasm for what I do. *Je t'aime*.

I am indebted to Dr. Edward Fon for his supervision, encouragement, and trust. I would also like to thank Dr. Heidi McBride for her personal and professional support; her contribution to the work contained within these pages was indispensable. Ted and Heidi have been instrumental in shaping my approach to experimentation, and taught me the importance of forward-thinking, big ideas, and having a scientific vision. I am eternally grateful to both of them.

I would like to thank Dr. Karl Grenier and Dr. Vincent Soubannier, both of whom trained me and witnessed my first, clumsy steps at the lab bench, as well as the many coworkers with whom I've worked alongside during my time at the MNI. Specifically, I'd like to thank Sydney Lee for sharing in my enthusiasm for membrane fusion, as well as Drs. Jean-François Trempe and Thomas Durcan for our discussions and collaborations, as well as their guidance. I'd like to also thank the members of my advisory committee, Drs. Peter McPherson and Eric Shoubridge, for both encouraging and challenging me. Finally, I'd like to acknowledge the various funding sources – CIHR, FRQS, Parkinson Society Canada and the Desjardins Foundation – that made this research possible.

## PREFACE and CONTRIBUTION of AUTHORS

This thesis describes the mechanistic involvement of parkin and PINK1 in a) a mitochondrial turnover pathway in which mitochondria shed vesicles that ultimately target to the lysosomal compartment and b) the destruction of membrane contact sites between mitochondria and the endoplasmic reticulum in the context of and a prerequisite for the autophagy of damaged mitochondria. Additionally, the SNARE-dependent mechanism by which mitochondrial vesicles fuse with the late endosome is also elucidated. All data described with Chapters II through IV are considered original scholarship.

Chapter II originally appeared as:

**McLelland GL**, Soubannier V, Chen CX, McBride HM, Fon EA (2014). Parkin and PINK1 function in a vesicular trafficking pathway regulating mitochondrial quality control. *EMBO Journal* 33(4):282-295, doi:10.1002/embj.201385902. PMID: 24446486

in which I conceived, planned, and analyzed experiments, along with VS, HMM and EAF. CXC performed experiments that did not make it into the manuscript. Save for the experiments in Fig. II.S3 describing the role of endogenous parkin in MDV generation which was performed and analyzed by VS, I generated all the data that went into the figures (a contribution of 13 out of 14 figures). EAF and I wrote the manuscript, which was edited by HMM.

Chapter III originally appeared as:

**McLelland GL**, Lee SA, McBride HM, Fon EA (2016). Syntaxin-17 delivers PINK1/parkin-dependent mitochondrial vesicles to the endolysosomal system. *Journal of Cell Biology* 214(3):275-291, doi:10.1083/jcb.201603105. PMID: 27458136

in which I conceived, planned, and analyzed experiments under the guidance of HMM and EAF. While SL optimized the SNARE immunoprecipitation protocol, I generated all the data that ultimately went into the figures (a contribution of 14 out of 14 figures). I wrote the manuscript, which was edited by HMM and EAF.

Chapter IV is currently a manuscript that is being prepared for submission:

**McLelland GL**, Dorval G, Lauinger ND, Rakovic A, Durcan TM, Trempe JF, Fon EA. Mitofusin-2 ubiquitination by PINK1/parkin gates the release of ER from mitochondria to drive mitophagy.

in which I conceived, planned, and analyzed experiments with the help of JFT and EAF. GD created the Mfn2 KO U2OS cell lines and NDL differentiated the iPSC-derived dopamine neurons, both under the guidance of TMD. AR contributed the *PARKIN* mutant cell line. Save for the acquisition and analysis the mass spectrometry data (Fig. IV.2E and F, and Table IV.S1) which was performed by JFT, I generated all the data that went into the figures (a contribution of ~13.5 out of 15 figures). I wrote the manuscript, which was edited by TMD, JFT and EAF.

In summary, Chapters II to IV comprises two first-author publications and one first-author manuscript in preparation, of which I have generated 40.5 out of 43 figures worth of data. Additionally, Chapters I and V contain 12 and 11 original figures, respectively, several of which will appear in a review article being prepared for submission:

**McLelland GL**, Fon EA. Principles of mitochondrial vesicle transport.

LIST of ABBREVIATIONS

**A**: alanine

**ACAT2**: acyl-CoA:cholesterol acyltransferase 2

**AD**: Alzheimer's disease

**AD**: autosomal dominant

**ADP**: adenosine diphosphate

**AFG3L2**: AFG3 ATPase family-like 2

**Ala**: alanine

**AMP**: adenosine monophosphate

**aMLS**: alternative mitochondrial localization signal

**APP**: amyloid precursor protein

**AR**: autosomal recessive

**AR-JP**: autosomal recessive juvenile parkinsonism

**Arg**: arginine

**Asn**: asparagine

**Asp**: aspartate

**ATF5**: activating transcription factor 5

**ATFS-1**: activating transcription factor associated with stress-1

**ATG**: autophagy-related gene

**ATG14L**: autophagy-related gene 14-like

**ATP**: adenosine triphosphate

**BAR**: Bin/Amphiphysin/Rvs-homology

**Barkor**: beclin-1-associated autophagy-related key regulator

**BAX**: B-cell CLL/lymphoma 2-associated X protein

**BCL**: B-cell CLL/lymphoma

**BID**: BH3 interacting-domain death agonist

**C**: cysteine

**C-terminus**: carboxy terminus

**$Ca^{2+}$**: calcium ion

**CCCP**: carbonyl cyanide m-chlorophenylhydrazone

**CFP**: cyan fluorescent protein

**Cho1**: choline-requiring 1

**CI (-V)**: electron transport chain complex I (to V)

**CLEAR**: coordinated lysosomal expression and regulation

**CLUH**: Clu1/CluA homologue

**CoA**: coenzyme A

**CoQ**: coenzyme Q

**Cys**: cysteine

**D**: aspartate

**DA(ergic)**: dopamine(rgic)

**$\Delta\Psi_m$**: mitochondrial membrane potential

**DFCP1**: double FYVE domain-containing protein 1

**Dnm1**: dynamin-related protein 1 (yeast)

**DRM**: detergent-resistant membrane

**Drp1**: dynamin-related protein 1 (mammals)

**DUB**: deubiquitinase

**E**: glutamate

**E1 (-n)**: enzyme one (to n) in a given enzymatic pathway

**EH**: epidermal growth factor receptor pathway substrate clone 15 homology

**EMC**: ER membrane protein complex

**EndoA1/B1**: endophilin A1/B1

**EOPD**: early-onset Parkinson's disease

**Eps15**: epidermal growth factor receptor pathway substrate clone 15

**ER**: endoplasmic reticulum

**ESCRT**: endosomal sorting complex required for transport

**ETC**: electron transport chain

**F**: phenylalanine

**FAD/$FADH_2$**: oxidized/reduced flavin adenine dinucleotide

**FBXO7**: F-box only protein 7

**FCHo**: F-BAR domain-containing Fer/Cip4 homology-domain-only protein

**Fis1**: mitochondrial fission protein 1

**FL**: full-length

**FUNDC1**: Fun14 domain-containing 1

**Fzo1**: fuzzy onions

**G**: glycine

**GABARAP(-L1/2)**: γ-amino butyric acid receptor associated protein (-like 1/2)

**GAP**: GTPase activating protein

**GDP**: guanosine diphosphate

**GEF**: GTP exchange factor

**GFP**: green fluorescent protein

**Glu**: glutamate

**Gln**: glutamine

**Gly**: glycine

**GRAMD1**: glucosyltransferases, Rab-like GTPase activators and myotubularins domain-containing 1

**GRP75**: gluocose-regulated protein 75 kDa

**GTP**: guanosine triphosphate

**H**: histidine

**HECT**: homologous to E6AP carboxy terminus

**HHARI**: human homologue of Ariadne

**His**: histidine

**HM**: heavy membrane fraction

**HOIL**: haem-oxidized IRP2 ubiquitin ligase

**HOIP**: HOIL interacting protein

**HOPS**: homotypic fusion and vacuole protein sorting

**HR**: heptad repeat region

**HRS**: hepatocyte growth factor-regulated tyrosine kinase substrate

**I**: isoleucine

**IBR**: in-between RING

**IDP**: intrinsically-disordered protein

**Ile**: isoleucine

**IM**: isolation membrane

**IMM**: inner mitochondrial membrane

**IMS**: intermembrane space

**$IP_3R$**: inositol-1,4,5-triphosphate receptor

**iPSC**: induced pluripotent stem cell

**K**: lysine

**$K_D$**: dissociation constant

**kDa**: kilo-Dalton

**KRD**: Kufor-Rakeb disease

**L**: leucine

**LAMP**: lysosome-associated membrane protein

**LB**: Lewy body

**LC3/MAP1LC3A(-C)**: microtubule-associated proteins 1A/1B light chain 3A (-C)

**Leu**: leucine

**LIR**: LC3 interacting region

**LLO**: listeriolysin O

**LM**: light membrane fraction

**LOPD**: late-onset Parkinson's disease

**LRRK2**: leucine-rich repeat kinase 2

**Ltc1**: lipid transfer at contact site 1

**Lys**: lysine

**M**: methionine

**m-AAA**: matrix-ATPase associated with diverse cellular activities

**MAM**: mitochondria-associated membrane of the ER

**MAPL**: mitochondria-anchored protein ligase

**MARF**: mitochondrial assembly regulatory factor

**MCU**: mitochondrial calcium uniporter

**MCUR1**: mitochondrial calcium uniporter regulator 1

**MDa**: mega-Dalton unit

**MDV**: mitochondrial-derived vesicle

**Met**: methionine

**Mff**: mitochondrial fission factor

**Mfn1/2**: mitofusin-1/2

**MICU1/2**: mitochondrial calcium uptake protein 1/2

**MiD49/51**: mitochondrial dynamics protein 49/51 kDa

**MIRO**: mitochondrial Rho GTPase

**MitAP**: mitochondrial antigen presentation

**MPP**: mitochondrial processing peptidase

**MS**: mass spectrometry

**mtDNA**: mitochondrial deoxyribonucleic acid

**mTOR**: mammalian target of rapamycin

**mTORC1/2**: mammalian target of rapamycin complex 1/2

**MVB**: multivesicular body

**N**: asparagine

**N-terminus**: amino terminus

**N-BAR**: N-terminal Bin/Amphiphysin/Rvs-homology

**$NAD^+$/NADH**: oxidized/reduced nicotinamide adenine dinucleotide

**nDNA**: nuclear deoxyribonucleic acid

**NDP52**: nuclear dot protein 52

**NLS**: nuclear localization sequence

**NMR**: nuclear magnetic resonance

**NSF**: *N*-ethyl-maleimide-sensitive factor

***O*-GlcNAc**: *O*-linked β-*N*-acetylglucosamine

**OMM**: outer mitochondrial membrane

**Opa1**: optic atrophy 1

**OPTN**: optineurin

**OXPHOS**: oxidative phosphorylation

**P**: proline

**PA**: phosphatidic acid

**PACS2**: phosphofurin acidic cluster sorting protein 2

**PARIS**: parkin interacting substrate

**PARL**: presinilin-associated rhomboid-like protease

**PAS**: phagophore assembly site

**PC**: phosphatidylcholine

**PD**: Parkinson's disease

**PDB**: Protein Data Bank

**PDH**: pyruvate dehydrogenase

**PDH E3bp**: pyruvate dehydrogenase E3 binding protein

**PE**: phosphatidylethanolamine

**PGC-1α**: peroxisome proliferator-activated receptor gamma-coactivator 1α

**Phe**: phenylalanine

**PHGH**: peptidyl glutamyl peptide-hydolyzing

**PI**: phosphatidylinositol

**PI3K**: phosphatidylinositol-3 kinase

**PI3P**: phosphatidylinositol-3-phosphate

**PI4P**: phosphatidylinositol-4-phosphate

**PI(4,5)$P_2$**: phosphatidylinositol-4,5-bisphosphate

**PICK1**: protein interacting with C kinase 1

**PINK1**: PTEN-induced putative kinase 1

**pKA**: negative logarithm (base 10) of the ionization constant of a given acid

**$PP_i$**: inorganic pyrophosphate

**Pro**: proline

**Pru**: pleckstrin-like receptor for ubiquitin

**PS**: phosphatidylserine

**pS65 Ub**: ubiquitin phosphorylated on serine-65

**PSEN**: presenilin

**PTDSS**: phosphatidylserine synthase

**pUb**: phosphoubiquitin

**pUbl**: phosphorylated ubiquitin-like domain

**PX**: phox homology

**pXX**: protein of XX kDa

**Q**: glutamine

**R**: arginine

**R0RBR**: RING0-RING1-IBR-RING2 parkin

**Rab**: Ras-related in brain

**RBR**: RING-IBR-RING

**redox**: oxidation-reduction

**REP**: repressor element of parkin

**RING**: really interesting new gene

**RNA**: ribonucleic acid

**RNS**: reactive nitrogen species

**ROS**: reactive oxygen species

**Rpn**: regulatory particle non-ATPase

**S**: serine

**S**: soluble fraction

**S**: Svedberg unit

**SD-OSR**: spinning disc Olympus superresolution

**Ser**: serine

**SH3**: Src homology 3

**SNARE**: soluble N-ethylmaleimide-sensitive factor attachment protein receptors

**SNP**: single nucleotide polymorphism

**SNpc**: substantia nigra pars compacta

**SNX**: sorting nexin

**SREBF1/2**: sterol regulatory binding factor 1/2

**STX**: syntaxin

**T**: threonine

**TAX1BP1**: TAX1 binding protein 1

**TBC1D15**: Tre-2/BUB2/CDC16 domain family member 15

**TBK1**: TANK-binding kinase 1

**TCA**: tricarboxylic acid

**TFEB**: transcription factor EB

**Thr**: threonine

**TIM23**: translocase of the inner membrane 23 kDa

**TMX1**: thioredoxin-related transmembrane protein 1

**TOM**: translocase of the outer membrane

**TPR**: tetratricopeptide repeat

**Trp**: tryptophan

**Tyr**: tyrosine

**Ub**: ubiquitin

**UBAN**: ubiquitin binding in ABIN and NEMO

**Ubl**: ubiquitin-like domain

**UBR**: E3 ubiquitin ligase N-recognin

**UIM**: ubiquitin interacting motif

**ULK**: unc-51-like autophagy activation kinase

**UPR$^{mt}$**: mitochondrial unfolded protein response

**UPS**: ubiquitin-proteasome system

**USP**: ubiquitin-specific protease

**V**: valine

**Val**: valine

**VAMP**: vesicle-associated membrane protein

**VARP**: VPS9-ankyrin-repeat protein

**VCP**: valosin-containing protein

**vMIA**: viral mitochondrion-localized inhibitor of apoptosis

**VPS**: vacuolar protein sorting

**W**: tryptophan

**WT**: wild-type

**Y**: tyrosine

**Zn$^{2+}$**: zinc ion

## NOTE on GENE NOMENCLATURE

Gene and protein product names are given using the human convention; i.e. *MFN2* for the gene name and mitofusin-2 for the protein. For the sake of simplicity and my sanity, these conventions are extended to all other organisms discussed within this thesis, *with the exception* of budding yeast, where – as a tribute to a long and distinguished history of taking the first steps into mechanistic descriptions of fundamental cell biology, including the secretory pathway, membrane trafficking and mitochondrial dynamics – the proper yeast nomenclature (i.e. Fzo1 and Fzo1p for the gene and protein, respectively) is used.

LIST of TABLES and FIGURES

# Chapter I

# INTRODUCTION

## I.I GENERAL INTRODUCTION

### I.I.i *Parkinson's disease: pathology and epidemiology*

Two hundred years ago, the English surgeon James Parkinson first described the eponymous disorder that came to be known as Parkinson's Disease (PD) in his *Essay on the Shaking Palsy* (Parkinson, 1817). PD is a neurodegenerative disease of unknown aetiology, and is the most common neurological motor disorder worldwide (Hirsch et al., 2016). Although Parkinson himself first speculated that the observed "involuntary tremulous motion" derived from spinal cord lesions (Parkinson, 1817), the primary motor symptoms of individuals suffering from PD – resting tremor, slowness of movement, muscle rigidity, and problems with posture, speech and handwriting – arise from a drastic reduction in striatal dopamine (DA) levels (Nagatsua and Sawadab, 2009). While observations that pharmacological reduction in striatal DA mimicked PD in animals (Carlsson et al., 1957; Carlsson et al., 1958) led to the development of DA replacement therapies in the 1960's (Hornykiewicz, 2010), there is currently no cure for PD.

The primary risk factor for PD is age, though the occurrence of the disease in men is higher than in women; according to a recent meta-analysis, the incidence of PD in men over the age of 50 is 318 cases per 100,000 individuals compared to 243 cases for women in the same age group (Hirsch et al., 2016). There is also a convergence between melanoma and PD diagnoses (Liu et al., 2011). A diagnosis of melanoma increased the risk of developing PD by almost 50% in two Scandinavian studies (Olsen et al., 2006; Wirdefeldt et al., 2014), whereas the incidence of melanoma development in PD patients is also increased compared to control individuals (Constantinescu et al., 2014; Constantinescu et al., 2007; Schwid et al., 2010). Other risk factors are less clear; for example, high levels of blood cholesterol and polyunsaturated fats were associated with decreased risk of PD, although only in certain populations and under certain

conditions (Ascherio and Schwarzschild, 2016). Moreover, the distribution of fat in the body (Abbott et al., 2002; Chen et al., 2004), rather than body-mass index, correlated with risk of PD (Ascherio and Schwarzschild, 2016). Environmental factors may also increase PD risk, with exposure to pesticides being a prime example (Hirsch et al., 2016).

The primary pathophysiological hallmark of PD is the loss of dopaminergic (DAergic) neurons within the *substantia nigra pars compacta* (SNpc) (Venderova and Park, 2012). The death of these neuromelanin-containing neurons is visible as a loss of pigmentation (hence the name of this part of the brain – *substantia nigra* or "black substance") in this area, as up to 90% of DAergic neurons are lost after only a few years post-diagnosis (Kordower et al., 2013). While DAergic neuron loss causes the visible motor symptoms, other catecholinergic systems are affected by the disease, notably the norepinephrine system of the *locus coeruleus* (Espay et al., 2014). In sporadic PD and many genetic forms of the disease, the remaining neurons contain proteinaceous inclusions termed Lewy bodies (LBs), whose primary component (by plurality) is α-synuclein (McCormack et al., 2016; Spillantini et al., 1997; Xia et al., 2008). The precise mechanisms of cell death in PD, however, remain unknown.

### I.I.ii *Genetics of Parkinson's disease*

Much of the insight into the pathophysiological mechanisms of PD have come from studies involving genes linked to PD. While most cases of PD arise from an unknown cause, 30% of PD cases have a direct genetic cause (Kumar et al., 2011). While many genes have been linked to PD, with others acting as risk factors, several well-validated genes (relevant to this thesis) that lead to monogenic forms of parkinsonism are listed in Table I.1 (adapted and modified from (Kumar et al., 2011) and (Abeliovich and Gitler, 2016)).

Table I.1. Descriptive table of several monogenic causes of PD

| Gene | Chromosomal location | Inheri-tance | Clinical phenotype | Protein function | First described |
|---|---|---|---|---|---|
| *ATP13A2* | 1p36 | AR | KRD | transporter | (Ramirez et al., 2006) |
| *DJ-1* | 1p36 | AR | AR-JP | glyoxalase | (Bonifati et al., 2003) |
| *LRRK2* | 12q12 | AD | LOPD | kinase/GTPase | (Paisan-Ruiz et al., 2004) |
| *PARKIN* | 6q25.2 to q27 | AR | AR-JP | Ub ligase | (Kitada et al., 1998) |
| *PINK1* | 1p35 to p36 | AR | AR-JP | kinase | (Valente et al., 2004) |
| *SNCA* | 4q21 | AD | EOPD | unknown | (Polymeropoulos et al., 1997) |
| *VPS13C* | 15q22.2 | AR | EOPD | unknown | (Lesage et al., 2016) |
| *VPS35* | 16q11.2 to q12 | AD | LOPD | retromer complex | (Vilarino-Guell et al., 2011; Zimprich et al., 2011) |

Abbreviations: AD, autosomal dominant; AR, autosomal recessive; AR-JP, autosomal recessive juvenile parkinsonism; EOPD, early-onset PD; LOPD, late-onset PD; KRD, Kufor-Rakeb disease; Ub, ubiquitin.

*SNCA*, encoding the LB protein α-synuclein, was the first gene linked to a familial form of early-onset PD (EOPD, early onset implies an age-of-onset of less than 50 years of age) with LB pathology (Polymeropoulos et al., 1997). EOPD due to *SNCA* mutations is thought to occur through a toxic gain-of-function mechanism, strongly evidenced by the fact that gene multiplications are pathogenic (Chartier-Harlin et al., 2004; Nishioka et al., 2006; Ross et al., 2008). Mutations in *LRRK2* (Paisan-Ruiz et al., 2004) and *VPS35* (Vilarino-Guell et al., 2011; Zimprich et al., 2011) also cause an autosomal dominant form of PD, although considered to be late-onset (LOPD). Although *VPS35* patients are rare, accounting for under 1.5% of familial PD cases, up to 41% of total familial PD is caused by mutations in *LRRK2* (Brice, 2005; Mohan and Mellick, 2016). Despite *LRRK2* patients presenting a heterogeneity of phenotypes, the patients

carrying the G2019S mutation are clinically indistinguishable from sporadic PD cases (Healy et al., 2008).

Mutations in *PARKIN* (also referred to as *PARK2*), *PINK1* and *DJ-1* are rare, but highly penetrant, and cause a syndrome known as autosomal-recessive juvenile parkinsonism (AR-JP), characterized by a very early onset of symptoms (Bonifati et al., 2003; Kitada et al., 1998; Valente et al., 2004). AR-JP patients are typically characterized by an unwavering responsiveness to DA therapy, slowness of disease progression, an intact sense of olfaction and typically, despite a rarity of studies on the matter, a paucity of LBs (Lucking et al., 2000; Malek et al., 2016; Mori et al., 1998). Truncating mutations in *VPS13C* cause recessive EOPD, although this is closer to sporadic PD rather than AR-JP, and characterized by a rapid disease progression and diffuse LB pathology

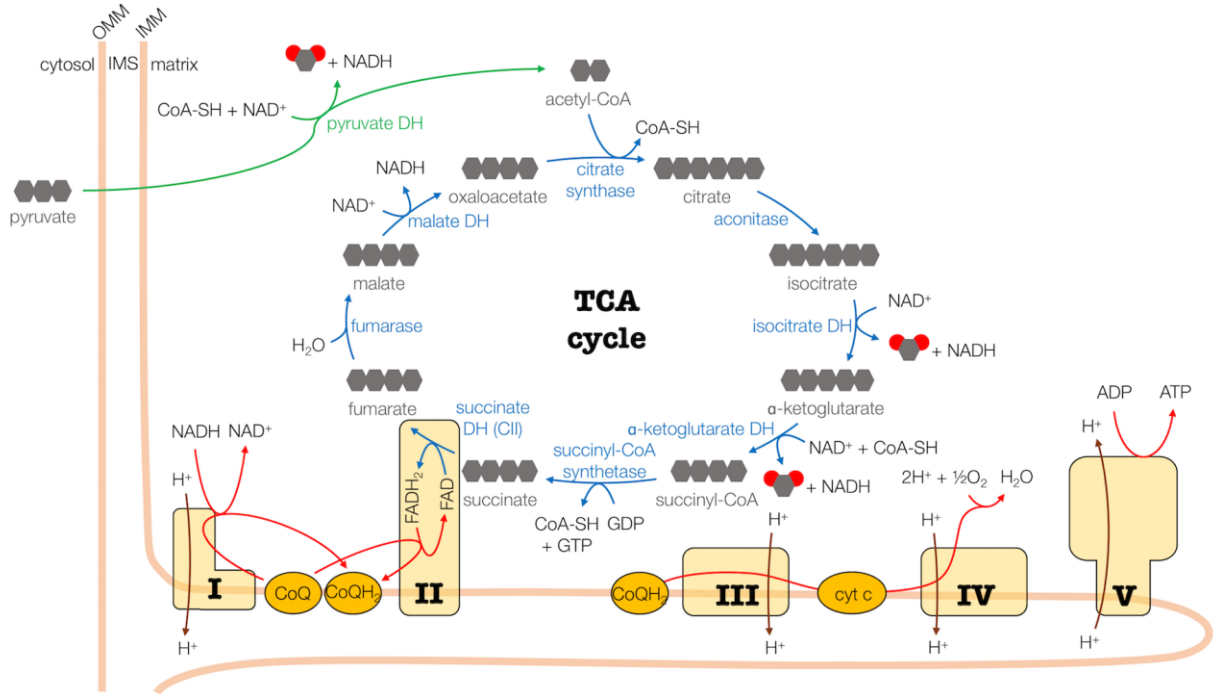


**Figure I.1**. *The TCA cycle and electron transport chain (ETC).* Pyruvate is transported into mitochondria, where it is converted to acetyl-CoA by pyruvate dehydrogenase (PDH), which then enters the TCA cycle. The number of carbons of each molecule is represented by grey hexagons, and $CO_2$ by a hexagon with two red circles. Electrons are transferred to $NAD^+$ and FAD, and then coenzyme Q (CoQ) through CI and CII, respectively, in the ETC, driving proton translocation across the IMM. Electrons pass from reduced CoQ ($CoQH_2$) through CIII, cytochrome c (cyt c), CIV and finally to water. The proton gradient is used by the $F_0F_1$-ATPase (CV) to phosphorylate ADP, forming ATP, the energy currency of the cell. TCA cycle metabolites are in grey, TCA enzymes in blue and the PDH-dependent step in green. Yellow shapes represent ETC complexes, and accessory ETC components are in orange.

(Lesage et al., 2016). Finally, mutations in *ATP13A2* cause a rare autosomal recessive form of PD known as Kufor-Rakeb disease (KRD), which encapsulates typical PD symptoms within a broader neurodegenerative spectrum (Ramirez et al., 2006; Williams et al., 2005). The ATP13A2 protein, like α-synuclein, has also been reported to be a component of LBs (Dehay et al., 2012).

### I.I.iii *Basics of mitochondrial function, and dysfunction in Parkinson's disease*

A deficit in the function of mitochondria has been associated with PD for almost 30 years (Bindoff et al., 1989; Schapira et al., 1989). Referring to the mitochondrion in 1957, Philip Siekevitz coined the term "powerhouse of the cell" (Siekevitz, 1957) in light of the organelle's apparent ability to generate the cell's energy in the form of adenosine triphosphate (ATP). At this time, future Nobel laureate (and Siekevitz's post-doctoral supervisor) George Palade had been performing pioneering electron microscopic studies on this organelle (among others), noting their double membrane structure limited by an inner and outer mitochondrial membrane (IMM and OMM, respectively), with the intermembrane space (IMS) existing between both membranes, and a matrix limited by the IMM (Palade, 1975; Palade, 1952; Palade, 1953). Palade correctly predicted that the morphological compartmentalization of the organelle implies functional specialization, building on the previous observation that enzymatic activities must be organized in a "definite spatial relationship" (Schneider and Hogeboom, 1951). Reducing equivalents – mostly in the form of pyruvate, a glucose breakdown product – are shuttled into the mitochondrial matrix, where they are stripped of their electrons through a cycle of chemical reactions referred to the tricarboxylic acid (TCA) cycle or Krebs cycle (Fig. I.1). Electrons are transferred to the carriers $NAD^+$ and FAD to form NADH and $FADH_2$, respectively, and are subsequently transferred to the electron transport chain (ETC), where they are shuttled through multi-subunit ETC complexes

(which also form higher-order supercomplexes) according to increasing (i.e. more positive) redox potential, to drive proton ($H^+$) translocation across the IMM, from the matrix into the IMS (Gu et al., 2016; Senior, 1988). This electrochemical gradient (equivalent to a mitochondrial membrane potential, $\Delta\Psi_m$) is utilized by complex V (also referred to as the $F_0F_1$-ATPase, CV), a phosphorylase, to couple proton flux back into the matrix with phosphorylation of adenosine diphosphate (ADP) to form ATP (Senior, 1988).

The mitochondrion arose from an endosymbiotic event that occurred roughly one billion years ago, where an α-proteobacterium (an obligate aerobe) was internalized into the primordial eukaryotic cell. Electron shuttling by the bacterium's primitive ETC – containing ancient homologues of all four respiratory complexes as well as the CV ATPase (Thrash et al., 2011) – allowed for the primitive eukaryote to greatly increase the energy yield per glucose molecule, conferring it an evolutionary advantage. This new reality of dealing with oxidative metabolism, and the damaging radicals associated with it, may have driven compartmentalization of the genome into the nucleus, as well as the biogenesis of the endomembrane system (Gould et al., 2016). Over millions of years, the ancestral bacterial genome was depleted through gene transfer to nuclear DNA (nDNA) (Berg and Kurland, 2000). Indeed, only thirteen ETC subunits are encoded by the mitochondrion's own genome (mtDNA), which also encodes the organelle's proper set of transfer and ribosomal RNAs (Anderson et al., 1981). While the driving force of this transfer remains unknown, it may have been a protective mechanism preventing the accumulation of deleterious mtDNA mutations through asexual reproduction of the mitochondrial genome – a phenomenon more generally known as Muller's ratchet (Felsenstein, 1974; Muller, 1964).

In addition to their fundamental role as powerhouses, mitochondria also perform crucial functions related to metabolism, lipid synthesis, iron handling, innate immunity, programmed cell

death, and biogenesis of other organelles (Naon and Scorrano, 2014; Newmeyer and Ferguson-Miller, 2003; Sugiura et al., 2017) – some of these roles will be expanded upon later in this work. One mechanism that mitochondria use to regulate this functional diversity throughout the mitochondrial network is by organellar fusion and division (Friedman and Nunnari, 2014). Regarding this point, Siekevitz was virtually prescient, writing in 1957 that mitochondria "are either spherical or rod-shaped, and they may change from one shape to another" (Siekevitz, 1957), referring to phenomenon which, four decades later, formed the basis for the field of mitochondrial dynamics.

In the context of PD, the earliest indication of a role for mitochondrial dysfunction in the disease came from observations that brains from PD patients had a selective CI functional deficit (Bindoff et al., 1989; Schapira et al., 1989). Indeed, mtDNA mutational abnormalities and decreased copy number, as well as increased deposition of elemental iron, have been measured in patient brains and at-risk neuronal populations (Barnham and Bush, 2008; Bender et al., 2006; Dexter et al., 1992; Grunewald et al., 2016; Perier et al., 2013; Pyle et al., 2016), which may contribute to the reported respiratory deficit. Moreover, associations between incidences of parkinsonism and *POLG1*, the gene encoding the mtDNA polymerase, have been reported (Anvret et al., 2010; Davidzon et al., 2006; Eerola et al., 2010; Gui et al., 2012; Luoma et al., 2007). AR-JP patients carrying *PARKIN* mutations have mitochondrial deficits similar to individuals affected by sporadic PD in primary patient cells (Mann et al., 1992; Muftuoglu et al., 2004; West and Maidment, 2004). Mitochondrial dysfunction has additionally been observed in both fibroblasts and induced pluripotent stem cells (iPSCs) isolated from *PARKIN* and *PINK1* AR-JP patients, in the form of decreased levels of respiration and cellular ATP, and alterations in $\Delta\Psi_m$ and mitochondrial morphology (Ambrosi et al., 2014; Chung et al., 2016; Shaltouki et al., 2015; van

der Merwe et al., 2014; Zanellati et al., 2015). Further observations that mitochondrial health is impaired in *LRRK2* G2019S carriers (Mortiboys et al., 2010) suggests that deficiencies in the function of these organelles may be a phenomenon common throughout different variations of parkinsonism. The answer to whether mitochondrial dysfunction is a cause or consequence of PD, however, has remained elusive.

## I.II PATHWAYS OF PINK1 AND PARKIN IN PARKINSON'S DISEASE

### I.II.i *PINK1 in mitochondrial health: import and CI deficiency*

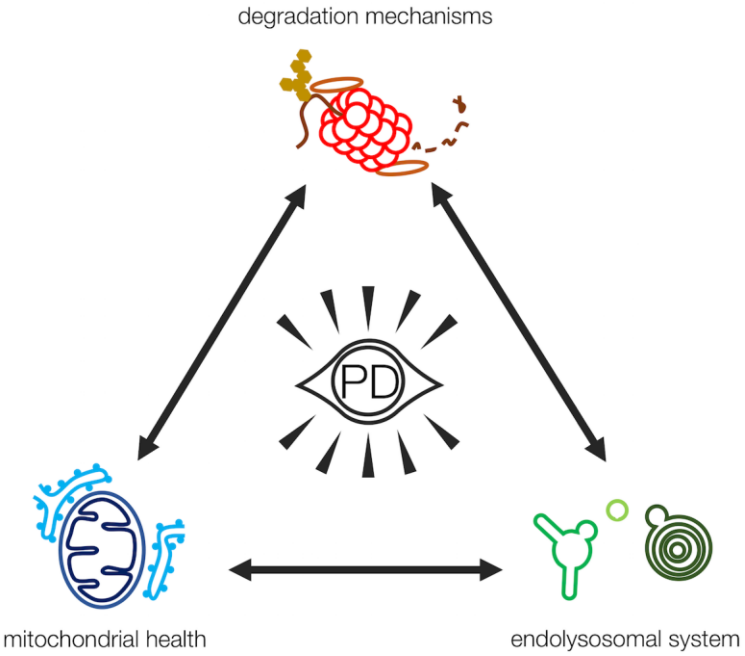


**Figure I.2**. *The three cornerstones of PD*. Recurring themes in the field of PD cell biology include mitochondrial health, mechanisms of protein/organelle degradation, and the endolysosomal system.

Despite the apparent prevalence of mitochondrial dysfunction in PD, alterations in endolysosomal trafficking, as well as protein turnover, are also suspected culprits in disease etiology (Abeliovich and Gitler, 2016); together, they complete the three "cornerstones" of PD (Fig. I.2). Returning to mitochondrial dysfunction, the most obvious PD gene linked to mitochondria is *PINK1* (PTEN-induced putative kinase 1), which encodes a 581 amino acid protein that contains a mitochondrial targeting sequence (MTS) at its N-terminus (Fig. I.3A) (Silvestri et al., 2005; Valente et al., 2004). The MTS is followed by a transmembrane (TM) domain and a serine/threonine (S/T) kinase domain that most closely resembles $Ca^{2+}$/calmodulin-

dependent protein kinases I and II, as well as dystrophia myotonica protein kinase (Cardona et al., 2011; Valente et al., 2004). PINK1 can autophosphorylate itself on residues S228 and S402 in cells (Okatsu et al., 2012), and the protein retains at least some of its neuroprotective activity even when the first 111 N-terminal amino acids (which cover the MTS and TM domains) of the protein are deleted (Haque et al., 2008), highlighting the importance of the cytoplasmic kinase domain in its function (Zhou et al., 2008).

In the absence of a ternary structure of PINK1, substrate and ATP, modeling the protein has proven to be difficult. PINK1 is an atypical S/T kinase, on its own branch of the human kinome tree (Fig. I.3B and C) (Eid et al., 2017). Initial protein modeling of human PINK1 predicted the conserved, critical lysine residue involved in ATP coordination to be K186 which, based on the

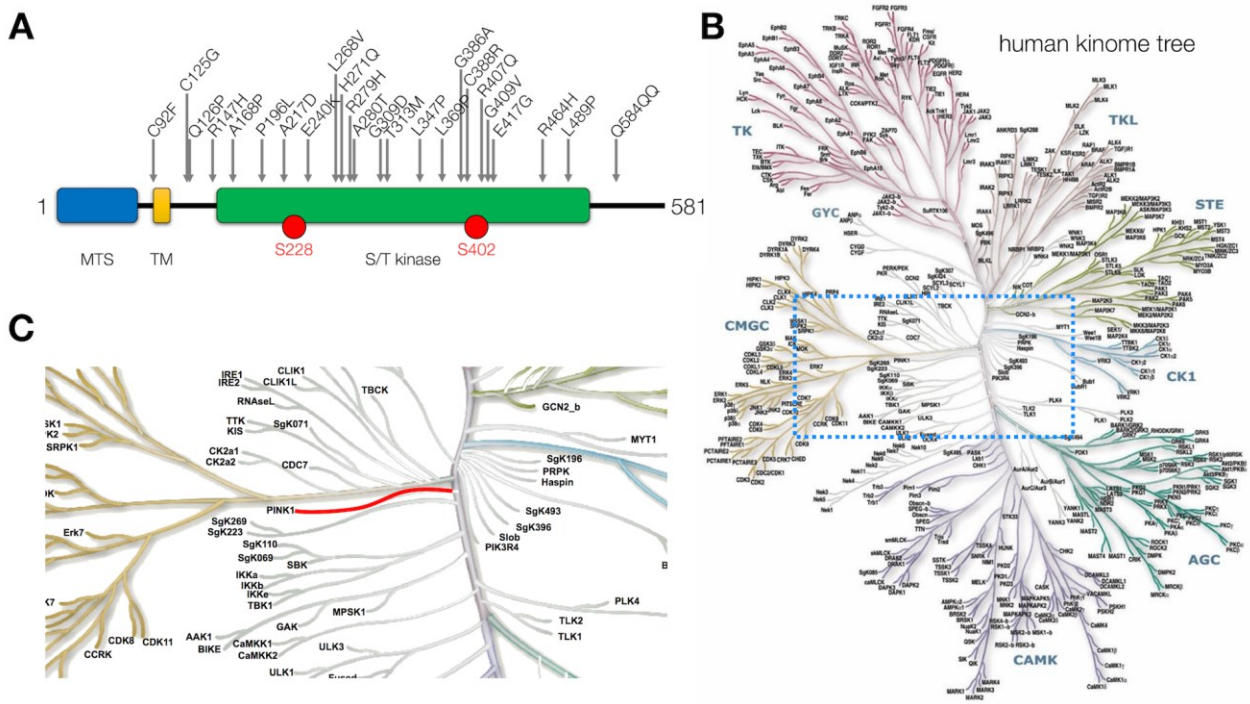


**Figure I.3**. *PINK1 domain structure, mutations and similarity to other kinases*. **A** Domain structure of human PINK1, including the mitochondrial targeting sequence (MTS, blue), transmembrane domain (TM, yellow) and S/T kinase domain (green). Grey arrows indicate PD mutations, as curated by Uniprot.org. Autophosphorylation sites are indicated by red circles. **B** The human kinome, produced using KinMap (Eid et al., 2017). Abbreviations: AGC, PKA-, PKC- and PKG-containing families; CAMK, $Ca^{2+}$/calmodulin-dependent protein kinase; CK1, casein kinase 1; CMGC, CDK-, MAPK-, GSK3- and CLK-containing families; GYC, guanylate kinase; STE, homologues of Sterile-7, -11 and -20 kinases in yeast; TK, tyrosine kinases; TLK, tyrosine kinase-like. **C** PINK1 and its surroundings in the human kinome (dotted blue box from **B**). The unique PINK1 branch is shown in red.

model, is in the proximity of G309 (Silvestri et al., 2005). By extension, the G309D PD mutation could affect phosphoryl transfer of the kinase (Silvestri et al., 2005; Valente et al., 2004). Further bioinformatic analyses, however, have instead shown K219 to be critical for ATP binding as part of the P-loop (Cardona et al., 2011; Petit et al., 2005). While mutation of this residue to methionine (K219M) is thought to supposedly abolish kinase activity (Beilina et al., 2005; Haque et al., 2008; Petit et al., 2005), PINK1$^{K219A}$ (alanine substitution) was shown to retain *in vitro* trans-phosphorylation activity (Pridgeon et al., 2007). In their bioinformatic study, Cardona *et al*. showed that K186, although in the kinase domain, is unconserved and PINK1 catalytic activity, like related S/T kinases, likely resides in the HRD motif (H360 to D362 in human PINK1) of the catalytic loop (Cardona et al., 2011). Indeed, mutation of either D362 in the catalytic loop or D384 in the activation loop results in a kinase-dead PINK1 variant (Pridgeon et al., 2007). A recent crystal structure of phosphomimetic PINK1 from *Tribolium castaneum* (the residue equivalent to the S228 phosphosite was mutated to glutamate) revealed several putative regulatory mechanisms, including interactions between the HRD motif and the activation loop in the absence of phosphorylation of the latter (Kumar et al., 2017b). The same study showed that autophosphorylation at the conserved S228 (pS205 in *Tc*PINK1) likely aids in the recognition of PINK1 substrates (Kumar et al., 2017b). It is important to note, however, that several insect homologues of PINK1 – including *Tc*PINK1 – show robust phosphorylation activity *in vitro* compared to the human form (Wauer et al., 2015a; Woodroof et al., 2011), and may accordingly lack additional regulatory mechanisms. We currently await structural data concerning human PINK1 in order to determine exactly how the protein is regulated and the mechanism of phosphoryl transfer.

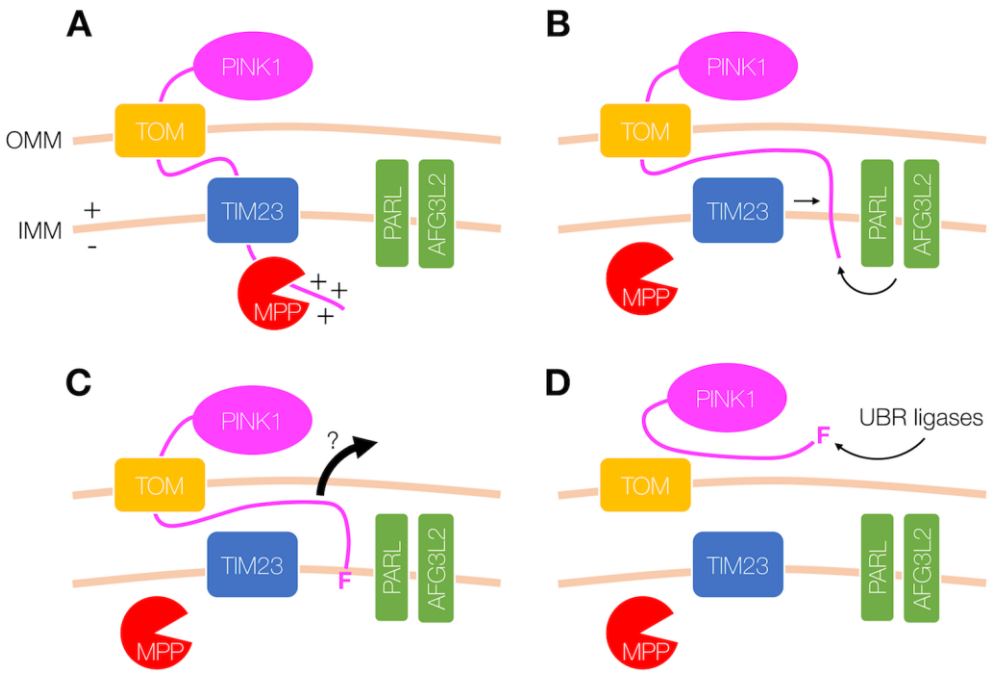


**Figure I.4**. *Proteolytic processing of PINK1*. PINK1 is processed in a stepwise manner. **A** MPP recognizes the MTS of FL PINK1 in the matrix and cleaves it. **B** PARL/AFG3L2 process cleaved PINK1 likely after its lateral release into the IMM, exposing the N-degron F104. **C** PINK1 is retrotranslocated into the cytoplasm by an unknown mechanism. **D** PINK1 is recognized by UBR ligases and turned over by the proteasome.

PINK1 protein is synthesized and then imported into mitochondria, potentially in a co-translational manner; evidence for co-translational import of mitochondrial proteins includes the observation that many mitochondrial proteins are translated on the surface of mitochondria (Williams et al., 2014), as well as a recent EM tomographic study demonstrating the presence of ribosomes on the OMM (Gold et al., 2017). PINK1 is imported through the translocase of the outer membrane (TOM) and translocase of the inner membrane 23 kDa (TIM23) machineries (Fig. I.4) (Harbauer et al., 2014). At the OMM, PINK1 can associate with TOM70 (Lazarou et al., 2012), and is translocated through the TOM complex, followed by the TIM23 complex; this latter step is electrophoretic due to the polarization of the IMM (Fig. I.1) (Harbauer et al., 2014; Lin and Kang, 2008). Once the N-terminus has been translocated into the matrix, the full-length (FL) 64 kDa protein is cleaved by the mitochondrial processing peptidase (MPP), a dimeric mitochondrial zinc metalloprotease, reducing the molecular weight of the protein to ~60 kDa (Greene et al., 2012). This form is further processed by the IMM proteases presinilin-

associated rhomboid-like protease (PARL) and the m-AAA (matrix-ATPase associated with diverse cellular activities) protease subunit AFG3 ATPase family-like 2 (AFG3L2) to create a 52 kDa form of PINK1 (Deas et al., 2011; Greene et al., 2012; Jin et al., 2010; Meissner et al., 2011). Accordingly, *PARL* and *PINK1* orthologues have been shown to interact genetically in *Drosophila* (Whitworth et al., 2008). Although PARL and AFG3L2 cleave ~60 kDa PINK1 in possibly redundant steps, recent evidence has shown that both proteins co-migrate in a ~2 MDa proteolytic complex (Wai et al., 2016). 52 kDa PINK1 is retrotranslocated to the cytosol by an unknown mechanism (Yamano and Youle, 2013). The cleavage of ~60 kDa PINK1 at A103 allows F104 to be recognized by Ub ligases involved in the N-end rule pathway, leading to turnover of the protein by the proteasome (Deas et al., 2011; Yamano and Youle, 2013). Indeed, treatment of cells with the proteasomal inhibitor MG132 stabilizes the 52 kDa form of PINK1, which collects in ubiquitinated inclusions (Greene et al., 2012; Jin et al., 2010; Yamano and Youle, 2013).

Classically, PINK1 has been implicated in promoting ETC activity. Replicating sporadic PD, a marked decrease in CI activity has been reported in PINK1 deficient cells and organisms (Grunewald et al., 2009; Morais et al., 2009), possibly resulting from disruption of electron transport between CI and coenzyme Q (CoQ, also termed ubiquinone) (Grunewald et al., 2009). Accordingly, PINK1-associated degenerative phenotypes can be rescued by either bypassing CI altogether through expression of an alternative NADH dehydrogenase (Vilain et al., 2012), by reverse electron transport through CI (Scialo et al., 2016), or by facilitating CI-CoQ reductive transfer through alternative electron carriers such as cardiolipin or menaquinone (vitamin K2) (Vos et al., 2012; Vos et al., 2017). These terminal mechanisms, however, may simply rescue PINK1 phenotypes by acting as electron sinks, as antioxidants also confer resistance to loss of PINK1 in flies (Wang et al., 2006). Along these lines, overexpression of the CI subunit NDUFA10, which is

positioned close by the CoQ binding pocket in CI (Sazanov, 2015), also rescues the CI defect in PINK1 null flies (Morais et al., 2014; Pogson et al., 2014). Thus, while the CI defect induced by PINK1 loss is responsive to several rescue mechanisms, how it arises in the first place remains to be determined.

### I.II.ii *Parkin and the ubiquitin system*

A gene closely related to *PINK1* – at least in what will become clear as function – is the AR-JP gene *PARKIN*, which encodes a 465 amino acid ubiquitin (Ub) ligase (Kitada et al., 1998; Shimura et al., 2000; Zhang et al., 2000). Ub ligases act as the E3 enzymatic component of protein ubiquitination. Ub, a small protein of 76 amino acids, is directly conjugated to substrate proteins through a covalent glycyl-lysine linkage between the C-terminal glycine in Ub and an ε-amino group in a lysine side chain of the substrate, forming a so-called isopeptide bond. Ub can also be conjugated to lysines in other Ub molecules to form chains of structurally distinct linkages, as Ub contains seven lysines – K6, K11, K27, K29, K33, K48 and K63 – in addition to the α-amino group of the N-terminal methionine (to form linear chains) (Fig. I.5A) (Komander and Rape, 2012). Conjugation to internal lysines is favoured as these side chain amino groups typically have higher pKa values relative to the N-terminus (values of ~10.5 to ~8.0, respectively), favouring deprotonation and nucleophillic attack (Grimsley et al., 2009). Chain branching (two Ub molecules conjugated to different lysines in another Ub molecule), linkage mixing (a Ub chain featuring conjugation at different lysines), as well as mixed chains (chains featuring Ub and other Ub-like proteins) create a complex and diverse "ubiquitin code" (Kravtsova-Ivantsiv and Ciechanover, 2012; Trempe, 2011).

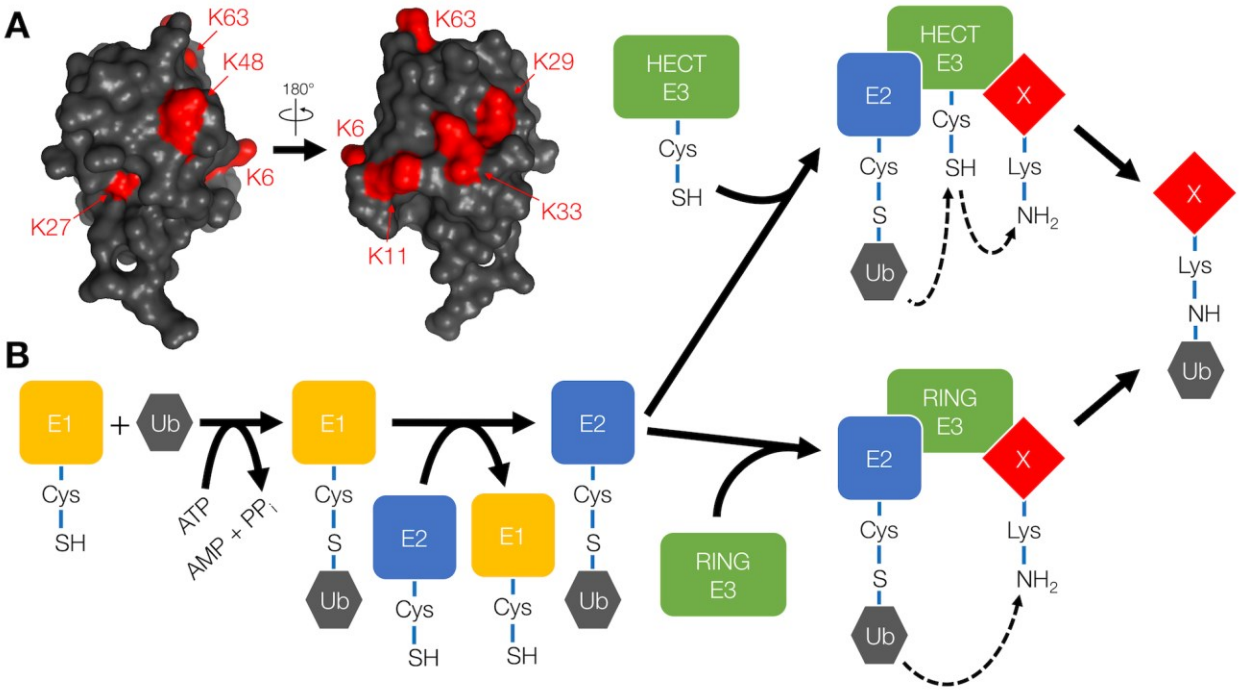


**Figure I.5**. *Catalytic mechanism of protein ubiquitination*. **A** Structure (surface) of human Ub (PDB ID 1UBQ, grey) with lysine residues available for conjugation highlighted in red. **B** Protein ubiquitination involves ATP-dependent charging of the E1 activating enzyme, followed by transfer of Ub to the E2 conjugating enzyme. While RING-type E3 ligases (lower path) bring charged E2 and the substrate protein (X) in close proximity for Ub transfer to occur between the E2 and the substrate, HECT-type ligases (upper path) receive Ub from the E2 prior to direct ligation to the substrate.

Conjugation of a single Ub moiety onto a lysine residue (monoubiquitination) or ubiquitin chain formation (polyubiquitination) is catalyzed by a series of enzymatic reactions (Fig. I.5B). Ub is first "activated" by an E1 activating enzyme in an ATP-dependent step, forming a glycyl-cysteine linkage (a thioester bond) between the Ub C-terminus and the E1 active site. Ub is then transferred to the active site cysteine of the E2 conjugating enzyme, which supplies Ub to E3 ligases for ligation onto substrate lysines (glycyl-lysine linkage). While HECT-type ligases form a transient thioester bond with the donor Ub C-terminus, RING-type ligases coordinate the E2 and substrate so that ubiquitination occurs directly from the E2 (Metzger et al., 2012).

Classically, polyubiquitination has been a key feature of the ubiquitin-proteasome system (UPS) – the major cellular turnover pathway of short-lived proteins (Arrigo et al., 1988; Hershko et al., 1980). Polyubiquitinated proteins are typically recognized by the proteasome – a massive

protein complex formed by a 20S core particle capped at one or both ends by a 19S regulatory particle. The barrel-shaped core particle catalyzes proteolysis and is formed of heptameric rings of α- and β-subunits with trypsin-like, chymotrypsin-like and PHGH-like activities (Besche et al., 2009; Goldberg, 2007). The regulatory particle acts to recognize Ub chains via the receptors Rpn10/S5a and Rpn13, and then unfold polypeptides through the activity of its AAA-ATPases in order to feed them into the core particle (Besche et al., 2009; Goldberg, 2007). Ub recognition by the proteasome occurs through interactions of Rpn receptors with the so-called "hydrophobic patch" on Ub, which includes residues L8, I44, H68 and V70 in Ub (Beal et al., 1996; Beal et al., 1998). Canonically, K48-linked chains are associated with proteasomal degradation, although there are exceptions; most notably, ornithine decarboxylase is not ubiquitinated yet turned over by the proteasome (Murakami et al., 1992).

With respect to the E3 ligase parkin, its domain structure consists of a Ub-like (Ubl) domain at its N-terminus, separated from four zinc-coordinating RING (really interesting new gene) domains, named RING0, RING1, IBR (in-between RING) and RING2, by a flexible linker (Fig. I.6A). A single α-helix, termed the repressor element of parkin (REP), is located between the IBR and RING2 domains (Trempe et al., 2013). Ligases with a RING-IBR-RING (RBR) domain module form a family of hybrid, RING-/HECT-type ligases, in which a thioester intermediate is formed and direct ligation of Ub to the substrate occurs despite a structure consisting of RING domains (Smit and Sixma, 2014); in parkin, the active site residue is C431 in the RING2 domain (Iguchi et al., 2013; Trempe et al., 2013; Wenzel et al., 2011). The RBR family, which includes other E3 ligases such as HHARI, HOIP and HOIL, are typically autoinhibited (Smit and Sixma, 2014). RING domains coordinate zinc ions through electrostatic interactions with cysteine and histidine (H) residues (four residues per ion). The importance of this structural element cannot be

understated, as incubation of parkin with EDTA, a chelator of divalent cations, unfolds the protein (Beasley et al., 2007; Hristova et al., 2009). Indeed, several Zn-coordinating cysteines are mutated in AR-JP (Fig. I.6B), and contribute to unfolding and aggregation of the protein (Gu et al., 2003; Hampe et al., 2006; Wong et al., 2007).

At the N-terminus, the Ubl domain was initially suggested to play a role as a negative regulator of enzymatic function and turnover stability (Burchell et al., 2012; Chaugule et al., 2011; Finney et al., 2003). It contains, as its name suggests, a high level of primary sequence homology to Ub and structurally adopts a ubiquitin superfold (Fig. I.6C) (Sakata et al., 2003; Tomoo et al., 2008; Vijay-Kumar et al., 1987). The domain's relevance to parkin function is highlighted by the R42P mutation, which unfolds the Ubl domain and causes AR-JP (Safadi and Shaw, 2007; Terreni

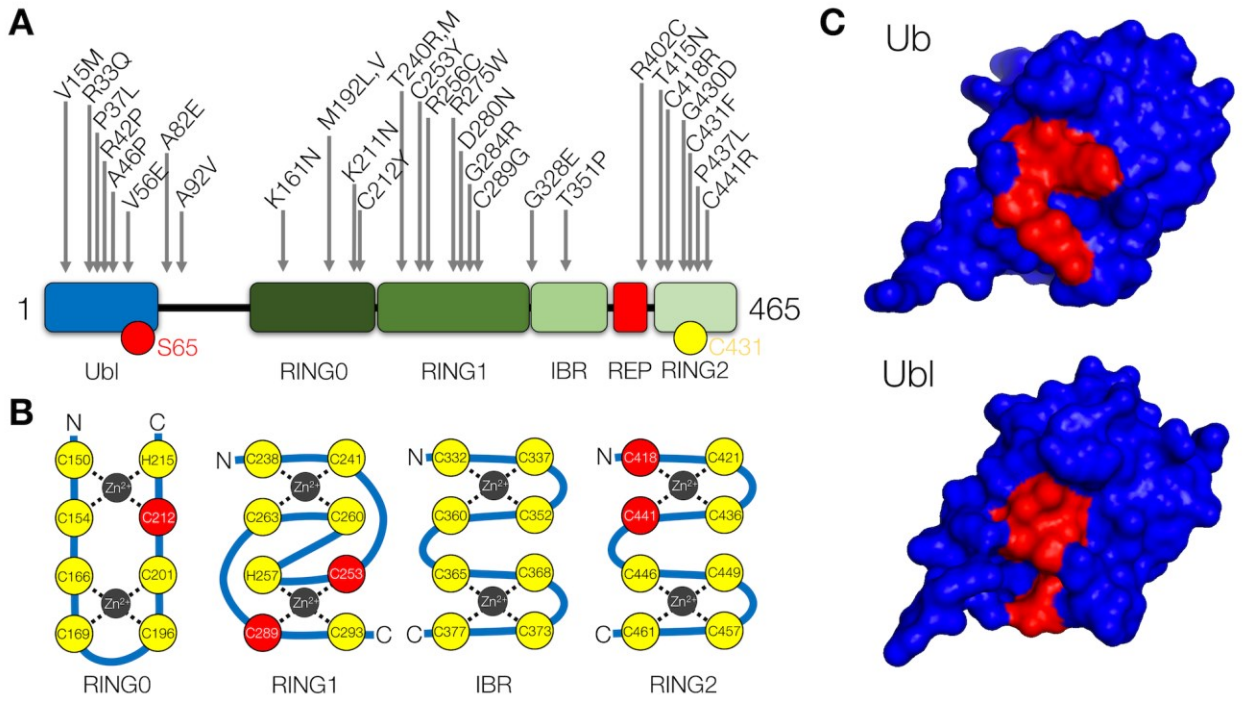


**Figure I.6**. *Parkin domain structure and mutations, zinc coordination and Ubl structure*. **A** Domain structure of human parkin, including the Ub-like domain (Ubl, blue), RING/IBR domains (different shades of green) and repressor element of parkin (REP, red). Grey arrows indicate PD mutations, as curated by Uniprot.org. The red circle indicates a site of phosphorylation, and the yellow circle indicates the active site residue. **B** Diagram of zinc ion coordination by C/H residues (yellow circles) within the RING domains, adapted from Trempe *et al.*, 2013. Red circles highlight residues mutated in PD. **C** Structure (surface) of human Ub (PDB ID 1UBQ) and the murine parkin Ubl domain (PDB ID 2ZEQ) (blue). The hydrophobic patch formed by L/N8, I44, H68 and V70 is highlighted in red in both proteins.

et al., 2001). Importantly, Ub residues corresponding to the hydrophobic patch are mostly conserved in the Ubl (L8 is an asparagine residue). Like Ub, the parkin Ubl can bind proteasomal Ub receptors through the association of its hydrophobic patch with the Ub interacting motifs (UIMs) of Rpn10 or the pleckstrin-like receptor for ubiquitin (Pru) domain of Rpn13 (Aguileta et al., 2015; Husnjak et al., 2008; Safadi and Shaw, 2010; Sakata et al., 2003; Schreiner et al., 2008). Although the affinity of the Ubl for Rpn13 was found to be ten-fold greater than the affinity of Ub for the same Ub receptor ($K_D$ values of ~3 μM and ~70 μM, respectively) and seventy-fold greater than the Ubl-Rpn10 interaction ($K_D$ of ~220 μM) (Aguileta et al., 2015; Safadi and Shaw, 2010), the affinity of Rpn13 for K48-linked diUb was measured to be in the nanomolar range (Husnjak et al., 2008). Regardless, this interaction may serve to promote the proteasomal degradation of parkin (Aguileta et al., 2015), whose stability is regulated by ubiquitination; ataxin-3 and USP8, two deubiquitinases (DUBs) – enzymes that cleave Ub molecules or entire chains off substrates – also function to control cellular levels of parkin (Durcan et al., 2011; Durcan et al., 2014).

Ubl interactions also highlight an apparent role for parkin in endocytic trafficking. Eps15 is an endocytic adaptor protein with tandem UIMs that, similar to Rpn10, bind parkin (Fallon et al., 2006; Safadi and Shaw, 2010). Parkin monoubiquitinates Eps15, a modification associated with the endocytic pathway, to prolong receptor tyrosine kinase signaling in the presence of growth factor (Fallon et al., 2006; Haglund et al., 2003). Parkin also monoubiquitinates other proteins involved in endocytosis, such as PICK1 and endophilin-A1 (EndoA1) (Joch et al., 2007; Trempe et al., 2009), and endocytic and trafficking defects have been observed in parkin-null cells (Cortese et al., 2016; Song et al., 2016). In the case of parkin-mediated EndoA1 ubiquitination, this is again achieved through an interaction with the parkin Ubl, although via the SH3 domain of EndoA1 (Trempe et al., 2009). In addition to the Ubl hydrophobic patch, this interaction also relies on basic

C-terminal residues that are unique to the parkin Ubl, termed the PaRK extension (P73-K76, with a PxRK consensus sequence) (Trempe et al., 2009). Accordingly, parkin levels were increased in the brains of EndoA-null mice (Cao et al., 2014), suggesting a functional interplay between these two proteins. Moreover, EndoA1 is phosphorylated by LRRK2 to promote protein turnover via the autophagy pathway at synapses (Soukup et al., 2016), highlighting the relevance of endocytic mechanisms to PD gene products.

I.II.iii *Fruit fly studies link AR-JP genes to mitochondrial dynamics and oxidative stress*

Despite its apparent importance in endocytosis, loss of *PARKIN* has, like *PINK1*, been associated with mitochondrial dysfunction (Ryan et al., 2015). Indeed, early studies on parkin suggested that it played a protective role in preventing apoptosis (Darios et al., 2003; Imai et al., 2000; Kahns et al., 2002). Despite a lack of an overt parkinsonian phenotype (Perez and Palmiter, 2005), both *PINK1*$^{-/-}$ and *PARKIN*$^{-/-}$ mice have increased susceptibility to oxidative stress and severe mitochondrial deficits, emphasized by reduced levels and activities of CI in the striatum and *substantia nigra* (Gautier et al., 2008; Gispert et al., 2009; Palacino et al., 2004; Stichel et al., 2007). The most prominent phenotype, however, appears in *Drosophila melanogaster*. While both fruit flies, as well as nematodes (*Caenorhabditis elegans*), have *PINK1* and *PARKIN* homologues, these are absent in fungi and plants, suggesting coevolution of both genes (Cardona et al., 2011; Marin and Ferrus, 2002). Both *PARKIN*- and *PINK1*-null flies have very similar phenotypes; in both cases, deletion or mutation of either gene resulted in male sterility, a wing phenotype resulting from degeneration of the indirect flight muscle, and death of a subset of DAergic neurons (Clark et al., 2006; Greene et al., 2003; Park et al., 2006; Yang et al., 2006). At the cellular level, these phenotypes were linked to mitochondrial defects in energy production, reactive oxygen species

(ROS) handling, and morphology (Clark et al., 2006; Greene et al., 2003; Park et al., 2006; Yang et al., 2006). Amazingly, these *PINK1* phenotypes could be rescued by overexpression of parkin, but not *vice versa*, indicating that both proteins function in the same genetic pathway, with *PINK1* acting upstream of *PARKIN* (Clark et al., 2006; Park et al., 2006; Yang et al., 2006). Since the *PARKIN* and *PINK1* fly phenotypes are tractable for genetic screening, suppressors of the wing phenotype were first sought in order to determine the nature of the PINK1/parkin pathway. Interestingly, the first group of genes interacting with the pathway were classical genes involved in mitochondrial dynamics; factors that regulate the shape (and, by extension, function) of the mitochondrial reticulum (Friedman and Nunnari, 2014).

Mitochondria undergo fission and homotypic fusion (Fig. I.7), and these processes are coordinated by large GTPases of the dynamin superfamily – a collection of homologous proteins involved in membrane tubulation and scission (Praefcke and McMahon, 2004). Much of the mitochondrial fusion and fission machinery was discovered in budding yeast (*Saccharomyces cerevisiae*). Dynamin-related protein 1 (Dnm1p or, in mammals, Drp1) was the first protein implicated in mitochondrial fission where, in budding yeast, it was shown to function in the maintenance of the reticulum through proper mitochondrial inheritance into the daughter bud during cell division (Nunnari et al., 1997; Otsuga et al., 1998; Pitts et al., 1999; Smirnova et al., 1998). Dnm1p/Drp1 is recruited to the OMM via receptor proteins – Fis1, MiD49, MiD51 and Mff in mammals – where it oligomerizes into a ring-like structure, constricting the OMM to between 80 and 150 nm (Bleazard et al., 1999; Ingerman et al., 2005; Lackner et al., 2009; Loson et al., 2013; Mozdy et al., 2000; Osellame et al., 2016; Rosenbloom et al., 2014). Once fully constricted, the ultimate step of mitochondrial scission is potentially mediated by dynamin-2 (Lee et al., 2016), a classical dynamin implicated in membrane scission (Praefcke and McMahon, 2004).

Conversely, mitochondrial fusion is achieved via the sequential activities of two large dynamin-like GTPases in mammals, mitofusin (Mfn) 1 and 2 (homologous to a single gene in yeast [Fzo1] and Drosophila [*MARF*]), that mediate OMM fusion, followed by fusion of the IMM by Opa1 (Chen et al., 2003; Friedman and Nunnari, 2014). Mfn molecules from opposing OMMs dimerize in order to bring both membranes into close proximity – forming a ring-like structure perpendicular to the membrane during tethering – and fusion is achieved via an unknown mechanism requiring GTP hydrolysis (Brandt et al., 2016; Ishihara et al., 2004). Mfn molecules

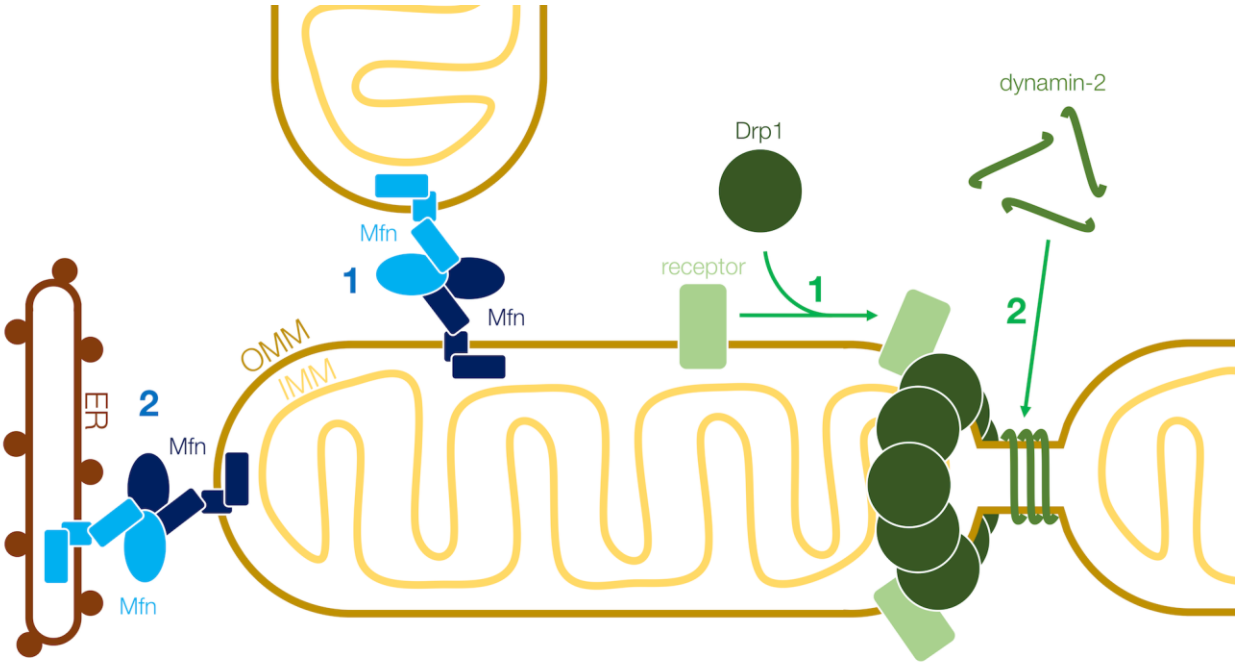


**Figure I.7**. *Mitochondrial dynamics are regulated by large GTPases*. The **green pathway** demonstrates mitochondrial fission. Drp1 receptors on the OMM recruit Drp1 (*1*) to sites of mitochondrial division, where it self-associates to constrict the membrane via a ring-like structure. Following membrane constriction, dynamin-2 is recruited (*2*) to mediate mitochondrial scission. For simplicity, the role of the ER and actin is not shown, and Drp1 is shown to be oligomerized on only one side of the division site. The **blue pathway** demonstrates OMM tethering and fusion. Mfn1/2 molecules from opposing OMMs bind (*1*) to bring the membranes into proximity for fusion by an unknown mechanism. IMM fusion is mediated by Opa1 (not shown). Mfn2 can also function as a tether (*2*) through the association of molecules on the OMM and ER. Note that each Mfn is coloured a different shade of blue to denote separate molecules (and not specifically Mfn1 or 2), and that the single-pass topology is depicted in the figure.

can also assemble into higher-order *cis*-oligomers dependent on redox state, possibly to promote mitochondrial fusion (de Brito and Scorrano, 2008; Karbowski et al., 2006; Shutt et al., 2012).

Both Mfns have very high primary sequence homology and exactly the same domain structure, with a N-terminal GTPase domain, followed by two coiled-coil domains termed heptad repeat (HR) 1 and 2, which flank a hydrophobic region (Praefcke and McMahon, 2004). This hydrophobic region is thought to contain two TM domains, giving Mfns a hairpin structure where the N- and C-termini face the cytoplasm, and is supported by recent crystal structures generated from truncated proteins (Cao et al., 2017b; Qi et al., 2016), although these conflict with a previous crystal structure of a self-associated HR2 dimer (Koshiba et al., 2004). However, bioinformatic and protease protection data suggest that the Mfns are single-pass transmembrane proteins, with the N-terminus (GTPase and HR1) facing the cytosol and the HR2 domain present in the IMS (Mattie et al., in revision). Thus, how exactly OMM fusion is catalyzed remains to be determined. Opa1 mediates fusion of the IMM in a process coupled to OMM fusion (Cipolat et al., 2004; Mishra et al., 2014; Song et al., 2009), in addition to its other proteolytically-regulated roles, such as cristae remodeling (Frezza et al., 2006; Ishihara et al., 2006).

Returning to *PARKIN* and *PINK1* null flies, suppressor screens revealed that inhibition of mitochondrial fusion or promotion of fission – either through Drp1 overexpression, or additional mutation of either *OPA1* or *MARF* – rescued the phenotype (Deng et al., 2008; Poole et al., 2008; Yang et al., 2008), although studies in mammalian cell lines were less conclusive (Exner et al., 2007; Lutz et al., 2009; Mortiboys et al., 2008; Yang et al., 2008; Yu et al., 2011). However, just as with *PINK1* null flies, *PARKIN* mutant fly phenotypes can be rescued by increasing cellular antioxidants, such as reduced glutathione (Greene et al., 2005; Trinh et al., 2008; Whitworth et al., 2005). Thus, increased oxidative stress and respiratory chain dysfunction – known triggers of mitochondrial fragmentation (Toyama et al., 2016) – in PINK1- or parkin-null conditions may stimulate fission, despite the contribution made by these proteins towards mitochondrial division;

here, physiology and pathophysiology converge in this experimental readout. It is important to note that parkin itself is inactivated by oxidation; specifically, via S-nitrosylation by reactive nitrogen species (RNS) (Chung et al., 2004; Yao et al., 2004). Thus, oxidative stress arising from mitochondrial dysfunction may contribute to or even cause AR-JP, and the PINK1/parkin pathway may act to neutralize these disease mechanisms.

Additionally, the implication of *DJ1* in AR-JP (Bonifati et al., 2003) supports a role for oxidative stress in disease pathogenesis. *DJ1* belongs to the ancient DJ-1/ThiJ/PfpI gene superfamily, which traces its origin to bacterial ThiJ phosphorylases involved in thiamine synthesis (Bandyopadhyay and Cookson, 2004). The DJ-1 protein itself appears to be a glyoxalase (Lee et al., 2012) – a function conserved in other superfamily homologues in other species (Bankapalli et al., 2015; Hasim et al., 2014; Kwon et al., 2013) – that catalyzes the removal of glyoxal and methylglyoxal adducts from side chain amines (Allaman et al., 2015). These reactive dicarbonyls arise as by-products of glycolysis (Allaman et al., 2015), and DJ-1 may help to buffer a reliance on glycolysis for ATP production during chronic mitochondrial dysfunction (Shi et al., 2015). Indeed, DJ-1 protects against oxidative stress, and its overexpression can rescue *PINK1*- but not *PARKIN*-null flies, suggesting it acts in parallel to the PINK1/parkin pathway to curb mitochondrial defects arising from *PINK1* loss (Hao et al., 2010; Meiser et al., 2016; Meulener et al., 2006; Thomas et al., 2011). The active site cysteine, C106, is sensitive to oxidation and possibly regulates localization of the protein to mitochondria (Andres-Mateos et al., 2007; Canet-Aviles et al., 2004). In summary, AR-JP genes genetically buffer mitochondrial dysfunction, with both *PINK1* and *PARKIN* acting in a common pathway, whereas *DJ1* operates independently. A loss of either *PARKIN* or *PINK1* is suppressed by increasing mitochondrial fission or curbing oxidative stress. Thus, what is the nature of the PINK1/parkin pathway?

## I.III MITOCHONDRIAL QUALITY CONTROL: MOLECULAR MECHANISMS

### I.III.i *The autophagy pathway: all roads lead to the lysosome*

Work from a number of laboratories over the past decade has revealed that PINK1 and parkin surveil the functionality of mitochondria by targeting damaged organelles for degradation; a type of "quality control" mechanism that maintains the health of the mitochondrial reticulum. Mitochondrial turnover is achieved via the autophagy pathway, a (normally) bulk degradative process that is conserved from yeast. There are many different types of autophagic mechanisms, both selective and non-selective, but all typically involved sequestration of cargo by an expanding membrane, termed a phagophore (yeast) or an isolation membrane (IM, mammals); a double-membrane structure that originates from the well-defined phagophore assembly site (PAS) in yeast, with the endoplasmic reticulum (ER), mitochondria, the ER-Golgi intermediate compartment (ERGIC) and the plasma membrane serving as proposed sources of autophagic membrane in mammals (Ge et al., 2013; Hailey et al., 2010; Hayashi-Nishino et al., 2009; Puri et al., 2013; Yang and Klionsky, 2010). Closure of the IM around the cargo creates a mature autophagosome and appears to require conjugation of ATG8/LC3 to phosphatidylethanolamine (PE) by the ATG conjugation system – requiring the E1-like ATG7 and E2-like ATG3 in a process similar to Ub charging – cementing the role of LC3 as an autophagosomal marker (Kabeya et al., 2000; Tsuboyama et al., 2016; Yang and Klionsky, 2010).

The involvement of lysosomal hydrolases at the end-stage of autophagy has been known for half a century (Deter et al., 1967); once closed, the autophagosome undergoes a maturation process before its fusion with lysosome (Reggiori and Ungermann, 2017). In a differing manner to homotypic mitochondrial fusion, heterotypic fusion between autophagosomes and lysosomes is achieved via a canonical SNARE-mediated mechanism, in which SNARE (soluble N-

ethylmaleimide-sensitive factor attachment protein receptor) proteins on opposing membranes complex via the formation of a four-helix bundle by their helical SNARE domains, which progressively zipper towards the membrane in a reaction driven by protein folding (Gao et al., 2012; Li et al., 2014; Rothman, 2014; Zhang, 2017). Complementary SNAREs on the autophagosome and lysosome allow for the proper targeting of both organelles, in an iteration of the "SNARE hypothesis" (Sollner et al., 1993). This process also requires lipid phosphorylation – specifically phosphatidylinositol (PI) phosphorylation to form phosphatidylinositol-4-phosphate (PI4P) (Dall'Armi et al., 2013; Wang et al., 2015a) – and the activity of the late endosome-associated Rab-family GTPase Rab7 (Ganley et al., 2011; Gutierrez et al., 2004; Jager et al., 2004), and thus shares similarities with the late endocytic pathway (Scott et al., 2014).

Canonical, starvation-induced autophagy is non-selective, evolutionarily-conserved and is coordinated by a cellular response to nutrient stress (Reggiori and Klionsky, 2013). Activity of the mammalian target of rapamycin (mTOR) complex 1 (mTORC1) kinase complex suppresses autophagy through phosphorylation of the upstream autophagy regulator ULK1/2 (Atg1p in yeast) (Laplante and Sabatini, 2012). Signaling complexes that sense nutrient abundance activate Rag GTPases – scaffolded with the lysosomal ATPase by the Ragulator complex at the lysosomal membrane – which act to translocate mTORC1 to the lysosomal surface and activate it (Bar-Peled et al., 2012; Chantranupong et al., 2016; Sancak et al., 2010; Zoncu et al., 2011). Downstream of

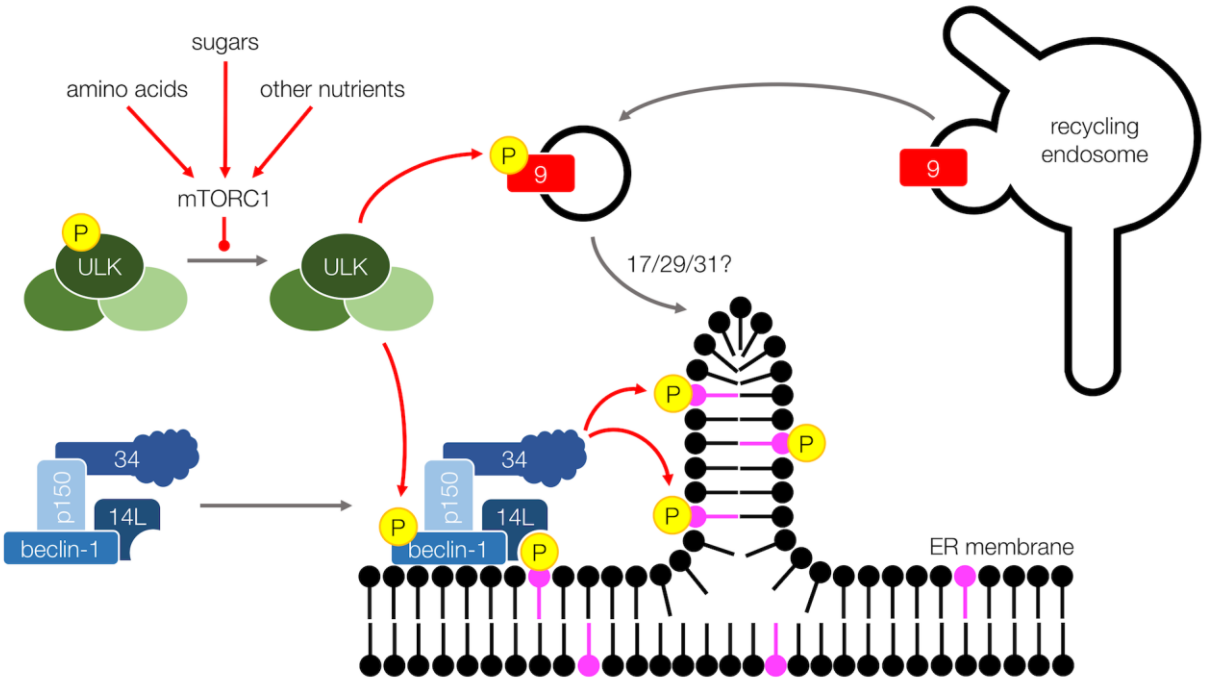


**Figure I.8**. *Autophagic membrane expansion*. Nutrient availability activates mTORC1, which inhibits the ULK complex via direct phosphorylation. Starvation inactivates mTORC1, activating the ULK complex, which in turn phosphorylates beclin-1 to activate the class III PI3K complex, comprising beclin-1, p150, ATG14L (14L) and VPS34 (34). The activated complex catalyzes the formation of PI3P from PI (denoted in pink) during membrane expansion from the ER (shown cross-sectionally), and remains tethered through ATG14L' s ability to bind PI3P. The ULK complex also directs ATG9-containing vesicles, originating from recycling endosomes, to the expanding isolation membrane to promote membrane addition in a manner potentially dependent upon the ATG17/ATG29/ATG31 (17/29/31) complex.

ULK1/2, the autophagosome is nucleated (Fig. I.8) through the activity of a conserved class-III PI3 kinase (PI3K) complex containing VPS34, ATG6/beclin-1, p150/VPS15 and ATG14L/Barkor (Itakura et al., 2008; Sun et al., 2008; Zhong et al., 2009). VPS34 is the catalytic subunit of the complex – harboring lipid kinase activity (Kihara et al., 2001; Schu et al., 1993) – while, based on homology to the yeast complex, the pseudokinase p150 likely serves to bridge VPS34 to a subcomplex composed of beclin-1 and ATG14L (Baskaran et al., 2014). Beclin-1 plays a regulatory role, wherein its phosphorylation by upstream signaling kinases (including ULK1) in turn controls the activity of VPS34 (Kim et al., 2013a; Russell et al., 2013). ATG14L acts to localize the complex to the ER via binding of its BATS domain to highly-curved membranes labeled with PI3P and PI(4,5)$P_2$ (another lipid involved in autophagosome formation) (Fan et al.,

2011; Matsunaga et al., 2010; Tan et al., 2016). Localization of the activated PI3 kinase complex to PI3P-labeled membranes to catalyze further PI3P production likely nucleates the formation of the nascent autophagosome.

Membrane is recruited for IM expansion from various sources (see above), but membrane delivery by ATG9-labeled vesicles plays an important role. During autophagosome formation, ATG9 (a multipass transmembrane protein) delivers membrane from the cell surface through recycling endosomes to sites of autophagosome biogenesis, where it is phosphorylated by ULK complexes in both yeast and mammals (Imai et al., 2016; Karanasios et al., 2016; Mari et al., 2010; Papinski et al., 2014; Popovic and Dikic, 2014; Puri et al., 2013; Yamamoto et al., 2012). These vesicles also likely incorporate PI into the elongating IM from the endosomal pool – in a manner that may depend on a complex of ATG17, ATG29 and ATG31 (at least in yeast) – thus increasing the amount of available substrate for VPS34 and driving nucleation (Ragusa et al., 2012; Schink et al., 2013). This process may additionally depend on ULK-mediated phosphorylation of ATG9, which regulates pathway processivity, allowing for the recruitment of lipidated ATG8 and conjugated ATG5-ATG12 to the expanding IM (Karanasios et al., 2016; Papinski et al., 2014). Colocalization and interaction between multiple corps of autophagic machineries at the ER highlights its role as a platform for IM expansion; indeed, the ER truly acts as a “cradle” during this process, as electron micrographs show ER present on both sides of the IM, with an in-depth tomographic study demonstrating that the biogenesis of autophagosomes occurs within a large cistern formed by a subdomain of the ER (Furuno et al., 1990; Hayashi-Nishino et al., 2009). This subdomain (termed the “omegasome”) is, expectedly, rich in PI3P and PI3P-binding proteins, such as double FYVE domain-containing protein 1 (DFCP1) (Polson et al., 2010; Uemura et al., 2014).

In summary, starvation-induced autophagosome formation is a localized process, driven by a positive feedback loop of lipid phosphorylation and membrane addition.

### I.III.ii *Proteasomes and isolation membranes converge at the mitochondrion during PINK1/parkin mitophagy*

While starvation-induced autophagy is a non-selective degradation pathway – stochastically engulfing cytoplasmic components and some organelles – parkin- and PINK1-mediated autophagy of mitochondria (termed "mitophagy") targets damaged organelles for turnover. Indeed, through this selective targeting of defective mitochondria, parkin (and perhaps PINK1 as well, although this has yet to be tested) can cleanse a mitochondrial population suffering

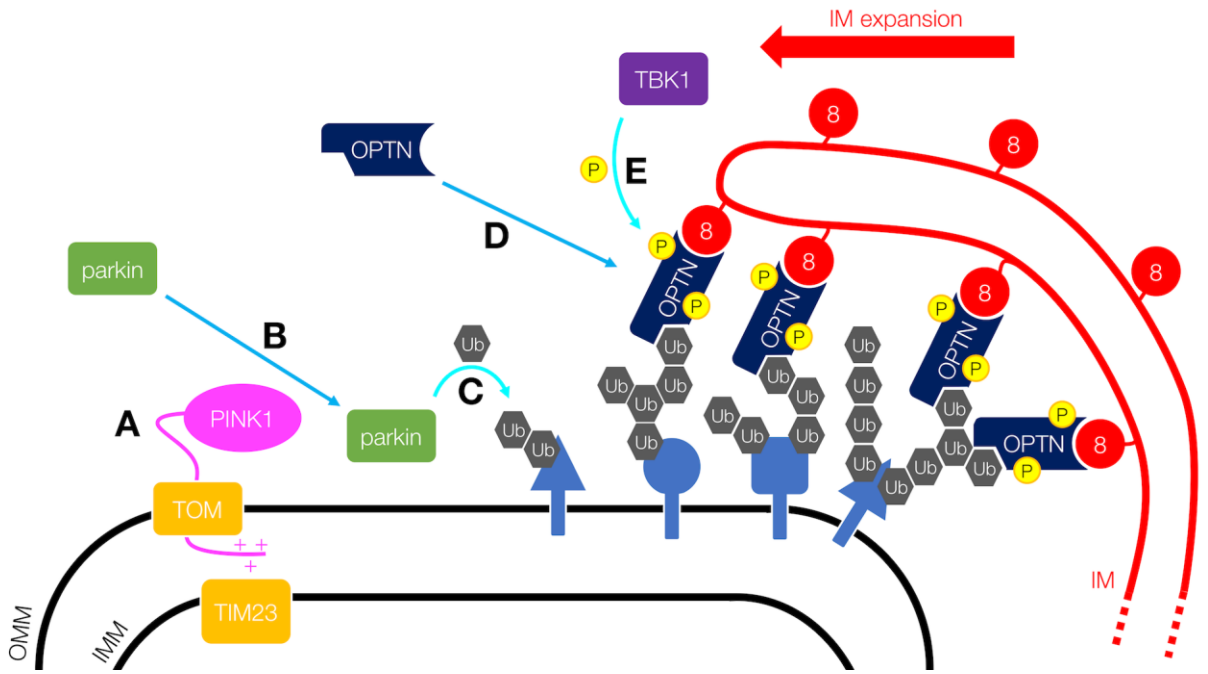


**Figure I.9**. *PINK1 and parkin initiate mitophagy*. **A** PINK1 is stabilized in a complex with the TOM channel on depolarized mitochondria as its $\Delta\Psi_m$-dependent import (see Fig. I.4) is prohibited. **B** PINK1 directs parkin to depolarized mitochondria, where parkin becomes activated (described in Fig. I.10). **C** Parkin ligates Ub to substrate proteins (blue shapes) on the OMM. **D** Ub chains on mitochondria recruit autophagy adaptor proteins, such as OPTN. **E** OPTN is phosphorylated by TBK1 on multiple residues to promote binding to Ub chains on mitochondria and lipidated ATG8-family proteins (8) on the expanding IM. Blue arrows indicate translocation events, while cyan arrows depict catalytic steps. The large red arrow indicates the direction of IM expansion.

from highly deleterious mitochondrial mutations, both in cells and *in vivo* (Pickrell et al., 2015; Suen et al., 2010). The participation of PINK1 and parkin in this type of pathway could explain the resulting mitochondrial phenotype described in *Drosophila* lacking either gene, and the mitochondrial dysfunction observed in patients (see section I.II.iii). A note on methods, however; while it is standard protocol in the field to induce mitochondrial damage experimentally through the use of pharmacological uncouplers (such as valinomycin or CCCP) – which completely depolarize mitochondria – the working assumption (and the one used in this section) is that these agents trigger a pathway that is perhaps characterized by a low number of events at the steady-state. While parkin and PINK1 regulate damage-induced mitophagy, additional mitophagy pathways – triggered by other stimuli, such as hypoxia in FUNDC1-mediated mitophagy or excessive mitochondrial fragmentation in BCL-rambo-/BCL2L13-induced mitophagy – are also used by the cell, and these complementary mechanisms may be able to buffer a loss of parkin-/PINK1-dependent mitophagy in certain systems (Liu et al., 2012; Murakawa et al., 2015; Yun et al., 2014).

To initiate damage-induced mitophagy (Fig. I.9), damaged mitochondria are sensed by PINK1 by an import-related mechanism (see Fig. I.4). Loss of $\Delta\Psi_m$ across the IMM of depolarized mitochondria (or very low $\Delta\Psi_m$ in highly damaged organelles) abolishes the electrophoretic force drawing polypeptides destined for the matrix through the membrane (Harbauer et al., 2014). Failure to import PINK1 because of compromised $\Delta\Psi_m$ results in its accumulation on the surface of damaged mitochondria (Jin et al., 2010; Narendra et al., 2010b; Vives-Bauza et al., 2010), where it stabilizes as a dimer in a ~700 kDa complex with TOM70 and other TOM subunits, in a manner that may require the TOM7 subunit of the TOM complex (Hasson et al., 2013; Lazarou et al., 2012; Okatsu et al., 2013). The dimer undergoes autophosphorylation – likely in *trans* – on S228

and S402 within the kinase domain (see Fig. I.3A) to become fully active (Okatsu et al., 2012). Stabilization of PINK1 on the OMM of depolarized mitochondria can be mimicked by depleting cells of the catalytic subunit of MPP (Greene et al., 2012). This, however, may hint at parallel mechanisms for PINK1 accumulation; indeed, PINK1 stabilization can occur on polarized mitochondria expressing misfolded proteins (Jin and Youle, 2013). Accordingly, PINK1 contains – ancillary to its N-terminal MTS – a cryptic, alternative mitochondrial localization signal (aMLS) (Becker et al., 2012; Okatsu et al., 2015a). While the MTS-dependent localization of PINK1 to mitochondria occurs regardless of polarization status, the aMLS is sufficient to selectively target PINK1 to depolarized mitochondria in a manner dependent on the TOM channel (Okatsu et al., 2015a). The MTS and aMLS may synergize to uniquely stabilize PINK1 (*versus* other mitochondrial proteins) on the OMM of depolarized mitochondria.

Parkin is basally present in an inactive conformation in the cytosol, but is recruited to and activated at depolarized mitochondria in a manner that requires PINK1 (Geisler et al., 2010; Narendra et al., 2008; Narendra et al., 2010b; Trempe et al., 2013; Vives-Bauza et al., 2010) (the precise mechanism of this activation is detailed in the next section). Once recruited to depolarized mitochondria by PINK1, parkin catalyzes the ubiquitination of a subset of OMM proteins – the Mfns and voltage-dependent anion channels (VDACs), among others – that ultimately serves to degrade the organelle (Rakovic et al., 2011; Sarraf et al., 2013; Tanaka et al., 2010; Ziviani et al., 2010). Initially, parkin-mediated ubiquitination may serve a role in sequestering damaged organelles from the reticulum. Ubiquitinated Mfns are extracted from the OMM by the AAA-ATPase p97/VCP and degraded by the proteasome, preventing re-insertion of the organelle into the mitochondrial population (Kim et al., 2013b; Kimura et al., 2013; Tanaka et al., 2010). Similarly, proteasomal degradation of ubiquitinated MIRO proteins – adaptors that recruit motors

to mitochondria – would serve to halt motility so that turnover of the organelle can occur (Wang et al., 2011). Ubiquitination also plays a more general role on the OMM, targeting resident proteins for proteasomal turnover to eventually rupture the membrane (Yoshii et al., 2011). Indeed, proteasomes translocate to mitochondria during mitophagy, and blocking proteasomal degradation impairs the pathway (Chan et al., 2011; Yoshii et al., 2011).

Once isolated, the organelle is engulfed by the IM and turned over lysosomally (Narendra et al., 2008). Unlike starvation-induced autophagy, mitophagy is highly discriminatory, and this selectivity is conferred by the recognition of ubiquitinated mitochondrial proteins by autophagic adaptor proteins, which contain Ub binding domains and LC3 interacting regions (LIRs) to bind Ub and LC3/ATG8 on the autophagosome, respectively (Khaminets et al., 2016). LIRs bind LC3- and the closely-related GABARAP-family proteins on the autophagosome through hydrophobic interactions, as well as acidic or phosphorylated residues upstream of the LIR (Rogov et al., 2014). Mitophagy is dependent upon the redundant activities of adaptor proteins optineurin (OPTN) and NDP52 (and possibly TAX1BP1), in the sense that clearance of mitochondria is impaired in cells lacking both factors (Heo et al., 2015; Lazarou et al., 2015; Moore and Holzbaur, 2016; Wong and Holzbaur, 2014). Other adaptors, such as p62, are recruited to ubiquitinated mitochondria during mitophagy as well, although these may not be considered core machinery (Geisler et al., 2010; Narendra et al., 2010a). Ub binding by NDP52 and OPTN is regulated via phosphorylation by the Ser/Thr kinase TBK1, which phosphorylates both proteins on multiple residues over many domains and is activated downstream of parkin ubiquitination (Heo et al., 2015; Richter et al., 2016). In the case of OPTN, phosphorylation N-terminal to the LIR promotes its interaction with LC3/GABARAP (Wild et al., 2011), while phosphorylation within its UBAN (Ub binding in ABIN and NEMO) domain promotes its binding to Ub chains (Heo et al., 2015; Richter et al.,

2016). Thus, autophagy adaptors link ubiquitinated mitochondrial proteins to ATG8 homologues on the expanding IM.

Autophagosome formation proceeds with the recruitment of ULK1, as well as ATG9-positive vesicles, to depolarized mitochondria in a parkin-dependent manner (Itakura et al., 2012a), as elaborated on in the previous section. While autophagy adaptors, through their association with ATG8-family proteins, may aid to guide the IM around the target mitochondrion and promote omegasome biogenesis (Lazarou et al., 2015), factors on the OMM may also serve a similar purpose. Notably, Fis1 – an OMM Drp1 receptor and parkin ubiquitination target – serves as a receptor for TBC1D15, a protein that serves the dual purpose of binding ATG8-family proteins on the IM to restrict autophagosome formation (TBC1D15-null cells have unrestrained LC3 tubulation) and inhibit Rab7 activation through TBC1D15's GAP activity, presumably to prevent the premature recruitment of factors associated with complete autophagosomes during IM expansion (Yamano et al., 2014). Indeed, association of mitochondria with LC3 is suppressed in nematodes harbouring Fis1 mutations (Shen et al., 2014). TBC1D15 binds GABARAP family members (GABARAP, GABARAPL1 and GABARAPL2) much more strongly than their LC3 family counterparts (LC3A, LC3B and LC3C) *in vitro* (Yamano et al., 2014). The role of both families in mitophagy is complex; while mitochondrial clearance was shown to be dependent upon GABARAPs rather than LC3 family proteins (in accordance with binding data), closure of autophagocytosed mitochondria (termed mitophagosomes) required both families (Nguyen et al., 2016). Clearance of autophagosomes in the absence of their closure is not a biological paradox, as unclosed mitophagosomes in LC3-null cells – or starvation-induced autophagosomes in cells lacking the conjugation system to produced lipidated LC3 – are still turned over, albeit with reduced kinetics (Nguyen et al., 2016; Tsuboyama et al., 2016). To summarize, while much of the

core autophagic machinery is shared between mitophagy and starvation-induced autophagy, the former includes added levels of complexity involving protein ubiquitination and pathway-specific factors such as Fis1 and TBC1D15.

### I.III.iii *Mitophagy reveals the mechanism of parkin activation by PINK1*

PINK1 and parkin act as the sensor and effector, respectively, during damage-induced mitophagy, despite their initially disparate subcellular locations. Accordingly, how PINK1 on the OMM of damaged mitochondria signals to parkin in the cytosol and how parkin remains localizaed to these organelles have become intense areas of study, notably because an interaction between parkin and PINK1 proved to be undetectable, and parkin is absent from the ~700 kDa PINK1-containing complex on depolarized mitochondria (Lazarou et al., 2012). Studies into this mechanism stemmed from an initial observation that catalytically-dead parkin harbouring either a C431S or C431A mutation at the active site failed to translocate to depolarized mitochondria (Lazarou et al., 2013; Zheng and Hunter, 2013). Strikingly, loss of parkin$^{C431S}$ translocation could be rescued by co-expression of the wild-type (WT) protein (Lazarou et al., 2013; Zheng and Hunter, 2013). Although this was initially thought to be due to parkin oligomerization at the membrane (Lazarou et al., 2013), an elegant rescue study utilizing chimeric constructs showed that co-expression of chimeras composed of the PINK1 N-terminus (lacking the kinase domain) and either the RBR portion of parkin or tetra-Ub (four linears Ub moieties in succession) was sufficient to rescue parkin$^{C431S}$ translocation (Zheng and Hunter, 2013).

While the above study suggested Ub chains conjugated to OMM proteins could act as a parkin tether, this explanation was only partial. The crystal structure of parkin (Fig. I.10A) was solved by several groups in 2013 and showed the protein to be autoinhibited (Riley et al., 2013;

Spratt et al., 2013; Trempe et al., 2013; Wauer and Komander, 2013). Firstly, the active site residue C431 – which forms the thioester bond with the ubiquitin C-terminus, coordinated by the other members of the catalytic triad, H433 and E444 – is occluded by a hydrophobic interaction with the RING0 domain. Moreover, the REP helix makes the E2 binding site in the RING1 domain inaccessible. Mutations that disrupt either of these interactions increase parkin ligase activity *in vitro* and increase the kinetics of its translocation to mitochondria as (this bears repeating) its recruitment is coupled to catalysis (Trempe et al., 2013; Zheng and Hunter, 2013). Interestingly, mapping of a selection of AR-JP-associated mutations on the surface of parkin revealed that these mutations cluster around functionally important areas of the protein, including the potential E2 binding face of RING1 and the catalytic RING2 domain (Riley et al., 2013). This approach, in addition to the concept that mutation of internal residues involved in or located near sites of $Zn^{2+}$ binding (see Fig. I.6B for examples) unfold the protein, supports a role for parkin inactivation as a primary cause of AR-JP.

If parkin is present in an autoinhibited state (presumably at the steady-state), how is it activated? This mechanism explains the PINK1-dependence of parkin function. PINK1 directly phosphorylates both Ub and the parkin Ubl domain on the homologous residue S65 to activate parkin ligase activity (Kane et al., 2014; Kazlauskaite et al., 2014a; Kazlauskaite et al., 2014b; Kondapalli et al., 2012; Koyano et al., 2014; Shiba-Fukushima et al., 2012). Phosphoubiquitin (pUb) is poorly ligated by parkin in *in vitro* ubiquitination assays, demonstrating that parkin is not an E3 pUb ligase (Wauer et al., 2015b). Rather, pUb activates parkin ligase activity allosterically by directly binding parkin on the backside of the RING1 domain (Fig. I.10B), coordinated by K151, H302 and R305 in the phosphate binding pocket (Sauve et al., 2015; Wauer et al., 2015a; Yamano et al., 2015). The hydrophobic patch of pUb also directly interacts with an extended

helical portion of RING1, and disruption of this interaction (via A320R substitution in parkin) abolishes binding (Wauer et al., 2015a). This helix changes conformation from a "kinked" to a "straight" shape, and accordingly displaces the IBR domain upwards (compare the position of the domain in Fig. I.10A to Fig. I.10B) where it can contact the C-terminus of pUb (Wauer et al., 2015a). Notably, structural determination of the pUb-parkin complex utilized a truncated form of parkin containing only the RING0-RING1-IBR-RING2 (R0RBR) domains; in fact, the Ubl is normally displaced in this complex as Ubl and pUb binding to the R0RBR module are mutually exclusive (Sauve et al., 2015).

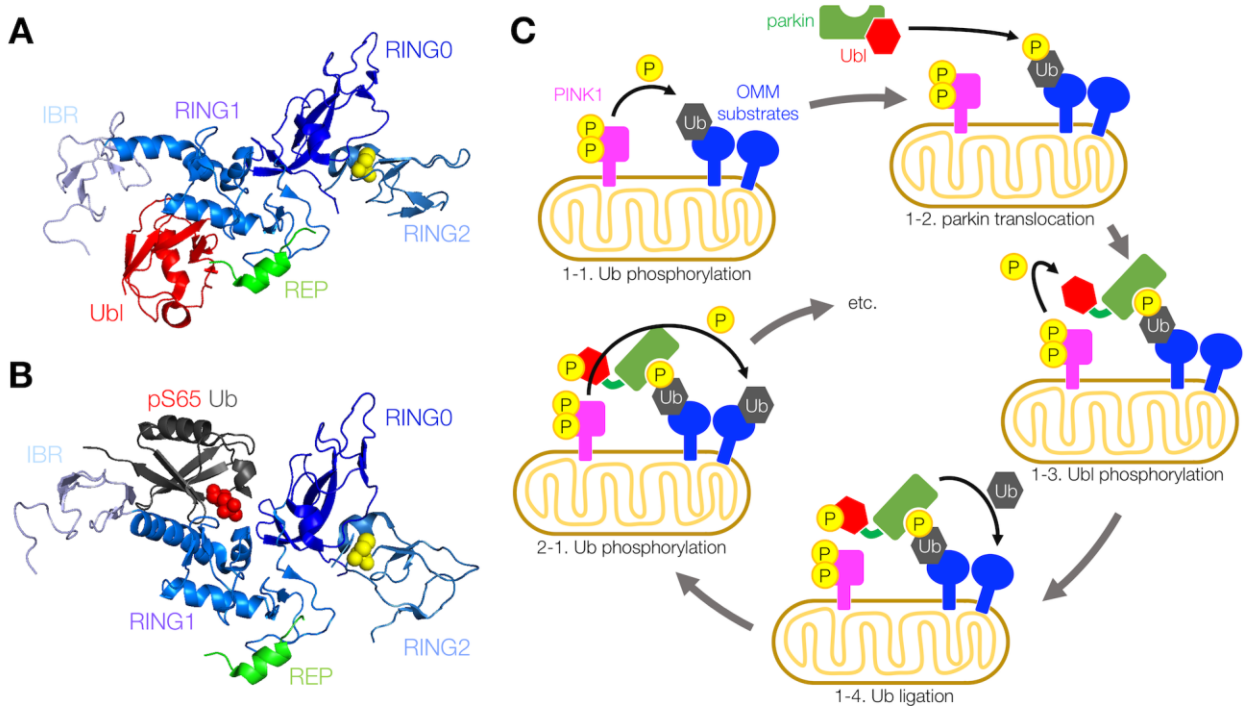


**Figure I.10**. *Parkin binds phosphorylated ubiquitin to induce mitophagy via a feed-forward mechanism*. **A** Structure (cartoon) of human parkin (PDB ID 4K95) in an autoinhibited conformation. The active site residue (C431) is labeled as yellow spheres. **B** Structure (cartoon) of flea parkin (lacking the Ubl domain) in a complex with pS65 Ub (PDB ID 5CAW). The active site cysteine (C428) of parkin and pS65 of pUb are labeled as yellow and red spheres, respectively. **C** Feed-forward mechanism of parkin activation and translocation. PINK1, stabilized on the OMM and activated by autophosphorylation, phosphorylates a Ub moiety already conjugated to a protein on the OMM (step 1-1), which binds parkin from the cytosol (step 1-2). PINK1 then phosphorylates the newly-dislodged parkin Ubl domain (step 1-3) to fully activate parkin ligase activity (step 1-4). Newly-ligated Ub is then phosphorylated by PINK1 (step 2-1) to drive further parkin translocation and OMM substrate ubiquitination. Conformational changes in parkin (see text) likely occur between steps 1-2 and 1-3 (Ubl disassociation from R0RBR) and steps 1-3 and 1-4 (opening of the RING0-RING2 interface for catalysis). This latter change is not illustrated.

With regards to the role of PINK1 in the process of parkin activation, S65-phosphorylation of the Ubl by PINK1 to form phosphoUbl (pUbl) disrupts the interaction of this domain with RING1 (Kazlauskaite et al., 2015; Sauve et al., 2015). Parkin phosphorylation also enhances the binding of both pUb and E2 enzyme by RING1 (Ordureau et al., 2014; Sauve et al., 2015). This latter observation implies that pUbl release facilitates de-repression of RING1 by the REP (this is mimicked by the W403A designer mutation in the REP helix) (Trempe et al., 2013). Finally, while two studies reported that the addition of pUb to maximally-phosphorylated parkin did not increase autoubiquitination *in vitro* – suggesting that pUb binding primes the Ubl for phosphorylation by PINK1 (Kazlauskaite et al., 2015; Sauve et al., 2015) – another study indeed reported a pUb-dependent enhancement (Ordureau et al., 2015). While this latter group also observed phosphorylation of parkin by PINK1 in cells despite the replacement of all Ub with non-phosphorylatable $Ub^{S65A}$ (Ordureau et al., 2015), this has also been challenged by the observation that parkin phosphorylation *in organello* by isolated mitochondria from depolarized cells is abolished by preventing its association with pUb (Tang et al., 2017). Despite the manner by which both phosphorylation steps are orchestrated, the above data provide a structural basis for the observation that both PINK1-phosphorylated parkin and ubiquitin are required for full activation of parkin *in vitro* and in cells (Kane et al., 2014; Kazlauskaite et al., 2014b; Koyano et al., 2014).

PINK1-mediated phosphorylation of Ub and parkin, pUb-parkin complex formation, and Ub ligation by parkin coordinate a feed-forward mechanism of parkin recruitment (Fig. I.10C). Targeting phosphomimetic Ub chains to mitochondria can trigger PINK1-independent recruitment of phosphomimetic parkin (but not the WT) (Okatsu et al., 2015b), indicating that parkin, PINK1 and Ub represent the core machinery required for parkin translocation. Indeed, as parkin and Ub are both initially cytosolic, an early result in which the PINK1 kinase domain ectopically targeted

to other cellular membranes induced parkin translocation to these compartments no longer seems surprising (Lazarou et al., 2012). While the precise mechanistic details of translocation are not fully clear at this time, data from Tang et al. suggest that Ub already present on mitochondria is first phosphorylated by PINK1, which directs parkin to mitochondria (FL parkin still binds pUb with an affinity [$K_D$] of ~400 nM) (Sauve et al., 2015; Tang et al., 2017). This event could dislodge the Ubl, making it amenable to phosphorylation by PINK1, which secures the parkin-pUb complex on mitochondria by increasing the interaction affinity twenty-fold (Sauve et al., 2015). Once phosphorylated and bound to pUb, parkin is "fully active" and likely exists in another conformation, as the RING0-RING2 interface must be loosened to allow C431 access to the charged E2 bound to RING1. Parkin is then free to ligate Ub to other mitochondrial substrates, to drive further Ub phosphorylation by PINK1, and parkin translocation and activation (Ordureau et al., 2014). This mechanism explains the aforementioned observations by Zheng and Hunter that describe the rescue of mitochondrial translocation of parkin$^{C431S}$ by chimeras of the PINK1 N-terminus combined with either the parkin RBR module or tetraUb (Zheng and Hunter, 2013). Here, exogenously increasing the levels of parkin receptors (i.e. S65-phosphorylated Ub) on mitochondria (which are normally increased via parkin-dependent Ub ligation) is the rescue mechanism, as endogenous PINK1 must phosphorylate overexpressed, mitochondrially-localized tetraUb. Alternatively, parkin RBR – defined by Zheng and Hunter as the C-terminal portion of parkin comprising the RING1, IBR, REP and RING2 domains – represents a likely semi-active form of parkin, as it lacks the portion of RING0 that typically acts to conceal the catalytic cysteine (Trempe et al., 2013). Targeting an active form of parkin on the OMM would increase the levels of mitochondrial Ub, and PINK1-mediated phosphorylation of Ub during mitochondrial

depolarization would drastically increase the number of parkin binding sites on the OMM, allowing for the recruitment of ligase-dead parkin.

On the surface of depolarized mitochondria, parkin catalyzes the formation of both canonical (K48- and K63-linked) and non-canonical (K6- and K11-linked) Ub chains (Cunningham et al., 2015; Ordureau et al., 2014), possibly via a combination of direct ubiquitination in addition to the activity of enzymes that elongate existing Ub chains with their own distinct linkages (i.e. E4 enzymes). Parkin also autoubiquitinates itself once activated, selectively forming predominantly K6-linked Ub chains (Durcan et al., 2014) – an observation that suggests that parkin is responsible for K6-linked Ub chain formation on the OMM during mitophagy. Parkin-mediated ubiquitination on mitochondria is antagonized by DUBs, namely USP15 and USP30, which act to deubiquitinate proteins on the OMM (Bingol et al., 2014; Cornelissen et al., 2014; Wang et al., 2015b). USP30 – an OMM-localized DUB – has a strong selectivity for K6- and K11-linked chains and potentially "sculps" Ub linkages to favour more canonical linkages (Cunningham et al., 2015). Mechanistically, K48- and K63-linked Ub chains may facilitate recognition by the p97 ATPase to mediate extraction of ubiquitinated OMM proteins (Tanaka et al., 2010). While the selectivity of p97 towards various linkages remains unknown, the complex is capable of binding both K48- and K63-linked chains (Hao et al., 2015; Meerang et al., 2011), and thus a model in which USP30 drives Ub linkage dynamics towards canonical chain formation to promote OMM protein extraction via p97 seems reasonable. However, depletion of USP30 promotes mitophagy, cementing its role as a pathway antagonist (Bingol et al., 2014); thus, the mechanistic purpose of the involvement of USP30 in mitophagy remains unclear. Another DUB, USP8, may also function to remove K6-linked Ub from parkin to drive its recruitment to depolarized mitochondria (Durcan et al., 2014). Thus, the coordination of Ub linkages during

mitophagy appears to have some importance with respect to the pathway. Interestingly, pUb appears to be resistant to DUBs in general, and USP8, USP15 and USP30 in particular (Wauer et al., 2015b). This supports a role for pUb in parkin activation; indeed, Ub phosphorylation plateaus at 20% of total Ub during mitophagy (Ordureau et al., 2014). Moreover, typical autophagy receptors bind weakly to pUb chains (Heo et al., 2015), although this data remains preliminary (Lazarou et al., 2015). Thus, mitophagy is driven by a feed-forward mechanism involving Ub ligation and phosphorylation, and is antagonized by deubiquitination. Importantly, the relative levels and activation states of the enzymatic factors involved in coordinating Ub chain formation are important to drive mitochondrial turnover.

### I.III.iv *Mitochondrial vesicular traffic: an emerging quality control mechanism?*

Table I.2. Drp1-independent drivers of OMM curvature and fission

| Factor | Curvature Type | Pathway | Mechanism | Reference(s) |
|---|---|---|---|---|
| BAX/BID | positive | apoptosis | form ring-like structures at OMM pores | (Terrones et al., 2004) |
| EndoB1 | positive | apoptosis | N-BAR domain, potentially downstream of BAX | (Rostovtseva et al., 2009) |
| HRS | negative | viral infection | presumably analogous to MVB formation | (Kopek et al., 2007; Richardson et al., 2014) |
| LLO | positive (fission) | bacterial infection | unknown; but associated with ER | (Stavru et al., 2013) |
| α-synuclein | positive (fission) | ? | directly binds and curves OMM | (Nakamura et al., 2011) |
| vMIA | positive (fission) | viral infection | unknown; potentially related to BAX | (McCormick et al., 2003) |

Abbreviations: BAX, B-cell CLL/lymphoma 2-associated X protein; BID, BH3 interacting-domain death agonist; EndoB1, endophilin B1; ER, endoplasmic reticulum; HRS, hepatocyte growth factor-regulated tyrosine kinase substrate; LLO,

listeriolysin O; MVB, multivesicular body; N-BAR, N-terminal Bin/Amphiphysin/Rvs-homology; OMM, outer mitochondrial membrane; vMIA, viral mitochondrion-localized inhibitor of apoptosis.

While the importance of mitophagy as a quality control pathway is apparent, other membrane trafficking-type pathways may be necessary for the maintenance of the mitochondrial reticulum. Notably, mitochondrial-derived vesicles (MDVs) represent an emerging, potential mitochondrial quality control mechanism. MDVs were first implicated in a trafficking pathway between mitochondria and peroxisomes, and were identified based on a) the incorporation of selected mitochondrial cargo, b) an independence from canonical, Drp1-mediated mitochondrial fission and c) ultrastructural imaging showing 70 to 100 nm-wide budding profiles on the OMM (Neuspiel et al., 2008). Mitochondria-anchored protein ligase (MAPL, also termed MUL1) was identified bioinformatically as a mitochondrially-localized E3 ligase, and was found to traffic to peroxisomes as cargo, given that delivery of a MAPL construct lacking the catalytic RING domain to peroxisomes was unobstructed (Neuspiel et al., 2008). Intriguingly, MAPL, a SUMO E3 ligase, promotes mitochondrial fission by stabilizing Drp1, yet its ability to traffic to peroxisomes is Drp1-independent (Neuspiel et al., 2008; Prudent et al., 2015). Delivery requires VPS35, a PD gene (see Table I.1) and subunit of the retromer complex, which is composed of a two subcomplexes; a

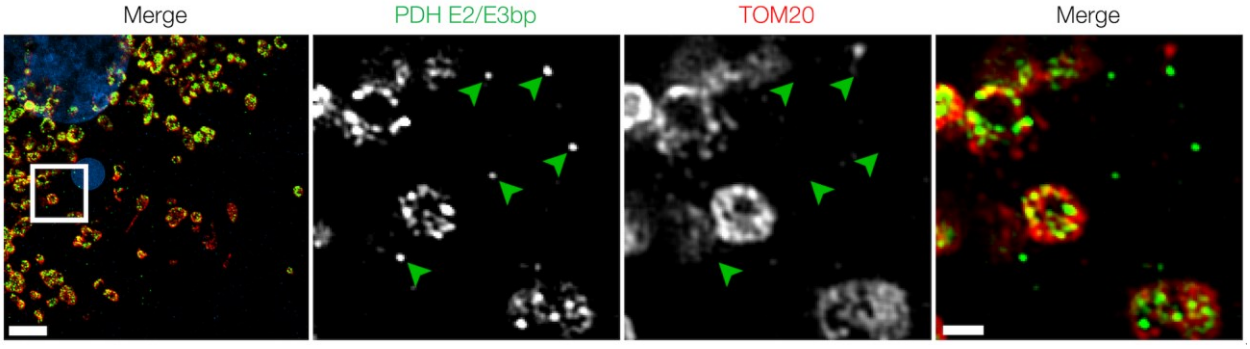


**Figure I.11**. *Cargo-selected transport of PDH E2/E3bp*. COS7 cells were stimulated with antimycin A to generate the formation of MDVs containing PDH E2/E3bp (green) but not TOM20 (red) prior to fixation, and imaged by super-resolution microscopy (see Chapter III for experimental details). The green arrows indicate cargo-selected structures *en route* to the lysosome that measure 150 to 180 nm in diameter (the resolution limit of this imaging technique). Scale bars, 5 (left) and 1 (right) microns.

membrane curvature-sensing sorting nexin (SNX) heterodimer and VPS26-VPS29-VPS35 subcomplex involved in sorting cargo (Cullen and Korswagen, 2012). VPS35 is recruited transiently to mitochondrial subdomains enriched in MAPL, where it may mediate sorting of cargo into MDVs; indeed, VPS35 depletion blocks delivery of MAPL to peroxisomes (Braschi et al., 2010).

How could Drp1-independent membrane scission be achieved? Table I.2 lists several factors involved in OMM shape and mitochondrial fission that function independently of Drp1. In the case of MAPL-positive vesicles – which contain a subset of OMM proteins, excluding TOM20 – the role of the retromer hints at a process involving at least some factors implicated in canonical membrane trafficking. While the VPS35-containing subcomplex functions in cargo binding and sorting, each subunit of the SNX heterodimer (canonically this is SNX1 and SNX2) contains a BAR domain for sensing membrane curvature, and a PX domain capable of detecting PI3P, potentially implicating lipid phosphorylation in MDV formation (Cullen and Korswagen, 2012).

More recently, two MDV pathways to the lysosome have been described (Soubannier et al., 2012a). Both pathways were identified as containing the reciprocally-exclusive cargo TOM20 (single membrane MDVs) and the E2/E3bp subunits of the pyruvate dehydrogenase complex (double membrane MDVs) (Soubannier et al., 2012a). Both pathways are triggered by oxidative stress and traffic to the lysosomal compartment in order to be turned over, likely transiting through the late endosome/multivesicular body (MVB) (Soubannier et al., 2012a). While the TOM20-containing MDVs may recycle portions of the OMM, the PDH-positive MDVs (Fig. I.11) deliver oxidized IMM and matrix cargo, including respiratory chain subunits, for degradation (Soubannier et al., 2012a; Soubannier et al., 2012b). Thus, one or both these pathways has the potential to function in mitochondrial quality control, delivering selected, damaged mitochondrial components

to the lysosome in order to preserve the function of the organelle. Clearly, more work is required to understand the machinery that regulates MDV formation and turnover, and whether these pathways may be related to human disease.

## I.IV MITOCHONDRIAL QUALITY CONTROL: INTEGRATION WITHIN THE CELL

### I.IV.i *Metabolism as a regulator of mitochondrial quality control*

It is crucial to recognize that mechanisms monitoring mitochondrial health exist within the cellular milieu, and are subject to regulation by external factors that do not directly impinge on quality control pathways themselves. For example, the lysosome – the end-of-the-line destination of mitophagosomes – is an important integrator of cellular metabolism (Lim and Zoncu, 2016). Lysosomal biogenesis is controlled through the coordinated lysosomal expression and regulation (CLEAR) gene network, and transcription factor EB (TFEB) acts as a "master regulator" at the top of this cascade by directly controlling the expression of almost five hundred genes (Palmieri et al., 2011; Sardiello and Ballabio, 2009). Upregulation of lysosome-related genes by TFEB occurs during the induction of starvation-induced autophagy, and involves the translocation of the protein from the cytosol to the nucleus in a manner dependent upon lysosomal calcium ($Ca^{2+}$) release to activate transcription (Medina et al., 2015; Settembre et al., 2011). A similar translocation event occurs with TFEB and associated family members in PINK1-/parkin-dependent mitophagy, and these factors are indeed required for efficient mitochondrial turnover to proceed (Ivankovic et al., 2016; Nezich et al., 2015). One notable difference between TFEB translocation during mitophagy and starvation-induced autophagy is that, in the case of the latter, TFEB is directly phosphorylated by mTORC1 at the lysosomal membrane during periods of nutrient availability to maintain TFEB in the cytosol, and thus lysosomal biogenesis is controlled

at the highest point in the cascade (Pena-Llopis et al., 2011; Settembre et al., 2012). However, in PINK1-/parkin-dependent mitophagy, while constitutively active Rag GTPases (simulating a "fed" state from the point of view of the mTORC1 complex) blocked translocation, loss of the early ATG genes ATG5 and ATG9 also prevented nuclear TFEB signaling. Thus, in the context of mitophagy, mTORC1-dependent derepression of TFEB nuclear translocation is therefore triggered downstream of mitophagosome formation (Nezich et al., 2015); conversely, in the context of starvation-induced autophagy, TFEB translocation occurs once mTORC1 is activated (Settembre et al., 2012). These observations imply that mitophagy feeds back onto the more general autophagy-lysosome pathway, and sustained mitophagy may in fact impair other turnover systems, perhaps through the sequestration of common factors. Lysosomal dyshomeostasis may also conversely impact mitophagy, either directly or by affecting mitochondrial health (Hughes and Gottschling, 2012; Soleimanpour et al., 2014). Accordingly, upregulation of the autophagy-lysosome system through TFEB-dependent driving of CLEAR gene expression is neuroprotective in *PINK1*-null organisms (Zhang et al., 2017b).

In addition to the transcriptional stimulation of CLEAR target genes, mitochondrial biogenesis (i.e. synthesis of mitochondrial proteins, ETC complex assembly, mtDNA replication, etc.) is also upregulated during mitophagy. Peroxisome proliferator-activated receptor gamma-coactivator 1α (PGC-1α) activity is stimulated during mitophagy in a TFEB-dependent manner, and has been proposed to be a TFEB target gene (Ivankovic et al., 2016). PGC-1α is another "master regulator" -type coactivator, and upregulates the transcription of genes associated with mitochondrial biogenesis, fatty acid oxidation, mtDNA replication and OXPHOS (Finck and Kelly, 2006). Parkin and PINK1 have been directly implicated in PGC-1α function, as parkin has been reported to ubiquitinate and degrade (via the proteasome) a transcriptional repressor of PGC-

1α, termed parkin interaction substrate (PARIS), in a PINK1-dependent manner (Lee et al., 2017; Shin et al., 2011). In parkin loss-of-function models, PGC-1α repression due to heightened PARIS levels leads to a loss of mitochondrial viability (Stevens et al., 2015). While PARIS represses PGC-1α by directly binding the promoter (Shin et al., 2011), parkin and PINK1 presumably collaborate to destroy it in the cytoplasm; perhaps, like TFEB, there is a component of nuclear-cytoplasmic – or mitochondrial – shuttling involving PARIS. A potentially similar mechanism occurs during the mitochondrial unfolded protein response ($UPR^{mt}$) in *C. elegans*. Activating transcription factor associated with stress-1 (ATFS-1) is imported into healthy mitochondrial, where it is normally degraded in the mitochondrial matrix (Nargund et al., 2012), analogous to the fate of PINK1. In instances of mitochondrial stress, ATFS-1 import is stalled, and its nuclear localization sequence (NLS) serves to target to protein to the nucleus where it drives the expression of chaperones, proteases and glycolytic enzymes in an effort to rescue OXPHOS function (Lin and Haynes, 2016; Nargund et al., 2015; Nargund et al., 2012). A similar mechanism involving ATF5, a potential ATFS-1 homologue, also occurs in mammals (Fiorese et al., 2016). Thus, there is precedence for direct communication between transcriptional regulators and mitochondria.

While parkin and PINK1 may regulate mitochondrial activity, mitochondrial activity reciprocally regulates mitophagy. For example, forcing mitochondrial respiration and energy production through OXPHOS greatly attenuates both the recruitment of parkin to mitochondria and mitophagy itself (McCoy et al., 2014; Van Laar et al., 2011). Cells whose mitochondria have been cleared by parkin-mediated mitophagy fail to grow in media containing galactose (as opposed to glucose) as, under these conditions, the TCA cycle is required for energy production (Narendra et al., 2008; Reitzer et al., 1979). Indeed, shifting ATP production to glycolysis is likely required during periods of increased mitophagy (and mitochondrial dysfunction), and is highlighted by a

requirement for hexokinase 1 – a known driver of high glycolytic metabolism – during parkin-mediated mitophagy (Bustamante and Pedersen, 1977; McCoy et al., 2014). While high ATP levels have been suggested to maintain PINK1 translation during mitophagy (Lee et al., 2015), other metabolites, such as pyruvate and certain fatty acids, may also affect PINK1 stabilization (Ivatt et al., 2014; Park et al., 2015b; Shi and McQuibban, 2017). Thus, it is important to consider parkin/PINK1 mitophagy within the context of the cellular state; not only is this mechanism vulnerable to the regulatory whim of the metabolic environment of the cell, but also directly and indirectly impacts other pathways.

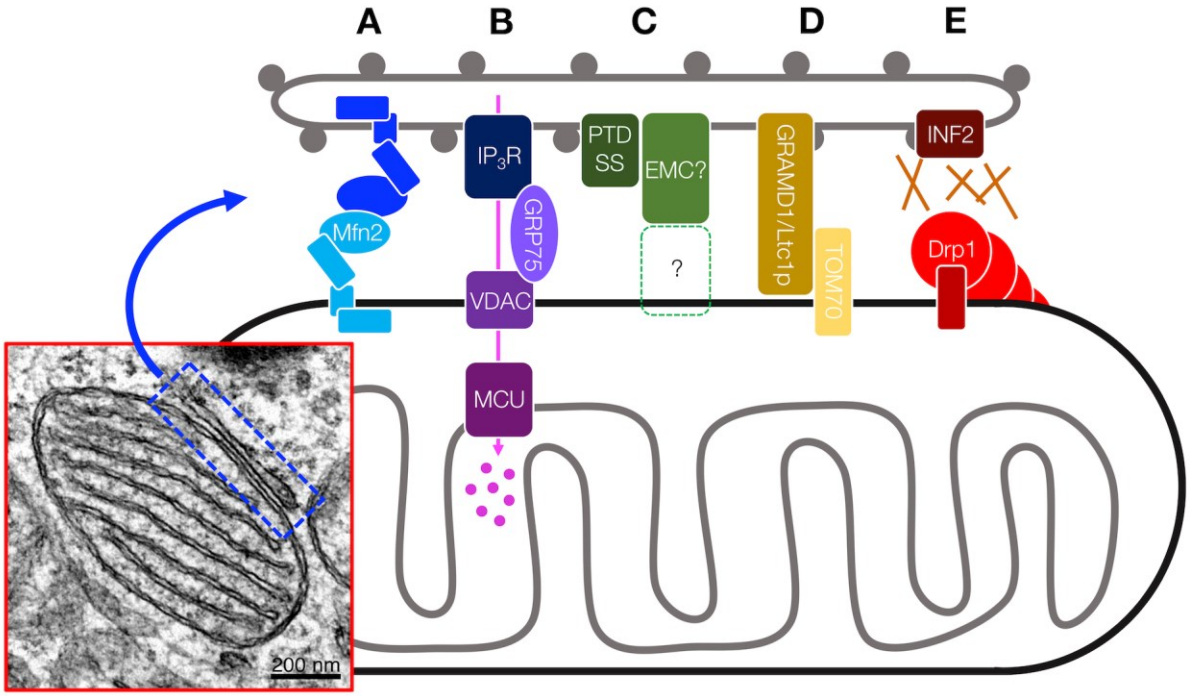


**Figure I.12**. *Roles of mitochondria-ER membrane contact sites*. Membrane contact sites between mitochondria and ER tubules are visible by EM; in the bottom-left micrograph, a U2OS cell mitochondrion is contacted by an ER tubule (blue box). These sites are physically and functionally regulated by several factors and physiological processes. **A** Mfn2 molecules on the OMM and the ER homo-oligomerize to tether the ER and mitochondria. **B** $Ca^{2+}$ transfer from the ER lumen to the mitochondrial matrix is achieved by the cooperative action of the $IP_3R$ and VDAC1 channels, which are physically linked by the chaperone GRP75, and MCU. **C** PS is synthesized by PTDSS on the ER membrane, and is channeled to mitochondria by a mechanism that involves EMC. **D** Sterol transport from the ER to mitochondria in mammals is presumably achieved by the GRAMD1 family of sterol transporters (Ltc1 in yeast), which are physically coupled to TOM70 on the OMM. **E** The ER controls mitochondrial division by INF2-dependent actin nucleation ( "X" ), which functions in the recruitment of Drp1 to the OMM by Drp1 receptors (dark red).

I.IV.ii *Membrane contact sites between mitochondria and the endoplasmic reticulum*

Membrane contact sites between mitochondria and other organelles represent important signaling hubs that are critical for mitochondrial function. The most studied contact is that between the mitochondrion and the ER (Fig. I.12), which regulates a number of mitochondrial and metabolic activities. Structurally, these sites are appositions of the ER and OMM, 9 to 30 nm in distance, held together by tethering proteins (Csordas et al., 2006). Mfn2 (first depicted in Fig. I.7 and additionally shown in Fig. I.12A) is thought to be a true tether; two Mfn2 molecules, one on each opposing membrane, form a homomeric complex to sustain the ER and OMM in proximity of one another (de Brito and Scorrano, 2008; Naon et al., 2016). Other molecules – such as PACS2, Stx17 and TMX1 – also promote ER-OMM tethering, but this may occur indirectly (Arasaki et al., 2015; Raturi et al., 2016; Simmen et al., 2005). Stx17, for example, may promote tethering through its proposed role in mitochondrial cholesterol uptake (Lin et al., 2016), as ER-OMM contacts, known biochemically as the mitochondria-associated membrane of the ER (MAM), constitute a detergent-resistant membrane (DRM) rich in cholesterol (Area-Gomez et al., 2012; Hayashi and Fujimoto, 2010). Factors involved in numerous cellular processes – including lipid synthesis, apoptosis, and innate immunity – cluster at this location (Horner et al., 2011; Phillips and Voeltz, 2016).

Mitochondria-ER coupling is crucial in metabolic regulation; in the context of starvation-induced autophagy, these contacts are where autophagosome biogenesis occurs (Hamasaki et al., 2013), potentially regulated by the lipid transfer that occurs at these sites (Lamb et al., 2013). During starvation, the class-III PI3K complex translocates to these sites, where it interacts with Stx17 – a SNARE protein that functions in autophagosome-lysosome fusion in addition to its proposed role in mitochondria-ER tethering (Hamasaki et al., 2013; Itakura et al., 2012b). Indeed,

ATG14L – which tethers the PI3K complex to membranes by binding phospholipids – clamps a binary complex composed of the SNAREs Stx17 and SNAP29 on the autophagosome and promotes their association with VAMP8 (to form a ternary SNARE complex) on lysosomes (Diao et al., 2015). In the absence of mitochondria-ER tethering, autophagosome formation is disrupted (Hamasaki et al., 2013). Indeed, other regulatory complexes, such as the growth factor-responsive mTORC2 (Betz et al., 2013), also localize to appositions between mitochondria and the ER, emphasizing the role of these locations in cellular metabolic and catabolic processes.

Mitochondria-ER contacts are also crucial for $Ca^{2+}$ dynamics between both organelles (de Brito and Scorrano, 2008). $Ca^{2+}$ transfer from the ER lumen to the mitochondrial matrix is an important driver of TCA cycle metabolism and ATP production (Llorente-Folch et al., 2015), and occurs through a system of channels (Fig. I.12B), beginning with the physical coupling of the inositol-1,4,5-triphosphate receptor ($IP_3R$) in the ER membrane to VDAC in the OMM through the chaperone GRP75, which acts a bridge molecule (Szabadkai et al., 2006). Flow of $Ca^{2+}$ across the IMM occurs through the mitochondrial $Ca^{2+}$ uniporter (MCU), a selective $Ca^{2+}$ channel ($K_D$ < 2 nM) (Kirichok et al., 2004; Mironova et al., 1994). Structurally, MCU homo-oligomers span the IMM to form the pore (Baughman et al., 2011; Chaudhuri et al., 2013; De Stefani et al., 2011; Oxenoid et al., 2016). Indeed, reconstitution assays in *S. cerevisiae* (which lack MCU) demonstrated that expression of exogenous MCU alone was sufficient to mediate mitochondrial $Ca^{2+}$ uptake (Kovacs-Bogdan et al., 2014). MCU is additionally regulated by soluble, accessory subunits such as mitochondrial $Ca^{2+}$ uptake protein 1 (MICU1) and MICU2 (Kamer and Mootha, 2015; Wang et al., 2014), as well as MCU regulator 1 (MCUR1) – although whether or not this latter factor regulates MCU directly remains unclear (Chaudhuri et al., 2016; Paupe et al., 2015; Vais et al., 2015).

In addition to $Ca^{2+}$ transfer, contacts between mitochondria and the ER have a functional role in the shuttling of phospholipids between both organelles. Phosphatidic acid (PA) is converted to phosphatidylserine (PS) by phosphatidylserine synthase (PTDSS, Cho1 in yeast) in the ER membrane (Phillips and Voeltz, 2016). PS is transported across the ER-mitochondrion interface by a mechanism that involves the conserved ER membrane protein complex (EMC, Fig. I.12C) (Lahiri et al., 2014). Indeed, perturbing the EMC itself or its interactors leads to mitochondrial lipid dyshomeostasis (Janer et al., 2016; Lahiri et al., 2014). This is one of the very first steps in a shuttling pathway, in which mitochondrial PS is then converted to phosphatidylethanolamine (PE), transported back to the ER to undergo enzymatic conversion to phosphatidylcholine (PC), and finally (likely) transported back to mitochondria (Phillips and Voeltz, 2016). Additionally, in yeast, sterols are transported from the ER to mitochondria via an interaction between the sterol transporter Ltc1p on the ER and Tom70p on mitochondria (Fig. I.12D) (Murley et al., 2015). This process is thought to be conserved in mammals, as the GRAMD1 family of proteins bears a domain configuration similar to Ltc1p and these proteins are highly-expressed in steroidigenic cell lines (McDowell et al., 2012; Murley et al., 2015; Rosenbloom et al., 2015). Additionally, organellar morphology itself is regulated by contact with the ER (Fig. I.12E); during mitochondrial fission, the ER contacts the OMM to label fission sites in order to stabilize Drp1 (Friedman et al., 2011; Prudent et al., 2015), likely through pre-constriction of the membrane via actin polymerization (Ji et al., 2015; Korobova et al., 2013). Thus, mitochondria-ER contact sites play critical and diverse functional roles in maintaining cellular homeostasis.

Returning to the PINK1/parkin quality control system, links between these disease genes and mitochondria-ER contacts are apparent, exemplified primarily by the association of PINK1 with $Ca^{2+}$ dynamics. In cultured cells, PINK1 depletion leads to an impairment of $Ca^{2+}$ uptake by

mitochondria – although this may be a secondary phenomenon arising from mitochondrial dysfunction – and, similarly, parkin-deficient cells have dysregulated $Ca^{2+}$ homeostasis (Heeman et al., 2011; Sandebring et al., 2009). Moreover, PINK1 deficiency in neurons – a cell type reliant on mitochondrially-generated energy production – sensitizes mitochondria to $Ca^{2+}$ overload, inducing cell death (Akundi et al., 2011; Almeida et al., 2004; Gandhi et al., 2009; Kostic et al., 2015), and deletion of MCU accordingly prevents dopaminergic degeneration in a zebrafish model of PINK1 loss (Soman et al., 2017). Conversely, highly glycolytic tissues (such as muscle) adapt to altered metabolism due to a loss of PINK1 by further increasing glycolysis and hyperpolarizing mitochondria, and become desensitized to $Ca^{2+}$-induced stress (Yao et al., 2011). Thus, the metabolic state of the cell can act as an important determinant for PINK1-related phenotypes. Both this observation and the inability of PINK1-null mitochondria to buffer $Ca^{2+}$ may sensitize DAergic neurons – which have an intrinsic pacemaking activity via $Ca^{2+}$ transients – to stress and cell death (Chan et al., 2007). More directly, perturbations in mitochondria-ER coupling have recently been described in *PARKIN* and *PINK1* loss-of-function systems, although these include both increases and decreases in contact (Celardo et al., 2016; Gautier et al., 2016; Gelmetti et al., 2017). Accordingly, dysregulation of lipid homeostasis has been reported in *PARKIN* mutant fibroblasts (Lobasso et al., 2017), and this may be due to dysregulation of mitochondria-ER uncoupling; indeed, the increase in PS observed by Lobasso *et al*. in mutant cells may be due to a failure of its ER-to-mitochondrion transfer, as PS synthesis is concentrated at these interorganellar junctions (Kannan et al., 2017). How parkin and PINK1 modulate mitochondria-ER contact remains unknown, although depolarization-stabilized PINK1 has recently been suggested to accumulate at contacts between both organelles (Gelmetti et al., 2017). Clearly, more study into

the direct, mechanistic role of PINK1 and parkin function at mitochondria-ER contact sites is required.

## I.V RATIONALE

Over the past decade, study of the cell biology of *PARKIN* and *PINK1*, building upon earlier work in *Drosophila*, has advanced significantly with respect to their roles in mitochondrial quality control. In focusing on how these proteins regulate mitophagy, the field has made significant progress in three major areas; *a*) how PINK1 transmits the mitochondrial damage signal to parkin, *b*) how parkin is activated, and *c*) how the mitochondrial ubiquitin signal is recognized by the cell to ensure degradation of the organelle. However, there is a significant dearth of knowledge concerning how parkin and PINK1 initiate mitophagy, and potentially other mitochondrial quality control mechanisms (i.e. between points *b* and *c*). Logically, regulatory mechanisms should precede the feed-forward cycle of ubiquitination and Ub phosphorylation – the point of no return – yet very little is known about factors modulating the pathway. Moreover, while transient or oscillating depolarizations have been measured in a variety of cell types (including DAergic neurons in *in situ* preparations), prolongued mitochondrial depolarization is rare under physiological conditions (Brady et al., 2004; Duchen et al., 1998; Guzman et al., 2010; Hattori et al., 2005; Li et al., 2012; Suen et al., 2010). Thus, the heavy reliance of the field on mitochondrial uncoupling agents and parkin overexpression to achieve phenotypes may mask the true nature of the parkin/PINK1 pathway; indeed, evidence in *Drosophila* suggests that these proteins regulate both autophagic turnover of mitochondria and selective degradation of mitochondrial proteins (Vincow et al., 2013). The overarching goal of the work contained within

this thesis was *to investigate how mitochondrial quality control pathways – specifically at the initiation step – are regulated by parkin, PINK1 and other factors*.

Chapter II

# PARKIN AND PINK1 FUNCTION IN A VESICULAR TRAFFICKING PATHWAY REGULATING MITOCHONDRIAL QUALITY CONTROL

The following Chapter originally appeared as a Research Article in the *EMBO Journal*:

**McLelland GL**, Soubannier V, Chen CX, McBride HM, Fon EA (2014). Parkin and PINK1 function in a vesicular trafficking pathway regulating mitochondrial quality control. *EMBO J.* 33(4):282-295, doi:10.1002/embj.201385902. PMID: 24446486

## II.I ABSTRACT

Mitochondrial dysfunction has long been associated with Parkinson's disease (PD). *PARKIN* and *PINK1*, two genes associated with familial PD, have been implicated in the degradation of depolarized mitochondria via autophagy (mitophagy). Here, we describe the involvement of parkin and PINK1 in a vesicular pathway regulating mitochondrial quality control. This pathway is distinct from canonical mitophagy and is triggered by the generation of oxidative stress from within mitochondria. Wild-type but not PD-linked mutant parkin supports the biogenesis of a population of mitochondria-derived vesicles (MDVs), which bud off mitochondria and contain a specific repertoire of cargo proteins. These MDVs require PINK1 expression and ultimately target to lysosomes for degradation. We hypothesize that loss of this parkin- and PINK1-dependent trafficking mechanism impairs the ability of mitochondria to selectively degrade oxidized and damaged proteins, leading, over time, to the mitochondrial dysfunction noted in PD.

## II.II INTRODUCTION

Mitochondrial quality control, a term encompassing various cellular pathways overseeing the regulated turnover of mitochondrial proteins and lipids, ensures the functionality of the mitochondrial reticulum throughout the lifetime of the cell (Youle and van der Bliek, 2012). The deterioration of these mechanisms has been hypothesized to underlie the pathogeneses of several neurodegenerative diseases, most notably Parkinson's disease (PD), the second-most common neurodegenerative disorder worldwide (Dawson et al., 2010; Schon and Przedborski, 2011; Tatsuta and Langer, 2008). PINK1 and parkin, two PD-linked genes initially implicated in a common pathway regulating mitochondrial function in *Drosophila*, have been shown to mediate the degradation of dysfunctional mitochondria that have become depolarized by treatment of cells

with the uncoupler CCCP (Clark et al., 2006; Greene et al., 2003; Park et al., 2006; Poole et al., 2008; Yang et al., 2006). In this paradigm, PINK1, a serine/threonine kinase, globally accumulates on depolarized mitochondria and recruits parkin from the cytosol to mitochondria in a manner dependent upon PINK1 phosphorylation activity (Greene et al., 2012; Matsuda et al., 2010; Narendra et al., 2008; Narendra et al., 2010b; Vives-Bauza et al., 2010). At depolarized mitochondria, parkin, an E3 ubiquitin ligase, catalyzes the polyubiquitination of several substrates, including the mitofusins and VDACs, and triggers whole-mitochondrial engulfment by autophagosomes and subsequent degradation through the autophagosome-lysosome pathway (a process known as mitophagy) (Geisler et al., 2010; Narendra et al., 2008; Poole et al., 2010; Sun et al., 2012; Tanaka et al., 2010; Wang et al., 2011; Ziviani et al., 2010). Kinetic studies of mitophagic clearance of entire mitochondria by PINK1 and parkin have demonstrated that this process occurs on the scale of several hours to days (Chan et al., 2011; Yoshii et al., 2011).

Recently, we showed that a subpopulation of mitochondrial-derived vesicles (MDVs) – cargo-selective vesicles that bud off mitochondria independently of the mitochondrial fission machinery – play a role in mitochondrial quality control (Neuspiel et al., 2008; Soubannier et al., 2012a; Soubannier et al., 2012b). We have shown that MDVs mediate transport between mitochondria and various other organelles in response to a variety of stimuli (Braschi et al., 2010; Neuspiel et al., 2008; Soubannier et al., 2012a). Correspondingly, upon generation of cytosolic oxidative stress, we observed the biogenesis of mitochondrial vesicles that ultimately targeted to lysosomes for degradation, on a scale of tens of minutes to an hour (Soubannier et al., 2012a). As *in vitro* reconstitution experiments demonstrated that these vesicles were enriched for oxidized proteins (Soubannier et al., 2012b), we hypothesized that certain populations of mitochondrial vesicles may regulate a form of mitochondrial quality control, kinetically faster than mitophagy,

which would function prior to total depolarization in an effort to preserve the integrity of the organelle.

Here, we demonstrate the involvement of parkin and PINK1 in the generation of MDVs in response to mitochondrial oxidative stress. Parkin colocalizes with MDVs in a PINK1-dependent manner, and stimulates their formation in response to antimycin A, a potent generator of reactive oxygen species (ROS). Once formed, these vesicles target to lysosomes for degradation in a manner independent of canonical mitophagy. These findings implicate PINK1 and parkin in a mitochondrial quality control pathway that operates at an early stage in order to salvage mitochondria by selectively extracting damaged components via vesicular carriers. We propose that it is only once this first line of defense is overwhelmed – and that mitochondria become irreversibly damaged – that the entire organelle is targeted for degradation by mitophagy.

## II.III RESULTS

### II.III.i *Mitochondrial ROS generate mitochondrial vesicles in a parkin-dependent manner*

To test whether parkin is involved in a mitochondrial vesicular trafficking pathway, we expressed GFP-parkin and a mitochondrial matrix-targeted DsRed2 (OCT-DsRed2) in HeLa cells, which express no endogenous parkin (Denison et al., 2003). Throughout this study, to ensure that we were examining MDVs rather than mitochondrial fragments generated by fission, Drp1-dependent fission was suppressed by either overexpressing a dominant-negative Drp1 mutant (CFP-Drp1$^{K38E}$, Fig. II.S1) (Harder et al., 2004) or by reducing endogenous Drp1 levels via siRNA. These cells, subjected to a variety of treatments, were fixed and immunostained against the outer mitochondrial membrane (OMM) protein TOM20 (Fig. II.1A). In untreated cells, GFP-parkin

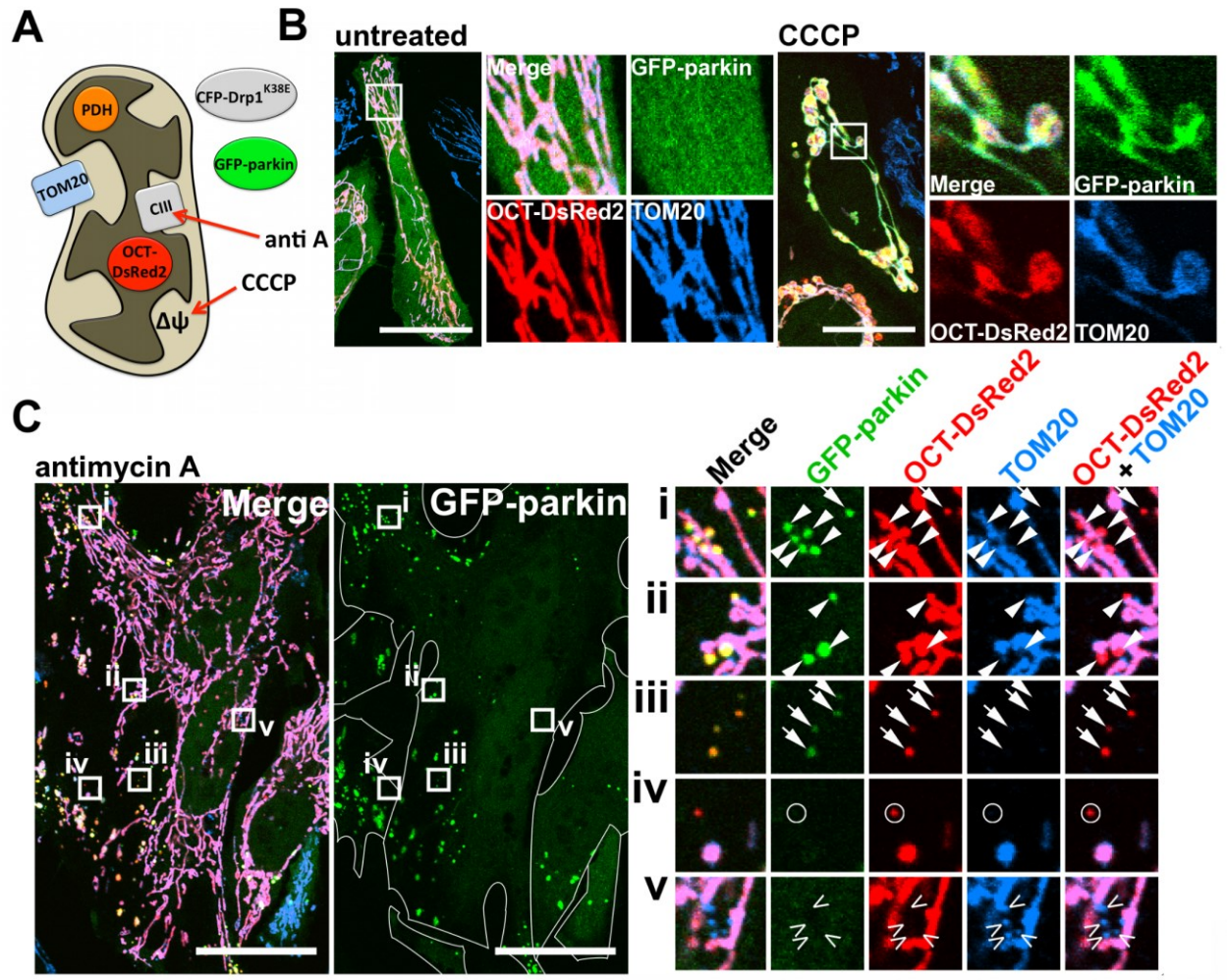


**Figure II.1**. *Parkin promotes the biogenesis of cargo-selective MDVs in response to mitochondrial ROS*. **A** Schematic depicting the location of relevant protein markers relative to the mitochondrion, as well as the site of action of pharmacological agents used. **B** HeLa cells expressing GFP-parkin (green), OCT-DsRed2 (red) and CFP-Drp1$^{K38E}$ were left untreated (untreated) or treated for two hours with 10 μM CCCP (CCCP), then fixed and stained for TOM20 (blue). Scale bars, 30 microns. **C** Cells prepared as in **B** were treated with 50 μM antimycin A for two hours. Arrows indicate OCT-DsRed2-positive/TOM20-negative MDVs that colocalize with GFP-parkin, while circles indicate MDVs that are parkin-negative. Arrowheads indicate "nascent" vesicles, adjacent to mitochondria, exhibiting cargo selectivity and parkin recruitment. Open arrowheads indicate parkin-negative MDVs containing the reciprocal cargo (TOM20-positive/OCT-DsRed2-negative). Cell boundaries are delineated in the GFP-parkin single-channel image. Scale bars, 30 microns.

remained predominantly cytosolic, and both mitochondrial markers overlapped almost perfectly (Fig. II.1B, *untreated*). As expected, disruption of $\Delta\psi_m$ with CCCP led to recruitment of parkin *en masse* to the mitochondrial reticulum (Fig. II.1B, *CCCP*), which remained elongated as Drp1-dependent fission was inhibited by CFP-Drp1$^{K38E}$. In our previous study, the generation of ROS within mitochondria in COS7 cells (which express low levels of endogenous parkin), using the

complex III inhibitor antimycin A, led to the formation of specific MDVs that incorporated selective cargo (Soubannier et al., 2012a). *In vitro* reconstitution followed by biochemical and ultrastructural analysis showed that these vesicles were enriched for oxidized cargo proteins, and that matrix cargo-containing MDVs, which excluded TOM20, were double-membrane structures containing both an inner and outer membrane (Soubannier et al., 2012b). Strikingly, treatment of HeLa cells with antimycin A for two hours led to the recruitment of GFP-parkin from the cytosol to puncta containing the matrix-targeted DsRed2 but not TOM20 (Fig. II.1C, boxes *i* to *iii*). Although we only observed these antimycin A-induced, matrix-positive/TOM20-negative MDVs in HeLa cells expressing GFP-parkin and not GFP alone (Fig. II.2A), only 20% to 40% of these structures colocalized with parkin, often at the periphery of mitochondria on what appeared to be nascent, budding vesicles (Fig. II.1C, arrowheads), as well as ones that had dissociated completely from mitochondria (Fig. II.1C, arrows). Thus, whereas both parkin and mitochondrial ROS are required to induce this population of double-membraned mitochondrial vesicles, it appears that the association of parkin with these structures is transient and occurs initially at sites of MDV budding.

Importantly, we found that the antimycin A-induced vesicular recruitment of parkin was specific to this OCT-DsRed2-positive/TOM20-negative MDV population, as vesicles with the reciprocal cargo (TOM20-positive/OCT-DsRed2-negative) lacked parkin (Fig. II.1C, open arrowheads). Moreover, treatment of GFP-parkin-expressing HeLa cells with antimycin A did not increase the overall number of this other, reciprocal vesicle population (Fig. II.S2A). When cells were treated with glucose oxidase, which induces ROS formation external to mitochondria, for two hours – a treatment that triggers the robust formation of TOM20-positive/matrix-negative vesicles (Soubannier et al., 2012a) – we again did not observe the recruitment GFP-parkin to these

MDVs (Fig. II.S2B, open arrowheads). Thus, parkin is recruited to a specific population of MDVs upon generation of mitochondrial ROS.

Next, we tested whether different PD-linked parkin mutants (depicted in Fig. II.2B) could induce MDVs in response to antimycin A. The number of matrix-positive, TOM20-negative structures was quantified in antimycin A-treated HeLa cells expressing GFP, GFP-parkin$^{WT}$, GFP-parkin$^{R42P}$, GFP-parkin$^{K211N}$ or GFP-parkin$^{C431F}$. Only upon expression of GFP-parkin$^{WT}$ did we

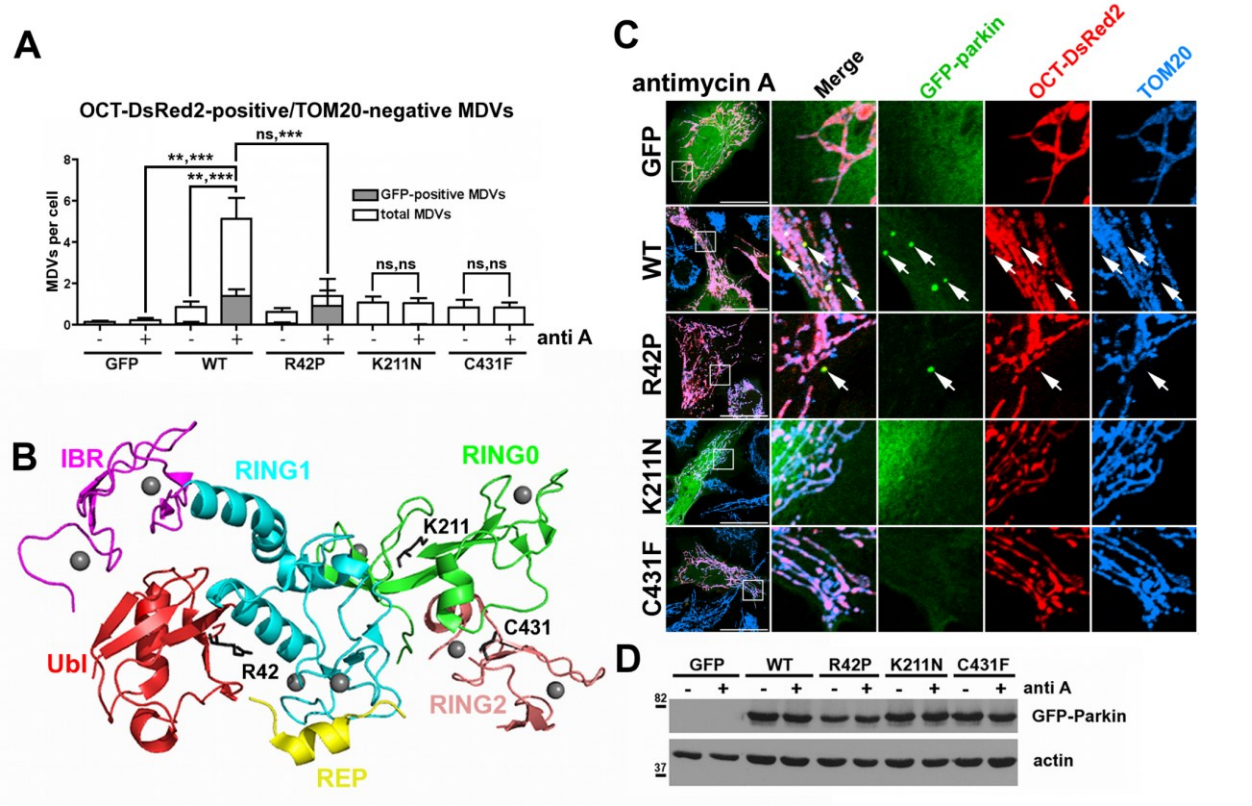


**Figure II.2**. *Wild-type parkin, but not PD-associated parkin mutants, promotes MDV biogenesis*. **A** Quantification of the number of OCT-DsRed2-positive/TOM20-negative vesicles in cells expressing GFP, GFP-parkin$^{WT}$, GFP-parkin$^{R42P}$, GFP-parkin$^{K211N}$, or GFP-parkin$^{C431F}$, treated with or without antimycin A; both total number (white bars) and the number colocalizing with GFP-parkin (gray bars) are indicated. Bars represent the mean±SEM. P-values are given first for GFP-/GFP-parkin-positive vesicles, then for total vesicle number (n = 49 to 68 cells in 2 to 3 experiments; ns, not significant; *, p<.05; **, p<.01; ***, p<.001). **B** Structure of parkin, with PD-linked residues from **D** highlighted in dark gray (PDB ID: 4K95). Ubl, ubiquitin-like domain (red); R0, RING0 domain (green); R1, RING1 (cyan); IBR, in-between RING (magenta); REP, repressor element of parkin (yellow); R2, RING2 (salmon). **C** HeLa cells expressing various GFP-parkin mutant contructs (green), pOCT-DsRed2 (red) and CFP-Drp1$^{K38E}$ were treated with 50 µM antimycin A for two hours, then fixed and immunostained against TOM20. Arrows indicate matrix-positive/TOM20-negative structures colocalizing with GFP-parkin. Scale bars, 30 microns. **D** Immunoblot of whole-cell lysates of HeLa cells expressing various GFP-parkin constructs, treated with 50 µM antimycin A or DMSO for two hours.

observe the formation of matrix-positive MDVs (Fig. II.2A and C). In contrast, both GFP-parkin$^{K211N}$ and GFP-parkin$^{C431F}$ failed to generate mitochondrial vesicles (Fig. II.2A and C). The mutation of the catalytic C431 abolishes parkin ubiquitin ligase activity (Trempe et al., 2013), suggesting a role for ubiquitination in MDV biogenesis, and the GFP-parkin$^{K211N}$ has been previously reported to be completely deficient in depolarization-induced parkin translocation (Geisler et al., 2010). In the case of cells expressing GFP-parkin$^{R42P}$, it was found that, although the antimycin A-dependent increase in total matrix-positive/TOM20-negative vesicles was not significant (Fig. II.2A and C), parkin colocalized with most of the few mitochondrial vesicles present in these treated cells (Fig. II.2A). The R42P mutation disrupts the folding of the Ubl domain but does not abolish CCCP-induced mitochondrial translocation (Geisler et al., 2010; Narendra et al., 2010b; Safadi and Shaw, 2007). Moreover, as an intact Ubl is critical for parkin to interact with membrane trafficking partners (Fallon et al., 2006; Trempe et al., 2009), we hypothesize that a functional Ubl domain may facilitate interactions between parkin and trafficking proteins downstream of vesicle formation. Additionally, we do not disregard the possibility that GFP-parkin$^{R42P}$-induced MDV formation may simply be kinetically slower in comparison to the wild-type.

To further extend our findings and show they were not cell-type specific, instead of HeLa cells, we used U2OS cells stably expressing either GFP (U2OS:GFP) or GFP-parkin (U2OS:GFP-parkin) and, instead of CFP-Drp1$^{K38E}$, we used Drp1 siRNA to inhibit mitochondrial fission (Fig. II.3A). To determine whether the parkin- and antimycin A-induced structures could incorporate endogenous mitochondrial proteins, instead of using OCT-DsRed2, the cells were stained with antibodies raised against the E2 and E3bp subunits of the pyruvate dehydrogenase complex (PDH E2/E3bp, localized to the mitochondrial matrix; Fig. II.1A) as well as TOM20. We again observed

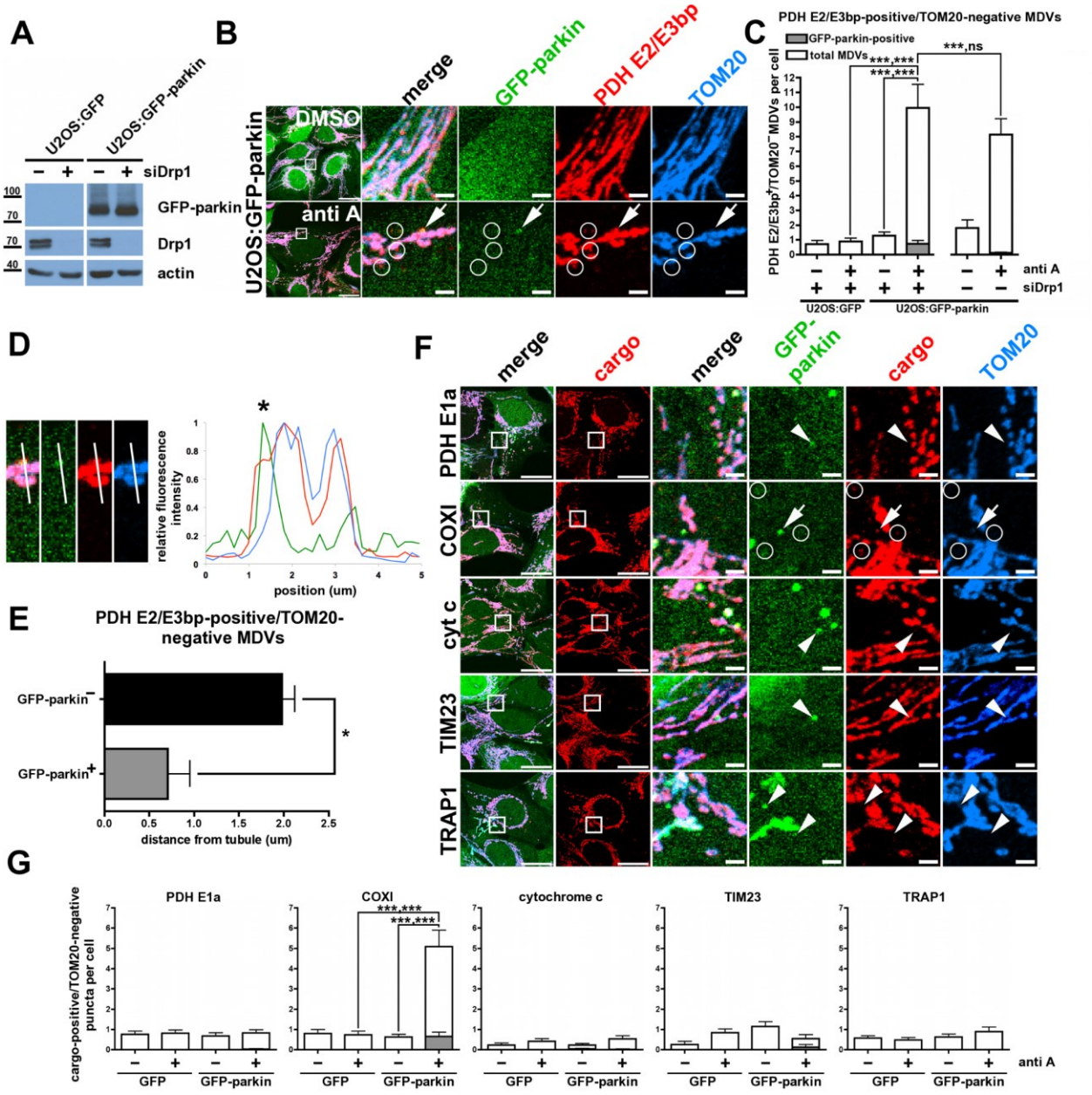


**Figure II.3**. *Parkin-dependent MDVs incorporate endogenous mitochondrial cargo*. See legend on the following page.

cargo-selective (PDH E2/E3bp-positive/TOM20-negative) structures that did (Fig. II.3B, arrows) or did not (Fig. II.3B, circles) colocalize with parkin after treatment. Expectedly, silencing of Drp1 had no effect on the total number of MDVs observed, confirming that MDVs are not a product of mitochondrial fission (Fig. II.3C). Again, only a fraction of the parkin-induced structures colocalized with GFP-parkin (Fig. II.3C) and those that did were predominantly adjacent to

**Figure II.3**. *Parkin-dependent MDVs incorporate endogenous mitochondrial cargo*. **A** Representative immunoblot of whole-cell lysates from U2OS:GFP and GFP-parkin cells transfected with non-targeting siRNA or siRNA targeting Drp1 (siDrp1). **B** U2OS:GFP-parkin cells transfected with siRNA targeting Drp1 were treated with DMSO (left panel set) or 25 μM antimycin A (anti A, right panel set) for 90 minutes, then fixed and immunostained against PDH (red) and TOM20 (blue). PDH E2/E3bp-positive/TOM20-negative MDVs colocalizing with GFP-parkin (arrows) or not (circles) are indicated. Scale bars, 20 and 2 microns. **C** Quantification of PDH-positive/TOM20-negative vesicles in U2OS:GFP and GFP-parkin cells, transfected with the indicated siRNA, treated with DMSO or antimycin A as in B; both total number (white bars) and the number colocalizing with GFP-parkin (gray bars) are indicated. Bars represent the mean±SEM. P-values are given first for GFP-/GFP-parkin-positive vesicles, then for total vesicle number (n = 48 to 85 cells in 2 to 3 experiments; ns, not significant; *, p<.05; **, p<.01; ***, p<.001). **D** 5 μm-long profile of the parkin-positive vesicle and adjacent mitochondrial tubule depicted in the antimycin A-treated cell from **B** (left). Increasing position values on the x-axis of the fluorescent intensity plot (right) correspond to moving from the top to the bottom of the profile. "*" denotes the MDV indicated by an arrow in **B**. **E** Quantification of the distance between the centres of GFP-parkin-negative (black bar) and -positive (gray bar) vesicles and the edge of the nearest mitochondrial tubule for the vesicles quantified in antimycin A-treated U2OS:GFP-parkin cells transfected with siDrp1 in **C**. Bars represent the mean±SEM. p<0.05 (*) was obtained by Student's t-test. **F** U2OS:GFP-parkin cells transfected with siRNA targeting Drp1 (siDrp1) were treated with 25 μM antimycin A for 90 minutes prior to fixation. Samples were immunostained against TOM20 (blue) and the indicated mitochondrial marker (red). PDH E2/E3bp-positive/TOM20-negative MDVs colocalizing with GFP-parkin (arrows) or not (circles) are indicated. Arrowheads show lack of colocalization between GFP-parkin and the indicated mitochondrial marker. Scale bars, 20 and 2 microns. **G** Quantification of TOM20-negative structures that stained positively for the indicated cargo in U2OS:GFP and GFP-parkin cells, transfected with the indicated siRNA, treated with antimycin A; both total number (white bars) and the number colocalizing with GFP-parkin (gray bars) are indicated. Bars represent the mean±SEM. P-values are given first for GFP-/GFP-parkin-positive vesicles, then for total vesicle number (n = 24 to 59 cells in 2 experiments; ns, not significant; *, p<.05; **, p<.01; ***, p<.001).

mitochondrial tubules (Fig. II.3D and E). Next, we asked whether parkin is required for the formation of this class of MDVs. We had previously shown that, in COS7 cells, a population of PDH E2/E3bp-positive, TOM20-negative MDVs was similarly induced by treatment with antimycin A (Soubannier et al., 2012a). Silencing of endogenous parkin with siRNA in these cells (Fig. II.S3A) significantly reduced the number of PDH E2/E3bp-positive, TOM20-negative MDVs that formed in response to antimycin A (Fig. II.S3B). Thus, the ROS-induced biogenesis of this class of MDV requires endogenous parkin in COS7 cells and is stimulated by parkin expression under multiple conditions in a variety of cell lines.

To further characterize the endogenous cargo being carried by these vesicles, we also screened a variety of other mitochondrial proteins to determine if they, like PDH E2/E3bp and OCT-DsRed2, were incorporated into the parkin-dependent MDVs in U2OS:GFP-parkin cells.

Strikingly, we did not observe sorting of the E1α subunit of the PDH complex (PDH E1a) in parkin-dependent MDVs (Fig. II.3F and G), suggesting that the megadalton PDH complex is at least partially disassembled before incorporation into vesicles. Moreover, while COXI (a transmembrane component of complex IV of the electron transport chain [ETC] located in the inner mitochondrial membrane [IMM]) was incorporated into the antimycin A/parkin-induced MDV population, several other mitochondrial proteins, including cytochrome c (intermembrane space [IMS]), TIM23 (IMM) and TRAP1 (IMS/matrix) were not (Fig. II.3F and G). These data confirm that cargo selection extends beyond the exclusion of TOM20 and suggest that components from the same mitochondrial locale and complex sort differentially into vesicles, in line with what has been observed in *in vitro* reconstitution assays (Soubannier et al., 2012b).

Mitochondrially-localized parkin has been shown to polyubiquitinate and mediate the degradation of OMM proteins in a manner dependent upon p97/VCP and the proteasome (Chan et al., 2011; Tanaka et al., 2010; Yoshii et al., 2011). Thus, it could be conceived that the exclusion of TOM20 from the observed parkin-dependent, antimycin A-induced MDV population may result from its proteasomal degradation. To test this, we treated HeLa cells expressing GFP-parkin with antimycin A in the presence of MG132 or epoxomicin, two proteasomal inhibitors (Fig. II.S4A). Under circumstances of proteasomal inhibition, we observed no decrease in the total number of antimycin A-induced PDH E2/E3bp-positive/TOM20-negative structures, or those colocalizing with parkin (Fig. II.S4B). Additionally, we did not observe a change in the ratios of PDH E2/E3bp-positive/TOM20-negative puncta (vesicles) with those that were doubly-positive (mitochondrial fragments) that colocalized with GFP-parkin (Fig. II.S4C), as would be expected if parkin were degrading TOM20 from the surface of these structures. We also did not observe any change in

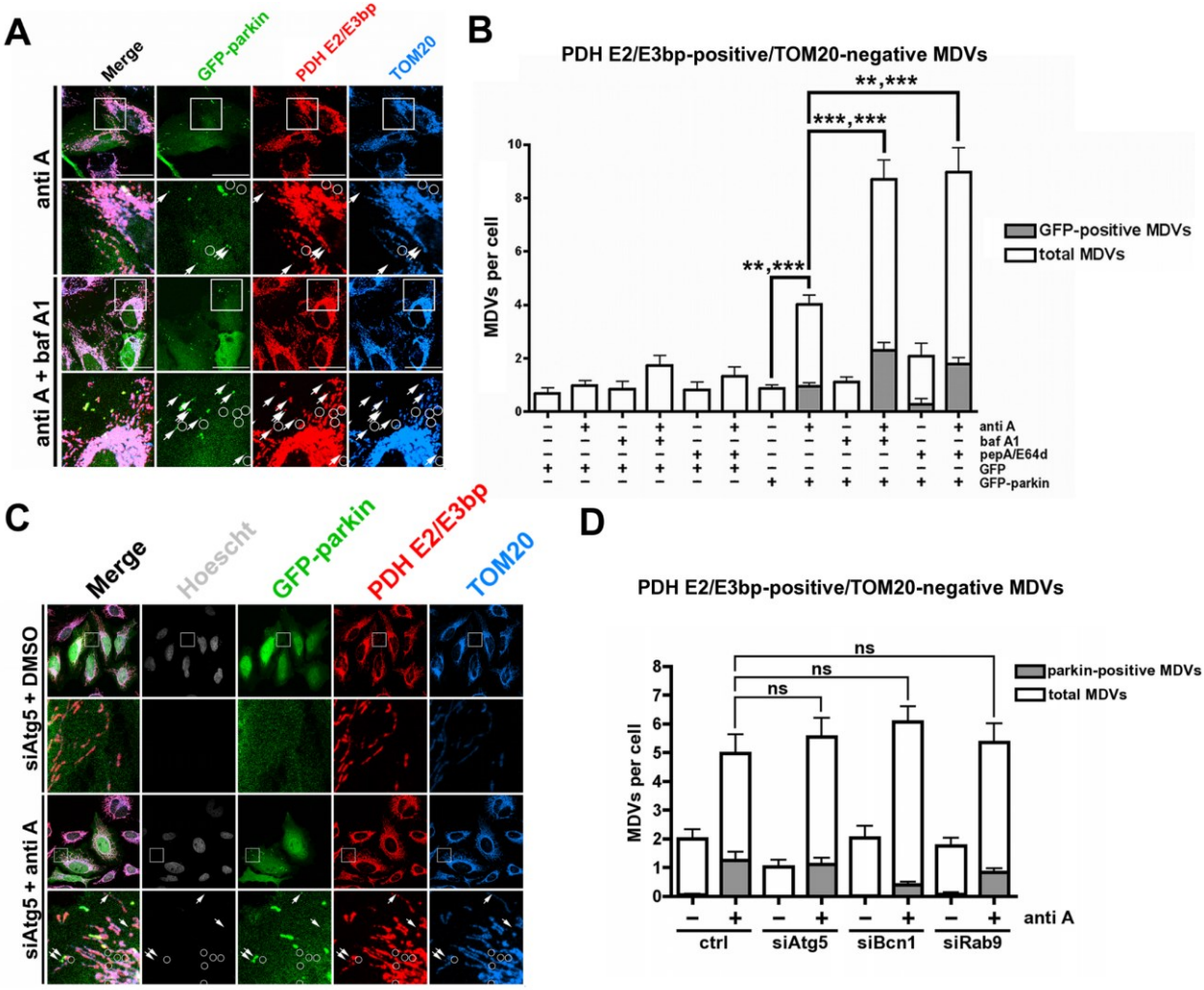


**Figure II.4**. *Parkin-dependent MDVs are targeted to lysosomes independently of autophagy.* **A** HeLa cells, transfected with siRNA targeting Drp1 and GFP-parkin (green), were treated with 25 μM antimycin A for 90 minutes following a 30-minute pretreatment with 50 nM bafilomycin, then fixed and immunostained against PDH E2/E3bp (red) and TOM20 (blue). PDH E2/E3bp-positive/TOM20-negative MDVs colocalizing with GFP-parkin (arrows) or not (circles) are indicated. Scale bar, 30 microns. **B** Quantification of PDH E2/E3bp-positive/TOM20-negative vesicles in HeLa cells treated with antimycin A in the presence of the lysosomal inhibitors bafilomycin $A_1$ or pepstatin A and E-64d; both total number (white bars) and the number colocalizing with GFP-parkin (gray bars) are indicated. Bars represent the mean±SEM. P-values are given for total vesicle number (n = 19 to 120 cells in 2 to 3 experiments; ns, not significant; *, p<.05; **, p<.01; ***, p<.001). **C** HeLa cells, transfected with GFP-parkin (green) and siRNA targeting Drp1 and Atg5, were treated with 25 μM antimycin A for 90 minutes, then fixed, immunostained for PDH E2/E3bp (red) and TOM20 (blue), and counterstained for Hoescht (gray). PDH E2/E3bp-positive/TOM20-negative MDVs colocalizing with GFP-parkin (arrows) or not (circles) are indicated. Scale bars, 20 microns. **D** Quantification of PDH E2/E3bp-positive/TOM20-negative vesicles from HeLa cells transfected with the indicated siRNA; both total number (white bars) and the number colocalizing with GFP-parkin (gray bars) are indicated. Bars represent the mean±SEM. P-values are given for total vesicle number (n = 42 to 64 cells in 2 to 3 experiments ns, not significant; *, p<.05; **, p<.01; ***, p<.001).

total levels of TOM20 in U2OS:GFP-parkin cells treated with antimycin A compared to those treated with DMSO (Fig. II.S4D and E). Finally, we silenced p97/VCP expression in U2OS:GFP-parkin cells (Fig. II.S4F), and observed no change in the total number of antimycin A-induced MDVs (Fig. II.S4G). Taken together with our data demonstrating differential sorting of endogenous cargo into vesicles (Fig. II.3), these results implicate *bona fide* selective incorporation – rather than selective degradation – in the generation of parkin-dependent MDVs.

II.III.ii *Parkin MDVs are targeted to lysosomes for degradation independently of autophagy*

As our previous study had shown that ROS-induced mitochondrial vesicles are targeted to lysosomes for degradation (Soubannier et al., 2012a), we suspected the fate of parkin-dependent vesicles to be similar. To address this, we first silenced Drp1 expression in HeLa cells (Fig. II.S5A), and overexpressed either GFP or GFP-parkin. In cells expressing GFP-parkin, we saw an increase in PDH E2/E3bp-positive/TOM20-negative structures after antimycin A treatment (Fig. II.S5B), similar to what we had observed in U2OS:GFP-parkin cells. We then incubated these HeLa cells with antimycin A in the presence of the V-ATPase inhibitor bafilomycin $A_1$ or the lysosomal hydrolase inhibitors pepstatin A and E64d; inhibitors commonly used in the study of the lysosomal degradative pathway (Klionsky et al., 2012; Mizushima et al., 2010). Both the total number of PDH E2/E3bp-positive/TOM20-negative MDVs, as well as the number of vesicles that colocalized with GFP-parkin, increased significantly in the presence of antimycin A and bafilomycin or pepstatin/E64d compared to treatment with antimycin A alone (Fig. II.4A and B). The increase resulting from lysosomal inhibition was parkin-dependent, as it was not observed in cells expressing an empty GFP vector (Fig. II.4B).

Given that parkin-dependent mitochondrial turnover via autophagy requires mitochondrial fission (Tanaka et al., 2010; Twig et al., 2008) and that Drp1 was suppressed in our cells, it is unlikely that the parkin-induced MDV biogenesis that we observed involved canonical autophagy pathways. To definitively test whether the role of parkin in the formation of mitochondrial vesicles is distinct from its established role in mitophagy, MDV formation in autophagy-deficient cell systems was investigated. We observed antimycin A-induced mitochondrial vesicles in parkin-expressing, immortalized mouse embryonic fibroblasts (MEFs) generated from both WT mice and mice lacking Atg5 (an essential component of the canonical autophagic machinery, and required for parkin-dependent mitophagy) (Fig. II.S6A). In HeLa cells, expression of Atg5, beclin-1 (a core component of the PI[3]K complex regulating autophagy) and Rab9 (implicated in an alternative autophagic pathway) were individually

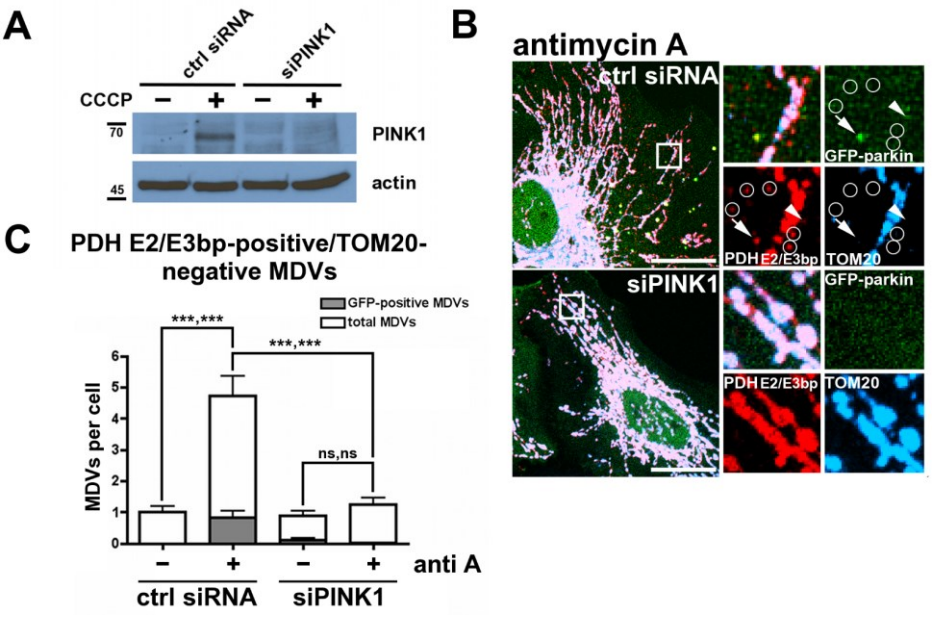


**Figure II.5**. *PINK1 is required for parkin-dependent MDV formation*. **A** Representative immunoblot of whole-cell lysates from HeLa cells transfected with non-targeting siRNA or siRNA targeting PINK1 (siPINK1), treated with 10 μM CCCP for 6 hours in order to stabilize the PINK1 full-length band. **B** HeLa cells, transfected with GFP-parkin (green) and siRNA targeting Drp1 and PINK1 (or non-targeting control), were treated with 25 μM antimycin A for 90 minutes, then fixed, immunostained for PDH E2/E3bp (red) and TOM20 (blue). PDH E2/E3bp-positive/TOM20-negative MDVs colocalizing with GFP-parkin (arrows) or not (circles) are indicated. Arrowheads indicate parkin-positive MDVs adjacent to mitochondria, possibly budding. **C** Quantification of PDH E2/E3bp-positive/TOM20-negative structures from **B**; both total number (white bars) and the number colocalizing with GFP-parkin (gray bars) are indicated. Bars represent the mean±SEM. P-values are given first for GFP-/GFP-parkin-positive vesicles, then for total vesicle number (n = 42 to 60 cells in 3 experiments; ns, not significant; *, p<.05; **, p<.01; ***, p<.001).

silenced using siRNA (Fig. II.S6B) (Narendra et al., 2008; Nishida et al., 2009; Xie and Klionsky, 2007). In these cells, autophagy was severely inhibited, as evidenced by the lack of GFP-LC3-positive autophagosomes (Fig. II.S6C). When GFP-parkin was expressed in these autophagy-deficient HeLa cells, we again observed an antimycin A-dependent increase in the total number of PDH E2/E3bp-positive/TOM20-negative vesicles (Fig. II.4C and D). As these numbers remained unchanged between autophagy-deficient and control cells, it is unlikely that these autophagy-related proteins play a role in parkin-dependent MDV biogenesis or degradation, as, in these instances, the number of vesicles would be expected to decrease or increase, respectively.

II.III.iii *PINK1 is required for parkin-dependent MDV biogenesis*

Given that parkin-dependent mitophagy has been shown to require PINK1 protein stabilization on mitochondria (Geisler et al., 2010; Matsuda et al., 2010; Narendra et al., 2010b; Vives-Bauza et al., 2010), the involvement of PINK1 in parkin-dependent MDV formation was investigated. PINK1 expression was silenced via siRNA-mediated knockdown in HeLa cells expressing GFP-parkin (Fig. II.5A), and the number of PDH E2/E3bp-positive/TOM20-negative structures was quantified after treatment with antimycin A. Interestingly, it was observed that, in cells lacking PINK1, antimycin A-induced, parkin-dependent MDV biogenesis was severely abrogated (Fig. II.5B and C). This finding indicates that PINK1 and parkin regulate both mitophagy and mitochondrial vesicle formation, and may do so in response to distinct stimuli. ROS generation may induce the formation of MDVs in an effort to preserve organelle integrity, while mitophagy may occur only once this vesicular system is overwhelmed and $\Delta\psi_m$ has been lost.

II.III.iv *Parkin-dependent MDV formation and turnover precedes mitophagy*

In order to test our hypothesis that, relative to mitophagy, parkin-dependent vesicle biogenesis represents an early response to mitochondrial stress, we performed kinetic experiments in U2OS:GFP-parkin cells, a cell line which undergoes parkin-dependent mitophagy in response to loss of $\Delta\psi_m$ by CCCP (Lefebvre et al., 2013). As we decided to monitor both MDV formation and mitophagy, we did not manipulate Drp1 levels. In addition to using antimycin A and CCCP to generate mitochondrial ROS and ablate $\Delta\psi_m$, respectively, we also chose to incubate cells with both antimycin A and oligomycin (a mitochondrial ATPase inhibitior). As oligomycin blocks both forward and reverse electron flow through the $F_1F_0$ ATP synthase, its use would prevent, during antimycin A-induced respiratory chain inhibition, the attempted repolarization of mitochondria through reverse ATP synthase activity (Hatefi, 1985).

We first monitored $\Delta\psi_m$ in these cells by TMRM fluorescence, and observed a sharp decline in TMRM fluorescence signal (down to 23.8% of DMSO-treated control cells) following CCCP treatment at 30 minutes (the first time point measured) that was maintained for the 6 hours of the experiment (Fig. II.6A, *CCCP*). As expected, antimycin A induced a much smaller decrease in TMRM signal after the first hour (67.0% of control at 60 minutes), which was then followed by a rebound in $\Delta\psi_m$ that, at 6 hours, had recovered almost completely (90.5% of control) (Fig. II.6A, *anti A*). This finding is consistent with the phenomenon of reverse proton flow through the $F_1F_0$ ATPase induced by compromised mitochondrial respiration (Campanella et al., 2008; Hatefi, 1985). Indeed, combined inhibition with antimycin A and oligomycin prevented this rebound, and $\Delta\psi_m$ decreased steadily over time (to 50.9% of control at 6 hours) (Fig. II.6A, *anti A + oligo*), although this decline was not as severe as cells treated with CCCP (17.2% of control at 6 hours, Fig. II.6A). Interestingly, we still observed global GFP-parkin recruitment in U2OS:GFP-parkin

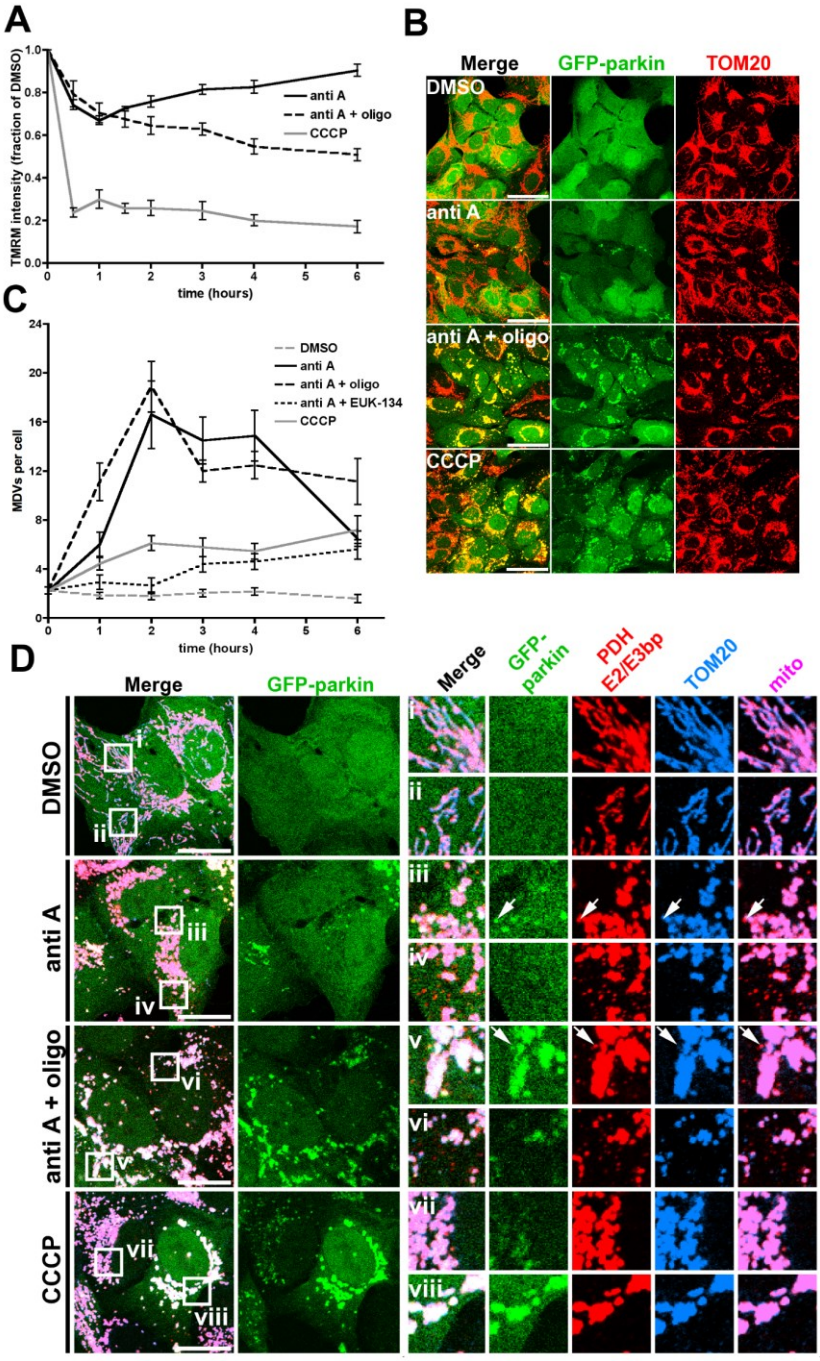


**Figure II.6**. *Parkin-dependent mitochondrial vesicle biogenesis is a rapid response triggered by ROS*. **A** Quantification of TMRM fluorescence by flow cytometry in U2OS:GFP-parkin cells treated with 25 µM antimycin A (anti A), 25 µM antimycin A and 10 µM oligomycin (anti A + oligo) and 20 µM CCCP for the indicated time, represented as a fraction of fluorescence intensity compared to DMSO-treated cells. Bars represent the mean±SEM (n = 3 experiments). **B** U2OS:GFP-parkin cells were treated with DMSO (DMSO), 25 µM antimycin A (anti A), 25 µM antimycin A and 10 µM oligomycin (anti A + oligo) or 20 µM CCCP (CCCP) for two hours, then fixed and immunostained for TOM20 (red). Scale bars, 50 microns. **C** Quantification of the total number of PDH E2/E3bp-positive/TOM20-negative structures in U2OS:GFP-parkin cells observed at various times for the indicated treatment. Bars represent the mean±SEM (n = 46 to 166 cells in 2 to 3 experiments; ns, not significant; *, p<.05; **, p<.01; ***, p<.001). **D** U2OS:GFP-parkin cells were treated with DMSO (DMSO), 25 µM antimycin A (anti A), 25 µM antimycin A and 10 µM oligomycin (anti A + oligo) or 20 µM CCCP (CCCP) for two hours, then fixed and immunostained for PDH E2/E3bp (red) and TOM20 (blue). A merged image of both mitochondrial markers (mito) is shown at the far right. Arrows indicate PDH E2/E3bp-positive/TOM20-negative structures colocalizing with GFP-parkin (green). Scale bars, 20 microns.

cells treated with both antimycin A and oligomycin for two hours (Fig. II.6B). This result supports previous data showing that perturbations in the $\Delta\psi_m$-dependent import machinery can have amplified effects on parkin recruitment to mitochondria (Greene et al., 2012), and is in line with a study demonstrating that $F_1F_0$ ATPase inhibition is sufficient to induce parkin recruitment in non-respiring cells (Suen et al., 2010).

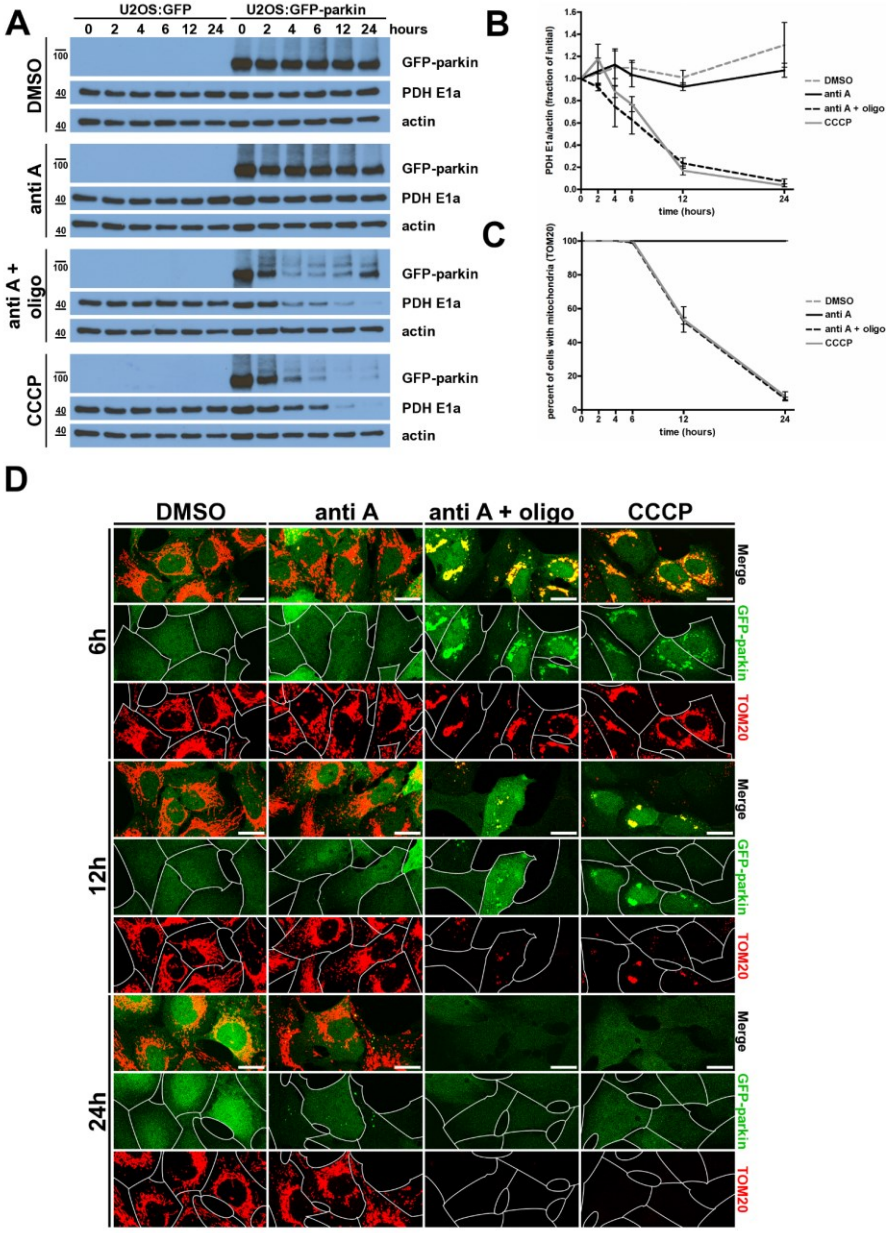


**Figure II.7**. *Cell-wide clearance of mitochondria via autophagy is triggered by depolarization and proceeds over a 24-hour time period.* **A** Representative immunoblot of whole-cell lysates from U2OS:GFP and GFP-parkin cells treated with DMSO, 25 μM antimycin A (anti A), 25 μM antimycin A with 10 μM oligomycin (anti A + oligo), or 20 μM CCCP for the indicated time period. **B** Quantification of PDH E1a signal intensity relative to that of actin in immunoblots from **A**. Bars represent the mean±SEM (n = 3 experiments). **C** Quantification of mitochondrial clearance in U2OS:GFP-parkin cells treated as in **A**, fixed and immunostained for TOM20. Data are shown as percentage of cells containing mitochondria, by TOM20 staining, visualized by fluorescence microscopy. Bars represent the mean±SEM (n = 3 experiments, with at least 85 cells quantified per condition, per experiment). **D** U2OS:GFP-parkin cells were treated as in A for the indicated time period, then fixed and immunostained for TOM20 (red). Cell boundaries are delineated in single-channel images. Scale bars, 20 microns.

We then addressed the kinetics of MDV formation by quantifying the total number of PDH E2/E3bp-positive/TOM20-negative structures over time in U2OS:GFP-parkin cells treated with DMSO, CCCP, antimycin A, antimycin A and oligomycin, and antimycin A and the ROS scavenger EUK-134 (Fig. II.6C and D). Both antimycin A and antimycin A combined with oligomycin triggered vesicle formation, which peaked at two hours (Fig. II.6C and D, *anti A* and *anti A + oligo*). Interestingly, the average number of vesicles per cell

decreased after this time, likely due to their lysosomal turnover, as well as decreased biogenesis owing to inhibition of forward electron flow through the ETC mitigating the amount of ROS generated by antimycin A (Fig. II.6A). Indeed, addition of EUK-134 decreased the observed number of antimycin A-induced MDVs, whereas incubation of cells with CCCP did not generate many vesicles (Fig. II.6C, *anti A + EUK-134* and *CCCP*), indicating that parkin MDV formation is a ROS-dependent process not induced by global depolarization.

Our observation that parkin-dependent MDV formation and turnover occur over a period of one to four hours (Fig. II.6C) contrasts this pathway with parkin-mediated mitochondrial turnover via autophagy, which occurs over a much larger scale of time (Geisler et al., 2010; Narendra et al., 2008). Indeed, depolarizing U2OS:GFP and GFP-parkin cells with CCCP or with antimycin A and oligomycin induced parkin-dependent mitophagy over a period of 4 to 24 hours, as assayed by the decrease in levels of several mitochondrial markers (Fig. II.7A and B and Fig. II.S7A). In contrast, no such effect was observed after treatment with antimycin A alone. Moreover, we observed cell-wide clearance of mitochondria in cells that had been depolarized for 12 hours, but not in cells treated with antimycin A alone (Fig. II.7C and D, Fig. II.S7B and C). These data support our view that parkin-dependent vesicle formation is a rapid response triggered by ROS, whereas turnover of the entire organelle is a relatively slow process initiated by depolarization.

## II.IV DISCUSSION

Parkin function has been implicated in both vesicular trafficking and mitochondrial quality control (Fallon et al., 2006; Fallon et al., 2002; Joch et al., 2007; Narendra et al., 2008; Trempe et al., 2009; Youle and Narendra, 2011). We recently identified MDV transport as a delivery

mechanism of selective, oxidized cargo to the late endosome (Soubannier et al., 2012a; Soubannier et al., 2012b). With this study, we greatly expand our understanding of this pathway with the identification of both parkin and PINK1 as core machinery required for the generation of double-membrane, matrix-containing MDVs. Thus, parkin and PINK1 sit at the crossroads of two distinct mitochondrial quality control mechanisms; the shuttling of selective cargo to lysosomes by autophagy-independent vesicular carriers, and the delivery of entire organelles to the autophagosome via autophagy. In contrast to mitophagy, parkin- and PINK1-dependent vesicles form in the absence of Drp1-dependent fission and are generated by ROS, not global mitochondrial depolarization. Additionally, these vesicles, whose formation can be induced by endogenous levels of parkin, preferentially incorporate certain endogenous mitochondrial cargo while excluding others, and target to lysosomes in a manner that is autophagy-independent. Kinetic studies demonstrate that much of the vesicle biogenesis and turnover occurs within the first few hours of treatment, whereas mitophagic clearance of mitochondria occurs over a period of days.

Both parkin-dependent mitophagy and vesicle formation may contribute to mitochondrial quality control, albeit it at differing levels. MDV formation *in vitro* shows that about 4% of the selected mitochondrial cargo can be sorted into vesicles per hour (Soubannier et al., 2012b), which is similar to the 6 to 12% of protein turnover generated by mitochondrial proteases in yeast (Augustin et al., 2005). Our data suggest that parkin may mediate the extraction of damaged respiratory proteins and chaperones by vesicular carriers that transport them to lysosomes for degradation, thus preserving the integrity of the whole mitochondrion at the steady state. If, however, these damaged proteins accumulate beyond a certain threshold, the dissipation of $\Delta\psi_m$ would trigger the autophagic engulfment and degradation by parkin-dependent mitophagy.

PINK1 may play a crucial role in the detection of this threshold. While CCCP triggers a massive PINK1 increase due to global import failure (Greene et al., 2012; Lazarou et al., 2012; Matsuda et al., 2010; Narendra et al., 2010b), antimycin A-induced ROS may cause PINK1 buildup at local or individual import channels. This interplay between local and global PINK1 accumulation may regulate the magnitudes of subsequent parkin recruitment and ubiquitin ligase activity. This latter point is intriguing, as while mitochondrial polyubiquitination has been implicated in autophagy (Chan et al., 2011; Geisler et al., 2010; Tanaka et al., 2010), we have previously shown that interactions between parkin and binding partners involved in endocytic trafficking and membrane curvature are regulated by monoubiquitination (Fallon et al., 2006; Joch et al., 2007; Trempe et al., 2009). Additionally, monoubiquitination and ubiquitin cycling are common themes in the endocytic system (d'Azzo et al., 2005). In our study, a role for ubiquitination in MDV formation is supported by the observation that vesicle formation is abolished upon expression of the ligase-dead parkin mutant.

Mounting evidence implicates the dysregulation of membrane trafficking pathways, as well as mitochondrial dysfunction, in the pathogenesis of PD. Recently, two exome sequencing analyses linked the retromer subunit Vps35 to PD (Vilarino-Guell et al., 2011; Zimprich et al., 2011). Vps35, along with Vps26 and Vps29, forms the so-called cargo recognition complex of the retromer, which cooperates with sorting nexins to mediate cargo selection and membrane curvature, respectively (Bonifacino and Hurley, 2008; Cullen and Korswagen, 2012). Interestingly, Vps35 localizes to mitochondria and is required for the formation of a population of mitochondrial vesicles that targets to peroxisomes (Braschi et al., 2010). Clearly, identification of the machinery regulating cargo selection and membrane dynamics, downstream of PINK1-dependent parkin recruitment to bud sites, requires further elucidation.

It is becoming evident that, in neurons, continued deregulation of mitochondrial quality control can lead to neurodegeneration (Rugarli and Langer, 2012). The existence of two distinct, yet complimentary, mitochondrial quality control pathways involving parkin and PINK1 is supported by a recent study in *Drosophila*, in which parkin/PINK1 mitochondrial quality control was shown to have both autophagy-dependent and -independent components at steady-state *in vivo* (Vincow et al., 2013). Additionally, Vincow *et al*. found that the turnover rates of individual subunits from the same multiprotein complex vary significantly, supporting our finding that different PDH subunits are sorted differentially into the MDV population that we observed.

In PD patients harbouring defects in parkin or PINK1, a loss of mitochondrial quality control mechanisms may lead to a buildup of mitochondrial damage, and ultimately mitochondrial dysfunction. This is supported by the observation that leukocytes collected from PD patients carrying parkin mutations have decreased mitochondrial respiratory capacity (Muftuoglu et al., 2004), similar to what has been observed in the *substantia nigra* of sporadic PD patients (Mann et al., 1992). Elucidating the precise role of PD-linked genes in the regulation of mitochondrial quality control, and how the loss of these processes may lead to the death of dopaminergic neurons, may point to specific degenerative mechanisms shared between genetic and sporadic forms of PD. Thus, further investigation of the exact role played by parkin and PINK1 in MDV biogenesis will enrich existing knowledge regarding mitochondrial quality control mechanisms and their relation to PD, and prospectively shed light on therapeutic possibilities regarding this debilitating, aging disease.

## II.V MATERIALS AND METHODS

*Reagents* – MG132 and epoxomicin were obtained from Boston Biochem. EUK-134 was purchased from Cayman Chemical. Tetramethylrhodamine methyl ester (TMRM) was purchased from Molecular Probes. All other reagents were purchased from Sigma-Aldrich.

*Plasmids* – pEGFP-C3 (Clontech), pEGFP-parkin, pECFP-Drp1$^{K38E}$ (Harder et al., 2004), pEGFP-LC3B and mito-DsRed2/pOCT-DsRed2 (Harder et al., 2004) were used in this study. pEGFP-parkin$^{R42P}$, pEGFP-parkin$^{K211N}$ and pEGFP-parkin$^{C431F}$ were generated from pEGFP-parkin$^{WT}$ using the QuikChange II site-directed mutagenesis kit (Agilent Technologies) according to the manufacturer's instructions.

*siRNA oligonucleotides – Stealth RNAi* siRNA oligonucleotides were purchased from Invitrogen. These included siRNA duplexes targeting Atg5 (5'-AACCUUUGGCCUAAGAAGAAAUGGA-3' (Chen et al., 2007)), beclin-1 (1:1 mixture of 5'-CAGUUUGGCACAAUCAAUAACUUCA-3' and 5'-CAGGAACUCACAGCUCCAUUACUUA-3' (Hoyer-Hansen et al., 2005)), Drp1 (5'-ACUAUUGAAGGAACUGCAAAAUAUA-3' (Taguchi et al., 2007)) and Rab9 (5'-AAGUUUGAUACCCAGCUCUUCCAUA-3' (Ganley et al., 2004)). Non-targeting siRNA was also obtained from Invitrogen. siRNA targeting parkin (ON-TARGETplus SMARTpool), PINK1 (ON-TARGETplus J-004030-07) and p97/VCP (ON-TARGETplus SMARTpool) were purchased from Dharmacon.

*Cell culture and transfection* – HeLa cells (ATCC), COS7 cells (ATCC), Atg5$^{+/+}$ and Atg5$^{-/-}$ MEFs (RIKEN BioResource Center, Ibaraki, Japan), and U2OS:GFP and GFP-parkin cells (Rob Screaton, University of Ottawa) were cultured in DMEM (Multicell) supplemented with 10% fetal

bovine serum, L-glutamine, penicillin and streptomycin at 37°C with 5% $CO_2$. HeLa cells and MEFs were plated on coverslips in 24-well plates (at 5 to $6x10^4$ cells per well). Cells were simultaneously infected with the $Drp1^{K38E}$-CFP adenovirus (MOI of 300) and transfected with 0.3 to 0.5 μg/ml of the indicated plasmid using jetPRIME transfection reagent (Polypus Transfection, Illkirch, France) according to the manufacturer's instructions. In the case of subsequent siRNA and DNA transfections, cells were first plated in 6-well or 10 cm plates, and transfected with 25 to 50 nM of each siRNA oligo using jetPRIME. At 24 hours post-transfection, cells were plated in 6-well plates or on coverslips in 24-well plates (at $2.5x10^5$ and 5 to $6x10^4$ cells per well, respectively). The following day (48 hours post-siRNA transfection), cells were transfected with DNA as indicated above. U2OS:GFP and GFP-parkin cells were plated for siRNA transfection, and then replated in 6-well plates or on coverslips in 24-well plates (at $2.5x10^5$ and $4x10^4$ cells per well, respectively) at 24 hours post-transfection. For the time-course experiment, U2OS:GFP-parkin cells were plated on coverslips in 24-well plates (at $8x10^4$ cells per well) the day prior to treatment.

*Cell treatments* – Unless otherwise specified, treatments were performed 24 hours after DNA transfection and/or 72 hours following siRNA transfection. Typically, cells were treated with 100 mU/ml glucose oxidase, 10 μM CCCP or 25 to 50 μM antimycin A for 90 to 120 minutes before fixation or lysis. In assays requiring lysosomal or proteasomal inhibition, cells were preincubated with 2 μM epoxomicin, 10 μM MG132, 50 nM bafilomycin $A_1$ or 10 μg/ml pepstatin A and 10 μg/ml E-64d for one hour, followed by an additional 90 minutes of the indicated inhibitor with antimycin A or DMSO. In the time-course experiment, cells were treated with DMSO, 25 μM

antimycin A, 25 μM antimycin A and 10 μM oligomycin, 25 μM antimycin A and 50 μM EUK-134, and 20 μM CCCP for the indicated time prior to fixation.

*Cell lysis and immunoblotting* – Cells were rinsed in ice-cold PBS and lysed in lysis buffer (20 mM Tris, 150 mM NaCl, 1 mM EDTA, 1 mM EGTA, 1% NP-40, 1% sodium deoxycholate, and a protease inhibitor cocktail [aprotinin, leupeptin, benzamidine and PMSF]) on ice. Protein content of the lysates was determined by BCA assay (Pierce/Thermo Scientific). 15 to 45 μg of protein were separated by SDS-PAGE and transferred to a nitrocellulose membrane. Primary antibodies were diluted in 5% milk or 3% BSA in PBS-Tween, and incubations with primary antibody were performed overnight at 4°C. Primary antibodies used in this study included anti-actin (Millipore, MAB1501, 1:100000), anti-Apg5 (Santa Cruz Biotechnology, sc-8667. 1:1000), anti-beclin-1 (BD Biosciences, 612113, 1:1000), anti-Drp1 (BD, 611113, 1:5000), anti-GAPDH (Novus Biologicals, NB300-320, 1:50000), anti-parkin (Santa Cruz, sc-32282, 1:2000 [endogenous parkin] or 1:100000 [ectopic parkin]), anti-PINK1 (Novus, BC100-494, 1:2500), anti-Rab9 (Abcam, ab2810, 1:1000), anti-TIM23 (BD, 611222, 1:40000), anti-TOM20 (Santa Cruz, sc-11415, 1:50000), anti-p97/VCP (Abcam, ab11433, 1:10000), anti-PDH E1a (Abcam, ab110330, 1:5000), anti-TRAP1 (Abcam, ab2721, 1:5000), anti-α-tubulin (Santa Cruz, sc-23948, 1:50000) and anti-VDAC1 (Abcam, ab14734, 1:40000). HRP-conjugated secondary antibodies were purchased from Jackson ImmunoResearch Laboratories, and were diluted in 5% milk in PBS-Tween. Incubations with secondary antibodies were performed at room temperature for one hour. Western Lightning ECL and Plus-ECL kits (PerkinElmer) were used to detect protein bands according to the manufacturer's instructions.

*Immunofluorescence* – Following treatments, cells were fixed in 6% paraformaldehyde and quenched with 50 mM $NH_4Cl$ in PBS. Cells were then permeabilized in PBS containing 0.25% Triton X-100 and blocked in 10% FBS in PBS. Primary antibodies were diluted in PBS containing 5% FBS. Primary antibodies used in this study included anti-COXI (Abcam, ab14705, 1:50), anti-cytochrome c (BD, 556432, 1:500), anti-PDH E1a (Abcam, ab110330, 1:50), anti-PDH E2/E3bp (Abcam, ab110333, 1:1000), anti-TIM23 (BD, 611222, 1:50), anti-TOM20 (Santa Cruz, sc-11415, 1:1000) and anti-TRAP1 (Abcam, ab2721, 1:100). Alexa Fluor 555- and 647-conjugated donkey anti-mouse and anti-rabbit secondary antibodies were purchased from Molecular Probes, and a DyLight 405-conjugated donkey anti-rabbit secondary antibody was purchased from BioLegend. Both primary and secondary antibody incubations were performed at room temperature for one hour. In certain cases, coverslips were counterstained with Hoescht 33342 (Molecular Probes) prior to mounting on glass slides using Aqua Poly/Mount (Polysciences Inc.).

*Confocal microscopy and vesicle quantification* – Confocal images (~0.8 μm-thick slices) were acquired either on an LSM 510 Meta confocal microscope (Zeiss) through a 100X, 1.4 NA objective or on an LSM 710 (Zeiss) through either a 40X, 1.3 NA or a 63X, 1.4 NA objective using excitation wavelengths of 405 nm, 458nm, 488 nm, 543 nm and 633 nm. Image files were analyzed using ImageJ (NIH, Bethesda, MD). Vesicles were identified by eye, based on cargo selectivity (i.e. the presence of one cargo and the absence of another) and quantified in two to three independent, blinded experiments. Typically, vesicles within 20 to 50 cells were counted per experiment.

*Determination of $\Delta\psi_m$ by fluorescence-activated cell sorting* – To quantitatively measure $\Delta\psi_m$, we modified a protocol established by Chazotte (Chazotte, 2011). U2OS:GFP-parkin cells were plated in 12-well plates (at $1.3x10^5$ cells per well) 12 hours prior to incubation with TMRM. Cells were then pulsed with 600 nM TMRM diluted in culture medium for 30 minutes, rinsed with PBS and incubated in culture medium containing 150 nM TMRM. All treatments were performed in the presence of 150 nM TMRM. Following treatment with various inhibitors, cells were trypsinized for 2 to 3 minutes at 37°C, collected in culture medium without TMRM and then kept on ice. Fluorescence-activated cell sorting measurements were performed with a FACSCalibur flow cytometer (BD Biosciences). Data was analyzed using FlowJo software (Tree Star Inc., Ashland, OR).

*Statistical analysis* – Histograms were generated from the mean number of vesicles per cell, obtained from two to three independent experiments in which the MDVs in at least 20 cells per experiment were counted. Error bars represent the mean±SEM, which was calculated using the total number of cells quantified as the n-value. Statistical significance was determined by one- or two-way ANOVA followed by a Bonferroni post-hoc analysis (Prism 5, GraphPad Software, La Jolla, CA). Differences were considered significant if $p<0.05$.

## II.VI ACKNOWLEDGEMENTS

We thank Miguel A. Aguileta and Marty Loignon (Montreal Neurological Institute) for the generation of the pEGFP-parkin mutants and technical assistance with the collection and analysis of FACS data, respectively. The Rab9 antibody was a gift from Peter S. McPherson (McGill University). The pEGFP-parkin and pEGFP-LC3 plasmids were provided by Michael G.

Schlossmacher (University of Ottawa) and Ron R. Kopito (Stanford), respectively. The $Atg5^{+/+}$ and $Atg5^{-/-}$ MEFs were provided by Noboru Mizushima (Tokyo Medical and Dental University). The U2OS:GFP and GFP-parkin cell lines were a gift from Rob Screaton (University of Ottawa). This work was supported by the Brain Repair Program from Neuroscience Canada as well as Operating Grants from the Canadian Institutes of Health Research (CIHR) to E.A.F. and H.M.M. G.L.M. has received support from the Fonds de la recherche du Québec – Santé (FRQS), Parkinson Society Canada, and the CIHR. E.A.F. is a Chercheur National of the FRQS.

## II.VII SUPPLEMENTARY FIGURES

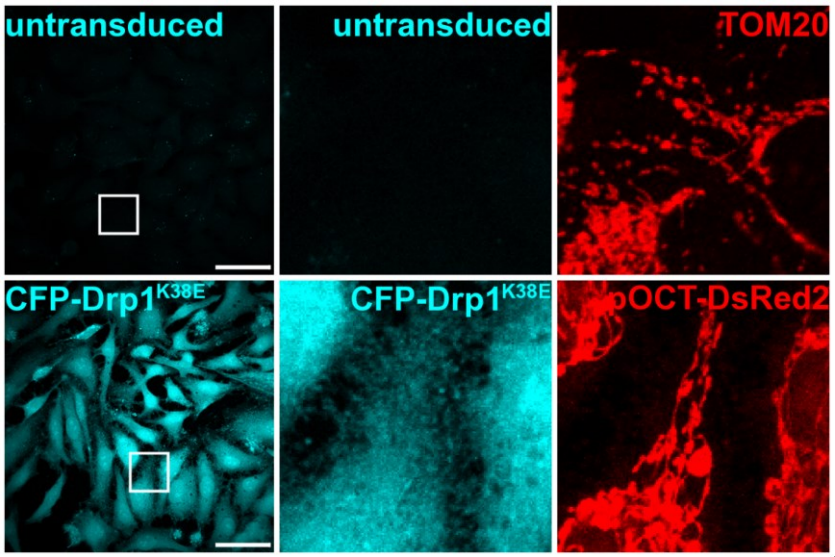


**Figure II.S1**. *Expression of CFP-Drp1$^{K38E}$ in HeLa cells*. Representative confocal images of HeLa cells left untransduced (top) or infected with adenovirus encoding CFP-Drp1$^{K38E}$ (bottom) and fixed 24 hours post-infection. Mitochondrial morphology was visualized by endogenous TOM20 immunostaining (red, top) or localization of ectopically-expressed pOCT-DsRed2 (red, bottom). Scale bars, 50 microns.

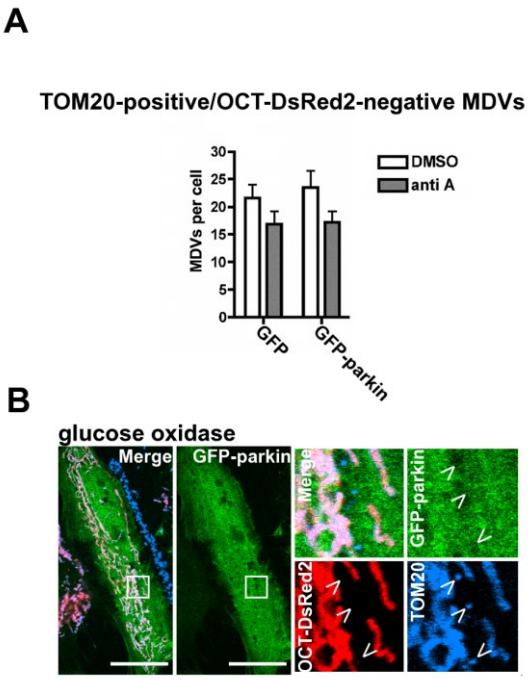


**Figure II.S2**. *Parkin does not associate with TOM20-positive MDVs*. **A** Quantification of the number of TOM20-positive/OCT-DsRed2-negative MDVs from GFP and GFP-parkin expressing cells from Fig. II.1C. Bars represent the mean±SEM. **B** HeLa cells expressing GFP-parkin (green), OCT-DsRed2 (red) and CFP-Drp1$^{K38E}$ were treated with 100 mU/ml glucose oxidase (GO) for two hours before fixation. Open arrowheads indicate TOM20-positive/OCT-DsRed2-negative structures that do not colocalize with GFP-parkin. Scale bars, 30 microns.

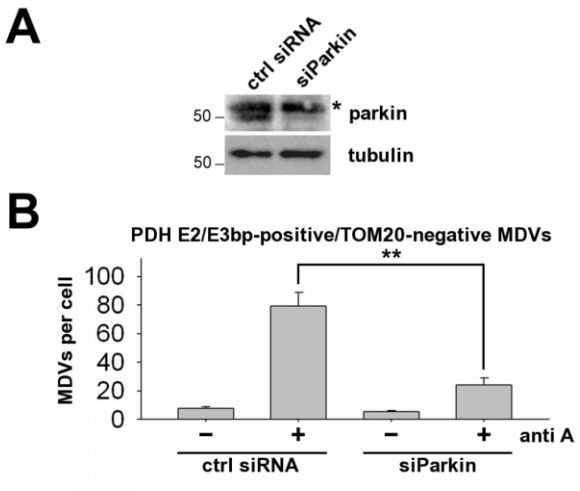


**Figure II.S3**. *Loss of parkin abolishes MDV formation in COS7 cells*. **A** Representative immunoblot of whole-cell lysates from COS7 cells transfected with non-targeting siRNA or siRNA targeting parkin (siParkin). The asterisk indicates a non-specific band. **B** Quantification of the total number of PDH E2/E3bp-positive/TOM20-negative structures from COS7 cells treated with or without 50 μM antimycin A for two hours prior to fixation. Bars represent the mean±SEM (n = at least 45 cells over 3 experiments; ns, not significant; *, p<.05; **, p<.01; ***, p<.001).

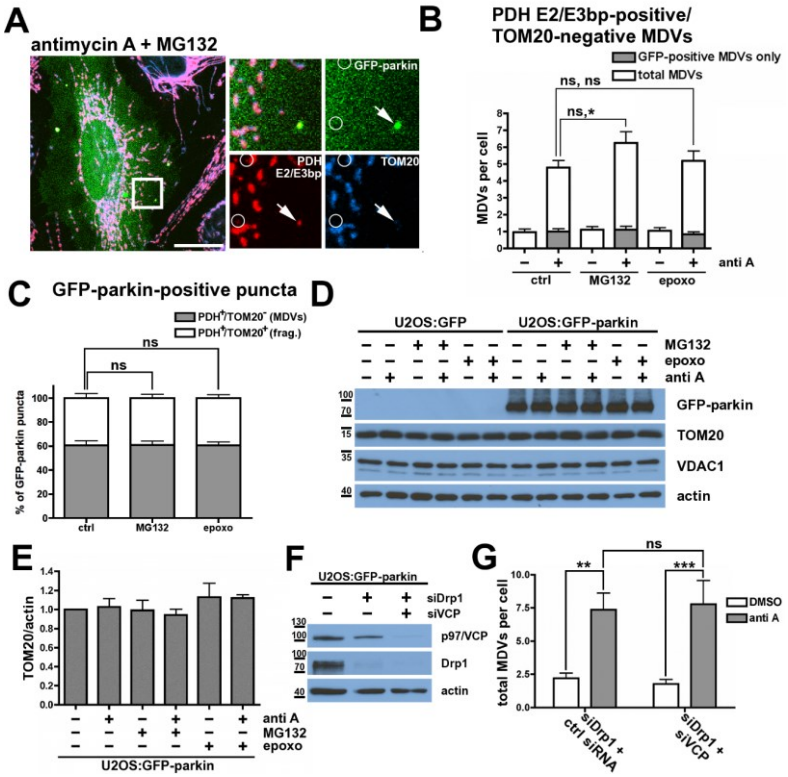


**Figure II.S4**. *Exclusion of TOM20 on MDVs does not occur through p97/VCP-dependent proteasomal degradation*. **A** HeLa cells transfected with siRNA targeting Drp1 and transiently expressing GFP-parkin (green) were pretreated for 30 minutes with 10 μM MG132 prior to treatment with 25 μM antimycin A (with MG132) for 90 minutes. After fixation, samples were immunostained against TOM20 (blue) and PDH E2/E3bp (red). PDH E2/E3bp-positive/TOM20-negative MDVs colocalizing

with GFP-parkin (arrows) or not (circles) are indicated. Scale bars, 20 microns. **B** Quantification of PDH E2/E3bp-positive/TOM20-negative structures from HeLa cells treated with antimycin A and 10 μM MG132 or 2 μM epoxomicin (epoxo); both total number (white bars) and the number colocalizing with GFP-parkin (gray bars) are indicated. Bars represent the mean±SEM. P-values are given first for GFP-/GFP-parkin-positive vesicles, then for total vesicle number (n = 61 to 73 cells in 3 experiments; ns, not significant; *, p<.05; **, p<.01; ***, p<.001). **C** Quantification of the ratio of parkin-positive MDVs (PDH E2/E3bp-positive/TOM20-negative, gray bars) to fragments (PDH E2/E3bp- and TOM20-positive, white bars) of all cells quantified in B (ns, not significant). **D** Representative immunoblot of whole-cell lysates from U2OS:GFP and GFP-parkin cells treated with antimycin A and proteasomal inhibitors depicting total TOM20 levels. VDAC1 is used as a mitochondrial loading control. **E** Quantification of TOM20 signal intensity relative to that of actin in immunoblots from D. Bars represent the mean±SEM (n = 3 experiments). **F** Representative immunoblot of whole-cell lysates from U2OS:GFP-parkin cells transfected with non-targeting siRNA, siRNA targeting Drp1 (siDrp1) and/or p97/VCP (siVCP). **G** Quantification of the total number of PDH E2/E3bp-positive/TOM20-negative structures from U2OS:GFP-parkin cells (transfected with the indicated siRNA) treated with 25 μM antimycin A for 90 minutes. Bars represent the mean±SEM (n = 48 to 62 cells in 2 experiments; ns, not significant; *, p<.05; **, p<.01; ***, p<.001).

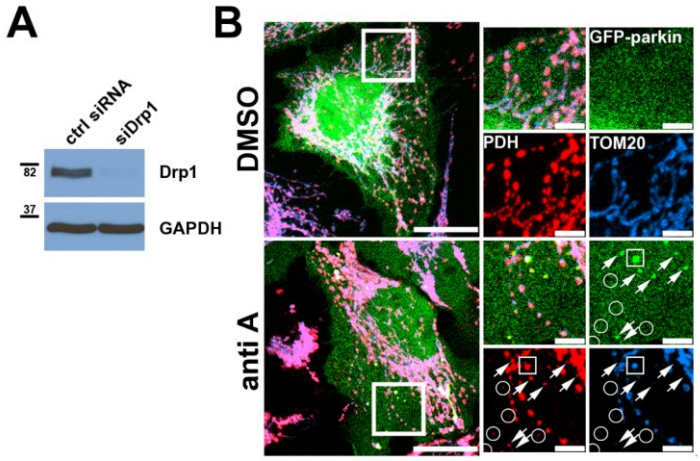


**Figure II.S5**. *Silencing of Drp1 in HeLa cells*. **A** Representative immunoblot of whole-cell lysates from HeLa cells transfected with non-targeting siRNA or siRNA targeting Drp1 (siDrp1). **B** GFP-parkin-expressing HeLa cells transfected with siRNA targeting Drp1 were treated with 25 μM antimycin A (anti A) or DMSO (DMSO) for 90 minutes, then fixed and immunostained against PDH E2/E3bp (red) and TOM20 (blue). PDH E2/E3bp-positive/TOM20-negative MDVs colocalizing with GFP-parkin (arrows) or not (circles) are indicated. Scale bars, 20 and 5 microns.

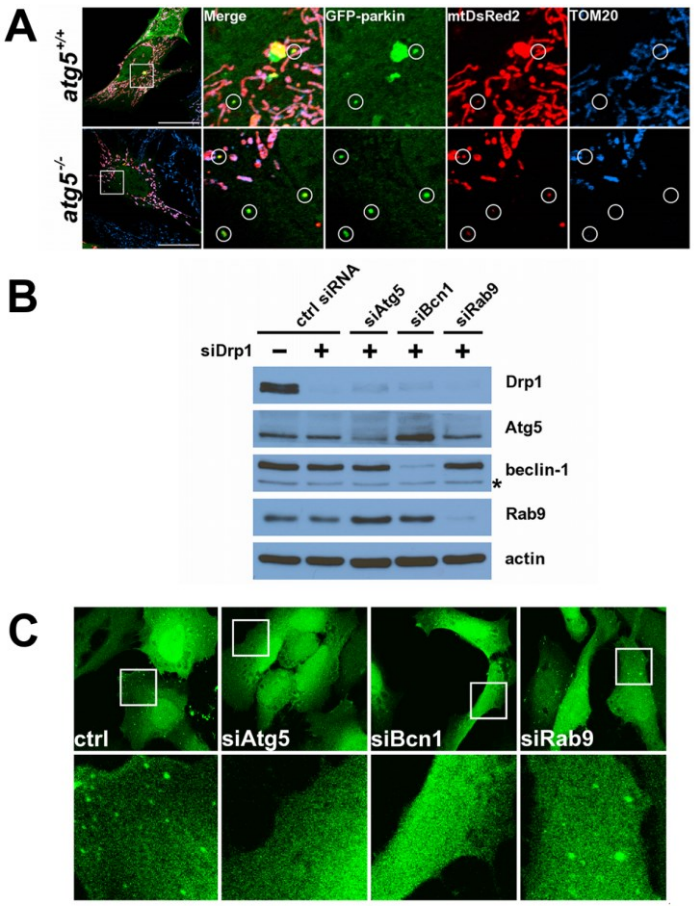


**Figure II.S6**. *Silencing of genes involved in autophagy in HeLa cells*. **A** $Atg5^{+/+}$ and $Atg5^{-/-}$ mouse embryonic fibroblasts (MEFs) were transfected with GFP-parkin (green), OCT-DsRed2 (red, mtDsRed2) and CFP-$Drp1^{K38E}$, treated with 40 μM antimycin A for two hours, fixed and immunostained against TOM20 (blue). Circles indicate OCT-DsRed2-positive/TOM20-negative MDVs colocalizing with GFP-parkin. Scale bars, 30 microns. **B** Representative immunoblots of whole-cell lysates depicting efficiency of siRNA-mediated knockdown of autophagy-related genes in HeLa cells. The asterisk indicates a non-specific band. **C** Representative images of HeLa cells transfected with GFP-LC3 (green) and siRNA targeting Drp1 and the indicated autophagy-related gene (or control), fixed 24 hours after plasmid transfection. Boxes highlight (lack of) GFP-LC3 clustering in untreated cells.

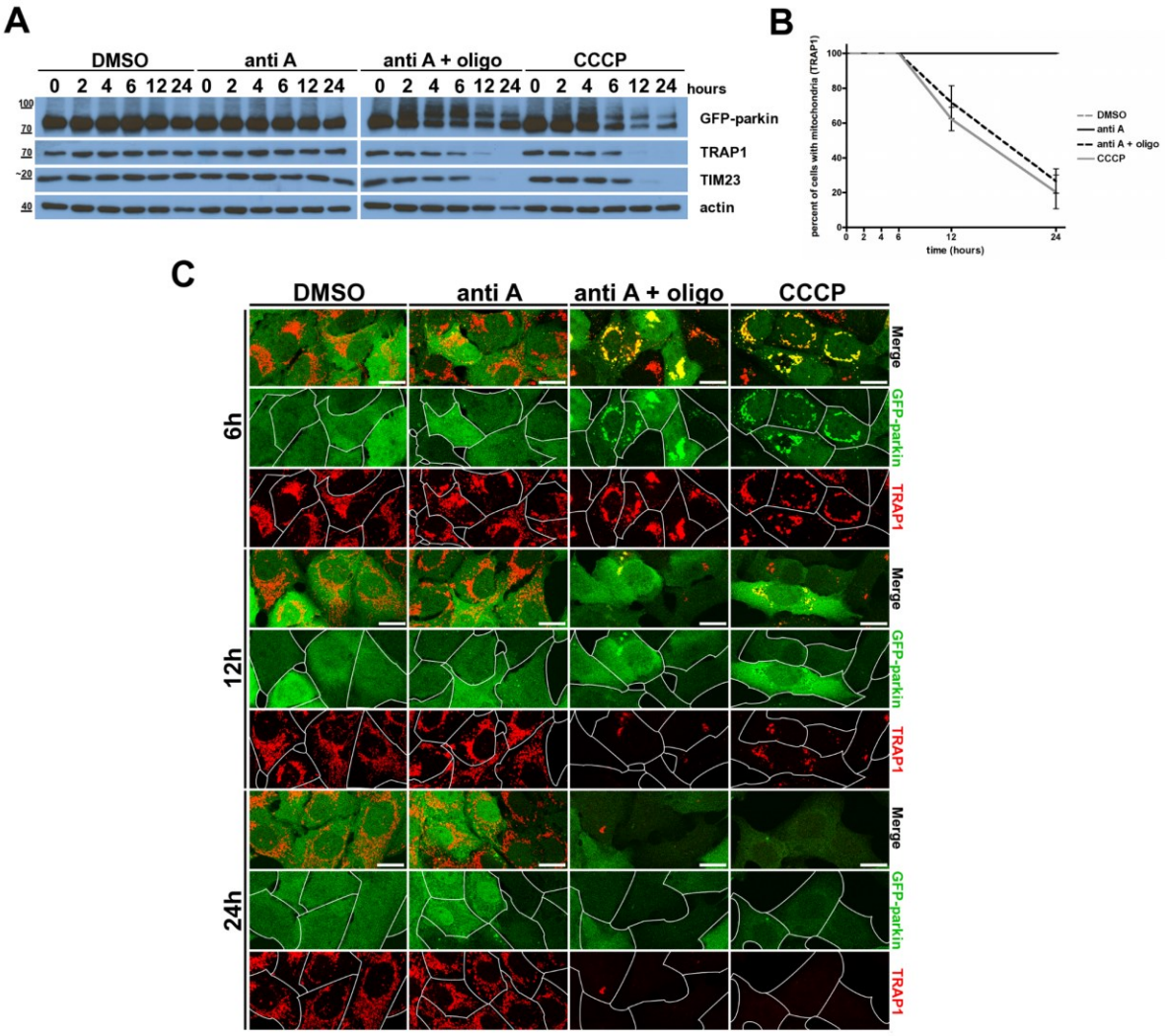


**Figure II.S7**. *Parkin-dependent mitophagy degrades mitochondria over 24 hours*. **A** Representative immunoblot of whole-cell lysates from U2OS:GFP-parkin cells treated with DMSO, 25 μM antimycin A (anti A), 25 μM antimycin A with 10 μM oligomycin (anti A + oligo), or 20 μM CCCP for the indicated time period. **B** Quantification of mitochondrial clearance in U2OS:GFP-parkin cells treated as in **A**, fixed and immunostained for TRAP1. Data are shown as percentage of cells containing mitochondria, by TRAP1 staining, visualized by fluorescence microscopy. Bars represent the mean±SEM (n = 3 experiments, with at least 85 cells quantified per condition, per experiment). **C** U2OS:GFP-parkin cells were treated as in **A** for the indicated time period, then fixed and immunostained for TRAP1 (red). Cell boundaries are delineated in single-channel images. Scale bars, 20 microns.

## II.VIII INTEGRATIVE SUMMARY

The work detailed in Chapter II shows that parkin and PINK1 play a critical role in the generation of a class of MDVs that transports components of the mitochondrial matrix and ETC to the lysosome for turnover. This study contains one of the first descriptions of core machinery involved in an MDV pathway, demonstrates a role for parkin and PINK1 in mitochondrial quality control in addition to mitophagy and implies that the parkin/PINK1 pathway surveys mitochondrial health across a spectrum of damage (Fig. II.8). This work underscores the importance of studying PINK1 and parkin function under more physiological conditions (although antimycin A is still a pharmacological inhibitor) and reveals a new facet of the relationship between parkin/PINK1 and mitochondrial biology. Of further interest is the notion that PINK1 and parkin are involved in the formation of $PDH^+$ vesicles, but not the $TOM20^+$ subpopulation (Fig. II.S2). Moreover, $MAPL^+$ vesicles are likely parkin-independent, as this pathway was first described in HeLa

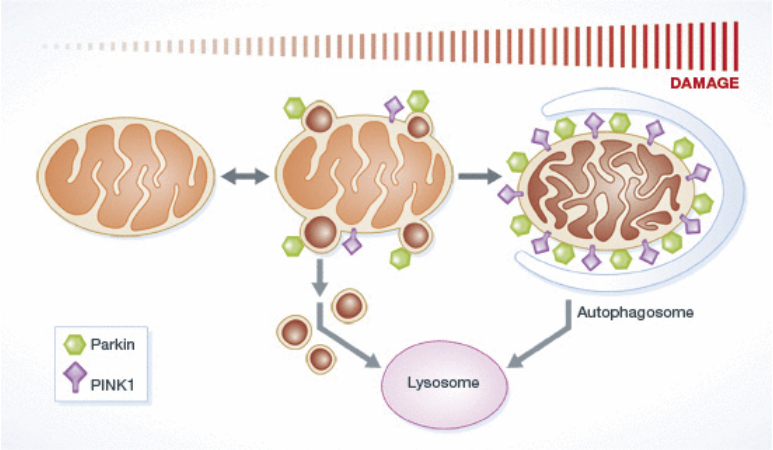


**Figure II.8**. *Parkin and PINK1 function in MDV formation and mitophagy*. Increasing mitochondrial damage triggers a differential PINK1/parkin quality control mechanism, with MDVs acting as a rapid, "first-line" response. This figure was reproduced from *EMBO J.*, 33(4), based on the original by the author.

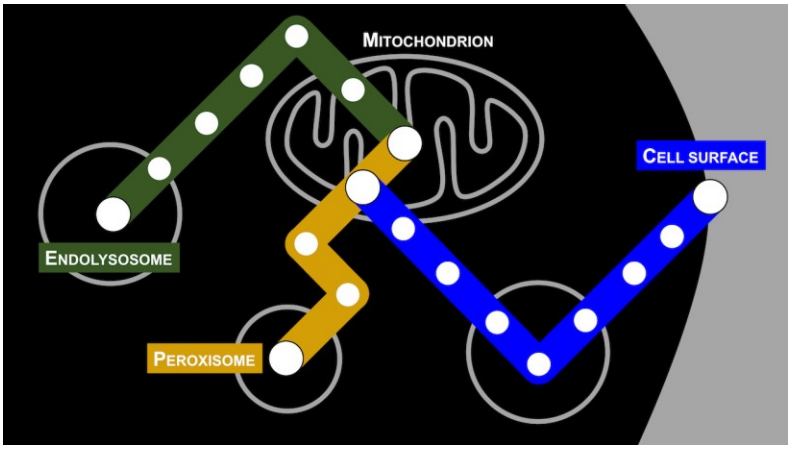


**Figure II.9**. *How do MDVs know where to go?*. Diagram highlighting the need for an understanding of mechanisms governing MDV targeting.

cells (which lack endogenous parkin) (Denison et al., 2003; Neuspiel et al., 2008). An emergent property of MDVs that stems from these observations is that distinct populations must target to specific destinations in pathway-specific manners (Fig. II.9). Thus, mechanisms intrinsic to these individual populations (i.e. $PDH^+$, $TOM20^+$, $MAPL^+$, etc.) must confer the selectivity of their targeting. This topic is addressed in Chapter III.

Chapter III

# SYNTAXIN-17 DELIVERS PINK1/PARKIN-DEPENDENT MITOCHONDRIAL VESICLES TO THE ENDOLYSOSOMAL SYSTEM

The following Chapter originally appeared as an Article in the *Journal of Cell Biology*:

**McLelland GL**, Lee SA, McBride HM, Fon EA (2016). Syntaxin-17 delivers PINK1/parkin-dependent mitochondrial vesicles to the endolysosomal system. *J. Cell Biol*. 214(3):275-291, doi:10.1083/jcb.201603105. PMID: 27458136

## III.I ABSTRACT

Mitochondria are considered autonomous organelles, physically separated from endocytic and biosynthetic pathways. However, recent work uncovered a PINK1/parkin-dependent vesicle transport pathway wherein oxidized or damaged mitochondrial content are selectively delivered to the late endosome/lysosome for degradation, providing evidence that mitochondria are indeed integrated within the endomembrane system. Given that mitochondria have not been shown to employ canonical SNARE machinery for fusion, the mechanism by which mitochondrial-derived vesicles (MDVs) are targeted to the endosomal compartment has remained unclear. In this study we identify syntaxin-17 as a core mitochondrial SNARE required for the delivery of stress-induced PINK1/parkin-dependent MDVs to the late endosome/lysosome. Syntaxin-17 remains associated with mature MDVs and forms a ternary SNARE complex with SNAP29 and VAMP7 to mediate MDV-endolysosome fusion in a manner dependent upon the HOPS tethering complex. Syntaxin-17 can be traced to the last eukaryotic common ancestor, hinting that the removal of damaged mitochondrial content may represent one of the earliest vesicle transport routes in the cell.

## III.II INTRODUCTION

Proper mitochondrial function is paramount to neuronal survival, and deficits in mitochondrial activity may underlie neurodegenerative diseases such as Parkinson's disease (PD). Mutations in *PARKIN* and *PINK1* cause recessive forms of PD (Kitada et al., 1998; Valente et al., 2004), and these genes – encoding parkin, an E3 ubiquitin ligase, and PINK1, a mitochondrially-targeted protein kinase – primarily function in the quality control of mitochondria; a collection of pathways regulating the removal of damaged proteins, lipids, and organelles from the mitochondrial reticulum to ensure its proper activity (Ryan et al., 2015). In one such mechanism,

parkin is recruited to depolarized mitochondria by PINK1, where it initiates their autophagic turnover (termed "mitophagy") (Ryan et al., 2015; Yamano et al., 2016). Alternatively, in response to oxidative stress, parkin and PINK1 deliver selective, oxidized components of the mitochondrial matrix and inner membrane to the late endosome for turnover via a class of mitochondrial-derived vesicles (MDVs) (McLelland et al., 2014; Soubannier et al., 2012a; Soubannier et al., 2012b). Whereas mitophagy describes the engulfment of a fusion-incompetent mitochondrial fragment within the autophagosome, PINK1-/parkin-dependent MDVs are mechanistically distinct in that vesicles containing highly-selected mitochondrial cargo bud off mitochondria independently of the core mitochondrial fission GTPase Drp1, and their turnover does not require canonical autophagy machinery (McLelland et al., 2014; Soubannier et al., 2012a). Indeed, evidence from parkin and PINK1 null flies has supported a role for these proteins in both mitophagy and selective mitochondrial protein turnover *in vivo* (Vincow et al., 2013). Moreover, a recent study in *Drosophila* revealed a strong genetic interaction between parkin and Vps35 (Malik et al., 2015), another PD-linked gene involved in the generation of other MDV populations (Braschi et al., 2010; Wang et al., 2016c), suggesting that defective MDV transport may play a role in PD pathogenesis.

While parkin and PINK1 activity are required for the generation of oxidative stress-triggered MDVs, the mechanism by which this vesicle population reaches the lysosome remains poorly understood. As mitochondrial vesicles are membrane-bound structures, a role for membrane fusion in turnover seems apparent (Sugiura et al., 2014). Soluble NSF attachment protein receptors (SNAREs) mediate most membrane fusion events in cells – mitochondrial membrane fusion being one exception – and associate via the formation of a four-helix bundle between their helical SNARE domains (designated Qa, Qb, Qc and R based on the amino acid present at the so-called zero layer) (Fasshauer et al., 1998; Sutton et al., 1998), which zipper

progressively towards the membrane-bound end of the complex in order to bring membranes together to fuse (Gao et al., 2012; Hanson et al., 1997; Li et al., 2014). As the compartmental specificity of fusion events is encoded by the SNAREs on the vesicle and target membrane (Sollner et al., 1993), the regulation of targeting and turnover of MDVs by SNARE-dependent membrane fusion presents itself as an intriguing and logical possibility. However, given the endosymbiotic origin of mitochondria, as well as the established roles of large GTPases involved in both homotypic and heterotypic mitochondrial fusion and tethering events, a role for SNAREs in MDV targeting and fusion is not a foregone conclusion.

Here, we demonstrate that syntaxin-17 (Stx17), a Qa-SNARE, is involved in the targeting of parkin/PINK1-generated MDVs to endolysosomal compartments. We observe the loading of Stx17 onto vesicles that were budded from mitochondria *in vitro*, and the enrichment of Stx17 on mitochondrial foci and nearby fully-formed vesicles in cells. Loss of Stx17 abrogates lysosomal targeting of MDVs and prevents pathway processivity. Stx17 assembles into a ternary SNARE complex with SNAP29 and VAMP7 to mediate MDV-endolysosome fusion, which can be disrupted using structure-based mutations. Strikingly, these SNAREs are dispensable for mitophagy, implying divergent targeting mechanisms in different parkin/PINK1 mitochondrial quality control pathways. These results demonstrate that MDVs are integrated within *bone fide* cellular membrane trafficking pathways, and identify machinery required for MDV turnover.

## III.III RESULTS

### III.III.i *Syntaxin-17 is biochemically enriched on mitochondrial-derived vesicles*

We sought to identify the manner by which oxidative stress-triggered MDVs target to the lysosome, reasoning that this turnover pathway – in a similar manner to lysosomally-directed

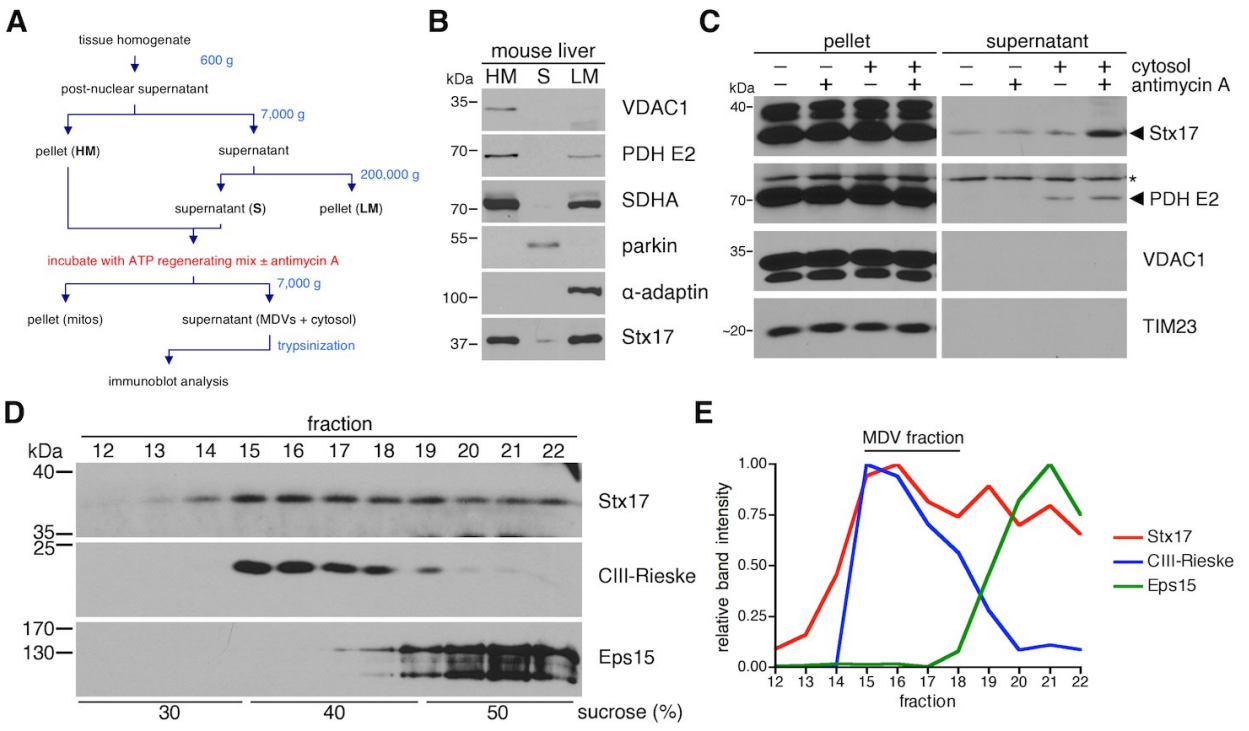


**Figure III.1**. *Stx17 is biochemically enriched on MDVs*. **A** Flowchart of cell-free MDV budding assay. See Materials and Methods for complete details. **B** Mouse liver was fractionated according to Materials and Methods, and 40 µg heavy membrane (HM), soluble (S) and light membrane (LM) fractions were separated by SDS-PAGE and analyzed by immunoblotting. **C** Trypsinized supernatants and pellets from *in vitro* MDV budding assays incubated in the presence of cytosol and/or 50 µM antimycin A (anti A) were separated, along with the reaction pellets (mitochondria), by SDS-PAGE and analyzed by immunoblotting. The asterisk indicates a non-specific band. **D** A large-scale budding reaction (incubated with cytosol and 50 µM antimycin A) was fractionated over a discontinuous sucrose gradient, separated by SDS-PAGE and analyze by immunoblotting. **E** Intensity profiles for the proteins probed for in **D**, expressed as a fraction of their maximum intensity.

endosomal transport – required SNARE-dependent targeting to reach the endolysosomal membrane. A portion of the Qa-SNARE syntaxin-17 (Stx17) localizes to mitochondria, in addition to the endoplasmic reticulum (ER) (Arasaki et al., 2015; Hamasaki et al., 2013; Hung et al., 2014). Moreover, Stx17 can form complexes with target R-SNAREs associated with lysosomes and late endosomes (Itakura et al., 2012b), and its assembly into these complexes is metabolically-regulated (Guo et al., 2014), making it a prime candidate for MDV-endolysosome fusion.

We began by testing whether Stx17 – which is unique among SNAREs with its two C-terminal transmembrane domains (Kloepper et al., 2008) – is biochemically enriched on MDVs, turning to *in vitro* MDV reconstitution assays (outlined in Fig. III.1A) that we adapted from

previous work (Soubannier et al., 2012b). We fractionated mouse liver into heavy membranes (HM; enriched in the mitochondrial proteins VDAC1, PDH E2 and SDHA), a soluble fraction (S; containing cytosol) and light membranes (LM; containing microsomes with some mitochondrial contamination) (Fig. III.1B). Endogenous Stx17 was evenly enriched in both membrane fractions (Fig. III.1B), as expected (Hamasaki et al., 2013). We then incubated the heavy membranes in the presence or absence of cytosol (fraction S) and/or antimycin A (a mitochondrial complex III inhibitor that causes oxidative stress; see Fig. III.1A or, for a detailed description of the assay, see *Materials and Methods*), as we have previously shown that mitochondrial cargo can be extracted from the HM fraction in a manner dependent on ROS generation and cytosolic components *in vitro* (Soubannier et al., 2012b). We then pelleted the mitochondria and trypsinized the MDV-containing supernatant; MDV cargoes remain trypsin-protected as they are contained within vesicles ((Soubannier et al., 2012b). Immunoblot analysis of trypsinized supernatants revealed that Stx17 was extracted from the mitochondrial fraction, along with PDH E2 (an established MDV cargo (McLelland et al., 2014)), in a cytosol- and antimycin A-dependent manner (Fig. III.1C). VDAC1 and TIM23, which do not enrich with this MDV population *in vitro* (Soubannier et al., 2012b) or in cells (McLelland et al., 2014), respectively, were not present in these supernatants, as expected (Fig. III.1C). Although Stx17, likely present on the outer MDV membrane, was available to trypsin digestion, its proteolytic protection in our assay was not surprising as SNAREs are often resistant to trypsin (Lawrence and Dolly, 2002a; Lawrence and Dolly, 2002b; Poirier et al., 1998).

To ensure that Stx17 was truly enriched on membranous structures, we fractionated the supernatant from the reaction containing both antimycin A and cytosol (not treated with trypsin) on a discontinuous sucrose gradient. We have previously shown that double-membrane MDVs (the population generated by antimycin A) enrich at the 30/40% sucrose interface (Soubannier et

al., 2012b). As expected, immunoblotting our fractionated sample showed an accumulation of the Rieske subunit of complex III (CIII-Rieske) around the 30/40% interface, while the soluble protein Eps15 remained at the bottom of the gradient, where the reaction supernatant was initially loaded (Fig. III.1D and E, blue and green lines for CIII-Rieske and Eps15, respectively). While a portion of Stx17 also remained at the bottom of the gradient, most Stx17 co-fractionated with the MDVs (Fig. III.1D and E, red line), corroborating our earlier results with trypsinized supernatants (Fig. III.1C). Thus, Stx17 is enriched on double-membrane MDVs generated *in vitro*.

III.III.ii *Syntaxin-17 is recruited to nascent vesicles prior to scission*

We next followed the dynamics of YFP-Stx17 by live-cell confocal microscopy in COS7 cells in order to determine the manner through which this SNARE was recruited to MDVs. We grew these cells in media containing galactose as a carbon source, as this increases steady-state MDV biogenesis through increased mitochondrial respiration (Soubannier et al., 2012a); unless explicitly stated, all cell-based experiments were performed under these bioenergetic conditions. In MitoTracker-labeled COS7 cells, steady-state formation and subsequent lateral disassociation of diffraction-limited YFP-Stx17 puncta on mitochondrial tubules were seen (Fig. III.2A, the white arrowheads indicate a ~0.3 micron-wide structure). We also observed much larger (>0.5 micron), stationary Stx17 structures adjacent to mitochondria (for example, the larger, brighter Stx17 structure in Fig. III.2A) that possibly corresponded to autophagosomes, as these structures form adjacent to mitochondria (Cheng et al., 2015; Hamasaki et al., 2013; Itakura et al., 2012b). Focusing on the smaller Stx17 structures on mitochondria, we were able to observe a buildup of YFP-Stx17 signal (depicted in Fig. III.2B) on the mitochondrial tubule prior to lateral release (Fig. III.2A, rapid release occurs between frames “+12 s” and “+13 s”). We have previously observed

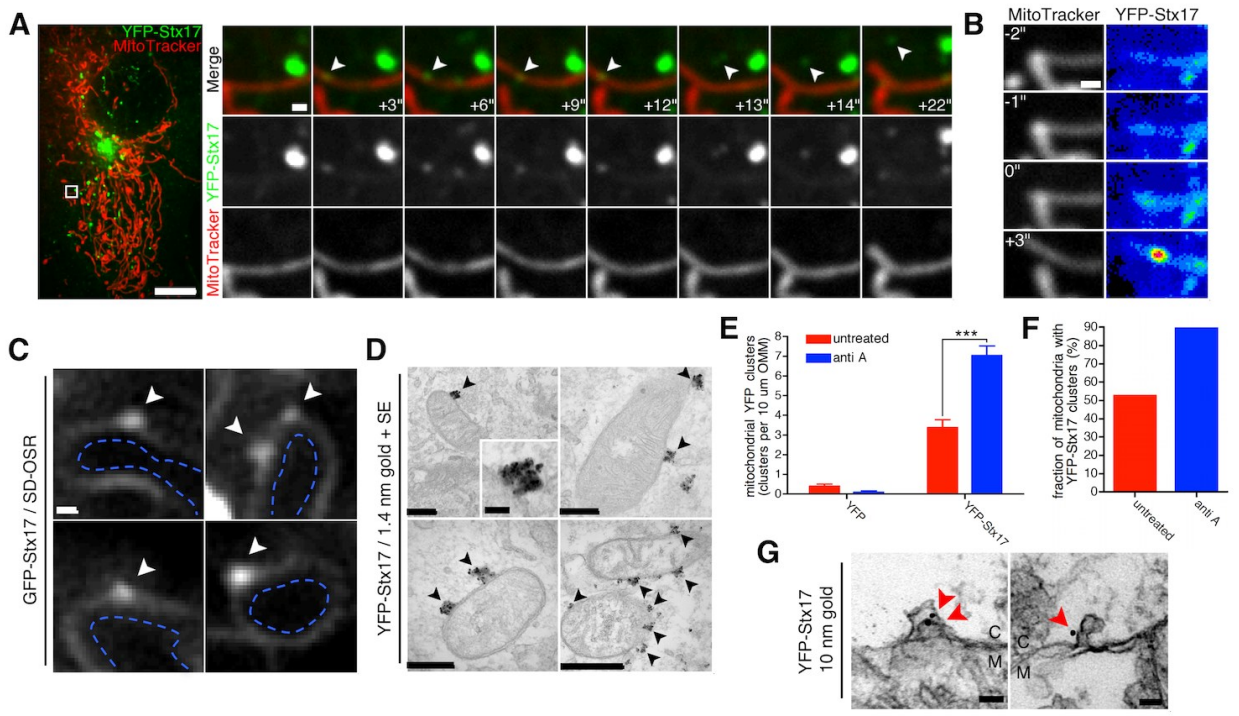


**Figure III.2**. *Dynamics and ultrastructure of mitochondrial Stx17 foci*. **A** Live-cell observation of Stx17 vesicle formation and release in an untreated COS7 cell expressing YFP-Stx17 (green, 800 ms exposure time) and stained with MitoTracker Deep Red FM (red, 50 ms exposure time) by spinning disc confocal microscopy. Elapsed time is indicated in the bottom-right of each merged image. The white arrowhead indicates a Stx17$^+$ structure that forms on and subsequently dissociates from the tubule. Scale bars, 10 (full image) and 0.5 (zoom-in) microns. **B** Stx17 concentrates on the tubule prior to release. In the same time series from **A**, YFP-Stx17 signal (right) concentrates on the MitoTracker-labeled tubule (left). The YFP-Stx17 image is represented as a heat map, and the brightness/contrast has been adjusted (from **A**) so that the fully-formed structure is almost saturating and the concentration of signal can be clearly seen. Scale bar, 0.5 microns. **C** Spinning-disc Olympus super-resolution (SD-OSR) images of live cells transfected with GFP-Stx17. The Stx17 signal is located on the outer mitochondrial membrane, and white arrowheads indicates Stx17 foci on the OMM. Dashed blue lines delineate the mitochondrial interior. Scale bar, 200 nm. **D** Representative transmission electron micrographs of COS7 cells expressing YFP-Stx17, immunostained against YFP and labeled with 1.4 nm gold particles and silver enhanced (SE). Cells were treated with 25 µM antimycin A for 45 minutes prior to fixation. Black arrowheads indicate YFP-Stx17 foci on the cytosolic face of the mitochondrial outer membrane. Scale bars, 250 nm (top-left), 50 nm (top-left inset), 250 nm (top-right), 200 nm (bottom-left), and 500 nm (bottom-right). **E** Quantification of the number of YFP-positive foci per distance of mitochondrial outer membrane, in antimycin A-treated and untreated cells expressing YFP and YFP-Stx17, in cells from **D**. Bars represent mean±SEM, n=80 to 112 mitochondria per condition. ***, p<.001. **F** Quantification of the proportion of mitochondria with YFP-Stx17 foci in cells from **D**. Bars represent the mean. **G** Representative transmission electron micrographs of COS7 cells expressing YFP-Stx17, immunostained against YFP and labeled with 10 nm gold particles. Red arrowheads indicate gold particles present on mitochondrial membrane deformations at the cytosolic face of the mitochondrial outer membrane. Scale bars, 50 nm.

this type of lateral release when studying the budding of MDVs off mitochondria (Neuspiel et al., 2008). Further analysis of GFP-Stx17 by super-resolution microscopy (using the spinning disk – Olympus super-resolution [SD-OSR] system) revealed a weak, diffuse signal along the outer

mitochondrial membrane (OMM), with clusters on the cytosolic side of the OMM that exceeded the resolution limit of this technique (Fig. III.2C, white arrowheads indicate GFP-Stx17 foci while the dashed blue markings delineate the inside of mitochondria). We then sought to analyze these mitochondrial Stx17 foci, which were continually beneath the resolution limit of our light microscopy techniques. To this end, we labeled YFP-Stx17 with 1.4 nm gold particles in semi-permeabilized cells, and analyzed the samples by electron microscopy (EM) after developing the gold signal by silver enhancement (SE) (Fig III.2D to F). Similar to what we had observed by super-resolution microscopy, we detected a strong enrichment of YFP-Stx17 within mitochondrial subdomains on the cytosolic face of the OMM (Fig. III.2D, black arrowheads), which increased in frequency with antimycin A treatment (Fig. III.2E and F), the trigger used to upregulate the biogenesis of double-membrane MDVs. Importantly, we did not observe any clustering in cells transfected with YFP alone (Fig. III.2E), and these <100 nm-wide mitochondrial Stx17 foci differed morphologically from mature or pre-autophagosomal structures (Kishi-Itakura et al., 2014). We also observed, by immunoEM using 10 nm gold particles (without enhancement, thus revealing membrane structure beneath the gold signal), YFP-Stx17 labeling on OMM deformations (Fig. III.2G, red arrowheads). Taken together, these confocal, super-resolution and ultrastructural data indicated that Stx17 is recruited to mitochondrial subdomains during vesicle formation and remains associated with fully-formed MDVs after scission, and supported our biochemical studies.

We next tested the link between these mitochondrial clusters of YFP-Stx17 and MDV biogenesis by parkin and PINK1. During biogenesis, nascent MDVs are visible under the electron microscope as 70 to 150 nm, double-membrane budding profiles (Neuspiel et al., 2008; Soubannier et al., 2012b) still attached to their parent mitochondrion via a constricted neck (Fig. III.3A). These

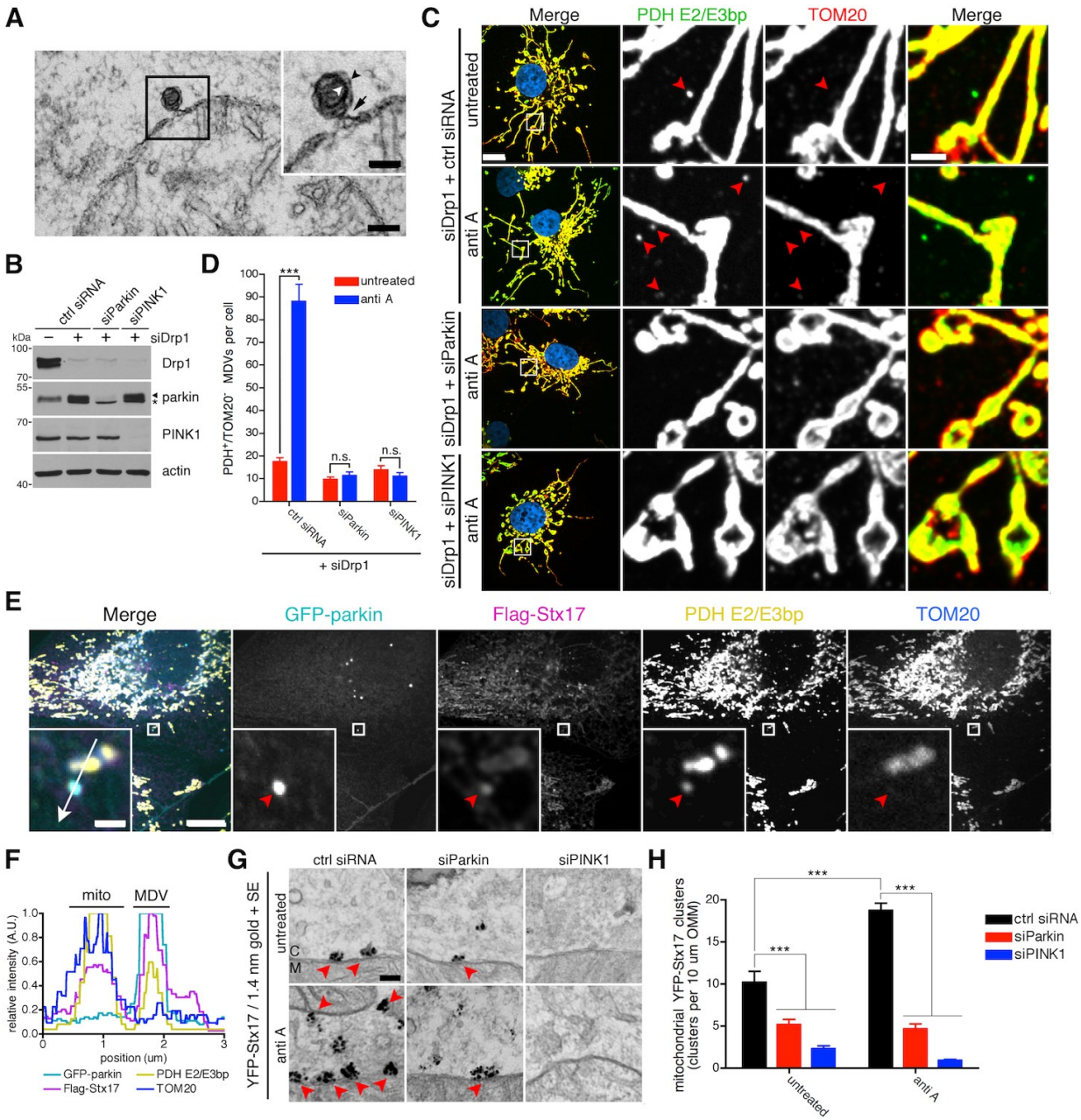


**Figure III.3**. *Stx17 localizes to parkin-/PINK1-dependent MDVs*. See legend on the following page.

vesicle necks are much smaller than the ~100 nm-wide ring formed by assembled Drp1 oligomers during mitochondrial division (Rosenbloom et al., 2014) – consistent with MDV formation being Drp1-independent (McLelland et al., 2014; Neuspiel et al., 2008; Soubannier et al., 2012a) – and much more reminiscent of a vesicular budding process. We have previously shown that the activity of parkin and PINK1 are required to generate double-membrane MDVs in response to oxidative

**Figure III.3**. *Stx17 localizes to parkin-/PINK1-dependent MDVs*. **A** Transmission electron micrograph of a COS7 cell treated with 25 μM antimycin A for 45 minutes prior to fixation. The inset (black box) shows a budding profile connected to the mitochondrial outer membrane. White and black arrowheads indicate the inner and outer vesicular membranes, respectively, and the black arrow indicates the vesicle neck. Scale bars, 100 (full image) and 50 (inset) nm. **B** COS7 cells were transfected with the indicated siRNA and 60 μg of lysate from untreated cells was separated by SDS-PAGE and immunoblotted against the indicated protein. The asterisk indicates a non-specific band. **C** Representative confocal images of antimycin A-treated cells immunostained for PDH E2/E3bp (green) and TOM20 (red) (Hoescht, blue). Selective, PDH E2/E3bp$^+$/TOM20$^-$ structures corresponding to MDVs are indicated by red arrowheads. Scale bars, 10 and 2 microns. **D** Quantification of the number of PDH E2/E3bp$^+$/TOM20$^-$ MDVs per cell in cells from **C** treated with or without 25 μM antimycin A for 45 minutes. Bars represent mean±SEM, n=23 to 29 cells per condition. ***, p<.001; n.s., not significant. **E** Confocal image of a U2OS:GFP-parkin (cyan) cell, expressing Flag-Stx17 (magenta), treated with 25 μM antimycin A for two hours, fixed and immunostained against PDH E2/E3bp (yellow) and TOM20 (blue). Red arrowheads in the insets indicate a PDH E2/E3bp$^+$/TOM20$^-$ structure colocalizing with GFP-parkin and Flag-Stx17. Scale bars, 10 (full image) and 1 (insets) microns. **F** Intensity plot through the 3-micron line drawn in the merged inset in **E**. The MDV indicated in **E**, as well as a mitochondrion (mito) are indicated. **G** Representative transmission electron micrographs of COS7 cells, transfected with control siRNA (ctrl siRNA) or siRNA targeting parkin (siParkin) or PINK1 (siPINK1), expressing YFP-Stx17, immunostained against YFP and labeled with 1.4 nm gold particles and silver enhanced (SE). Cells were treated with 25 μM antimycin A for 45 minutes or left untreated prior to fixation. M, mitochondrion; C, cytosol. Scale bar, 100 nm. **H** Quantification of the number of YFP-positive foci per distance of mitochondrial outer membrane, in antimycin A-treated and untreated cells expressing YFP-Stx17, in cells from **G**. Bars represent mean±SEM, n=105 to 207 mitochondria per condition. ***, p<.001.

stress, which contain, among other cargoes, the mitochondrial matrix protein PDH E2/E3bp (detected by an antibody raised against homologous regions of the E2 and E3bp subunits, herein referred to as "PDH"), but lacking the OMM marker TOM20 (McLelland et al., 2014; Soubannier et al., 2012a). Despite an absence of TOM20, matrix-containing MDVs have an outer membrane (Fig. III.3A). We first confirmed the involvement of endogenous parkin and PINK1 in PDH-positive/TOM20-negative MDV generation in COS7 cells by silencing both parkin and PINK1, as well as Drp1 (Fig. III.3B). In cells transfected with only siDrp1, we observed few cargo-selective puncta in the cytosol, which increased after antimycin A treatment (Fig. III.3C and D). As expected, additional silencing of parkin or PINK1 abolished MDV formation in these cells (Fig. III.3C and D). In U2OS cells stably over-expressing GFP-parkin (U2OS:GFP-parkin cells), we confirmed that Flag-Stx17 localized to PDH-positive/TOM20-negative MDVs, along with GFP-parkin (Fig. III.3E, red arrowhead), enriching on these vesicles compared to mitochondria (Fig. III.3F). Returning to ultrastructural studies, we repeated our 1.4 nm gold labeling and silver

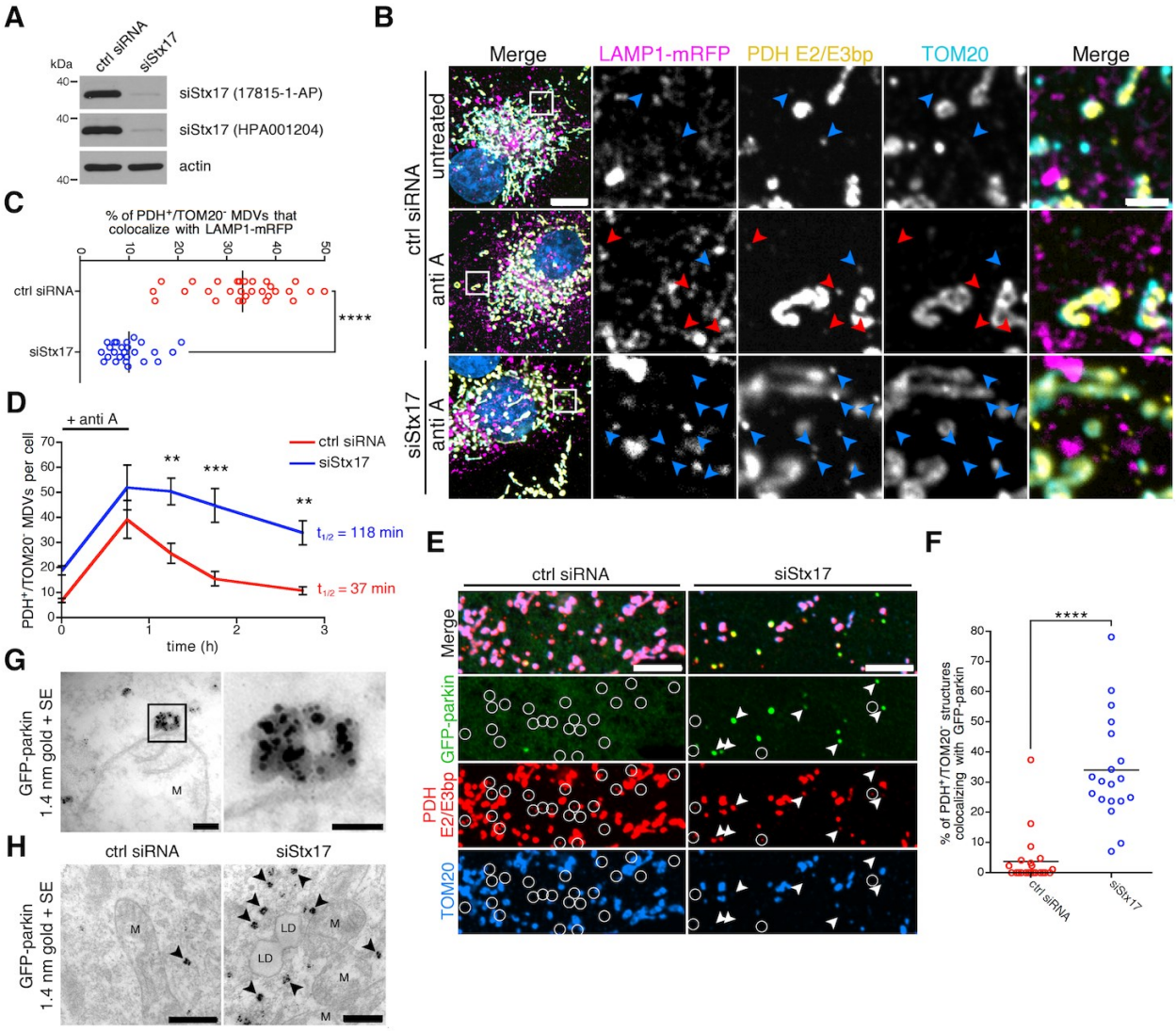


**Figure III.4**. *Stx17 is required for the lysosomal turnover of parkin-/PINK1-dependent MDVs*. See legend on the following page.

enhancement of YFP-Stx17 in cells in which parkin or PINK1 were silenced. Upon quantification of the number of clusters, we observed that YFP-Stx17 cluster formation on the OMM in the absence of parkin or PINK1 in both untreated cells and cells treated with antimycin A was greatly reduced (Fig. III.3G and H, red arrowheads). Thus, parkin and PINK1 are required for Stx17 clustering on the OMM.

**Figure III.4**. *Stx17 is required for the lysosomal turnover of parkin-/PINK1-dependent MDVs*. **A** Stx17 silencing was detected in COS7 cells by immunoblot using two different antibodies. **B** Representative confocal images of cells expressing LAMP1-mRFP (magenta) treated with antimycin A, fixed and immunostained for PDH E2/E3bp (yellow) and TOM20 (cyan) (Hoescht, blue). PDH E2/E3bp$^+$/TOM20$^-$ structures that are positive (red arrowheads) or negative (blue arrowheads) for LAMP1 are indicated. Scale bars, 10 and 2 microns. **C** Quantification of the percent of PDH E2/E3bp$^+$/TOM20$^-$ MDVs that colocalize with LAMP1-mRFP in the antimycin A-treated cells from **B**. Bars represent the mean, n=29 and 25 cells for ctrl siRNA and siStx17, respectively. ****, p<.0001. **D** Pulse-chase analysis of MDV turnover in siStx17 cells. Cells were pulsed with 25 μM antimycin A for 45 minutes in COS7 cells tranfected with control siRNA (red line) or siRNA targeting Stx17 (blue line), then chased with media lacking drug for 0.5 to 2 hours prior to fixation. The number of PDH E2/E3bp$^+$/TOM20$^-$ structures were counted for the indicated times. Bars represent the mean±SEM, n=19 to 23 cells per condition. **, p<.01; ***, p<.001. MDV half-lives were calculated from fitted decay plots (outlined in Materials and Methods; $r^2$=0.98 for ctrl siRNA, $r^2$=0.91 for siStx17). **E** Stx17 silencing delays parkin dissociation from MDVs. U2OS:GFP-parkin cells were transfected with the indicated siRNA and treated with 25 μM antimycin A for 4 hours, fixed and immunostained for PDH E2/E3bp (red) and TOM20 (blue). PDH E2/E3bp$^+$/TOM20$^-$ MDVs that are also positive (arrowheads) or negative (circles) for GFP-parkin (green) are indicated. Scale bars, 5 microns. **F** Quantification of the percent of PDH E2/E3bp$^+$/TOM20$^-$ MDVs that colocalize with GFP-parkin in cells from **E**. Bars represent the mean, n=22 and 19 cells for ctrl siRNA and siStx17, respectively. ****, p<.0001. **G** Transmission electron micrograph of antimycin A-treated U2OS:GFP-parkin cells, immunostained against GFP and labeled with 1.4 nm gold particles. The black box (left) magnifies a GFP-parkin cluster on the cytosolic face of the OMM (right). M, mitochondrion. Scale bars, 100 nm (left) and 50 nm (right). **H** Transmission electron micrographs of antimycin A-treated U2OS:GFP-parkin cells transfected with ctrl siRNA (left) or siRNA targeting Stx7 (siStx17, right), immunostained against GFP and labeled with 1.4 nm gold particles. Black arrowheads indicate cytosolic clusters of GFP-parkin. M, mitochondrion; LD, lipid droplet. Scale bars, 500 nm.

### III.III.iii *Syntaxin-17 mediates MDV turnover and pathway processivity*

Given its previously known role in targeting starvation-induced autophagosomes to lysosomes, we next asked whether Stx17 played an analogous role in MDV trafficking. When Stx17 was silenced (siStx17) in COS7 cells (Fig. III.4A), colocalization of MDVs with LAMP1-mRFP-positive endolysosomes in antimycin A-treated cells was severely reduced in siStx17 versus control cells (Fig. III.4B and C). This suggested that loss of Stx17 may impact MDV turnover. We tested this by measuring MDV turnover kinetics in siStx17 and control cells, where cells pulsed with antimycin A were chased with media lacking the inhibitor. Here, we observed a defect in MDV degradation in cells where Stx17 was silenced (Fig. III.4D) – with MDV half-lives of 37 and 118 minutes for control siRNA (red line) and siStx17 (blue line) conditions, respectively – supporting our lysosomal targeting data in demonstrating a role for Stx17 in MDVs turnover.

We previously suggested that parkin dissociates from matrix-containing MDVs during vesicle maturation (after scission but prior to fusion with the late endosome) (McLelland et al., 2014), thus a loss of Stx17-dependent MDV turnover may slow the rate of parkin dissociation from vesicles. Indeed, more parkin remained colocalized with MDVs in Stx17-silenced, antimycin A-treated U2OS:GFP-parkin cells compared to control (Fig. III.4E and F). When we immunogold-labeled GFP-parkin in antimycin A-treated, control siRNA-transfected cells, we observed few clusters of GFP-parkin, either on the cytosolic face of the OMM (Fig. III.4G, compare to YFP-Stx17 in Fig. III.2D) or in the cytosol (Fig. III.4H, left panel). In contrast, we observed many cytosolic GFP-parkin structures in siStx17 cells treated with antimycin A (Fig. III.4H, right panel). This confirmed that the accumulation of parkin seen by confocal microscopy was predominantly on ~100 nm cytosolic structures, and not on mitochondria.

Finally, these Stx17-mediated targeting defects were specific to this MDV subpopulation, as the targeting of two other classes of mitochondrial vesicles – TOM20-containing MDVs to lysosomes and MAPL-containing MDVs to peroxisomes – showed no dependence on Stx17 (Fig. III.S1A and B for TOM20 carriers, and III.S1C and D for MAPL-containing MDVs, respectively). This pathway specificity is in line with our YFP-Stx17 immunogold labeling experiment in parkin and PINK1 knockdown cells (Fig. III.3F and G), as neither of these other MDV pathways require parkin or PINK1 (McLelland et al., 2014; Neuspiel et al., 2008). Thus, Stx17 is required for lysosomal targeting and turnover of stress-induced MDVs, and loss of Stx17-mediated fusion delays parkin dissociation from the fully-formed vesicle.

III.III.iv *SNAP29 and VAMP7 target MDVs to endolysosomes*

As the ultimate fate of parkin-/PINK1-dependent MDVs is lysosomal turnover (Soubannier et al., 2012a), we accordingly sought to identify the Stx17-containing SNARE complex that mediates fusion of MDVs with endolysosomes. Stx17 (a Qa-SNARE) has already been shown to complex with the Qbc-SNARE SNAP29 and the lysosomal R-SNARE VAMP8 in the context of starvation-induced autophagosome-lysosome fusion in mammals (Diao et al., 2015; Guo et al., 2014). Additionally, co-immunoprecipitation data has indicated that Stx17 also binds the R-SNARE VAMP7 in mammalian cells and in *Drosophila* (Itakura et al., 2012b; Takats et al., 2013). Both VAMP7 and VAMP8 are transmembrane proteins that localize to late endocytic and lysosomal compartments (Fig. III.S2). We confirmed the above interaction data in COS7 cells, where Flag-VAMP7 and Flag-VAMP8, as well as endogenous SNAP29, co-immunoprecipitated with YFP-Stx17 (Fig. III.5A). While PDH-positive/TOM20-negative structures colocalized with both VAMP7 and VAMP8, we observed higher colocalization with Flag-VAMP7 compared to Flag-VAMP8 in both antimycin A-treated U2OS:GFP-parkin (Fig. III.5B and C) and COS7 (Fig. III.5D) cells. To then determine whether these SNAREs, like Stx17, were involved in MDV delivery to endolysosomes, we silenced SNAP29, VAMP7 and VAMP8 in U2OS:GFP-parkin cells (Fig. III.5E). In these cells, loss of SNAP29 or VAMP7 almost completely abolished the lysosomal targeting of MDVs, with a less pronounced (but still significant) inhibition caused by VAMP8 silencing (Fig. III.5F and G); a pattern that was also observed in COS7 cells (Fig. III.5H). We reasoned that the minor targeting defect in the siVAMP8 condition may have resulted from a general impairment of lysosomal pathways, as silencing of the other SNAREs reduced endolysosomal targeting of MDVs to less than 10%, and further supported the selectivity of this pathway for VAMP7 rather than VAMP8.

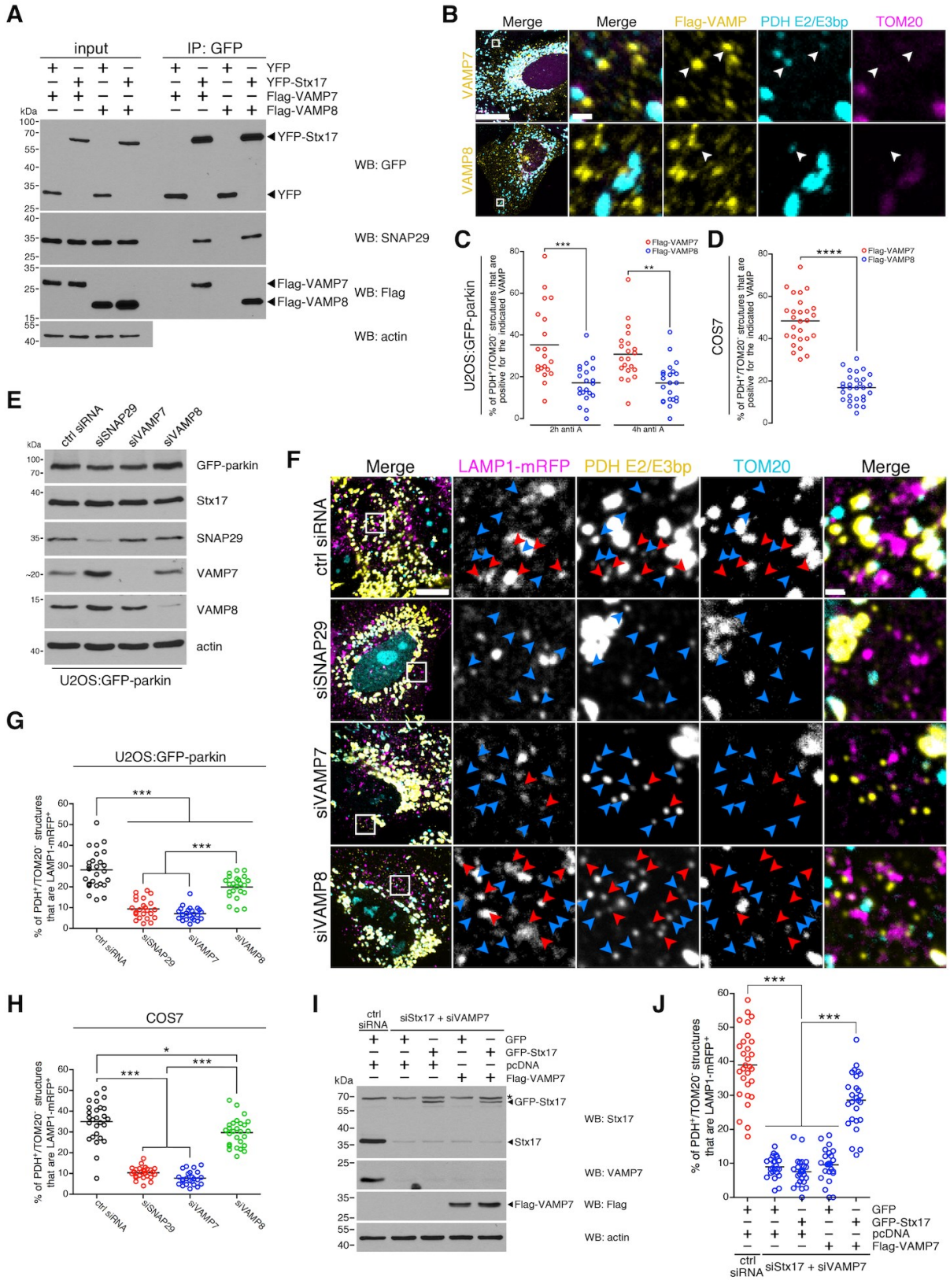


**Figure III.5**. *The Stx17-associated SNAREs SNAP29 and VAMP7 are required for MDV turnover*. See legend on the following page.

**Figure III.5**. *The Stx17-associated SNAREs SNAP29 and VAMP7 are required for MDV turnover*. **A** Co-immunoprecipitation of endogenous SNAP29 and either Flag-VAMP7 or Flag-VAMP8 with YFP-Stx17 in COS7 cells, immunoprecipitated using an anti-GFP antibody. Immunoprecipitates were separated, along with 8% input, by SDS-PAGE and immunoblotted for the indicated protein. **B** U2OS:GFP-parkin cells expressing either Flag-tagged VAMP7 or VAMP8 (yellow) were treated with 25 μM antimycin A for 2 hours, fixed and immunostained for PDH E2/E3bp (cyan) and TOM20 (magenta). Arrowheads indicate PDH E2/E3bp$^+$/TOM20$^-$ structures that colocalize with the related VAMP. Scale bars, 20 and 1 microns. **C** Quantification of the percent of PDH E2/E3bp$^+$/TOM20$^-$ structures that colocalize with VAMP7 (red dots) or VAMP8 (blue dots) in cells from **B** treated for two and four hours. Bars represent the mean, n= 20 to 22 cells. **D** Quantification of the percent of PDH E2/E3bp$^+$/TOM20$^-$ structures that colocalize with VAMP7 (red dots) or VAMP8 (blue dots) in COS7 cells treated with 25 μM antimycin A for 45 minutes. Bars represent the mean, n= 27 and 29 cells for VAMP7 and VAMP8, respectively. **E** Stx17-associated SNAREs were silenced in U2OS:GFP-parkin cells, and silencing was confirmed by immunoblotting. **F** Representative confocal images of U2OS:GFP-parkin cells transfected with the indicated siRNA and LAMP1-mRFP (magenta) that were treated with 25 μM antimycin A for 2 hours, fixed and immunostained for PDH E2/E3bp (yellow) and TOM20 (cyan). PDH E2/E3bp$^+$/TOM20$^-$ structures that are positive (red arrowheads) or negative (blue arrowheads) for LAMP1 are indicated. Scale bars, 10 and 1 microns. **G** Quantification of the percent of PDH E2/E3bp$^+$/TOM20$^-$ structures that colocalize with LAMP1-mRFP in the cells from **F**. Bars represent the mean, n=23 to 26 cells per condition. ***, p<.001. **H** Quantification of the percent of PDH E2/E3bp$^+$/TOM20$^-$ structures that colocalize with LAMP1-mRFP in antimycin A-treated COS7 cells. Bars represent the mean, n=24 to 27 cells per condition. *, p<.05; ***, p<.001. **I** GFP-Stx17 and Flag-VAMP7 were expressed in a 1:3 ratio, along with LAMP1-mRFP, in COS7 cells in which endogenous Stx17 and VAMP7 were silenced. GFP and pcDNA were used as control plasmids. Cells were lysed, and 20 μg of cell lysate was separated by SDS-PAGE and immunoblotted for the indicated protein. The asterisk indicates a non-specific band. Note that the antibody against endogenous VAMP7 does not recognize Flag-VAMP7, as this construct was created using cDNA from mouse. **J** Quantification of PDH E2/E3bp$^+$/TOM20$^-$ structures that colocalize with LAMP1-mRFP in GFP-positive, antimycin A-treated cells from **I**. Bars represent the mean, n=24 to 29 cells per condition. ***, p<.001.

To confirm that the targeting defect was not an off-target effect resulting from the siRNA, we re-expressed GFP-Stx17 and/or Flag-VAMP7 in COS7 cells in which both endogenous Stx17 and VAMP7, which induced the most severe defect, were silenced (Fig. III.5I). In these cells, only the expression of both GFP-Stx17 and Flag-VAMP7 partially rescued the targeting of MDVs to endolysosomes (Fig. III.5J and Fig. III.S3). Thus, Stx17, SNAP29 and VAMP7 are required for the targeting of MDVs to lysosomes, and Stx17 and VAMP7, integral membrane proteins on MDVs and endolysosomes, respectively, likely mediate fusion between their respective compartments.

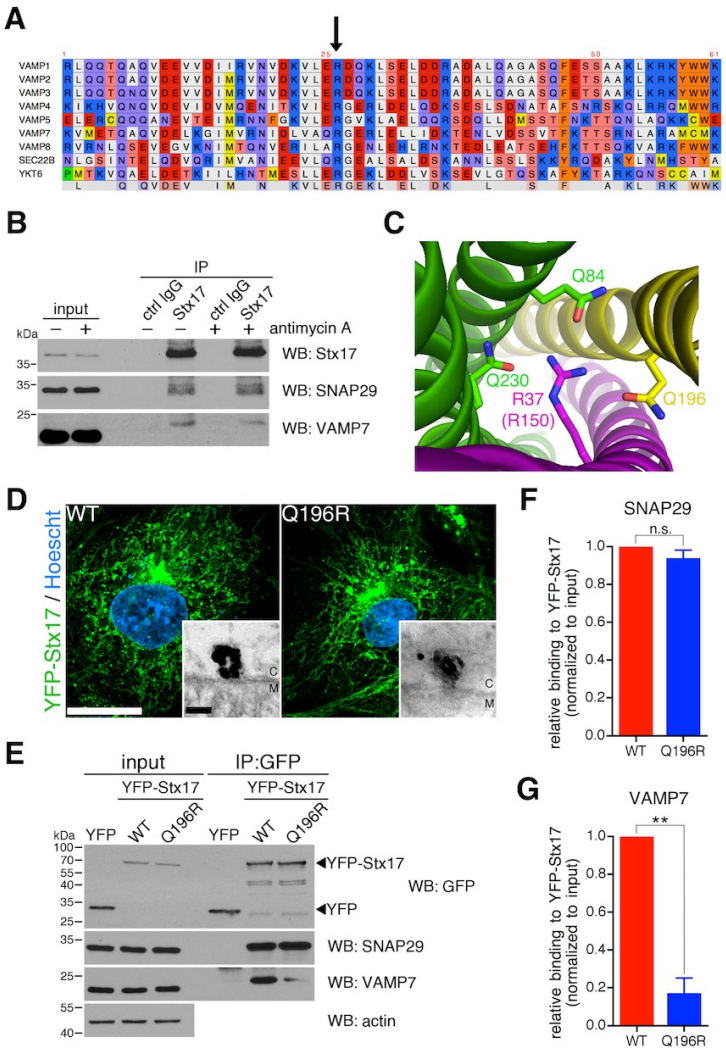


**Figure III.6**. *Manipulation of the Stx17/VAMP7 zero layer affects complex formation and MDV turnover*. **A** Primary sequence alignment of the SNARE domain of human R-SNARE proteins. The arrow indicates the conserved arginine that participates in the central ionic layer of the SNARE ternary complex. **B** Co-immunoprecipitation of endogenous SNAP29 and VAMP7 from untreated and antimycin A-treated COS7 cells with endogenous Stx17 immunoprecipitated with anti-Stx17 antibody. Anti-GFP is used as a control. Immunoprecipitates were separated, along with 5% input, by SDS-PAGE and immunoblotted for the indicated protein. Note that the VAMP7 band is shifted in the IP lanes due to increased glycerol content of the immunoprecipitated sample compared to the input, resulting in slower migration by SDS-PAGE. **C** Structure of the central ionic layer of the ternary SNARE complex formed by Stx17 (yellow), SNAP29 (green) and VAMP8 (magenta) solved by Diao *et al.* (PDB ID 4WY4). Participating residues are indicated. Note that arginine-37 in VAMP8 is equivalent to arginine-150 in VAMP7. **D** Wild-type (WT) or mutant (Q196R) YFP-Stx17 were expressed in COS7 cells, which were then fixed and prepared for immunofluorescence (YFP-Stx17, green; Hoescht, blue) or, in the case of the insets, immunoEM. M, mitochondrion; C, cytosol. Scale bars, 20 microns and 50 nm. **E** Co-immunoprecipitation of endogenous SNAP29 and VAMP7 from COS7 cells expressing either an empty YFP vector, wild-type (WT) or mutant (Q196R) YFP-Stx17, immunoprecipitated using an anti-GFP antibody. Immunoprecipitates were separated, along with 2.5% input, by SDS-PAGE and immunoblotted for the indicated protein. **F**, **G** Quantification of the amounts of SNAP29 (**F**) and VAMP7 (**G**) co-immunoprecipitated by YFP-Stx17 WT compared to Q196R, normalized to the input. Bars represent mean±SEM, n=3 experiments. **, p<.01; n.s., not significant.

### III.III.v *Stx17, SNAP29 and VAMP7 form a SNARE complex that mediates MDV turnover*

The simplest interpretation of our loss-of-function targeting experiments was that a Stx17/SNAP29/VAMP7 complex mediates fusion between MDVs and endolysosomes, analogous to the Stx17/SNAP29/VAMP8 complex involved in autophagy in mammals (Itakura et al., 2012b); indeed, the SNARE domain is highly conserved across R-SNAREs (Fig III.6A, the arrow indicates the conserved arginine at the centre of the domain). Interestingly, in *Drosophila*, an organism that

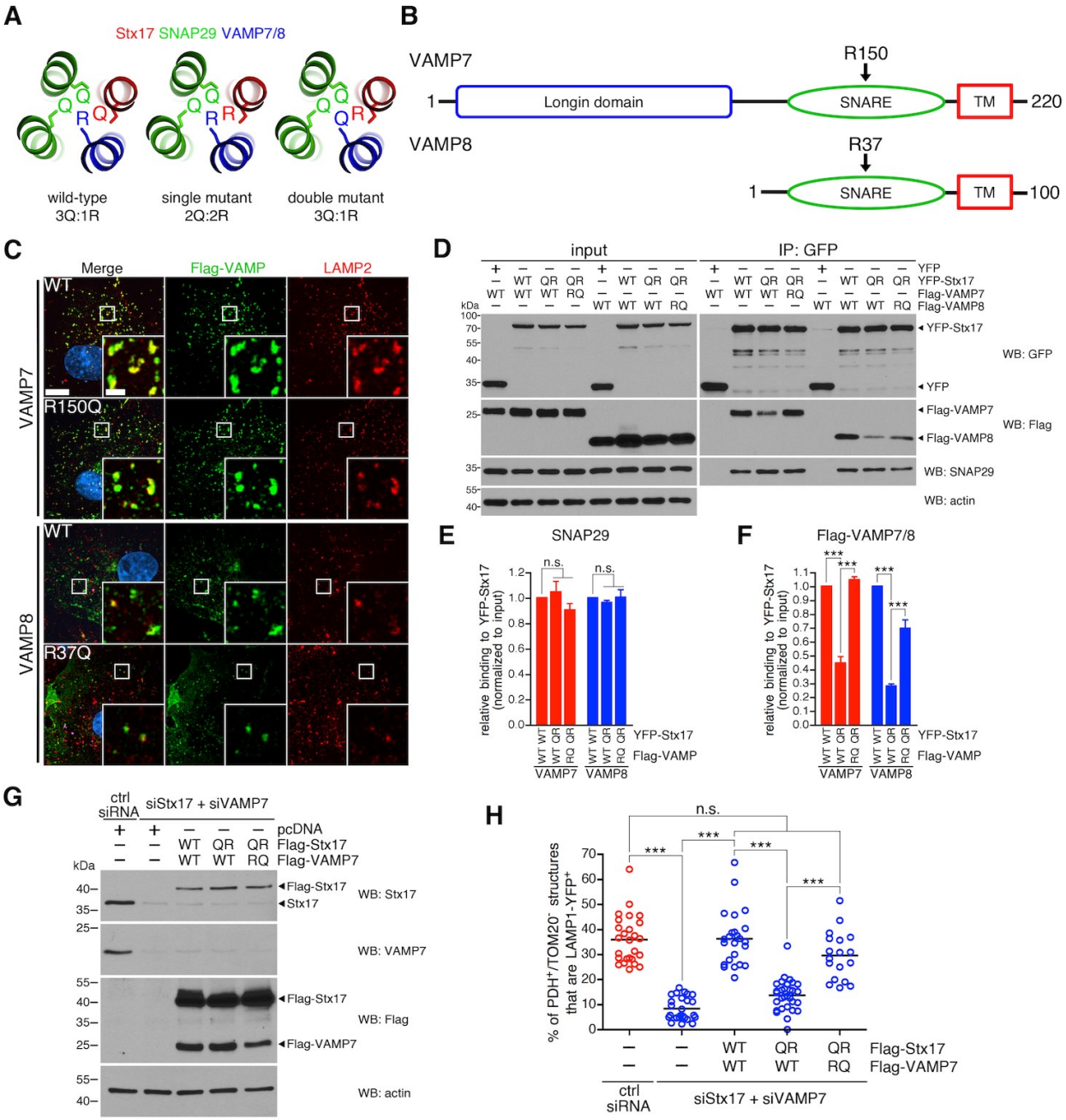


**Figure III.7**. *SNARE complex formation and MDV turnover require a proper zero layer ratio*. See legend on the following page.

lacks VAMP8, autophagosome-lysosome fusion is achieved via a Stx17/SNAP29/VAMP7 complex (Kloepper et al., 2008; Takats et al., 2013). Although we were able to co-immunoprecipitate endogenous VAMP7 and SNAP29 with Stx17, the amounts of VAMP7 and SNAP29 binding Stx17 remained unchanged when cells were treated with antimycin A (Fig.

**Figure III.7**. *SNARE complex formation and MDV turnover require a proper zero layer ratio*. **A** Organization and mutation of zero layer residues in a ternary complex composed of Stx17 (red), SNAP29 (green) and VAMP7/8 (blue), based on the structure solved by Diao *et al.* (PDB ID 4WY4). **B** Domain structure of VAMP7 and VAMP8. The arrows indicate the conserved zero layer residue in the SNARE domains. TM, transmembrane domain. **C** Flag-tagged VAMP7 and VAMP8 constructs were expressed in COS7 cells, then fixed and immunostained against Flag (green) and LAMP2 (red). Scale bars, 10 and 2 microns. **D** Co-immunoprecipitation of endogenous SNAP29 and Flag-tagged VAMP7 or VAMP8 zero layer mutants with YFP, YFP-Stx17 WT or Q196R in COS7 cells, using an anti-GFP antibody. Immunoprecipitates were separated, along with 8% input, by SDS-PAGE and immunoblotted for the indicated protein. **E**, **F** Quantification of the amounts of SNAP29 (**E**) and Flag-tagged VAMP7 and VAMP8 (**F**) co-immunoprecipitated by YFP-Stx17 WT compared to Q196R, normalized to the input. Bars represent mean±SEM, n=3 experiments. ***, p<.001; n.s., not significant. **G** Flag-Stx17 (WT or Q196R), Flag-VAMP7 (WT or R150Q) and LAMP1-YFP were expressed in a 3:3:1 ratio in COS7 cells in which endogenous Stx17 and VAMP7 were silenced (pcDNA3 was used as a control for the Flag vectors). Cells were lysed, and 20 µg of cell lysate was separated by SDS-PAGE and immunoblotted for the indicated protein. **H** Quantification of PDH E2/E3bp$^{+}$/TOM20$^{-}$ structures that colocalize with LAMP1-YFP in antimycin A-treated COS7 cells transfected with constructs from **G**. Bars represent the mean, n=18 to 30 cells per condition. ***, p<.001; n.s., not significant.

III.6B). Thus, we turned to a structure-function approach in order to determine the role of a Stx17/SNAP29/VAMP7 complex in MDV turnover.

To first test whether Stx17, SNAP29 and VAMP7 formed a ternary SNARE complex *in vivo*, we manipulated the zero layer (also known as the central ionic layer) of the potential complex (Fig. III.6C). To this end, we mutated glutamine-196 in Stx17 to arginine (Stx17$^{Q196R}$) in order to disrupt the 3:1 ratio of glutamine to arginine at the zero layer (Diao et al., 2015; Ossig et al., 2000). In COS7 cells, we found that YFP-Stx17$^{Q196R}$ assembled on mitochondrial foci and localized to mitochondria in a similar manner to the wild-type (WT) construct (Fig. III.6D). Intriguingly, co-immunoprecipitation of YFP-Stx17 revealed that, while both the WT and Q196R mutant could interact with SNAP29 (Fig. III.6E and F), the Q196R mutation drastically reduced the interaction of Stx17 with VAMP7 (Fig. III.6E and G). Stx17 and SNAP29 have previously been shown to exist in a binary complex prior to ternary complex formation (Diao et al., 2015), analogous to the syntaxin-1/SNAP25 binary complex and VAMP2 on opposing membranes in the context of neuronal secretion (Rothman, 2014).

We next sough to rescue VAMP7 binding to Stx17 by restoring the 3Q:1R ratio at the zero layer (summarized in Fig. III.7A), and made the corresponding R-to-Q mutation in VAMP7

(R150Q) in parallel with VAMP8 (R37Q) (Fig. III.7B), using this latter VAMP as a control for binding as it has already been shown to form a ternary SNARE complex with Stx17 and SNAP29 (Diao et al., 2015; Itakura et al., 2012). Both Flag-VAMP7$^{R150Q}$ and Flag-VAMP8$^{R37Q}$ localized to LAMP2-positive compartments, like their WT counterparts (Fig. III.7C). We then expressed combinations of zero layer mutants of YFP-Stx17 and either Flag-VAMP7 or Flag-VAMP8 in COS7 cells. As before, the binding of SNAP29 to Stx17 was unaffected by mutation of the zero layer residues of Stx17, VAMP7 or VAMP8 (Fig. III.7D and E). While both Flag-VAMP7$^{WT}$ and

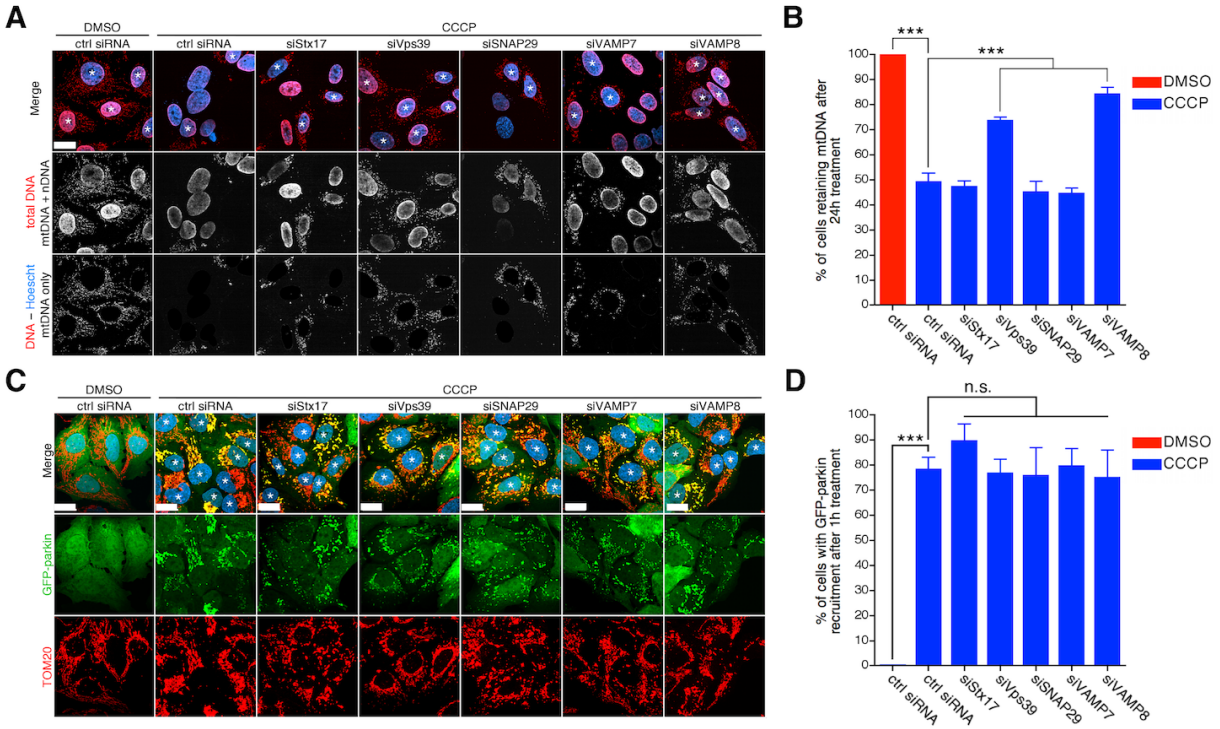


**Figure III.8**. *Stx17 is dispensable for depolarization-induced mitophagy*. **A** Representative confocal images of U2OS:GFP-parkin (not shown) cells (grown on glucose) treated with 20 μM CCCP or DMSO for 24 hours. Mitophagy was monitored by then fixing and immunostaining for DNA (red) and counter-staining with Hoescht 33342 (blue). Cells that have retained their mitochondria are marked by asterisks. To make the presence of mitochondrial DNA (mtDNA) clearer to the reader, the Hoescht image (pertaining to nuclear DNA [nDNA]) was thresholded and subtracted from the total DNA staining to yield an image of solely mtDNA (bottom row). Scale bars, 20 microns. **B** Quantification of the percent of cells retaining mitochondria from cells in **A**. Bars represent mean±SEM, n=3 replicates cells per condition, with >100 cells counted per condition for each replicate. ***, p<.001. **C** Representative confocal images of U2OS:GFP-parkin (cells (grown on glucose) treated with 20 μM CCCP or DMSO for one hour to monitor GFP-parkin (green) recruitment (cells marked with asterisks) to mitochondria (TOM20, red) (Hoescht, blue) Scale bars, 20 microns. **D** Quantification of the percent of cells display parkin recruitment to mitochondria in cells from **C**. Bars represent mean±SEM, n=3 replicates cells per condition, with >100 cells counted per condition for each replicate. ***, p<.001; n.s., not significant.

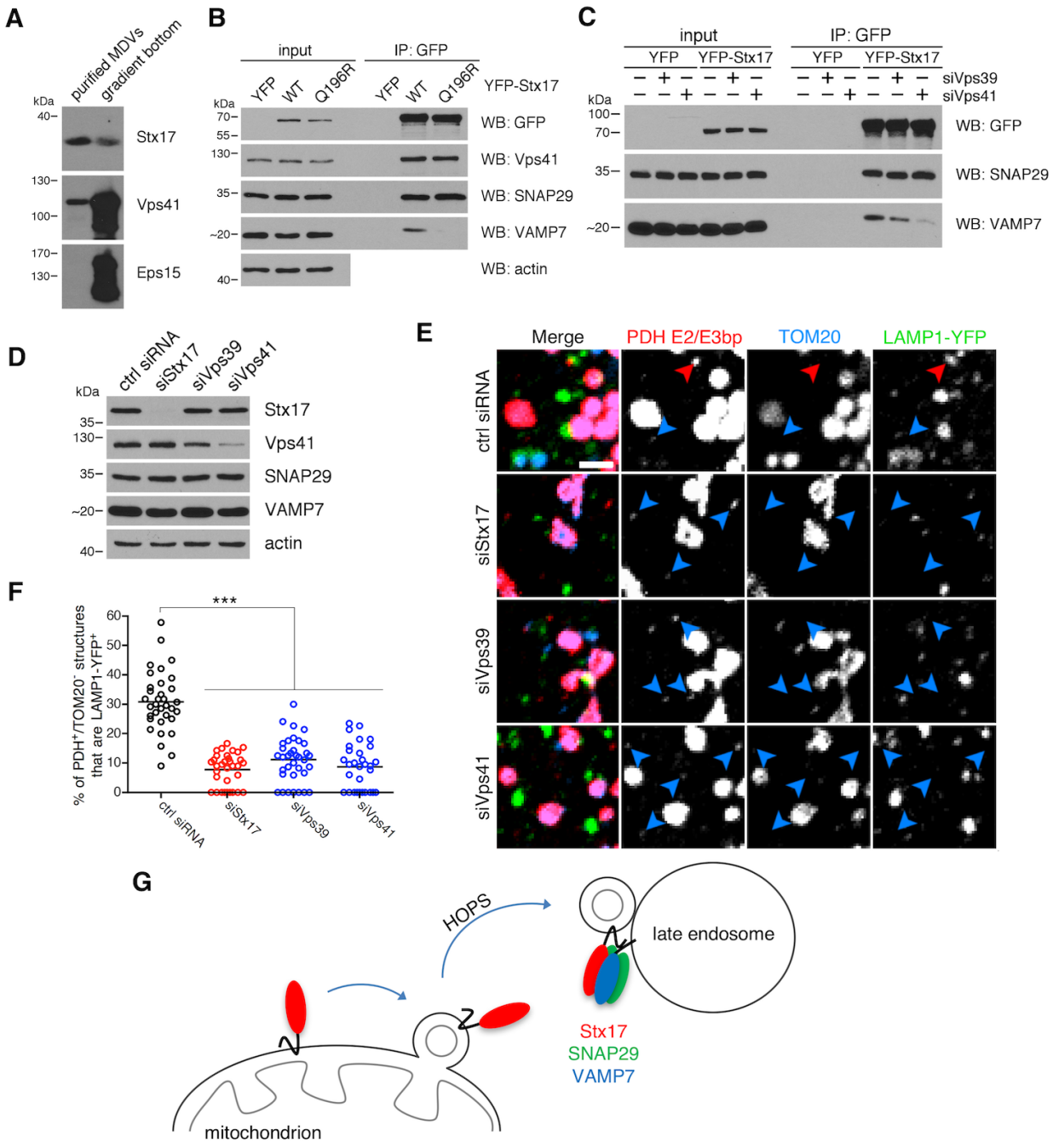


**Figure III.9**. *The HOPS complex acts as a tether during MDV turnover*. See legend on the following page.

Flag-VAMP8$^{WT}$ robustly bound YFP-Stx17$^{WT}$, binding to YFP-Stx17$^{Q196R}$ was again significantly reduced (Fig. III.7D and F). Strikingly, correcting the zero layer ratio back to 3Q:1R from 2Q:2R with Flag-VAMP7$^{R150Q}$ and Flag-VAMP8$^{R37Q}$ rescued YFP-Stx17$^{Q196R}$ binding (Fig. III.7D and F). Thus, the binding of Stx17 to cognate R-SNAREs is dependent upon a proper 3Q:1R ratio at

**Figure III.9**. *The HOPS complex acts as a tether during MDV turnover*. **A** The HOPS subunit Vps41 is present on MDVs generated *in vitro*. Equal volumes of purified MDVs (equivalent to fraction 16 in Fig. III.1D) generated in a cell-free assay as in Fig. III.1D (with cytosol and 50 μM antimycin A), as well as material present at the bottom of the gradient (equivalent to fraction 22 in Fig. III.1D) were separated by SDS-PAGE and immunoblotted for the indicated protein. Eps15 is included as a control for soluble proteins. **B** Co-immunoprecipitation of endogenous Vps41 from COS7 cells expressing either an empty YFP vector (YFP, note that the blot is cropped above the ~30 kDa band corresponding to YFP), wild-type (WT) or mutant (Q196R) YFP-Stx17, immunoprecipitated using an anti-GFP antibody. Immunoprecipitates were separated, along with 2.5% input, by SDS-PAGE and immunoblotted for the indicated protein. **C** Co-immunoprecipitation of endogenous SNAP29 and VAMP7 from control, Vps39- or Vps41-depleted COS7 cells expressing YFP or YFP-Stx17, immunoprecipitated using an anti-GFP antibody. Immunoprecipitates were separated, along with 2.5% input, by SDS-PAGE and immunoblotted for the indicated protein. **D** Immunoblot analysis of COS7 cells transfected with the indicated siRNA. **E** Representative confocal images of COS7 cells transfected with the indicated siRNA and LAMP1-YFP (green) that were treated with 25 μM antimycin A for 45 minutes, fixed and immunostained for PDH E2/E3bp (red) and TOM20 (blue). PDH E2/E3bp$^+$/TOM20$^-$ structures that are positive (red arrowheads) or negative (blue arrowheads) for LAMP1 are indicated. Scale bar, 2 microns. **F** Quantification of the percent of PDH E2/E3bp$^+$/TOM20$^-$ structures that colocalize with LAMP1-YFP in the cells from **E**. Bars represent the mean, n=30 to 35 cells per condition. ***, p<.001. **G** Model of MDV-late endosome fusion mediated by Stx17. Stx17 is recruited to MDVs during budding, likely mobilized from a diffuse pool present on the OMM. In a HOPS-dependent manner, Stx17 forms a ternary SNARE complex with SNAP29 and VAMP7 at the late endosome to mediate fusion.

the zero layer of the four helix bundle, and indicates that Stx17, SNAP29 and VAMP7 form a ternary SNARE complex in cells.

To then determine the effect of zero layer manipulation on MDV trafficking, we reconstituted the Stx17-VAMP7 interaction in COS7 cells. We again silenced both Stx17 and VAMP7, and then re-expressed combinations of Flag-Stx17 and Flag-VAMP7 mutants (Fig. III.7G). When we looked at MDV targeting in these cells, we found that Flag-Stx17$^{Q196R}$ disrupted colocalization of MDVs with LAMP1-YFP compared to WT in cells co-expressing Flag-VAMP7$^{WT}$, and that this, like binding, was rescued by expression of Flag-VAMP7$^{R150Q}$ (Fig. III.7H and Fig. III.S4). Taken together, these data demonstrate the existence of a ternary Stx17/SNAP29/VAMP7 SNARE complex that mediates the fusion of MDVs with endolysosomes.

### III.III.vi *MDV and mitophagosome turnover utilize different sets of SNAREs but both employ the HOPS tethering complex*

Stx17 is involved in the fusion of starvation-induced autophagosomes with lysosomes, and it has been suggested that it is the SNARE responsible for mitophagosome-lysosome fusion during parkin-/PINK1-mediated mitophagy (Yoshii and Mizushima, 2015). Given our current data implicating Stx17 in MDV-endolysosome fusion, we thus sought to identify a role for this molecule in depolarization-induced mitophagy, reasoning that Stx17 may be common to both pathways. To this end, we silenced Stx17 and its associated SNAREs in U2OS:GFP-parkin cells that were grown in glucose medium – a metabolic condition under which mitophagy is permitted (Lee et al., 2015; McCoy et al., 2014; Van Laar et al., 2011) – in order to determine which relevant membrane fusion-related genes would impair mitophagy. We additionally silenced Vps39, a component of the HOPS tethering complex that regulates autophagosome-lysosome fusion and other late endosomal tethering events (Balderhaar and Ungermann, 2013; Jiang et al., 2014; Takats et al., 2014), to serve as a positive control. After these cells were depolarized for 24 hours, to our surprise, only cells in which either Vps39 or VAMP8 were silenced displayed a reduced rate of mitophagy (as visualized by a loss of either mitochondrial DNA or TOM20), with loss of any of Stx17, SNAP29 or VAMP7 having a negligible effect (Fig. III.8A and B for mtDNA, and Fig. III.S5 for TOM20). To ensure that the effects seen by silencing Vps39 and VAMP8 were occurring upstream of mitophagosome turnover, we quantified the recruitment of GFP-parkin after one hour of CCCP – a time frame in which delays in recruitment are visible (Durcan et al., 2014) – and saw no significant delay in any condition (Fig. III.8C and D).

We next tested a role for the HOPS complex in MDV turnover. Similarly to Stx17, the HOPS-specific Vps41 subunit co-purified with MDVs generated in cell-free reconstitution assays (Fig. III.9A), and we confirmed the association of Stx17 with the HOPS complex in cells by co-immunoprecipitating Vps41 with Stx17 (Fig. III.9B) (Jiang et al., 2014; Takats et al., 2014).

Interestingly, we saw no difference in Vps41 binding between WT Stx17 and the Q196R zero layer mutant (which cannot bind cognate R-SNAREs, Fig. III.6E and G). Taken together, these data indicated that Stx17 can recruit the HOPS complex to MDVs prior to binding VAMP7 on the late endosome. Indeed, silencing either Vps39 or Vps41 abrogated the binding of YFP-Stx17 to VAMP7 (Fig. III.9C), as would be expected if the complex was acting as a tether. When we silenced the Vps39 and Vps41 HOPS subunits in COS7 cells (Fig. III.9D), we observed an MDV targeting defect similar to that obtained with Stx17 depletion (Fig. III.9E and F). In summary, the HOPS complex binds Stx17 on MDVs and is required for their efficient targeting to endolysosomes, likely through a conserved role in coordinating interactions at the zero layer (Baker et al., 2015; Starai et al., 2008) between Stx17 and VAMP7. Additionally, while mitophagosomes generated by depolarizing insults are degraded in a HOPS-dependent manner, this occurs largely independently of Stx17, SNAP29 and VAMP7.

## III.IV DISCUSSION

In this study, we have demonstrated the molecular principles that govern MDV transport to the lysosome, showing a requirement for evolutionarily conserved SNARE machinery in this process. The Qa-SNARE Stx17 localizes to the mitochondrial outer membrane, building up at foci that are then released as vesicles, and remains present on MDVs that have dissociated from the mitochondrial tubule. Stx17 also promotes the turnover of mitochondrial vesicles, and MDV-endolysosomal fusion is achieved via a Stx17/SNAP29/VAMP7 ternary SNARE complex. Endolysosomal targeting is regulated via Stx17-VAMP7 binding, as revealed by mutations that disrupt this interaction. While the Stx17/SNAP29/VAMP7 ternary SNARE complex identified in

this study is not involved in parkin-mediated mitophagy, both processes utilize the HOPS tethering complex for turnover (Fig. III.9G).

Manipulation of residues at the zero layer of the helical bundle identified SNARE machinery involved in the turnover of MDVs. The physiological role of residues at this position remains contentious; an all-Q zero layer can still support vacuolar fusion and exocytosis in yeast (Fratti et al., 2007; Katz and Brennwald, 2000; Ossig et al., 2000), whereas other exocytic studies have provided little coherence as to the function of disrupting the 3Q:1R ratio (Gil et al., 2002; Graham et al., 2001; Lauer et al., 2006; Watanabe et al., 2013). Here, we show that zero layer mutations in Stx17 prevent fusion of MDVs with endolysosomes through a reduction in Stx17-VAMP7 binding, and are the first to demonstrate, to our knowledge, that defects resulting from an aberrant zero layer ratios can be functionally rescued via compensatory mutation in a mammalian system.

Accompanying our findings that SNAREs are required for heterotypic fusion between the MDV outer membrane (which is derived from the OMM) and the endolysosomal limiting membrane is the notion that this machinery is distinct from the mitochondrion's own fuseogenic GTPases involved in homotypic fusion of the organelle (Scorrano, 2013). Indeed, while MDV transport to the lysosome is directional and destructive, the major role of mitochondrial fusion is the mixing of mitochondrial contents (Mishra and Chan, 2016), and thus co-evolution of distinct membrane fusion machineries would allow for segregated regulation of these two processes. Drawing this ancestral parallel further, the evolutionary origin of Stx17 is, like the mitochondrion, also primordial – traceable to the so-called last eukaryotic common ancestor (Arasaki et al., 2015; Koumandou et al., 2013). Moreover, Stx17 is a phylogenic "outlier" compared to its most immediate family members – Stx7, Stx13 and Stx20, all of which are much more closely

interrelated (Kloepper et al., 2008) – indicative of an early evolutionary origin. Together, these observations highlight the fundamental concept that, in a similar manner to other conserved trafficking pathways, vesicular trafficking from mitochondria to the lysosome may be an ancient process (Sugiura et al., 2014). Indeed, MDV release may have its origins in the ancestor of the mitochondrion itself; that is, vesicle shedding by α-proteobacteria (Deatherage and Cookson, 2012). Thus, the co-evolution of mitochondria and MDV transport to the lysosome (or vacuole) remains an intriguing area of future work.

The precise mechanism by which Stx17 is recruited into clusters on the OMM is another further area of study. We provide evidence that Stx17 likely assembles at locations of parkin-/PINK1-dependent MDV formation, implicating Stx17 specificity for this MDV subpopulation versus others. While a direct interaction between Stx17 with parkin or PINK1 is unlikely, an unbiased screen for interactors of S65-phosphorylated ubiquitin (the major PINK1 enzymatic product at depolarized mitochondria (Kane et al., 2014; Kazlauskaite et al., 2014b; Koyano et al., 2014)) revealed SNARE-family proteins as a top hit of preferential binding partners in yeast (Swaney et al., 2015). Thus, phosphoubiquitin itself may recruit Stx17 to sites of vesicle formation. Alternatively, Stx17 may be recruited to sites of MDV formation indirectly, or in parallel with other factors. For example, Stx17 may use its two transmembrane domains to detect OMM curvature – a more passive version of how atlastin, another hairpin transmembrane protein, can itself bend ER membranes (Byrnes et al., 2013; Daumke and Praefcke, 2011; Hu et al., 2009) – and thus preferentially collect at sites of membrane deformation.

In the current study, the identification of a canonical SNARE pairing mechanism driving the process of MDV-endolysosomal fusion confirms that this transport route employs established, cellular trafficking machinery, and highlights the integration of mitochondrion-to-lysosome

vesicular transport within the cellular milieu. Additionally, in studying the mechanism of MDV delivery to lysosomes and contrasting this to mitophagy, we have further distinguished MDV transport from parkin-/PINK1-dependent mitophagy, highlighting the divergence of their downstream targeting mechanisms. Studying MDV biology at the molecular level will help us understand how disruption of this mitochondrial quality control mechanism may lead to neuronal degeneration.

## III.V MATERIALS AND METHODS

*Antibodies and other reagents*

Antibodies used in this study include anti-actin (Millipore, MAB1501), anti-α-adaptin (Santa Cruz Biotechnology, sc-17771), anti-CD63 (BD Pharmigen, 556019), anti-DNA (Progen, 61014), anti-Drp1 (BD Biosciences, 611113), anti-Eps15 (Santa Cruz, sc-534), anti-Flag (anti-DDDDK, Abcam, ab1257), anti-Flag (Sigma, F1804), anti-GFP (Abcam, ab6673), anti-GFP (Invitrogen, A6455), anti-LAMP2 (Santa Cruz, sc-18822), anti-LBPA (Eschelon, Z-SLBPA), anti-parkin (Santa Cruz, sc-32282), anti-PDH E2/E3bp (Abcam, ab110333), anti-PINK1 (Cell Signaling Technology, 6946), anti-PMP70 (Sigma, SAB4200181), anti-SDHA (Abcam, ab14715), anti-SNAP29 (Abcam, ab138500), anti-Stx17 (ProteinTech, 17815-1-AP), anti-Stx17 (Sigma, HPA001204), anti-TIM23 (BD, 611222), anti-TIP47 (Novus), anti-TOM20 (Santa Cruz, sc-11414), anti-UQCRFS1 (referred to herein as CIII-Rieske, Abcam, ab14746), anti-VAMP7 (Santa Cruz, sc-166394), anti-VAMP8 (Abcam, ab76021), anti-VDAC1 (Abcam, ab14734) and anti-Vps41 (Abcam, ab181078). Unless otherwise specified, all reagents were purchased from Sigma-Aldrich.

*Plasmids, subcloning and mutagenesis*

Flag-Stx17 (#45911), Flag-VAMP8 (#45912), Flag-VAMP7 (#45913) and LAMP1-mRFP (#1817) were purchased from Addgene (Cambridge, MA) and are described elsewhere (Itakura et al., 2012b; Sherer et al., 2003). MAPL-YFP has also been previously described (Neuspiel et al., 2008). YFP-Stx17 was constructed by first performing sequential digestions of Flag-Stx17 with XbaI and then EcoRI (NEB, Ipswitch, MA). YFP-C1 (mVenus-C1, Addgene plasmid #27794) was cut in the same manner, but dephosphorylated using SAP (Affymetrix, Cleveland, OH) prior to separation on the gel. As the Stx17 cDNA contains an internal EcoRI site, XbaI-cut Flag-Stx17 was partially digested with EcoRI to yield a ~950bp band (representing the full cDNA) that was excised and purified. Purified components were ligated using Rapid DNA Ligation Kit (Thermo Scientific) according to the manufacturer's instructions, and positive clones were identified by sequencing. GFP-Stx17 was constructed by double-digesting YFP-Stx17 and pEGFP-C1 (Clontech) with XhoI and XbaI, followed by a ligation as above. Flag- and YFP-tagged $Stx17^{Q196R}$ were generated using a Quik Change II site-directed mutagenesis kit (Agilent Technologies) by mutagenizing $Stx17^{WT}$ with the primer pair of 5'-CTCCTAGTGAATTCTCGGCAGGAGAAGATTGAC-3' and 5'-GTCAATCTTCTCCTGCCGAGAATTCACTAGGAG-3' according to the manufacturer's instructions. Flag-$VAMP7^{R150Q}$ and Flag-$VAMP8^{R37Q}$ were generated by the same method, using the primer pairs of 5'-CATAGATTTAGTTGCTCAACAGGGAGAAAGGTTGGAATTGC-3'/5'-GCAATTCCAACCTTTCTCCCTGTTGAGCAACTAAATCTATG-3' and 5'-GGATCCTGGCCCAGGGGGAAAACTTG-3'/5'-CAAGTTTTCCCCCTGGGCCAGGATCC-3' for Flag-VAMP7 and Flag-VAMP8, respectively. LAMP1-YFP was constructed by double-

digesting LAMP1-mRFP with BamHI and EcoRI, and ligating (as above) the 1200 bp insert into YFP-N1 (mVenus-N1, Addgene plasmid #27793) that had been cut in the same manner.

*RNA interference*

siRNA oligonucleotides targeting Drp1, parkin and PINK1 have been described previously (McLelland et al., 2014). Non-targeting siRNA, as well as siRNA targeting Stx17 (5'-GGAAACCUUAGAAGCGGACUUAAUUdTdT-3') (Jiang et al., 2014), SNAP29 (5'-AGACAGAAAUUGAGGAGCAdTdT-3') (Guo et al., 2014), VAMP8 (5'-GCAACAAGACAGAGGAUCUdTdT-3') (Guo et al., 2014), Vps39 (5'-GGUAAAGAAGCUGAAUGACUCUGAUdTdT-3') (Jiang et al., 2014) and Vps41 (5'-GAGAAUGAAUGUAGAGAUUdTdT-3') (McEwan et al., 2015) were purchased from Life Technologies. siRNA targeting VAMP7 (ON-TARGETplus J-020864-05) was purchased from Dharmacon (Lafayette, CO).

*Cell culture and transfection*

COS7 cells were purchased from ATCC (Manassas, VA), and the U2OS:GFP and U2OS:GFP-parkin stable cell lines have been described previously (McLelland et al., 2014). Cells were maintained in DMEM supplemented with L-glutamine, penicillin/streptomycin, and 10% FBS in the presence of 10 mM galactose (Wisent, Saint-Bruno, QC). Alternatively, for the experiments depicted in Fig. III.8, 25 mM glucose was used as a carbon source. Cells were typically transfected with 40 nM siRNA, or 0.5 ug/ml DNA for experiments involving a single construct, via lipofection using jetPRIME transfection reagent (Polyplus Transfection, New York, NY) according to the manufacturer's instructions. Cells were treated and analyzed three days post-transfection for

siRNA, and one day post-transfection for DNA transfections. In the case of siRNA/DNA double-transfections, cells were first transfected in 6-well plates with siRNA, then replated the next day in 24-well plates with coverslips (for imaging) or 6-well plates (for immunoblotting). The following day, cells were transfected with the indicated DNA construct, and analysis was performed the next day. In the case of rescue experiments (Fig. III.5I, J and III.S3 and Fig. III.7G, H and III.S4), cells were transfected initially with 40 nM of each siRNA oligonucleotide (as above). For Fig. III.5I, J and III.S3, cells were then transfected with 0.5 ug/ml LAMP1-mRFP, 0.2 ug/ml GFP/GFP-Stx17 and 0.6 ug/ml pcDNA/Flag-VAMP7 (transfection was monitored by GFP fluorescence). For Fig. III.7G, H and III.S4, cells were transfected with 0.5 ug/ml LAMP1-YFP, 0.6 ug/ml pcDNA/Flag-Stx17 and 0.6 ug/ml pcDNA/Flag-VAMP7 (transfected was monitored by YFP fluorescence).

*Immunofluorescence, fluorescence microscopy and microscope image acquisition*

Cells on coverslips were fixed in 6% formaldehyde, washed with PBS and permeabilized in PBS containing 0.25% Triton X-100. Coverslips were then blocked in 10% FBS in PBS. Primary antibodies were diluted in 5% FBS/PBS and incubations were performed for one hour at room temperature. Coverslips were then washed three times in 5% FBS/PBS, then incubated with Alexa Fluor-conjugated secondary antibodies (Molecular Probes, ThermoFisher), diluted as above, for one hour at room temperature. Cells were then washed three times in PBS and mounted on glass slides using Aqua Poly/Mount (Polysciences Inc.). Cells were often counterstained with Hoescht 33342 prior to mounting. Confocal slices (<1 μm-thick) were acquired via an LSM710 laser scanning confocal microscope (Zeiss) through a 63x, 1.4 NA or a 40x, 1.3 NA objective lens, or an Olympus IX81 (with Andor Yokogawa system) spinning disc microscope through either a 100x,

1.4 NA or a 60x, 1.4 NA objective lens using excitation wavelengths of 405, 488, 543 and 633 nm or 405, 488, 515, 561 and 640 nm for the laser scanning and spinning disc microscopes, respectively. Live-cell imaging was performed in a chamber heated to 37°C at 5% $CO_2$, with images acquired every second at 800 ms (YFP) and 50 ms (MitoTracker Deep Red FM) exposure times. Cells were loaded with 225 nM MitoTracker Deep Red FM (Invitrogen) for 30 minutes, then rinsed three times with media without dye, prior to imaging. Super-resolution was performed on an equivalent spinning disc set-up as above and was achieved using the spinning disc – Olympus super-resolution (SD-OSR) system (Olympus), and images were acquired using 2000 ms exposure times. Image files were analyzed using ImageJ (NIH, Bethesda, MD). While vesicles were counted by eye, peroxisomes were counted using the particle counting feature of ImageJ.

*Immunoprecipitation and immunoblotting*

Cells were rinsed in ice-cold PBS and lysed in lysis buffer (20 mM HEPES pH 7.2, 1% NP-40 substitute, 150 mM NaCl, supplemented with protease inhibitors benzamidine, PMSF, aprotinin and leupeptin) on ice. Lysates were clarified by centrifugation and protein concentration was determined by BCA assay (Pierce/Thermo Scientific). Lysates were diluted to 1 to 2 mg/ml and incubated with the indicated primary antibody overnight at 4˚C. The following day, samples were incubated with protein G-Sepharose (GE Healthcare Bio-Sciences) for 4 h. Immunoprecipitates were washed five times in lysis buffer and eluted by incubating at 90˚C. Samples were separated by SDS-PAGE and transferred to nitrocellulose membrane. Membranes were blocked in 5% milk in PBS plus 0.1% Tween-20 (PBST), and primary antibodies were diluted in blocking buffer or 3% BSA/PBST. Primary antibody incubations were performed overnight at 4˚C. The following day, membranes were washed with PBST, blocked again as before, and incubated with HRP-

conjugated secondary antibodies, diluted in 5% milk/PBST, for one hour at room temperature. Membranes were then washed with PBST before protein detection with Western Lightning ECL and Plus-ECL kits (PerkinElmer) according to the manufacturer's instructions.

*Isolation of mitochondria and reconstitution of MDV formation* in vitro

Mitochondrial isolation from mouse liver was adapted from a protocol by Frezza *et al*. (Frezza et al., 2007). Tissue and fractions were kept on ice at all times, and centrifugation was done at 4°C using pre-cooled rotors. Six to eight week-old mice were euthanized with $CO_2$, and the liver was excised and cut into small pieces before homogenization (4 passes at 1,600 rpm) in cold isolation buffer (20 mM HEPES pH 7.4, 220 mM mannitol, 68 mM sucrose, 76 mM KCl, 4 mM KOAc, 2 mM $MgCl_2$, supplemented with protease inhibitors benzamidine, PMSF, aprotinin and leupeptin). The post-nuclear supernatant was collected by centrifuging the homogenate at 600 g for 10 minutes in an Avanti J-25I centrifuge using a SLA-25.50 rotor (Beckman Coulter). This supernatant was collected and centrifuged again at 7,000 g for 10 minutes as above. The pellet (heavy membrane fraction, HM) was resuspended in a large volume of isolation buffer and centrifuged again, then stored in isolation buffer on ice. The 7,000 g supernatant was then centrifuged at 200,000 g for 90 minutes in an Optima L-90K ultracentrifuge using a 70 Ti rotor. The resulting supernatant (soluble cytosolic fraction, S) was stored on ice, and the pellet (light membrane fraction, LM) was resuspended in isolation buffer with 2% Triton X-100. Protein concentrations were determined by BCA assay as mentioned above. MDV formation was reconstituted according to Soubannier *et al*. (Soubannier et al., 2012b). The HM fraction was first washed twice in isolation buffer without protease inhibitors (10,000 rpm for 10 minutes in a microfuge at 4°C). The S fraction was added to the HM in a 1:4 ratio (by protein weight) in the presence of an ATP regenerating mixture (1

mM ATP, 5 mM succinate, 80 μM ADP, 2 mM $K_2HPO_4$ pH 7.4) and 50 μM antimycin A, topped up with isolation buffer. For small scale reactions, the total reaction volume was 250 μl (HM, 6 mg/ml; S, 1.5 mg/ml). These were incubated at 37°C for 2 hours (vortexing every 30 to 45 minutes), and then centrifuged at 10,000 rpm for 10 minutes in a microfuge at 4°C. The pellet was resuspended in SDS-PAGE sample buffer. 0.5 mg/ml trypsin was added to the supernatants, and this was incubated on ice for 10 minute, after which 0.5 mg/ml soybean trypsin inhibitor was added to quench the proteolysis, followed by SDS-PAGE sample buffer. In the case of larger scale reactions (1 ml total volume, with the same fraction concentrations as above), the reaction was centrifuged as above. 900 μl of the supernatant was equilibrated to ~50% sucrose by mixing with 1.35 ml 80% sucrose dissolved in isolation buffer. 2 ml of this was loaded at the bottom of a 14x89 mm Ultra-Clear ultracentrifuge tube (Beckman Coulter). Subsequent 2 ml steps of 40%, 30%, 20%, 10% sucrose (dissolved in isolation buffer), followed by buffer alone, were added slowly to establish a discontinuous sucrose gradient. Gradients were centrifuged overnight (minimum 12 hours) at 35,000 rpm in an Optima ultracentrifuge using a SW41 Ti swinging-bucket rotor. The following day, 500 μl fractions were collected in SDS-PAGE sample buffer.

*Transmission electron microscopy and immunogold labeling*

Cells expressing YFP-Stx17 or GFP-parkin were prepared for immunoelectron microscopy by fixation in 5% formaldehyde and 0.1% glutaraldehyde in PBS for 15 minutes at 37°C. Cells were washed in PBS, quenched with 50 mM glycine in PBS for 15 min, and washed again. Cells were semi-permeabilized in 0.1% saponin, 5% BSA in PBS for 30 min, followed by three 5-min washes in 5% BSA in PBS. Cells were then incubated with anti-GFP antibody (Invitrogen) diluted 1:2000 in 1% BSA for one hour, washed in 1% BSA/PBS three times for 5 min each, then incubated with

nanogold-conjugated (1.4 nm colloidal gold) goat anti-rabbit IgG (Nanoprobes, Yaphank, NY) for another hour (diluted 1:200 as before). Cells were then washed three times in PBS and post-fixed with 1.6% glutaraldehyde for 10 minutes at room temperature, then rinsed extensively with water. Gold particles were enhanced for 5 minutes using the HQ Silver Enhancement Kit (Nanoprobes) according to the manufacturer's instructions, and cells were washed extensively in water afterward and stored in 1.6% glutaraldehyde at 4°C until EM processing. For immunogold labeling using 10 nm gold, cells were prepared as above, but incubated with 10 nm gold-conjugated goat anti-rabbit IgG (Abcam) overnight at 4°C (diluted 1:20) and were not subsequently silver enhanced. For preparation of samples for morphological analysis, cells were fixed in 2.5% glutaraldehyde for 2 hours at room temperature and then stored at 4°C before processing. Thin sections on grids were observed in a Tecnai 12 BioTwin transmission electron microscope (FEI) at 120 keV and images were acquired with an XR80C CCD camera (AMT).

*Statistical analyses, graphing and protein structure/alignment graphic generation*

Unless otherwise indicated in the figure legends, all quantitative experiments were performed two to four times. The numbers of cells quantified per experiment are indicated in the figure legends. No statistical method was used to predetermine the experimental sample size. Statistical tests and representations of the data were generated using Prism (GraphPad Software, La Jolla, CA). For histograms, data are given as the mean ± standard error of the mean (SEM), while the mean is indicated on dot plots. Statistical significance was determined by the appropriate statistical test; one- (Fig. III.4C) and two- (Fig. III.3G, III.4D, III.5F, III.5G, III.S1D) tailed t-tests, and one- (Fig. III.5G, III.5H, III.5J, III.7E, III.7F, III.7H, III.9F) and two-way (Fig. III.2E, III.3D, III.3H, III.4D, III.5C, III.8B, III.8D, III.S5B) ANOVAs followed by Bonferroni *post-hoc* tests. Differences were

considered significant if $p<.05$. Note that for Fig. III.8B and D, DMSO-treated samples, of which all but one were left out of the histogram (as they were identical to the DMSO-treated ctrl siRNA sample), were accounted for in the statistical analyses. The MDV half-lives in Fig. III.4D were estimated from fitting a decay plot to the graph with Microsoft Excel, using the antimycin A-treated and untreated data as maximum and baseline MDV levels, respectively ($r^2=0.98$ for ctrl siRNA; $r^2=0.91$ for siStx17). Diagrams of the structure of the SNARE tetrad and the R-SNARE sequence alignment were created with PyMOL and eBioX, respectively.

*Summary of supplemental material*

Fig. III.S1 examines the effect of Stx17 depletion on the targeting of other MDV populations to other cellular destinations. Fig. III.S2 demonstrates that VAMP7 and VAMP8 localize to late endosomes and lysosomes. Fig. III.S3 shows that the targeting of MDVs to LAMP1-positive compartments is rescued in siStx17/siVAMP7 double-knockdown cells by the re-introduction of Stx17 and VAMP7 (see also Fig. III.5I and J). Fig. III.S4 demonstrates that a 3Q:1R zero layer ratio is required in the Stx17-/VAMP7-containing SNARE complex in order for proper MDV targeting (see also Fig. III.7G and H). Fig. III.S5 identifies a role for Vps39 and VAMP8 (but not Stx17) in TOM20 turnover by mitophagy (see also Fig. III.8A and B).

## III.VI ACKNOWLEDGEMENTS

This work was supported by operating grants from the Canadian Institutes for Health Research (CIHR) to H.M.M. and E.A.F. G.L.M. is supported by a Canada Graduate Scholarship from the CIHR. The authors would like to thank Jeannie Mui and the Facility for Electron Microscopy

Research (McGill) for TEM sample processing and technical advice. The TIP47 antibody was a kind gift from Peter McPherson (McGill). The authors declare no competing financial interests.

## III.VII SUPPLEMENTARY FIGURES

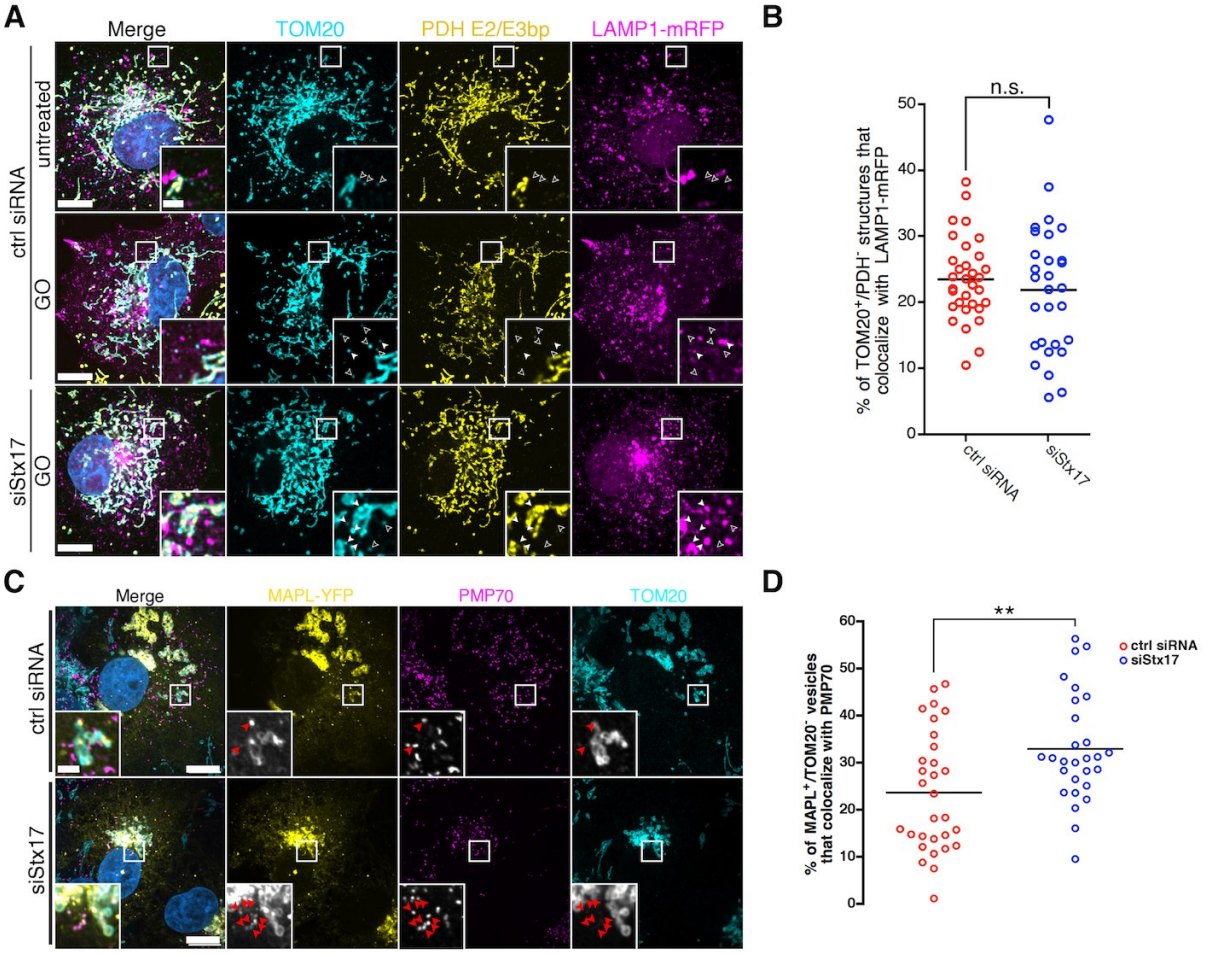


**Figure III.S1**. *Silencing of Stx17 does not perturb other MDV pathways*. **A** Representative confocal images of cells expressing LAMP1-mRFP (magenta) treated with GO, fixed and immunostained for PDH E2/E3bp (yellow) and TOM20 (cyan) (Hoescht, blue). $TOM20^{+}/PDH\ E2/E3bp^{-}$ structures that are positive (white arrowheads) or negative (empty arrowheads) for LAMP1 are indicated. Scale bars, 10 and 2 microns. **B** Quantification of the percent of $TOM20^{+}/PDH\ E2/E3bp^{-}$ structures that colocalize with LAMP1-mRFP in Stx17-silenced COS7 cells treated with 50 mU/ml glucose oxidase (GO) or left untreated. Bars represent mean, n=32 to 39 cells per condition. n.s., not significant. **C** COS7 cells transfected with MAPL-YFP (yellow) and the indicated siRNA were fixed and immunostained for TOM20 (cyan) and PMP70 (magenta, a peroxisomal marker) (Hoescht, blue). Red arrowheads indicate PMP70-labeled peroxisomes that also contain MAPL-YFP. Scale bars, 10 and 2 microns. **D** Quantification of the percent of PMP70-labeled peroxisomes that also contain MAPL-YFP per cell of cells from **C**. Bars represent the mean, n=30 and 28 cells for ctrl siRNA and siStx17, respectively. **, $p<.01$.

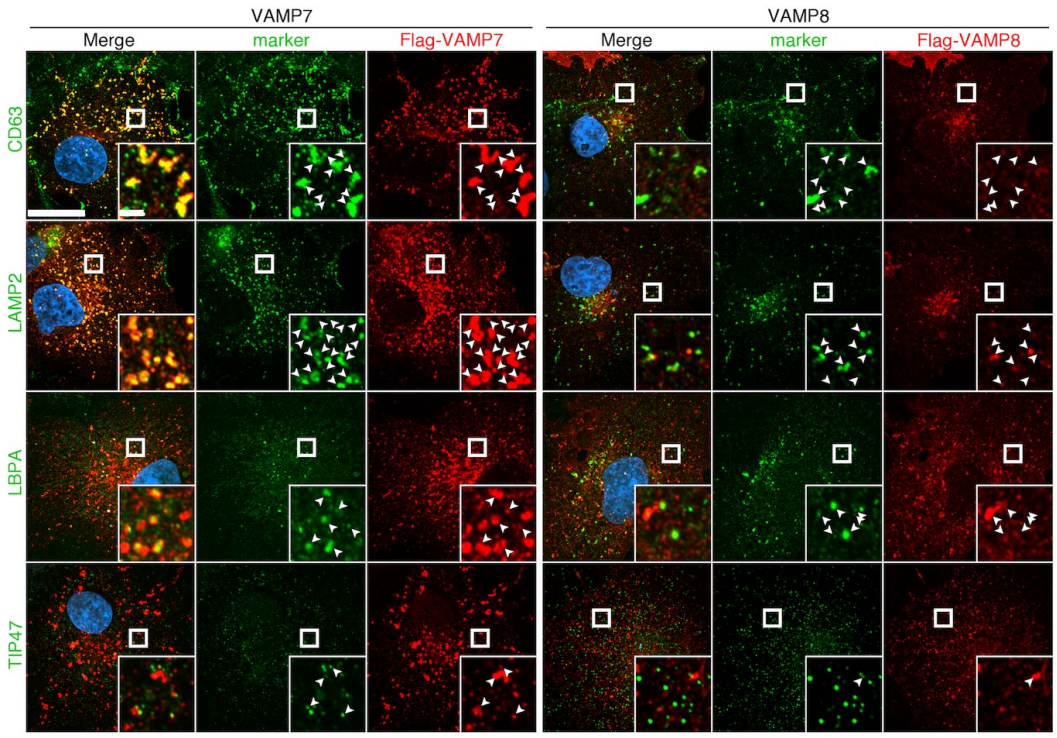


**Figure III.S2**. *VAMP7 and VAMP8 localize to late endosomes and lysosomes*. COS7 cells expressing Flag-VAMP7 (left) or Flag-VAMP8 (right) were fixed and immunostained for the Flag tag (red) and the indicated late endosomal/lysosomal (CD63, LAMP2) or strictly late endosomal (TIP47, LBPA) marker (green) (Hoescht, blue). White arrowheads indicate structures that are positive for both the Flag-VAMP and the corresponding marker. Scale bars, 20 and 2 microns.

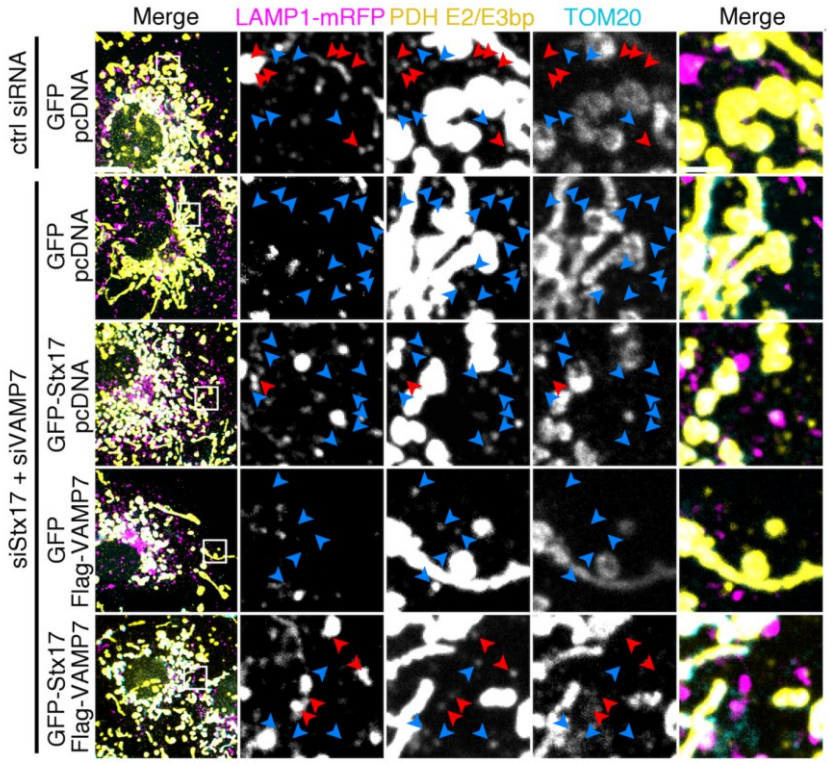


**Figure III.S3**. *MDV targeting in cells lacking Stx17-associated SNAREs*. Representative confocal images of COS7 cells from Fig III.5I and J treated with 25 µM antimycin A for 45 minutes, fixed and immunostained against PDH E2/E3bp (yellow) and TOM20 (cyan) (LAMP1-mRFP, magenta). PDH E2/E3bp$^{+}$/TOM20$^{-}$ structures that are positive (red arrowheads) or negative (blue arrowheads) for LAMP1 are indicated. Scale bars, 10 and 2 microns.

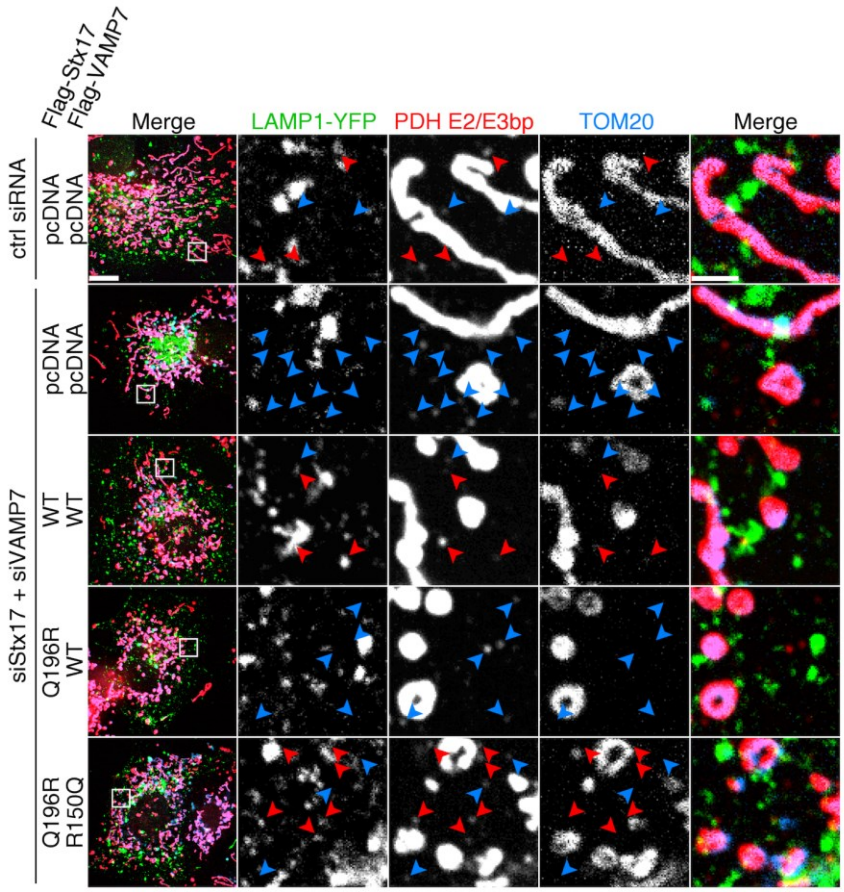


**Figure III.S4**. *MDV targeting in cells reconstituted with zero layer mutants*. Representative confocal images of COS7 cells from Fig. III.7G and H treated with 25 µM antimycin A for 45 minutes, fixed and immunostained against PDH E2/E3bp (red) and TOM20 (blue) (LAMP1-YFP, green). PDH E2/E3bp$^{+}$/TOM20$^{-}$ structures that are positive (red arrowheads) or negative (blue arrowheads) for LAMP1 are indicated. Scale bars, 10 and 2 microns.

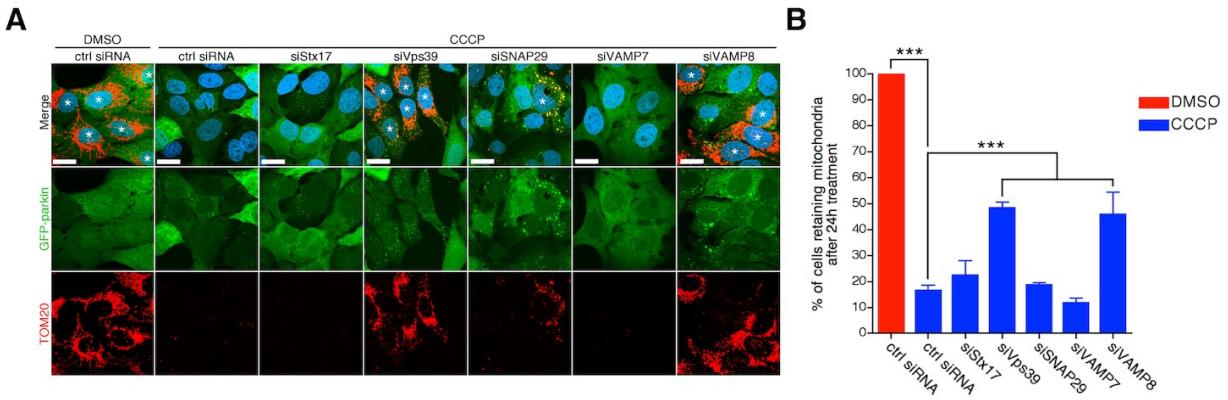


**Figure III.S5**. *Stx17 is dispensable for depolarization-induced mitophagy.* **A** Representative confocal images of U2OS:GFP-parkin (green) cells (grown on glucose) treated with 20 µM CCCP or DMSO for 24 hours. Mitophagy was monitored by then fixing and immunostaining for TOM20 (red) (Hoescht 33342, blue). Cells that have retained their mitochondria are marked by asterisks. Scale bars, 20 microns. **B** Quantification of the percent of cells retaining mitochondria from cells in **A**. Bars represent mean±SEM, n=3 replicates cells per condition, with >100 cells counted per condition for each replicate. ***, p<.001.

## III.VIII INTEGRATIVE SUMMARY

While Chapter II described core machinery involved in the generation of MDVs carrying ETC/matrix components, Chapter III provides a detailed description concerning how these vesicles target to and fuse with the late endosome, revealing that they use a canonical SNARE-pairing mechanism. While the mechanistic relationship between Stx17 and parkin/PINK1 remains unknown – although this SNARE is clearly a component of MDVs, as revealed by cell-free reconstitution assays and live-imaging microscopy – this study identifies more players involved in this mitochondrion-to-lysosome vesicular pathway, and provides tractable molecules that can be followed in future studies of how this and potentially other classes of MDVs are formed. This work demonstrates that parkin-/PINK1-dependent MDV biogenesis is truly a stand-alone pathway separate from mitophagy, and implies that other machineries involved in cellular membrane trafficking pathways – such as Rabs, membrane-deforming molecules, motors, etc. – are likely associated with MDV biogenesis and delivery to the late endosome.

Chapter II and III covered molecular mechanisms associated with parkin/PINK1-dependent MDV formation. Chapter IV, on the other hand, identifies a mitophagic regulatory mechanism centered on the activity of PINK1 and parkin on Mfn2, showing that PINK1/parkin regulate contact between the OMM and ER (see section I.IV.ii) via Mfn2 destruction as an early step in the mitophagic cascade.

Chapter IV

# MITOFUSIN-2 UBIQUITINATION BY PINK1/PARKIN GATES THE RELEASE OF ER FROM MITOCHONDRIA TO DRIVE MITOPHAGY

The following Chapter is a manuscript being prepared for submission:

**McLelland GL**, Dorval G, Lauinger ND, Rakovic A, Durcan TM, Trempe JF, Fon EA. Mitofusin-2 ubiquitination by PINK1/parkin gates the release of ER from mitochondria to drive mitophagy.

## IV.I ABSTRACT

Despite their importance as signaling hubs, the function of mitochondria-ER contact sites in mitochondrial quality control pathways remains unexplored. Here we describe a mechanism by which mitofusin-2 (Mfn2), a mitochondria-ER tether, gates the autophagic turnover of mitochondria by PINK1 and parkin. Mitochondria-ER appositions are destroyed during mitophagy, and reducing mitochondria-ER contacts increases the rate of mitophagy. Mechanistically, parkin and PINK1 catalyze a rapid burst of Mfn2 phosphoubiquitination to trigger the p97-dependent extraction of high molecular weight Mfn2 complexes from the outer mitochondrial membrane, resulting in the disassociation of mitochondria from the ER. Finally, we demonstrate that a major portion of the facilitatory effect of p97 on mitophagy is epistatic to Mfn2 and promotes parkin substrate availability. Our data show that mitochondria-ER tethering antagonizes mitophagy, and reciprocally describe a parkin- and PINK1-dependent mechanism that regulates the destruction of mitochondria-ER contact sites.

## IV.II INTRODUCTION

Loss of *PRKN* or *PINK1* results in an early-onset form of hereditary Parkinson's disease (PD), a neurological disorder that is linked to mitochondrial dysfunction (Kitada et al., 1998; Ryan et al., 2015; Valente et al., 2004). Accordingly, parkin and PINK1 promote mitochondrial health through several mitochondrial quality control mechanisms; the turnover of outer mitochondrial membrane (OMM) proteins by the proteasome, the generation of mitochondrial-derived vesicles, and whole-organellar degradation by autophagy (termed "mitophagy") (Sugiura et al., 2014; Yamano et al., 2016). During mitophagy, PINK1, a mitochondrial kinase, builds up on the surface of damaged mitochondria where it activates parkin directly via phosphorylation and allosterically

through the generation of phosphoubiquitin (pUb) (Kane et al., 2014; Kazlauskaite et al., 2014b; Kondapalli et al., 2012; Koyano et al., 2014; Shiba-Fukushima et al., 2012). Parkin, an E3 ubiquitin (Ub) ligase, mediates the ubiquitination of resident OMM proteins, recruiting Ub-binding autophagic machinery through a feed-forward mechanism to ultimately degrade the organelle via the lysosome (Heo et al., 2015; Lazarou et al., 2015; Ordureau et al., 2015).

Contact sites between mitochondria and the endoplasmic reticulum (ER) act as crucial signaling hubs in the context of starvation-induced autophagy, where they serve as the site of autophagosome formation (Hamasaki et al., 2013; Kishi-Itakura et al., 2014). Indeed, autophagosome biogenesis is impaired in cells with defective mitochondria-ER tethering (Hamasaki et al., 2013), as lipid transfer between organelles may be important for their formation (Hailey et al., 2010; Klecker et al., 2014). As steady-state mitophagy in yeast requires mitochondria-ER contacts (Bockler and Westermann, 2014), it has been assumed that parkin-dependent mitophagy follows a similar mechanism (Yoshii and Mizushima, 2015). However, this model directly conflicts with the observation that mitofusin-2 (Mfn2) – a mitochondria-ER tether required for starvation-induced autophagosome formation in mammals (de Brito and Scorrano, 2008; Hamasaki et al., 2013; Naon et al., 2016) – is ubiquitinated by parkin and rapidly turned over by the proteasome (Tanaka et al., 2010). Thus, how mitophagy is regulated by contacts between mitochondria and the ER (if at all), and the location from which the mitophagic membrane originates, remain open questions in the field.

## IV.III RESULTS

### IV.III.i *Parkin and PINK1 destroy mitochondria-ER contact during mitophagy*

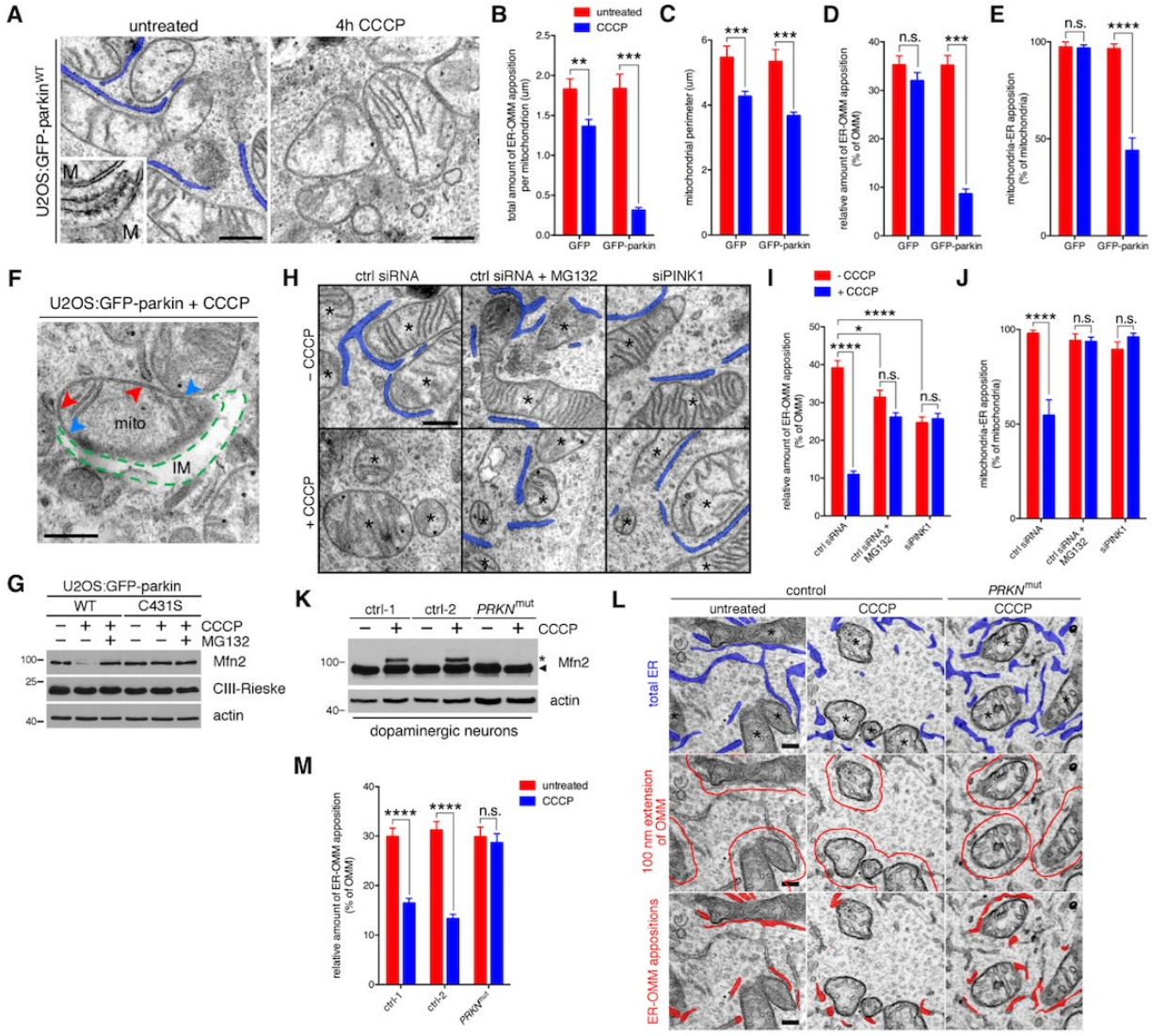


**Figure IV.1**. *Ultrastructural analysis of ER-mitochondria contact during mitophagy in U2OS cells and dopaminergic neurons.* See legend on the following page.

We hypothesized that PINK1 and parkin may regulate contact between both organelles during mitophagy, based on studies demonstrating high levels of parkin ubiquitination activity on Mfn2 in both cells and *in organello* ubiquitination assays (Tanaka et al., 2010; Tang et al., 2017). To first determine whether parkin destroys the OMM-ER interface of depolarized mitochondria, we analyzed contacts between the two organelles by EM (Csordas et al., 2006). We quantified ER tubules within 100 nm of the OMM, as this distance is enough to capture tubules closely associated with the OMM (Fig. IV.1A, left panel and inset). To induce PINK1-/parkin-mediated mitophagy,

**Figure IV.1**. *Ultrastructural analysis of ER-mitochondria contact during mitophagy in U2OS cells and dopaminergic neurons*. **A** Representative TEM images of mitochondria ("M") in contact with ER (pseudocoloured blue) in untreated and CCCP-treated U2OS:GFP-parkin cells. Scale bars, 500 nm. **B**-**E** Quantification of TEM from **A** in U2OS:GFP and GFP-parkin$^{WT}$ cells, left untreated (red bars) or treated with 20 μM CCCP for four hours (blue bars). Total apposition length (**B**), mitochondrial size (**C**), and the percent of OMM per mitochondrion (**D**) and mitochondria per field (**E**) in contact with the ER was quantified. Bars represent mean±SEM, n=82 to 152 mitochondria in 15 to 19 fields per condition. n.s., not significant; **, p<.01; ***, p<.001; ****, p<.0001. **F** TEM image of an isolation membrane ("IM", broken green line) wrapping a mitochondrion ("mito"). Blue arrowheads indicate the boundaries of OMM rupture, while red arrowheads indicate ER tubules in contact with the intact portion of the OMM. Scale bar, 500 nm. **G** Immunoblot analysis of whole-cell lysates from U2OS:GFP-parkin WT and C431S cells treated with 20 μM CCCP for four hours with or without 10 μM MG132. In the case of MG132 treatment, cells were first pre-incubated with 10 μM MG132 for 30 minutes prior to addition of CCCP. **H** Representative TEM images of mitochondria ("*") in contact with ER (pseudocoloured blue) in U2OS:GFP-parkin cells transfected with the indicated siRNA, and treated with 20 μM CCCP ("+CCCP") for four hours, in the presence or absence of 10 μM MG132 as in **G**. Scale bar, 500 nm. **I**,**J** Quantification of TEM from **H** in cells treated with (blue bars) or without (red bars) 20 μM CCCP for four hours. The percent of OMM per mitochondrion (**I**) and mitochondria per field (**J**) in contact with the ER was quantified. Bars represent mean±SEM, n=101 to 203 mitochondria in 14 to 16 fields per condition. n.s., not significant; *, p<.05; ***, p<.001; ****, p<.0001. **K** Immunoblot analysis of whole-cell lysates from dopaminergic neurons, derived from iPSCs isolated from control (ctrl) individuals and a *PRKN* patient (*PRKN*$^{mut}$), treated with 20 μM CCCP for one hour. The arrowhead indicates the unmodified Mfn2 band, while the asterisk indicates ubiquitinated Mfn2. **L** Representative TEM images of mitochondria ("*") in contact with ER in iPSC-derived dopaminergic neurons treated with 20 μM CCCP for one hour. In the top row, the ER is pseudocoloured blue. In the second row, the red line denotes an area within 100 nm of the OMM. In the bottom row, ER tubules within the 100 nm area are psedocoloured red. Scale bars, 200 nm. **M** Quantification of the percent of the OMM apposed to the ER in cells from **L**, corresponding to the labeled ER in the bottom row of **L**. Bars represent mean±SEM, n=80 to 131 mitochondria per condition. n.s., not significant; ****, p<.0001.

we treated U2OS cells stably-expressing GFP-parkin (U2OS:GFP-parkin) and control U2OS:GFP cells with CCCP for four hours, and observed by EM a decrease the total length of ER-OMM contact in both cell lines, although this decrease was greater in magnitude in cells expressing GFP-parkin (Fig. IV.1A, quantified in 1B). However, when CCCP-induced, parkin-independent mitochondrial fragmentation was taken into account (Fig. IV.1C), parkin had a specific effect on reducing the percentage of the OMM that remained in contact with the ER in depolarized cells (Fig. IV.1D), as well as the percentage of total mitochondria that were still connected to the ER (Fig. IV.1E). Given that the mitochondria observed by EM were still intact organelles and not yet engulfed by the isolation membrane (IM) of the autophagosome (Fig. IV.1A, right panel), we concluded that parkin ablates contact between mitochondria and the ER as an early step during depolarization-induced mitophagy in cells.

We next took a closer look at how this process of contact site removal may occur. Parkin has been reported, through its ability to ubiquitinate OMM proteins and target them for proteasomal degradation, to eventually mediate the rupture the OMM prior to or during engulfment by the autophagosome (Yoshii et al., 2011). Indeed, we observed rare (likely transient) mitochondrial structures in which OMM rupture was apparently occurring at the time of fixation (Fig. IV.1F, the blue arrowheads indicate the limits of OMM rupture, where the organelle is being wrapped by the IM [indicated by the broken green line]). Concordantly, ER contacts with the still-intact OMM were observed (Fig. IV.1F, red arrowheads), leading us to postulate that the removal of OMM-ER contacts may precede OMM rupture. To this end, we quantified ER-OMM contacts in CCCP-treated cells that were co-incubated with the proteasome inhibitor MG132, which stabilizes the unmodified band of OMM parkin substrates, including Mfn2, and prevents rupture of the OMM (Chan et al., 2011; Rakovic et al., 2011; Yoshii et al., 2011) (Fig. IV.1G, GFP-parkin$^{C431S}$, which cannot ligate Ub (Trempe et al., 2013), is used as a negative control). MG132 co-incubation rescued ER-OMM contact in U2OS:GFP-parkin cells treated with CCCP (Fig. IV.1H, I and J). Expectedly, we also prevented OMM-ER disruption in cells depleted of PINK1 (Fig. IV.1H, I and J).

Finally, we replicated our U2OS cell data in human dopaminergic neurons derived from induced pluriopotent stem cells (iPSCs) isolated from either control individuals or a patient carrying compound heterozygous mutations in the *PRKN* gene (*PRKN*$^{mut}$; see *Materials and Methods*). iPSC-derived dopaminergic neuronal cultures express detectable amounts of endogenous parkin (Jiang et al., 2012). Upon treatment of these neurons with CCCP for only one hour, we observed Mfn2 ubiquitination in both control lines but not in the parkin mutant line (Fig. 1K). When we analyzed mitochondria-ER appositions in these cells (Fig. IV.1L, bottom row), we

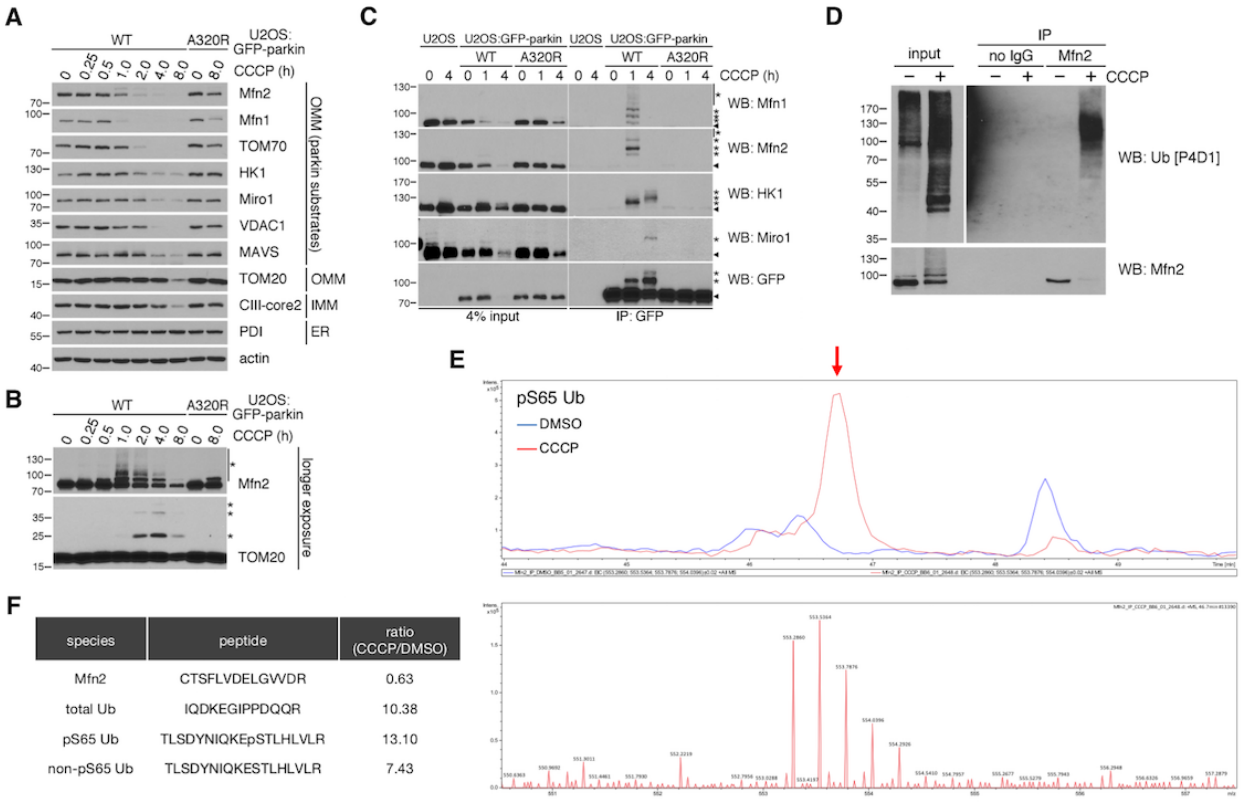


**Figure IV.2**. *Mfn2 is rapidly phosphoubiquitinated upon induction of mitophagy*. **A** Immunoblot analysis of protein turnover in glucose-maintained U2OS:GFP-parkin WT and A320R cells treated with 20 µM CCCP for the indicated time. **B** Higher exposures of Mfn2 and TOM20 immunoblots from **A**. Asterisks indicate ubiquitinated forms of Mfn2 and TOM20. **C** Co-immunoprecipitation of parkin substrates with GFP-parkin WT or A320R in U2OS cells treated with 20 µM CCCP for the indicated time, using an anti-GFP antibody. Immunoprecipitates were separated, along with 4% input, by SDS-PAGE and immunoblotted for the indicated protein. The arrowhead indicates the unmodified form of the protein, while the asterisks denote ubiquitinated forms. **D** Immunoprecipitation of Mfn2 under denaturing conditions. Immunoprecipitates were separated, along with 4% input, by SDS-PAGE and immunoblotted for Ub. **E** Extracted ion chromatogram for the pS65 Ub peptide (TLSDYNIQKEpSTLHLVLR, a.a. 55-72) from Mfn2 immunoprecipitates from DMSO- (blue line) and CCCP- (red line) treated U2OS:GFP-parkin$^{WT}$ cells, immunoprecipitated as in **D**. The red arrow indicates the peak corresponding to the peptide. **F** Table depicting the ratios of integrated MS peaks from CCCP-treated cells compared to DMSO for species of interest. See Supplementary Table IV.S1 for more information.

again observed a CCCP-dependent decrease in the amount of <100 nm ER-OMM appositions in both control lines (Fig. IV.1M). However, this decrease was absent in the parkin mutant line (Fig. IV.1M), supporting our previous overexpression data in U2OS cells (Fig. IV.1A to E). Thus, PINK1 and parkin function to destroy contacts between the ER and mitochondria during mitophagy, likely through parkin-mediated OMM protein ubiquitination and turnover, as this

process can be prevented by inhibiting proteasomal degradation. Moreover, this is a relevant biological process in dopamine neurons, where it is regulated by endogenous parkin.

IV.III.ii *Phosphoubiquitination of Mfn2 by the PINK1/parkin system disrupts its antagonistic effect on mitophagy*

Our EM data demonstrated that ER-mitochondria uncoupling occurs as an early step in the mitophagy pathway, prior to autophagosomal engulfment of the organelle (Fig. IV.1F). We thus pursued the mechanism of this phenomenon. Mfn2 is both a mitochondria-ER tether and parkin ubiquitination substrate (de Brito and Scorrano, 2008; Sarraf et al., 2013; Tanaka et al., 2010), and thus the modulation of interorganellar contact by PINK1/parkin may occur through their effect on Mfn2. We began by examining the ubiquitination (via the disappearance of the unmodified band) of various parkin substrates (Khan et al., 2016; Sarraf et al., 2013) during a CCCP time course in U2OS:GFP-parkin cells. Turnover of both Mfn1 and Mfn2 occurred early (almost complete disappearance by two hours) compared to other OMM proteins (Fig. IV.2A). Upon higher exposure (Fig. IV.2B) of these immunoblots (from Fig. IV.2A), we observed a rapid "burst" of Mfn2 ubiquitination that occurred between 30 and 60 minutes CCCP. When compared to TOM20, a protein that is not robustly ubiquitinated by parkin (Sarraf et al., 2013), the rapidity of this Ub burst on Mfn2 was emphasized as TOM20 ubiquitination occurs gradually over a period of hours, rather than rapidly over a period of minutes (Fig. IV.2B). Thus, ubiquitination of the mitofusins is one of the very first steps after the induction of mitophagy.

Mechanistically, this Ub burst would require local activation of parkin by PINK1 in the vicinity of Mfn2, which could be achieved by PINK1-catalyzed phosphorylation of the resulting Ub chains – events that would dually serve to activate parkin and tether it in place (Okatsu et al.,

2015b). To test this, we first immunoprecipitated WT GFP-parkin or the A320R mutant – which fails to bind pUb (Wauer et al., 2015a; Yamano et al., 2015), the major PINK1 phosphorylation product on depolarized mitochondria – from cells treated with CCCP over time. We observed robust coimmunoprecipitation of ubiquitinated Mfn1 and Mfn2 with GFP-parkin$^{WT}$ at one hour CCCP (corresponding to the Ub burst observed in Fig. IV.2B), with no apparent binding at four hours (Fig. IV.2C), likely due to turnover of the Mfns by the proteasome at this time (Fig. IV.2B and (Tanaka et al., 2010)). When we analyzed other parkin substrates that are ubiquitinated less rapidly than the Mfns (Fig. IV.2A), we observed binding to WT parkin only at four hours of CCCP treatment in the case of ubiquitinated Miro1, and binding of mono-ubiquitinated HK1 at one hour CCCP, which was further shifted at four hours, indicative of processivity of HK1 ubiquitination (Fig. IV.2C). None of these ubiquitinated species coimmunoprecipitated with GFP-parkin$^{A320R}$ (Fig. IV.2C) indicating that these proteins were likely phosphoubiquitinated and binding parkin through its pUb-binding helix (Wauer et al., 2015a). We confirmed phosphoubiquitination of Mfn2 by its immunoprecipitation under denaturing conditions. By immunoblot, we detected Ub-modified species in the immunprecipitate from cells that were treated with CCCP for one hour (Fig. IV.2D). Liquid-chromatography coupled to mass spectrometry (LC/MS) confirmed that the Mfn2 immunoprecipitate from CCCP-treated cells contained a mixture of both unphosphorylated and S65-phosphorylated Ub (Fig. IV.2E and F). Overall, we observed a CCCP-dependent, ~10-fold increase in Mfn2 ubiquitination (all species), which was concomitant with a decrease in Mfn2 abundance (Fig. IV.2F, Fig. IV.S1 and Supplementary Table 1). Taken together, these data demonstrate that a burst of phosphoubiquitination occurs on Mfn2 at an early time point in the mitophagy pathway.

Our observations so far demonstrated that mitochondria are separated from the ER during mitophagy, and that the OMM-ER tether Mfn2 is rapidly degraded at the onset of the pathway. We thus hypothesized that Mfn2 may antagonize mitophagy through its ability to tether mitochondria and the ER, necessitating its destruction. To test this, we silenced Mfn2 (siMfn2) in U2OS:GFP-parkin cells, as well as Mfn1 – which promotes mitochondrial fusion without any apparent role in interorganellar tethering (de Brito and Scorrano, 2008) – to control for phenomena resulting from fusion defects. We confirmed Mfn1 and Mfn2 depletion by immunoblot (Fig. IV.3A), and observed mitochondrial fragmentation in both siMfn1 and siMfn2 cells (Fig. IV.3B) with an ER-OMM apposition defect unique to the siMfn2 condition (Fig. IV.S2), as expected. Next, we investigated the kinetics of parkin recruitment to depolarized mitochondria in these cells (in our analyses, a cell is considered to have recruited parkin if the parkin signal covers the mitochondrial reticulum in its entirety). Moreover, we took advantage of delayed pathway kinetics of respiring cells by culturing cells in growth medium containing galactose as a carbon source (rather than glucose). This forces ATP generation through the electron transport chain and mitigates parkin-dependent mitophagy (Lee et al., 2015; McCoy et al., 2014). Mitochondrial translocation of parkin, and the buildup of Ub, p62 and LC3 on mitochondria are slowed in galactose-grown cells (Fig. IV.S3). Remarkably, we observed faster mitochondrial recruitment in siMfn2 (but not siMfn1) cells, under both bioenergetic conditions (Fig. IV.3C and D). A significant difference was visible within one hour of CCCP treatment in glucose-cultured cells, and was exacerbated in their galactose-grown counterparts, owing to their slower kinetics in the control siRNA-transfected condition (Fig. IV.3E). Strikingly, Mfn2 silencing increased recruitment in galactose-grown cells to levels seen in glucose-maintained cells transfected with control siRNA (Fig. IV.3E). Silencing Mfn1 and Mfn2 simultaneously (Fig. IV.S4A) did not further enhance the

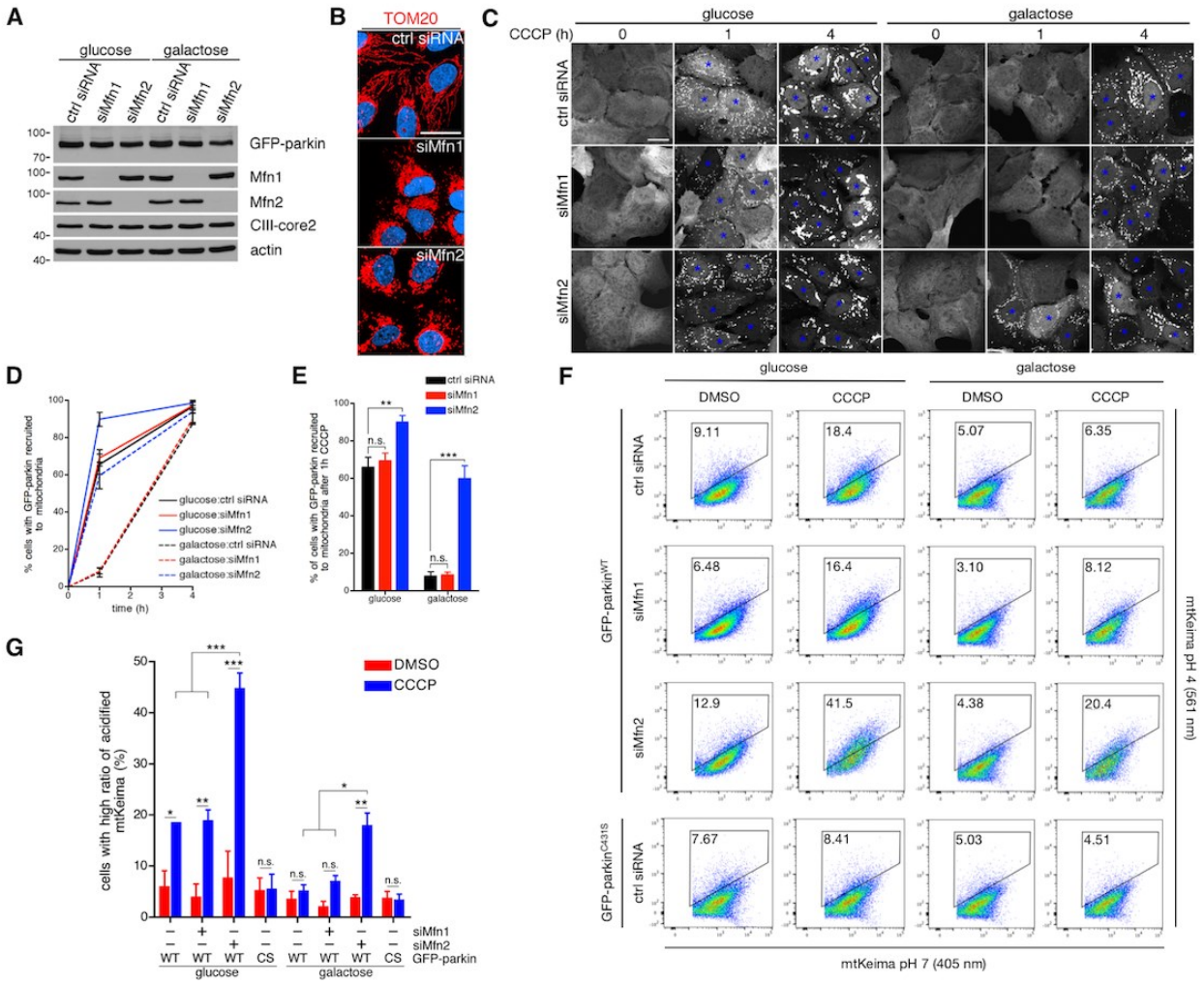


**Figure IV.3**. *Mfn2 antagonizes mitophagy*. **A** Immunoblot analysis of whole-cell lysates from cells cultured in glucose or galactose transfected with control siRNA or siRNA targeting Mfn1 ( "siMfn1" ) or Mfn2 ( "siMfn2" ). **B** Mitochondrial morphology in glucose-maintained cells transfected with the indicated siRNA, as revealed by confocal imaging of TOM20 (red) staining (Hoescht, blue). Scale bar, 30 microns. **C** Representative confocal images of GFP-parkin recruitment to mitochondria as a function of time in U2OS:GFP-parkin cells treated with 20 μM CCCP. Blue asterisks indicate cells in which GFP-parkin has fully translocated to mitochondria. Scale bar, 20 microns. **D** Quantification of parkin recruitment in cells from **C**. Data points represent mean±SEM, n=3 replicates cells per condition, with >100 cells counted per condition for each replicate. **E** Parkin recruitment at one hour CCCP in cells from **C** arranged as a histogram. Bars represent mean±SEM. n.s., not significant; **, p<.01; ***, p<.001. **F** U2OS:mtKeima cells were transfected with the indicated siRNA and GFP-parkin WT or C431S, and were treated with 20 μM CCCP (or DMSO) for four hours. mtKeima fluorescence in GFP-positive cells was measured using flow cytometry by excitation at 405 nm (neutral pH) and 561 nm (acidified). The data are represented as scatter plots of fluorescence emission from excitation at both wavelengths. The gated area encloses cells undergoing mitophagy (high acidified:neutral Keima ratio), and the percentage of cells within this gate is indicated in the top-left corner of each plot. **G** Quantification of the percent of cells undergoing mitophagy in cells from **F** treated with DMSO (red bars) or CCCP (blue bars) for four hours. Bars represent mean±SEM, n=2 experiments. n.s., not significant; *, p<.05; **, p<.01; ***, p<.001.

kinetics of parkin recruitment beyond single, Mfn2-depleted cells (Fig. IV.S4B-D), implying that this phenotype was Mfn2-specific and unrelated to a loss of mitochondrial fusion.

We next determined whether, more generally, this increase in recruitment kinetics could be induced by disrupting mitochondria-ER contacts via means other than removing Mfn2. To test this, we silenced two other genes that have been shown to promote mitochondria-ER association; PACS2 and Stx17 (Fig. IV.S4E) (Arasaki et al., 2015; Simmen et al., 2005). Unlike Mfn2 knockdown, we did not observe mitochondrial fragmentation in either PACS2- or Stx17-silenced cells (Fig. IV.S4F). When we tested parkin recruitment in these cells, we saw that, similarly to Mfn2 knockdown, silencing of either PACS2 (siPACS2) or Stx17 (siStx17) increased the translocation of parkin to mitochondria (Fig. IV.S4G and H). Again, the increase was most pronounced in galactose-cultured cells that were treated with CCCP for one hour, where parkin was recruited to near-glucose levels in Mfn2-, PACS2- and Stx17-silenced cells despite remaining predominantly cytosolic in cells transfected with control siRNA at this time point (Fig. IV.S4I). Thus, disruption of mitochondrion-ER tethering increases the kinetics of parkin translocation to depolarized mitochondria.

We next directly tested the effect of Mfn2 depletion on mitochondrial turnover using quantitative, ratiometric measurements of mitochondrially-targeted mKeima (mtKeima), a protein that shifts its fluorescence excitation when acidified by the lysosome (Katayama et al., 2011). We transfected U2OS cells stably-expressing mtKeima (U2OS:mtKeima), grown on either glucose or galactose, with siRNA targeting Mfn1 or Mfn2, followed by wild-type (WT) GFP-parkin, using the ligase-dead C431S mutant as a negative control. Next, we treated these cells with CCCP (or DMSO) for four hours and then determined the ratio of acidified mtKeima per cell by FACS (see *Materials and Methods*) as a quantitative indicator of mitophagy (Katayama et al., 2011; Tang et

al., 2017). In the glycolytic, CCCP-treated condition, a higher proportion of control siRNA-transfected cells had an increased ratio of acidified mtKeima compared with DMSO-treated counterparts – expectedly, these cells were undergoing mitophagy – and this population shift was similarly replicated in siMfn1 cells (Fig. IV.3F and G). However, in Mfn2-depleted cells, we observed a ~2-fold increase in the proportion of cells undergoing mitophagy (Fig. IV.3F and G). In respiring conditions, we did not observe a shift at all in either control siRNA-transfected or Mfn1-depleted cells but observed a level of mitophagy in siMfn2 cells similar to control cells cultured in glucose medium (Fig. IV.3F and G). These data demonstrate that, in Mfn2-depleted cells, depolarization-induced mitophagy is enhanced, in line with our parkin recruitment experiments (Fig. IV.3A to E), and demonstrate that Mfn2 represses mitophagy at the level of pathway initiation.

To ensure that we were observing on-target effects from depletion of our siRNA targets, we replicated our recruitment data in Mfn2 knock-out (KO) U2OS cells that were generated using the CRISPR-Cas9 system. Genetic disruption was confirmed by sequencing in two clones (A4 and A5) in which a premature stop codon was introduced via a single base-pair frame shift following the codon corresponding to leucine-29 in the Mfn2 gene (Fig. IV.S5A). We validated these KO cells by immunoblot, along with a clone that underwent the complete procedure and selection but in which Mfn2 knock out failed (B4) as a further negative control; importantly, Mfn1 levels remained similar across all lines, and the core subunits of the mitochondrial $Ca^{2+}$ uniporter remained unperturbed (Fig. IV.S5B, compensation in the latter has been reported in MEFs isolated from $Mfn2^{-/-}$ mice (Filadi et al., 2015)). Accordingly, Mfn2 KO cells had fragmented mitochondrial reticula (Fig. IV.S5C). Corroborating our earlier data in siMfn2 cells, Mfn2 KO cells (grown on glucose) transiently transfected with GFP-parkin displayed increased recruitment

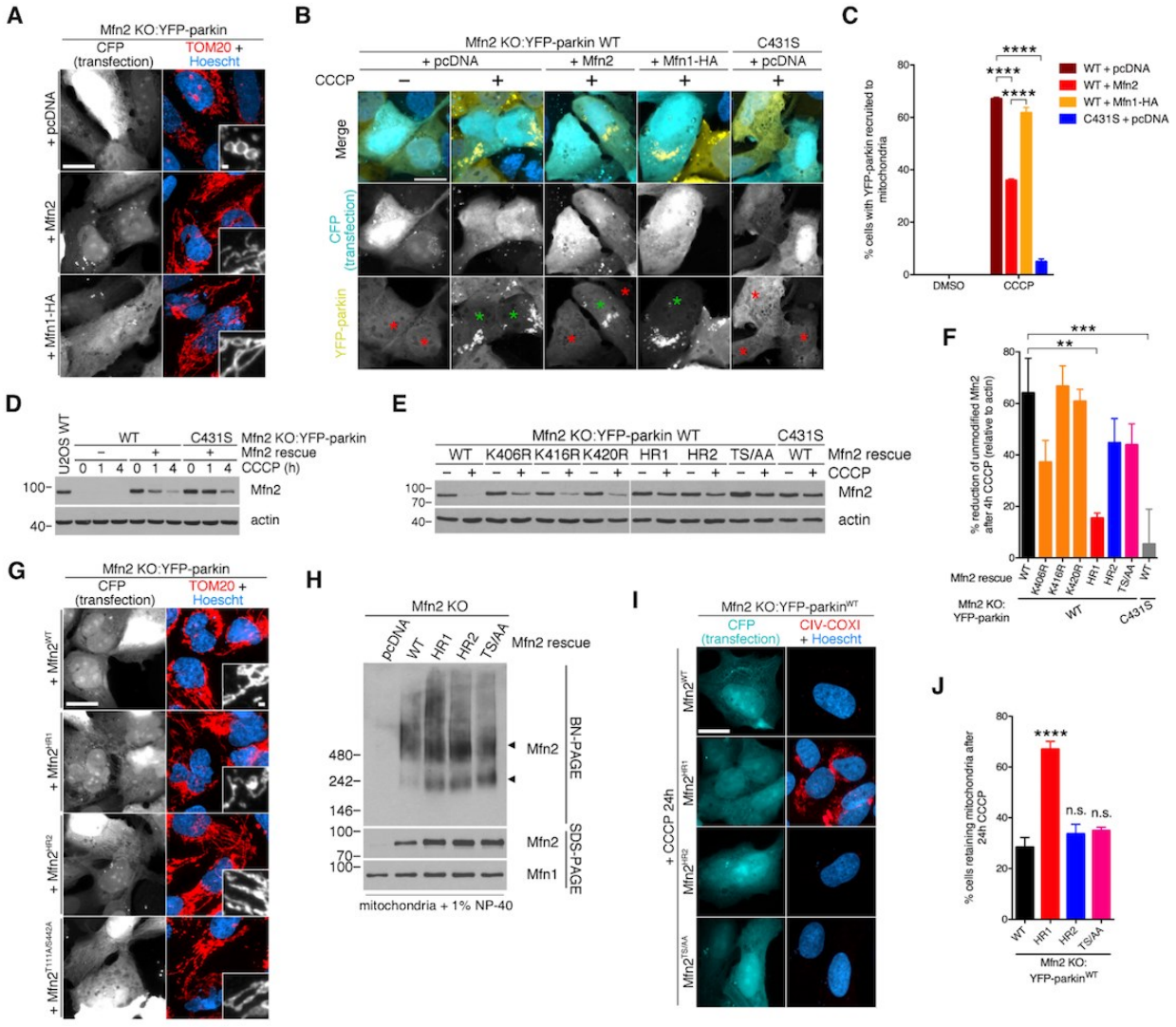


**Figure IV.4**. *Parkin ubiquitinates Mfn2 in the HR1 domain to derepress mitophagy.* See legend on the following page.

kinetics (Fig. IV.S5D and E) and increased mitophagy (Fig. IV.S5F and G). Finally, we ensured that parkin translocation in Mfn2 KO cells (Fig. IV.S6A to C) and U2OS:GFP-parkin cells depleted of Mfn2 (Fig. IV.S6D) was PINK1-dependent. Moreover, cells expressing GFP-parkin$^{A320R}$ (Fig. IV.S6E) failed to translocate under conditions of Mfn2-depletion (Fig. IV.S6F and G). This indicates a clear requirement for PINK1 and Ub phosphorylation for parkin translocation in Mfn2-depleted cells, demonstrating that Mfn2 reduction increases on-pathway mitophagy kinetics. Taken together, our data not only show that mitochondria-ER contact is

**Figure IV.4**. *Parkin ubiquitinates Mfn2 in the HR1 domain to derepress mitophagy*. **A** Mnf2 KO:YFP-parkin$^{WT}$ cells were transfected with the indicated plasmid and CFP in a 3:1 ratio, then fixed and immunostained for TOM20 (red) and counterstained with Hoescht 33342 (blue). Scale bars, 20 and 1 microns. **B** Mfn2 KO:YFP-parkin WT and C431S cells, transfected as in **A**, were treated with 20 μM CCCP for four hours prior to fixation, then scored for YFP-parkin recruitment. Green and red asterisks indicated CFP-positive cells with mitochondrial and cytosolic YFP-parkin, respectively. Scale bar, 20 microns. **C** Quantification of recruitment in **B**. Bars represent mean±SEM, n=3 replicates cells per condition, with >50 cells counted per condition for each replicate. ****, p<.0001. **D** Immunoblot analysis of Mfn2 KO:YFP-parkin cells (WT and C431S) transfected with Mfn2 and treated with 20 μM CCCP for the indicated time. An untreated U2OS cell lysate is included as a control for endogenous Mfn2 levels. **E** Representative immunoblot analysis of Mnf2 KO:YFP-parkin$^{WT}$ cells transfected with the indicated Mfn2 mutant and treated with 20 μM CCCP for four hours. **F** Quantification of Mfn2 modification in immunoblot analyses from **E**, given as the percent of Mfn2 reduction after CCCP relative to actin. Bars represent mean±SEM, n=4 replicates. **, p<.01; ***, p<.001. **G** Mnf2 KO:YFP-parkin$^{WT}$ cells were transfected with the indicated plasmid and CFP in a 3:1 ratio, then fixed and immunostained for TOM20 (red) and counterstained with Hoescht 33342 (blue). Scale bars, 20 and 1 microns. **H** Immunoblot analysis of BN- and SDS-PAGE gels of solubilized mitochondria from cells from **G**. Arrows indicated two Mfn2-containing complexes in the native condition. **I** Representatitve widefiled images of Mfn2 KO:YFP-parkin$^{WT}$ cells transfected with the indicated Mfn2 construct. Cells were treated with 20 μM CCCP for 24 hours prior to fixation, then stained with CIV-COX1 (red) and Hoescht (blue). Scale bar, 20 microns. **J** Quantification of mitophagy in **I**. Bars represent mean±SEM, n=4 replicates per condition, with >50 cells counted per condition for each replicate. ****, p<0.0001; n.s., not significant.

dispensable for mitophagy, but that this type of organellar coupling in fact antagonizes the pathway.

We next sought to demonstrate that the antagonistic effect of mitochondria-ER tethering on mitophagy was functioning directly through the degradation of Mfn2. Conceivably, we could manipulate the pathway by preventing ER-OMM dissociation through the blockage of Mfn2 turnover, which is mediated by proteasomal degradation coupled to parkin ubiquitination (Tanaka et al., 2010; Ziviani et al., 2010). This is in line with our EM data demonstrating that MG132 blocks mitochondria-ER uncoupling during mitophagy (Fig. IV.1H to J). To achieve this, we created Mfn2 KO cells stably-expressing YFP-parkin (Mfn2 KO:YFP-parkin) and re-expressed ectopic Mfn2, which was able to rescue mitochondrial morphology from a fragmented reticulum to a collection of tubules (Fig. IV.4A; CFP is used to identify cells expressing untagged Mfn2). We could additionally rescue morphology by overexpression of Mfn1 (Fig. IV.4A), a phenomenon that has been described previously (Chen et al., 2003). Turning to recruitment assays – in which we observed faster GFP-parkin recruitment in Mfn2 KO cells (Fig. IV.S5D and E) – we observed

that ectopic expression of Mfn2, but not Mfn1, was able to suppress the recruitment of YFP-parkin to depolarized mitochondria (Fig. IV.4B and C). This is in line with our previous data showing that the antagonistic effect of Mfn2 on mitophagy occurs through its ability to tether mitochondria to the ER (Fig. IV.S4H to J) and not its effect on mitochondrial fusion (Fig. IV.S4A to D). Immunoblot analysis of Mfn2 KO:YFP-parkin$^{WT}$ cells ectopically expressing Mfn2 revealed that it was expressed at near endogenous levels in the parental U2OS line and degraded rapidly upon CCCP treatment compared to the control Mfn2 KO:YFP-parkin$^{C431S}$ cell line (Fig. IV.4D). Mfn2 is ubiquitinated by parkin on at least ten lysine residues, although several sites are clustered in the heptad repeat (HR) domains (Sarraf et al., 2013). Additionally, Mfn2 itself has been reported to be directly phosphorylated by PINK1 on T111 and S442, and that these phosphorylation events are critical for the interaction of parkin with Mfn2 and parkin recruitment in cardiomyocytes (Chen and Dorn, 2013). Focusing on these putative phosphorylation sites and the clustered ubiquitination sites in the HR1 and HR2 domains, phylogenic analysis of their conservation demonstrated that only T111 in the GTPase domain and K737 in the HR2 domain were completely conserved from human Mfn2 to the sole *Drosophila* mitofusin, MARF (Fig. IV.S7A and B). However, in the case of the sites of ubiquitination, at least two HR1 sites and three HR2 sites were conserved as lysines down through *Xenopus* Mfn2, while MARF retained one site each in HR1 and HR2 (Fig. IV.S7A). Thus, it was likely that mutation of several lysine residues would be required to abolish Mfn2 ubiquitination. While mutation of all major sites of Mfn2 ubiquitination almost completely abolishes its modification by parkin (Heo et al., 2015), we found that mutation of K406, K416 and K420 in the HR1 domain (Mfn2$^{HR1}$) reduced its CCCP-induced ubiquitination by ~75%, as measured by the disappearance of the unmodified band by immunoblot (Fig. IV.4E and F). This effect was greater than what we observed with the single mutant, Mfn2$^{K406R}$ (K416 and K420

appear dispensable in this assay), and mutation of all four sites in HR2 ($Mfn2^{HR2}$) or the double T111A/S442A phosphomutant ($Mfn2^{TS/AA}$) failed to significantly reduce Mfn2 modification (Fig. IV.4E and F). We thus considered $Mfn2^{HR1}$ as a "hypomorph" with respect to parkin ubiquitination. Introduction of either $Mfn2^{HR1}$, $Mfn2^{HR2}$ or $Mfn2^{T111A/S442A}$ into Mfn2 KO:YFP-parkin cells rescued morphology in a similar manner to WT Mfn2 (Fig. IV.4G), demonstrating these mutations did not disrupt mitochondrial fusion. We also monitored the ability of these Mfn2 mutants to form high molecular weight (HMW) complexes (Karbowski et al., 2006) that function in mitochondria-ER tethering (de Brito and Scorrano, 2008). By blue native polyacrylamide gel electrophoresis (BN-PAGE), we observed that all three mutants (HR1, HR2 and T11A/S442A) formed HMW complexes similar to WT in solubilized mitochondria (Fig. IV.4H). When we assayed mitophagy in Mfn2 KO:YFP-$parkin^{WT}$ cells, we found that only rescue of Mfn2 with $Mfn2^{HR1}$ – the ubiquitination of which is compromised (Fig. IV.4E and F) – blocked the turnover of mitochondria (Fig. IV.4I and J). Thus, ubiquitination of Mfn2 by parkin is required for efficient mitophagy and, taken together with our previous mitophagic data in Mfn2-depleted cells, demonstrates that parkin and PINK1 directly counter Mfn2-mediated mitochondria-ER tethering through Mfn2 turnover to promote mitophagy.

### IV.III.iii *Mfn2 complexes are extracted by p97 to drive mitochondria and the ER apart*

We next investigated exactly how parkin and PINK1 act on Mfn2-mediated OMM-ER tethering. Examining HMW complexes by BN-PAGE in untreated U2OS:GFP-$parkin^{WT}$ cells (expressing endogenous Mfn2), we observed a bimodal distribution of Mfn2 into two complexes, weighing approximately ~250 kDa and ~500 kDa (Fig. IV.5A, leftmost lane, similar to what was seen in Fig. 4H). By contrast, Mfn1 – which, in our assays, appears dispensable for mitochondria-

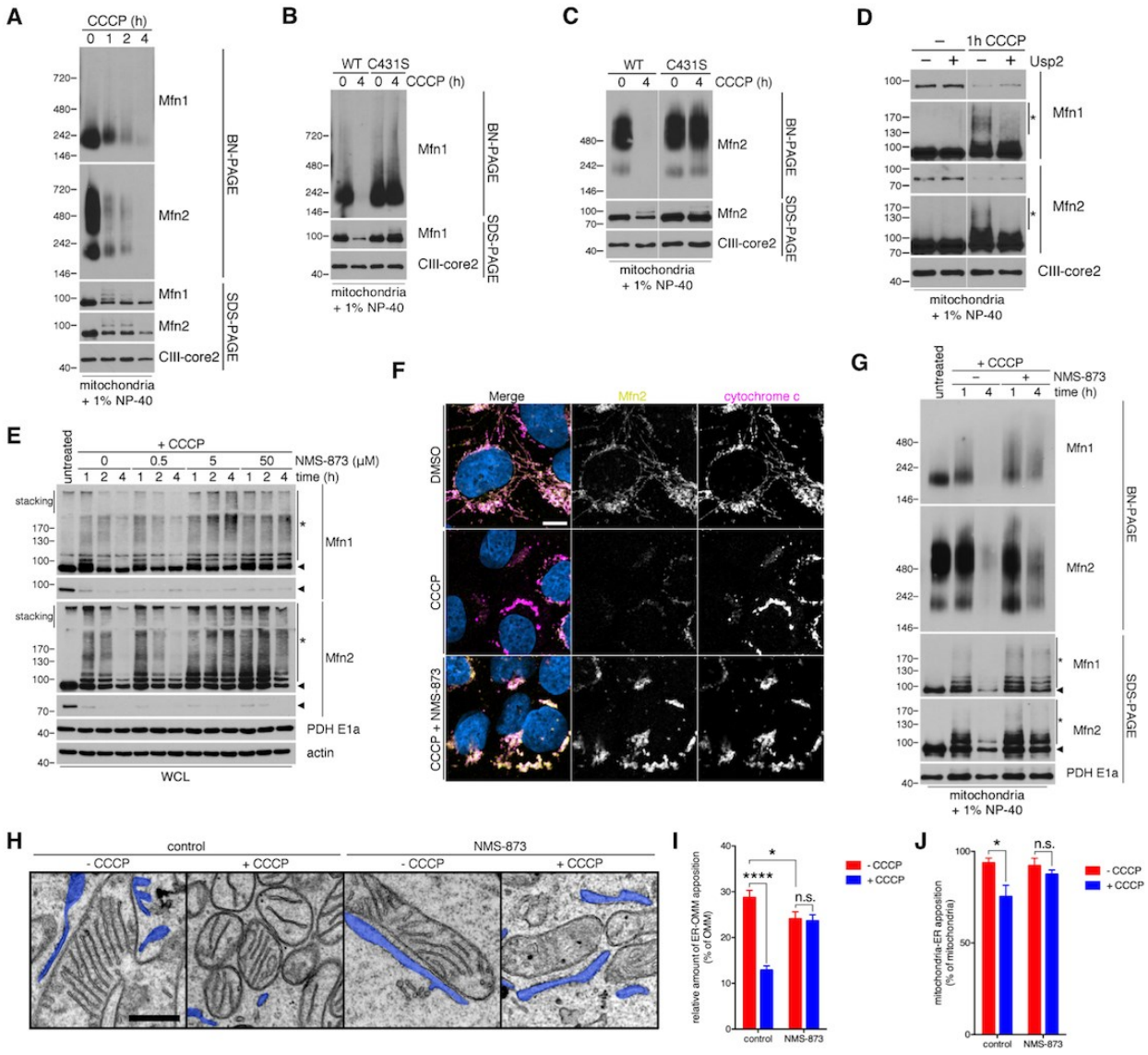


**Figure IV.5**. *p97 governs ER-OMM contact via the extraction of Mfn2 complexes*. See legend on the following page.

ER tethering as assayed by EM (Fig. IV.S2) and its effect on parkin recruitment (Fig. IV.3C to E) – only formed a ~250 kDa HMW complex (Fig. IV.5A). We thus considered the ~500 kDa complex containing solely Mfn2 as a dimer of the ~250 kDa Mfn2-containing subcomplex that potentially bridges the ER and OMM. We then monitored the stability of Mfn2- (and Mfn1-) containing HMW complexes during mitophagy. Upon CCCP treatment, we observed a rapid loss Mfn2- (and Mfn1-) containing complexes (Fig. IV.5A), concomitant with its phosphoubiquitination (Fig. IV.2) and dependent upon parkin ligase activity (Fig. IV.5B and C).

**Figure IV.5**. *p97 governs ER-OMM contact via the extraction of Mfn2 complexes*. **A** Immunoblot analysis of NP-40-solubilized mitochondria, isolated from U2OS:GFP-parkin$^{WT}$ cells treated with 20 μM CCCP for the indicated time, separated by blue native- (BN-) and SDS-PAGE. **B**, **C** Immunoblot analysis of Mfn1- (**B**) and Mfn2- (**C**) containing complexes in NP-40-solubilized mitochondria, isolated from U2OS:GFP-parkin WT and C431S cells treated with 20 μM CCCP for four hours, separated by BN- and SDS-PAGE. **D** Mitochondria isolated from U2OS:GFP-parkin$^{WT}$ cells treated with 20 μM CCCP for one hour were, after solubilization in NP-40, incubated with 1 μM Usp2 for 30 minutes at 37°C prior to separation by SDS-PAGE. Asterisks indicate ubiquitinated species of Mfn1 and Mfn2. **E** Immunoblot analysis of whole-cell lysates (WCL) from U2OS:GFP-parkin cells treated with 20 μM CCCP and the specified concentration of NMS-873 for the indicated time, separated by SDS-PAGE. For each Mfn, longer (upper panel) and shorter (lower panel) exposures are shown. Asterisks indicate ubiquitinated Mfn species, while the arrowheads denote the unmodified band. **F** U2OS:GFP-parkin cells were treated with 20 μM CCCP in the presence or absence of 25 μM NMS-873 for four hours, then fixed and immunostained for Mfn2 (yellow) and cytochrome c (magenta). Scale bar, 10 microns. **G** Immunoblot analysis of NP-40-solubilized mitochondria, isolated from U2OS:GFP-parkin$^{WT}$ cells treated with 20 μM CCCP in the presence or absence of 25 μM NMS-873 for the indicated time, separated by blue native- (BN-) and SDS-PAGE. Asterisks indicate ubiquinated Mfn species visible by SDS-PAGE, while the arrowhead denotes the unmodified band. **H** Representative TEM images of mitochondria in contact with ER (pseudocoloured blue) in U2OS:GFP-parkin cells treated with 20 μM CCCP ( "+CCCP" ) for four hours in the presence or absence of 25 μM NMS-873. Scale bar, 500 nm. **I**, **J** Quantification of TEM from **H** in cells treated with (blue bars) or without (red bars) 20 μM CCCP for four hours. The percent of OMM per mitochondrion (**I**) and mitochondria per field (**J**) in contact with the ER was quantified. Bars represent mean±SEM, n=99 to 187 mitochondria in 12 to 14 fields per condition. n.s., not significant; *, p<.05; ***, p<.001; ****, p<.0001.

Treatment of mitochondrial lysates with Usp2 deubiquitinase, which is active on both ubiquitin and phosphoubiquitin chains (Wauer et al., 2015b), did not robustly rescue the unmodified Mfn1 or Mfn2 band (Fig. IV.5D), indicating that the disappearance of HMW Mfn complexes are due to their extraction from the OMM (and not a high level of modification by Ub). This process is thought to be mediated by the AAA-ATPase p97/VCP (Tanaka et al., 2010) and, accordingly, when we treated U2OS:GFP-parkin$^{WT}$ cells with CCCP in the presence of the non-competitive p97 inhibitor NMS-873 (Magnaghi et al., 2013), we were able to block turnover of both Mfn1 and Mfn2, resulting in a buildup of ubiquitinated Mfn1 and Mfn2 species in a dose-dependent manner (Fig. IV.5E, asterisks). When we immunostained these cells for Mfn2, we observed that Mfn2 was stabilized on mitochondria in the presence of NMS-873 (Fig. IV.5F); extraction of HMW complexes containing either Mfn1 or Mfn2 was accordingly repressed under conditions of p97 inhibition (Fig. IV.5G). Indeed, both ~250 kDa (containing Mfn1 and/or Mfn2) and ~500 kDa (Mfn2 only) complexes were stabilized in the presence of NMS-873, with smearing occurring due

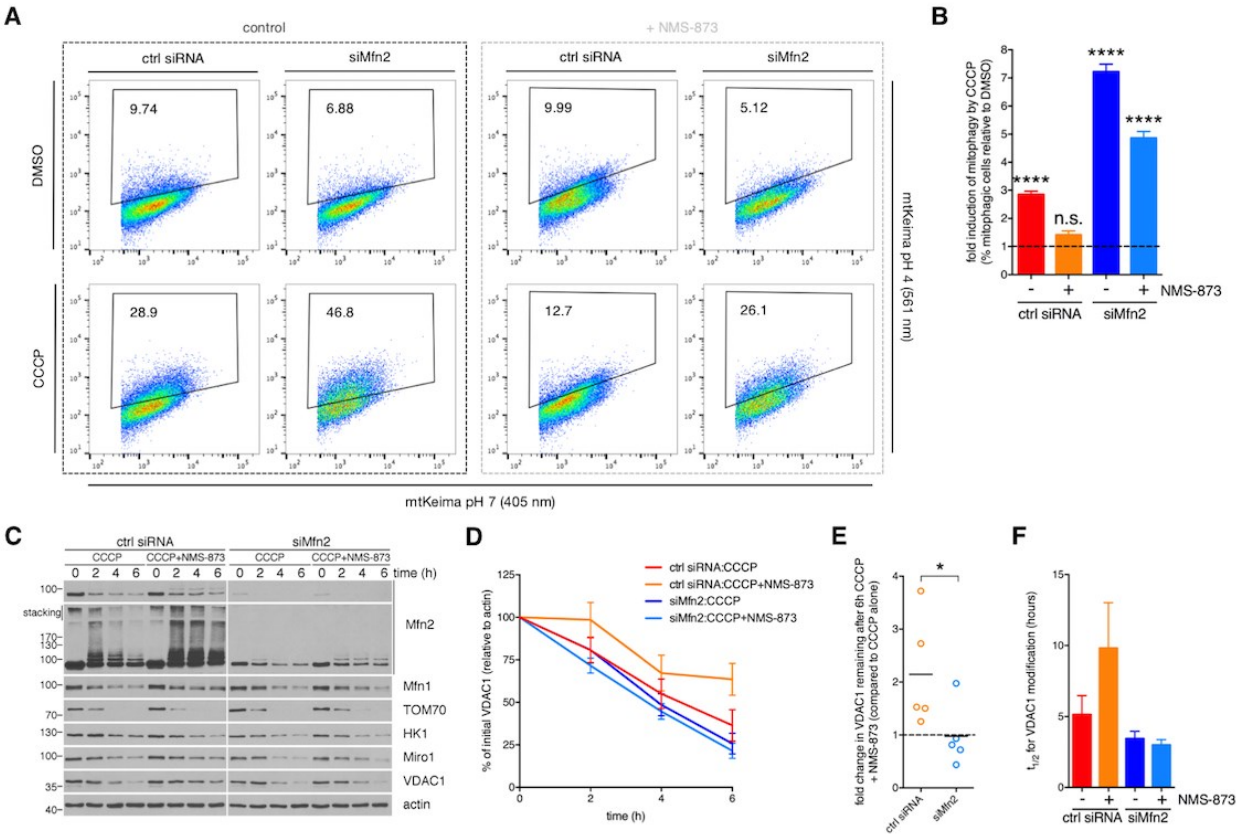


**Figure IV.6**. *p97 and Mfn2 effect mitophagy through parkin substrate availability.* **A** U2OS:mtKeima cells were transfected with the indicated siRNA and GFP-parkin$^{WT}$, and were treated with 20 µM CCCP (or DMSO) for five hours in the presence (dark grey box) or absence (light grey box) of 25 µM NMS-873. mtKeima fluorescence in GFP-positive cells was measured using flow cytometry by excitation at 405 nm (neutral pH) and 561 nm (acidified). The data are represented as scatter plots of fluorescence emission from excitation at both wavelengths. The gated area encloses cells undergoing mitophagy and the percentage of cells within this gate is indicated in the top-left corner of each plot. **B** Quantification of the percent of cells undergoing mitophagy in cells from **A**, expressed as a ratio of CCCP-treated cells to those treated with DMSO. Bars represent mean±SEM, n=2 experiments. n.s., not significant; ****, p<.0001. **C** Immunoblot analysis of U2OS:GFP-parkin cells, transfected with siRNA targeting Mfn2 (siMfn2) or control (ctrl siRNA), treated with 20 µM CCCP in the presence or absence of 25 µM NMS-873 over a period of six hours. **D** Immunoblot quantification of VDAC1 levels (relative to actin) from cells from **C**. Bars represent mean±SEM, n=5 experiments. **E** The 6 hour time-point data from **D** is represented as a fold change in VDAC1 remaining when NMS-873 is added. Data points are represented on the graph, n=5 experiments. *, p<0.05. **F** Quantification of VDAC1 half-lives ($t_{1/2}$) in cells from **C** over 6 hours. Half-lives were obtained from decay curves generated with the time-points in **C**. Bars represent mean±SEM, n=5 experiments.

to Mfn ubiquitination (Fig. IV.5G), indicating that parkin-mediated ubiquitination itself was not sufficient to drive apart the ~500 kDa Mfn2-containing interorganellar bridge. Analysis of OMM-ER appositions in these cells revealed that p97 inhibition prevented the dissociation of mitochondria from the ER (Fig. IV.5H to J). Thus, p97-dependent extraction of Mfn2 HMW

complexes, flagged by parkin-mediated ubiquitination, from the OMM separates mitochondria from the ER during mitophagy.

The herein-described role of p97 in separating mitochondria from the ER is critical; parkin-mediated ubiquitination on its own appears to be insufficient to drive the disassembly of Mfn2 HMW complexes (Fig. IV.5G) or to dissociate the ER from the OMM (Fig. IV.5H-J) in the absence of p97 activity. To clarify the role of p97 in mitophagy, we investigated the potentially epistatic relationship between p97 and Mfn2. We first measured mitophagy in U2OS:mtKeima cells expressing GFP-parkin$^{WT}$, comparing the effect of p97 inhibition in cells depleted of Mfn2 to control cells. In control siRNA-transfected cells, inhibition of p97 by NMS-873 abolished the CCCP-dependent, ~3-fold increase in cells with acidified mtKeima (Fig. IV.6A and B, red and orange bars in Fig. IV.6B). When cells were depleted of Mfn2 (siMfn2), p97 inhibition reduced the rate of mtKeima acidification (Fig. IV.6A and B, dark and light blue bars), but mitophagy was still permissive. Indeed, the number of cells with acidified mtKeima in siMfn2 cells treated with NMS-873 was still ~5-fold greater than their DMSO treated counterparts (Fig. IV.6B, light blue bar), which was more of an increase that was observed for control cells with active p97 (Fig. IV.6B, red bar). Thus, in the absence of Mfn2, inhibition of p97 fails to suppress the enhancement of mitophagy that it induces in control cells, demonstrating that a significant component of the role of p97 in mitophagy functions through Mfn2. As p97 extracts Mfn2-containing interorganellar bridges to uncouple mitochondria from the ER (Fig. IV.5), we reasoned that Mfn2-mediated mitochondria-ER tethering may protect certain OMM substrates from parkin-mediated ubiquitination. Thus, we analyzed a sample of parkin substrates by immunoblot in CCCP-treated cells depleted of Mfn2 compared to control, in the presence or absence of NMS-873 (Fig. IV.6C). We observed that the parkin-dependent ubiquitination of VDAC1 – which has been reported to

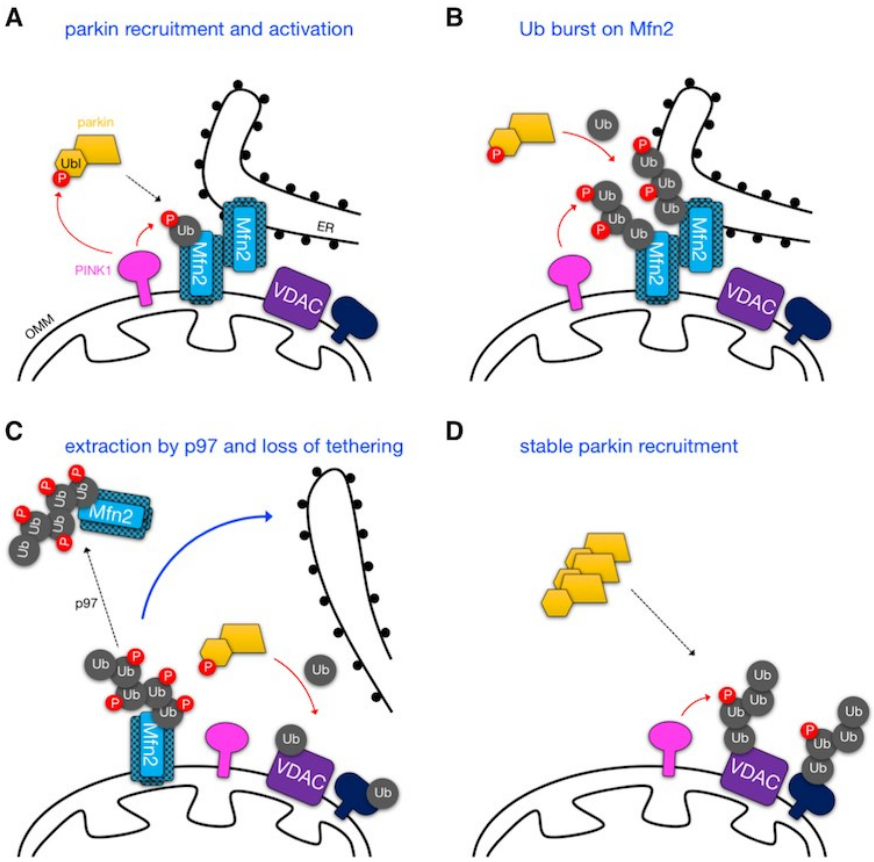


**Figure IV.7**. *Dismantling of Mfn2 interorganellar bridges by p97/VCP gates the release of endoplasmic reticulum from mitochondria to drive PINK1/parkin mitophagy.* **A** PINK1-phosphorylated Ub on Mfn2 initially recruits parkin to Mfn2 complexes, where it is phosphorylated and activated by PINK1. **B** Parkin and PINK1 cooperate to catalyze a pUb burst on Mfn2. **C** Ubiquitinated Mfn2 HMW complexes are recognized by p97, extracted from the OMM, and degraded by the proteasome. **D** VDACs and possibly other substrates become available to the parkin/PINK1 system, and their phosphoubiquitination stabilizes parkin on mitochondria to drive mitophagy.

form a complex with phosphoubiquitin and parkin that is stable over a period of hours (Callegari et al., 2016) – was selectively-dependent upon p97 activity in control cells, but not cells depleted of Mfn2 (Fig. IV.6C to E). Indeed, the half-life of unmodified VDAC1 during mitophagy increased two-fold in the presence of NMS-873 specifically in control cells compared to cells transfected with siMfn2 (Fig. IV.6F). Thus, p97 relieves Mfn2-dependent inhibition of the ubiquitination of VDAC1 (and possibly other OMM substrates). In this manner, Mfn2 (which is a transient parkin interactor on the OMM as it is rapidly extracted by p97 [Fig. IV.S8]) gates the availability of the stable parkin receptor VDAC1 (Callegari et al., 2016), and mechanistically reconciles our earlier data concerning the destruction of ER-OMM contacts during mitophagy, Mfn2-dependent mitophagy inhibition, and p97-mediated facilitation of ER-OMM uncoupling.

## IV.IV DISCUSSION

Here, we have described a reciprocal relationship between mitochondria-ER tethering and mitophagy. Contacts between both organelles are destroyed during mitophagy, in both cell lines and cultured dopaminergic neurons, and we demonstrate a requirement for parkin, PINK1 and proteasomal activity in this process. Complementarily, mitochondria-ER contacts themselves are negative regulators of mitophagy, as their reduction facilitates parkin substrate ubiquitination, its translocation to mitochondria and mitochondrial turnover. We identify the known mitochondria-ER tether Mfn2 as a factor that is rapidly phosphoubiquitinated upon the induction of mitophagy, and show that Mfn2-containing HMW complexes are extracted from the OMM by p97. Both reduction of Mfn2 ubiquitination and p97 inhibition repress mitophagy. We identify a regulatory role for Mfn2-mediated mitochondria-ER coupling within the parkin/PINK1 pathway, which is counteracted by the ubiquitination of Mfn2 by parkin and its p97-dependent turnover.

We propose a model in which the PINK1/parkin/p97 axis acts rapidly on Mfn2 HMW complexes to separate mitochondria from the ER in order to facilitate mitophagy, potentially by making more substrates available to the parkin/PINK1 system (Fig. IV.7). Emerging from this model is the intriguing possibility that mitochondria-ER contacts are initial sites of PINK1/parkin activity and Ub phosphorylation, and would thus be critical loci of mitophagic regulation by deubiquitinating enzymes and as-yet unidentified ubiquitin phosphatases. A recent cryoelectron tomographical study on the ancestral yeast mitofusin Fzo1p demonstrated the existence of a ring-like structure formed by Fzo1p during the docking stage of mitochondrial fusion (Brandt et al., 2016). Mfn2 bridges between mitochondria and the ER may therefore form a similar type of ring, potentially restricting the availability of non-mitofusin OMM substrates such as VDAC1 (Fig. 6C to F) to parkin and/or PINK1. With respect to the latter case, PINK1 has recently been shown to

localize to the mitochondria-associated membrane of the ER (MAM) upon depolarization (Gelmetti et al., 2017), and a physical interaction between VDACs on the OMM and $IP_3$ receptors on the ER places this parkin substrate at contacts between both organelles (Szabadkai et al., 2006). The existence of a ~500 kDa Mfn2-containing interorganellar bridge is supported by our BN-PAGE data (Fig. IV.5A) demonstrating that Mfn2 uniquely exists in a homotypic dimer of ~250 kDa subunits, as it has been demonstrated that ~500 kDa mitofusin complexes form from subcomplexes on adjacent membranes (Ishihara et al., 2004). Our observation of a steady-state ~500 kDa complex containing Mfn2 but not Mfn1 correlates with the reduced activity of the Mfn2 GTPase domain in comparison to Mfn1 (Ishihara et al., 2004), and fits a model in which Mfns tether membranes in the GTP-bound state (Brandt et al., 2016; Ishihara et al., 2004; Qi et al., 2016). Here, we show that the stability of these complexes can be negatively regulated by parkin-mediated Mfn2 ubiquitination coupled to p97-dependent extraction. Taken together with another study demonstrating that MITOL-mediated Mfn2 ubiquitination (on different lysine residues) can positively regulate complex formation and mitochondria-ER tethering (Sugiura et al., 2013), these data emphasize Mfn2 ubiquitination as an important regulator of mitochondria-ER contact.

Robust parkin activation during mitophagy occurs through a feed-forward mechanism (Ordureau et al., 2014). PINK1-phosphorylated Ub serves to both activate and anchor parkin to the OMM, where it can ligate more Ub moieties that are subsequently phosphorylated (Okatsu et al., 2015b; Ordureau et al., 2014). Here, our data hint at a hierarchy of parkin substrates. The Mfns undergo a burst of phosphoubiquitination at the onset of mitophagy, driven by localized parkin activation – potentially due to their proximity to PINK1 (Chen and Dorn, 2013). Indeed, our GFP-parkin immunoprecipitation and OMM substrate turnover kinetics (Fig. IV.2A to C) clearly show a preference for the Mfns above other parkin substrates such as HK1 and Miro1. The Mfns are

then rapidly extracted from the OMM by p97 (Fig. IV.5A and G) in a step that coincides temporally with parkin translocation to mitochondria. It is therefore unlikely that Mfn1 or Mfn2 act as a parkin receptor in this paradigm – as others have suggested (Chen and Dorn, 2013) – for this reason, especially when our recruitment data in Mfn2-deficient cells (Fig. IV.3C to E and Fig. IV.S6) are taken into account. Indeed, we demonstrate that Mfn2 acts as a stable parkin tether only under conditions of p97 inhibition (Fig IV.S8). Our data support a role for the involvement of VDAC1 in a stable complex that tethers parkin to the OMM (Callegari et al., 2016); indeed, as β-barrel channels fully integrated into the membrane, VDACs may not be amenable to p97-dependent extraction. Mfn2 may act as a parkin receptor in cardiomyocytes (Chen and Dorn, 2013), where parkin-dependent clearance of mitochondria by autophagy plays a role in metabolic development (Gong et al., 2015) rather than quality control, and thus may occur by a distinct mechanism; the phosphomutant $Mfn2^{T111A/S442A}$ or Mfn2 deletion blocks parkin-mediated mitophagy in the heart but not in cell lines (Fig. IV.4I and J, Fig. IV.S5, and (Narendra et al., 2008)). Conceivably, phosphorylation of Mfn2 on T111 and S442 by a cardiac-specific S/T kinase (or cardiac PINK1, as has been proposed (Chen and Dorn, 2013)) may facilitate mitophagy in the heart by uncoupling mitochondria from the sarcoplasmic reticulum.

Our study describes an antagonistic, reciprocal relationship between mitophagy and interorganellar tethering between mitochondria and the ER. This highlights a fundamental difference between mitophagy and the more canonical starvation-induced autophagy pathway, the latter of which requires mitochondria-ER contact sites for autophagosome formation (Hamasaki et al., 2013). While mitophagy functions as a quality control mechanism (Ryan et al., 2015), starvation-induced autophagy is a metabolic response, and thus its initiation at contact sites between mitochondria and the ER may serve to decode the metabolic needs of the cell.

Mechanistically, both mitochondria (Hailey et al., 2010) and the ER (Hayashi-Nishino et al., 2009) have been reported to function as autophagosomal membrane sources during starvation, and mitochondrial damage may preclude the former from participating in this process during mitophagy. Accordingly, the SNARE Stx17, which governs autophagosome-lysosome fusion during starvation (Itakura et al., 2012b), is dispensable for mitophagy (McLelland et al., 2016; Nguyen et al., 2016). Indeed, Stx17 appears to suppress mitophagy (Fig. IV.S4G to I) through its role in supporting mitochondria-ER contact (Arasaki et al., 2015). While mitophagy does indeed share morphological and several mechanistic similarities with canonical macroautophagy – including the recruitment of ULK1 complexes and ATG9A vesicles to depolarized mitochondria (Itakura et al., 2012a; Lazarou et al., 2015) – molecular dissection of mitophagosome formation and fusion requires further study.

Finally, our data posit the possibility of steady-state regulation of mitochondria-ER contact by PINK1/parkin, separately from mitophagy. In flies, phenotypes of *PINK1* and *PRKN* mutants are duplicated by overexpression of the sole *Drosophila* mitofusin MARF, and suppressed by p97 overexpression (Yun et al., 2014; Zhang et al., 2017a). Thus, PINK1/parkin/p97 counteract MARF *in vivo* through its ubiquitination and turnover (Wang et al., 2016d; Zhang et al., 2017a; Ziviani et al., 2010). Indeed, a proposed mechanism of cell death due to deletion of *PINK1* is the sensitization of mitochondria to $Ca^{2+}$ overload (Akundi et al., 2011; Gandhi et al., 2009; Kostic et al., 2015), the root cause of which may be dysregulation of mitochondria-ER contact. Accordingly, deletion of the mitochondrial $Ca^{2+}$ uniporter protects dopaminergic neurons from cell death in *PINK1*-deficient zebrafish (Soman et al., 2017). While we did not observe any steady-state differences in the extent of mitochondria-ER coupling in either parkin overexpression (Fig. IV.1A to E) or loss-of-function (Fig. IV.1L and M) systems, others have observed an increased degree of contact and

metabolite transfer in both fibroblasts from *PRKN* and *PINK1* patients, as well as brains from *PINK1* and *PRKN* mutant flies (Celardo et al., 2016; Gautier et al., 2016). Conversely, we (Fig. IV.1H to J) and others (Gelmetti et al., 2017) measured a destabilization of mitochondria-ER tethering when PINK1 was transiently depleted. While differences between studies can be attributed to cell type and culture conditions, how mitochondria-ER contact is quantified is certainly a determinant; whereas we quantified ER tubules within 100 nm of the OMM, Gautier *et al*. extended this distance to 500 nm, and this may effectively account for observed differences. For this study, our <100 nm criterion was sufficient to capture ER tubules directly opposite the OMM (see OMM extension outlines in Fig. IV.1L). Future studies will aim to a) address when and where PINK1/parkin act to regulate the OMM-ER interface via Mfn2, and b) understand how dysregulation of mitochondria-ER contact during mitophagy and at the steady-state may contribute to disease pathology. The work described here lays the foundation for these future studies, identifying a molecular mechanism for contact site destabilization through the ubiquitination of Mfn2 tethering complexes by the PINK1/parkin system and their extraction and destruction via p97 and the proteasome.

## IV.V MATERIALS AND METHODS

*Antibodies and other reagents*

Antibodies used in this study include anti-actin (Millipore, MAB1501), anti-Cardif (referred to herein as MAVS, Enzo Life Sciences, ALX-210-929-C100), anti-cytochrome c (BD Biosciences, 556432), anti-GFP (ab6673, Abcam), anti-GFP (A6455, Invitrogen), anti-HA (Abcam, ab9134), anti-HK1 (Cell Signaling Technology, 2024S), anti-Mfn1 (Santa Cruz, sc-50330), anti-Mfn2 (Sigma Aldrich, M6319), anti-Mfn2 (Cell Signaling, 9482), anti-MTCO1 (herein referred to as

CIV-COXI, ab14705), anti-p62 (Progen, GP62-C), anti-PDH E1a (Abcam, ab110330), anti-PDI (Abcam, ab2792), anti-PINK1 (Cell Signaling, 6946), anti-pS65 ubiquitin (Millipore, ABS1513-I), anti-Rhot1 (referred to herein as Miro1, Sigma, HPA010687), anti-SDHA (referred to herein as CII-SDHA, Abcam, ab14715), anti-Stx17 (ProteinTech, 17815-1-AP), anti-TOM20 (Santa Cruz, sc-11414), anti-TOM70 (Santa Cruz, sc-390545), anti-ubiquitin [FK2] (Enzo Life Sciences, BML-PW8810), anti-ubiquitin [P4DI] (Santa Cruz, sc-8017), anti-UQCRC2 (referred to herein as CIII-core2, Abcam, ab14745), anti-UQCRFS1 (referred to herein as CIII-Rieske, Abcam, ab14746), and anti-VDAC1 (Abcam, ab14734). Halt phosphatase inhibitor cocktail was purchased from Thermo Fisher Scientific, and NMS-873 was purchased from ApexBio. Unless otherwise specified, all other reagents were purchased from Sigma-Aldrich.

*Cell culture and iPS cell differentiation*

U2OS cells were maintained in DMEM supplemented with L-glutamine, penicillin/streptomycin, and 10% FBS in the presence of either 25 mM glucose or 10 mM galactose (Wisent, Saint-Bruno, QC). Glucose-maintained cells were cultured in galactose-containing medium for at least seven days before use in experiments. The parkin mutant iPSC line (*PRKN*$^{mut}$) was initially isolated from a patient carrying compound heterozygous mutations (delEx7/c.1072delT) in the *PRKN* gene (Grunewald et al., 2010). Control lines used in this study were NCRM1 (NIH, Bethesda, MD) and L2131 (Chung et al., 2016). Differentiation of iPSCs into dopaminergic neurons was based on a protocol by Xi and colleagues (Xi et al., 2012). iPSCs were initially grown in non-coated flasks for one week in DMEM/F12 supplemented with N2 and B27, in the presence of 10 μM SB431542, 200 ng/ml noggin, 1 μM CHIR99021, 200 ng/ml Shh and 100 ng/ml FGF-8. Embryoid bodies were transferred to polyornithine- and laminin-coated flasks to form rosettes, grown in the

presence and then absence of the above-indicated differentiation factors for one week each. Neural progenitors were then cultured in 50% DMEM/F12 and 50% Neurobasal medium, supplemented with N2 and B27, in the presence of 1 μg/ml laminin, 500 μM db-cAMP, 20 ng/ml BDNF, 20 ng/ml GDNF, 200 μM ascorbic acid, 50 μM valproic, 100 nM Compound A and 1 ng/ml TGF-β. Progenitors were then grown in 25% DMEM/F12 and 75% Neurobasal medium, supplemented as above, for three days, and final differentiation into dopaminergic neurons occurred over four weeks in Neurobasal medium (supplemented as above).

*Plasmids and transfection*

Cells were transfected with siRNA or DNA using jetPRIME transfection reagent (Polyplus Sciences) according to the manufacturer's instructions. Cells were typically analyzed three or one days after siRNA or DNA transfection, respectively. The DsRed-LC3 (Boland et al., 2008), HA-Ub (Durcan et al., 2014) and Mfn2 (Neuspiel et al., 2005) plasmids have been described previously. Mfn mutants were generated using the QuikChange II site-directed mutagenesis kit (Agilent Technologies) according to the manufacturer's instructions and confirmed by sequencing. While duplexed oligonucleotides were used in the mutagenesis reactions, only forward primers are listed below. $Mfn2^{HR1}$ was created by sequential reactions with 5'-CTGAAATTTATTGACAGACAGCTGGAGCTCTTG-3' and 5'-CTTGGCTCAAGACTATAGGCTGCGAATTAAGCAG-3' to create $Mfn2^{K406R/K416R}$, then with 5'-CTATAGGCTGCGAATTAGGCAGATTACGGAGGAAG-3' to make $Mfn2^{HR1}$, as this last primer contains the K416R substitution already present. Likewise, $Mfn2^{HR2}$ was created by sequential reactions with 5'-CCGCCATGAACAAGAGAATTGAGGTTCTTG-3', 5'-CTCACTTCAGAGCAGAGCAAAGCTGCTC-3' and 5'-

CTGCTCAGGAATAGAGCCGGTTGGTTG-3' to make Mfn2$^{K720R/K730R/K737R}$, and then with 5'-GCCGCCATGAACAGGAGAATTGAGGTTC-3' to make the final K719R mutation. Mfn2$^{T111A/S442A}$ was created using 5'-CAATGGGAAGAGCGCCGTGATCAATGC-3' and 5'-GAGGAGATCAGGCGCCTCGCAGTACTGGTGGACGATTAC-3'. U2OS:GFP, U2OS:GFP-parkin$^{WT}$, U2OS:GFP-parkin$^{C431S}$ and U2OS:mtKeima stable cell lines have been described previously (Tang et al., 2017), and the Mfn2 KO:YFP-parkin$^{WT}$ and Mfn2 KO:YFP-parkin$^{C431S}$ lines were created in the same manner using YFP-parkin constructs generated in that study. To create the initial Mfn2 KO U2OS cell lines, the human *MFN2* gene was disrupted in exon 3 using the following guide RNA: 5'-CACUUAAGCACUUUGUCACU-3'.

*RNA interference*

siRNA targeting PINK1 and Stx17 have been previously described (McLelland et al., 2016). Non-targeting siRNA oligonucleiotides, as well as siRNA targeting Mfn1 (5'-GAUACUAGCUACUGUGAAAdTdT-3') (Zhao et al., 2013), Mfn2 (5'-GGAAGAGCACCGUGAUCAAdTdT-3') (Zhao et al., 2013) and PACS2 (5'-AACACGCCCGUGCCCAUGAACdTdT-3') (Simmen et al., 2005) were purchased from Thermo Fisher Scientific.

*Cell lysis and immunoblotting*

Cells were lysed in lysis buffer (20 mM Tris pH 7.5, 150 mM NaCl, 1 mM EDTA, 1 mM EGTA, 1% NP-40 substitute, 1% sodium deoxycholate, protease inhibitor cocktail [aprotinin, leupeptin and benzamidine], and phosphatase inhibitor cocktail) on ice. Lysates were cleared by centrifugation, protein was quantified by BCA assay (Pierce/Thermo Scientific), separated by

SDS-PAGE over Tris-glycine gels and transferred to nitrocellulose membrane. Primary antibodies were diluted in 3% BSA in PBS-Tween and incubations performed overnight at 4°C. The following day, membranes were washed and incubated in HRP-conjugated secondary antibodies (Jackson ImmunoResearch Laboratories), diluted in 5% milk in PBS-Tween, at room temperature for one hour. Protein bands were detected using Western Lightning ECL and Plus-ECL kits (PerkinElmer), according to the manufacturer's instructions.

*Immunoprecipitation*

Cells were lysed in HEPES-IP buffer (20 mM HEPES pH 7.2, 150 mM NaCl, 1% NP-40 substitute, 0.1% sodium deoxycholate, and protease/phosphatase inhibitor cocktails) or denaturing IP buffer (20 mM Tris pH 7.5, 300 mM NaCl, 1% NP-40 substitute, 0.5% sodium deoxycholate, 0.1% SDS and protease/phosphatase inhibitor cocktails) and protein content was quantified by BCA assay after clearing by centrifugation. Lysates were equilibrated to 1 to 2 mg/ml protein and immunocapture was performed with the indicated antibody overnight at 4°C at a 1:10 to 1:100 dilution. The following day, immunoprecipitation was performed with protein A- or protein G-sepharose (GE Healthcare) for four hours at 4°C. Immunoprecipitates were washed five times in buffer and eluted by incubating in SDS-PAGE sample buffer at 90°C.

*Mitochondrial isolation and BN-PAGE*

After treatment, U2OS cells were collected from 2 x 15-cm plates per condition in isolation buffer (20 mM Hepes pH 7.4, 220 mM mannitol, 68 mM sucrose, 76 mM KCl, 4 mM KOAc, and 2 mM $MgCl_2$, supplemented with protease inhibitors benzamidine, PMSF, aprotinin, and leupeptin) and passed through a 27.5-gauge syringe twenty times. Cell lysates were centrifuged at 600 g for 10

minutes at 4°C. Supernatants were then centrifuged at 10,000 g for 10 minutes at 4°C. The mitochondrial pellet was resuspended in isolation buffer and centrifuged again at 12,000 g for 10 minutes at 4°C. Protein content of mitochondria was determined by BCA assay, and equilibrated to 1 mg/ml prior to lysis with 1% NP-40 substitute at 4°C for 30 minutes. Mitochondrial lysates were clarified by centrifugation and added to sample buffer and Coomassie Blue G-250. Solubilized complexes were separated over 4-16% and 3-12% Bis-Tris gels and transferred to PVDF membrane using the NativePAGE Novex Bis-Tris gel system (Life Technologies) according to the manufacturer's instruction prior to immunoblotting. In addition, certain samples were incubated with 1 μM Usp2 (Boston Biochem) for 30 minutes at 37°C following NP-40 lysis, then separated by SDS-PAGE as above.

*LC/MS*

Mfn2 was immunoprecipitated under denaturing conditions as described above. Immunoprecipitates were washed twice in PBS, then twice more in 50 mM ammonium acetate pH 7.0, and eluted twice in 50% acetic acid on ice for 10 minutes. Eluates were pooled, cleared by centrifugation and dried by speedvac. Pellets were resuspended in 8 μl 6M urea, 50 mM TEAB pH 8.5, and added to 40 μl 50 mM TEAB pH 8.5. The sample was reduced in 2 mM TCEP at 37°C for ten minutes, and then alkylated in 20 mM iodoacetamide for 30 minutes at room temperature in the dark. The 50 μl sample was then digested with 0.2 μg of trypsin for two hours at 37°C, and then quenched in 0.5% trifluoroacetic acid (TFA) and 5% acetonitrile. Digests were C18-purified using ZipTips (Millipore), eluted in 0.1% TFA/80% acetonitrile, and evaporated and resuspended in 0.1% TFA/4% acetonitrile. Peptides were diluted in 0.1% TFA and 4% acetonitrile, and eluted from an Acclaim PepMap100 C18 column (75 μm × 25cm) with a 1h 5-40% gradient of

acetonitrile in 0.1% formic acid at 300 nL/min. The eluted peptides were analyzed with an Impact II Q-TOF spectrometer equipped with a Captive Spray nano electrospray source (Bruker). Data was acquired using data-dependent auto-MS/MS with a range 150-2200 m/z range, a fixed cycle time of 3 sec, a dynamic exclusion of 1 min, m/z dependent isolation window (1.5-5 Th) and collision energy 25-75 eV (Beck et al., 2015). MS/MS data were analyzed using MASCOT using a standard search procedure against the human proteome, or using Biotools (Bruker) to find ubiquitin and phospho-ubiquitin peptides. Extracted ion chromatograms were integrated using the Data Analysis software (Bruker).

*Transmission electron microscopy*

After treatment, cells grown in chamber slides were fixed in 2.5% glutaraldehyde in PBS for one hour at room temperature, then stored at 4°C overnight before processing. Thin sections on grids were observed in a Tecnai 12 BioTwin transmission electron microscope (FEI) at 120 keV. Images were acquired with a charge coupled device camera (AMT).

*Immunofluorescence and fluorescence microscopy*

Cells were grown on glass coverslips, treated then fixed in 6% formaldehyde in PBS for 15 minutes 37°C. Fixed cells were permeabilized in 0.25% Triton X-100 in PBS for 10 minutes, and blocked in 10% FBS in PBS. Primary antibodies were diluted in 5% FBS in PBS, and incubations were performed for one hour at room temperature. Alexa Fluor-conjugated secondary antibodies (Thermo Fisher Scientific) were performed in the same manner. Cells were counterstained with Hoescht 33342 (Invitrogen) and mounted on glass slides using Aqua Poly/Mount (Polysciences Inc.). Confocal slices (<1 micron-thick) were acquired via a spinning disc confocal microscope

(with Andor Yokogawa system IX81, Olympus) through a 100X, 1.4 NA or 60X, 1.4 NA objective lens. Widefield microscopy was performed using a Zeiss AxioObserver Z1 microscope through a 63X, 1.4 NA objective lens.

*Fluorescence-activated cell sorting and mtKeima measurements*

Quantitative analysis of mitophagy was performed as described previously (Tang et al., 2017). U2OS:mtKeima were first transfected with siRNA targeting Mfn1 or Mfn2. Two days later, mtKeima was induced with 10 μM ponasterone A, and cells were transfected with GFP-parkin WT or C431S for 12 to 18h. The next day (3 days post-siRNA transfection), cells were treated with 20 μM CCCP (or DMSO) for four hours, trypsinized and collected in PBS. Cell fluorescence was analyzed by an LSR Fortessa (BD Bioscience) fluorescence-activated cell sorter, using excitation wavelengths of 405 nm and 561 nm to detect Keima at pH 7.0 and 4.0, respectively, and 488 nm to detect GFP-parkin. Cell fluorescence data were analyzed using FlowJo (Tree Star). For each condition, $10^5$ cells, gated for GFP-parkin expression, were used for the analysis.

*Image and statistical analyses*

The numbers of cells quantified per experiment are explicitly indicated in the figure legends. No statistical method was used to predetermine the experimental sample size. Statistical tests and representations of the data were generated using Prism (GraphPad Software, La Jolla, CA). Data are displayed as the mean ± standard error of the mean (SEM). Statistical significance was determined by one- (Fig. IV.S2B, IV.S2C, IV.S2D, IV.4F, IV.4J) and two-way (Fig. IV.1B, IV.1C, IV.1D, IV.1E, IV.1I, IV.1J, IV.1M, IV.3E, IV.3G, IV.S3B, IV.S4D, IV.S4I, IV.S5E, IV.S5G, IV.S6C, IV.S6D, IV.S6G, IV.4C, IV.5I, IV.5J, IV.6B) ANOVAs followed by Bonferroni *post-hoc*

tests, or one-tailed t-test (Fig. IV.6E). Differences were considered significant if $p<.05$. The diagram of the crystal structure of the pUb-parkin complex was created with PyMOL. Images were analyzed using ImageJ (NIH), and analyses were performed blindly.

## IV.VI ACKNOWLEDGEMENTS

This work was supported by an operating grant from the Canadian Institutes for Health Research (CIHR) to E.A.F. G.L.M. was supported by a Canada Graduate Scholarship from the CIHR and a *Mouvement Desjardins* award from the Montreal Neurological Institute. The authors are grateful to Matthew Tang for technical advice regarding mtKeima acquisition experiments, stable cell line creation and cell sorting. The authors also thank Jeannie Mui and the Facility for Electron Microscopy Research (McGill) for TEM sample processing and technical advice, and Carol Chen (iPSC-CRISPR platform, Montreal Neurological Institute) for technical help with iPSC differentiation. The antibodies against MCU, MICU1 and MICU2 were kind gifts from Heidi McBride (McGill). All cell lines and reagents generated by the Montreal Neurological Institute (MNI) IPSC/CRISPR Platform are available without restriction via the MNI Tanenbaum Open Science Institute.

# IV.VII SUPPLEMENTARY FIGURES

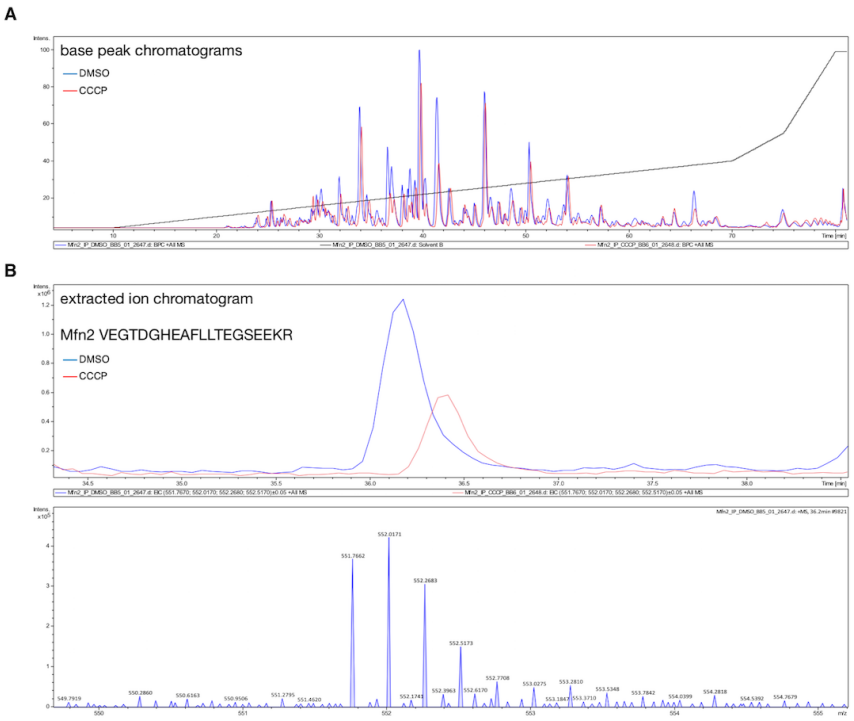


**Figure IV.S1**. *LC/MS of immunoprecipitated Mfn2*. **A** Base peak chromatograms indicating equal loading of both DMSO- and CCCP-treated samples from Fig. IV.2E and F. **B** Extracted ion chromatogram of the indicated Mfn2 peptide (a.a. 136-155) from both DMSO- (blue line) and CCCP- (red line) treated samples.

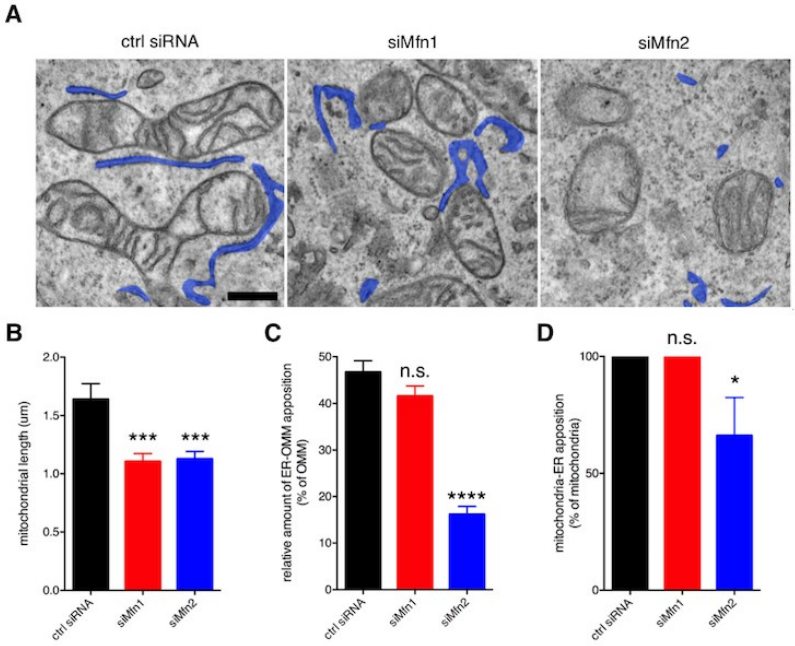


**Figure IV.S2**. *Mfn2 is a mitochondrion-ER tether*. **A** Representative TEM images of U2OS:GFP-parkin cells transfected with the indicated siRNA. ER tubules are pseudocoloured blue. Scale bar, 500 nm. **B**-**D** Quantification of mitochondrial length (**B**), relative percentage of OMM in contact with the ER (**C**) and percentage of mitochondria in contact with ER per field of view (**D**) in cells from **A**. Bars represent mean±SEM, n=66 to 70 mitochondria in 5 to 7 fields per condition. n.s., not significant; *, p<.05; ***, p<.001; ****, p<.0001.

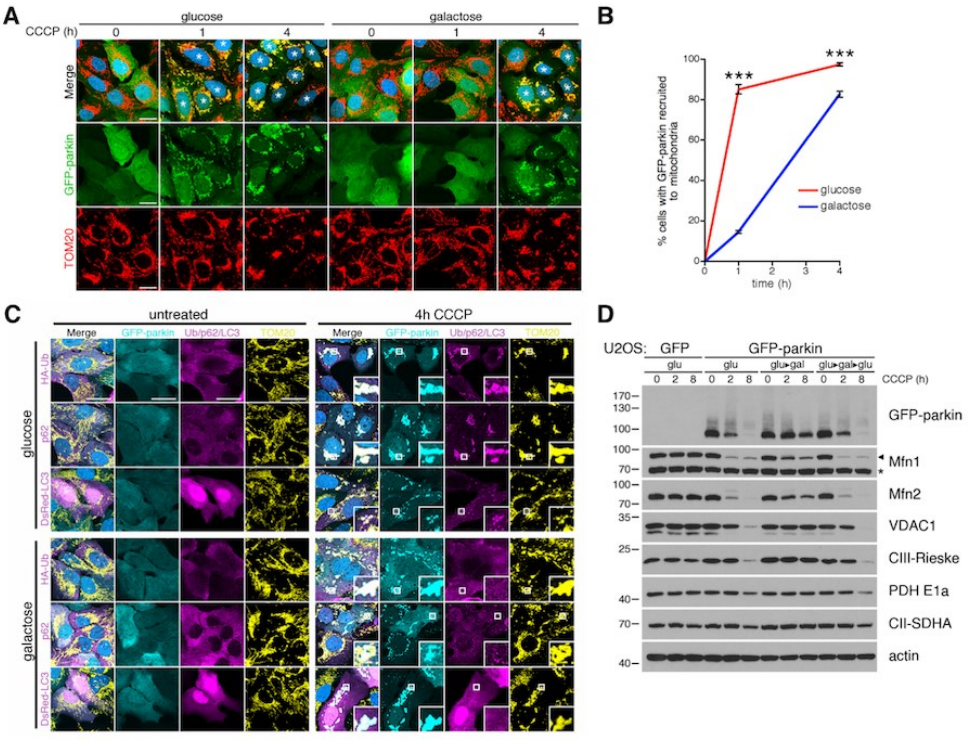


**Figure IV.S3**. *Mitochondrial respiration impedes mitophagy*. **A** Representative confocal images of U2OS:GFP-parkin (green) cells, grown on either glucose or galactose, treated with 20 μM CCCP for the indicated times. Cells were then fixed and stained for TOM20 (red) (Hoescht, blue). Cells marked with asterisks display parkin fully translocated to mitochondria. Scale bars, 20 microns. **B** Quantification of parkin recruitment to mitochondria in cells treated in **A**. Bars represent mean±SEM, n=3 replicates cells per condition, with >100 cells counted per condition for each replicate. ***, p<.001. (C) Representative confocal images of U2OS:GFP-parkin (cyan) cells expressing the indicated construct, treated with 20 μM CCCP for four hours and then fixed and stained for TOM20 (yellow) and the indicated tag (magenta) (Hoescht, blue). In the case of p62 (middle panels), an antibody against endogenous p62 was used. Scale bars, 30 microns. **D** Immunoblot analysis of whole-cell lysates from U2OS:GFP and GFP-parkin cells – grown either on glucose ( "glu" ), converted to galactose ( "glu>gal" ) or back to glucose ( "glu>gal>glu" ) – treated with 20 μM CCCP for the indicated times. The asterisk indicates a non-specific band.

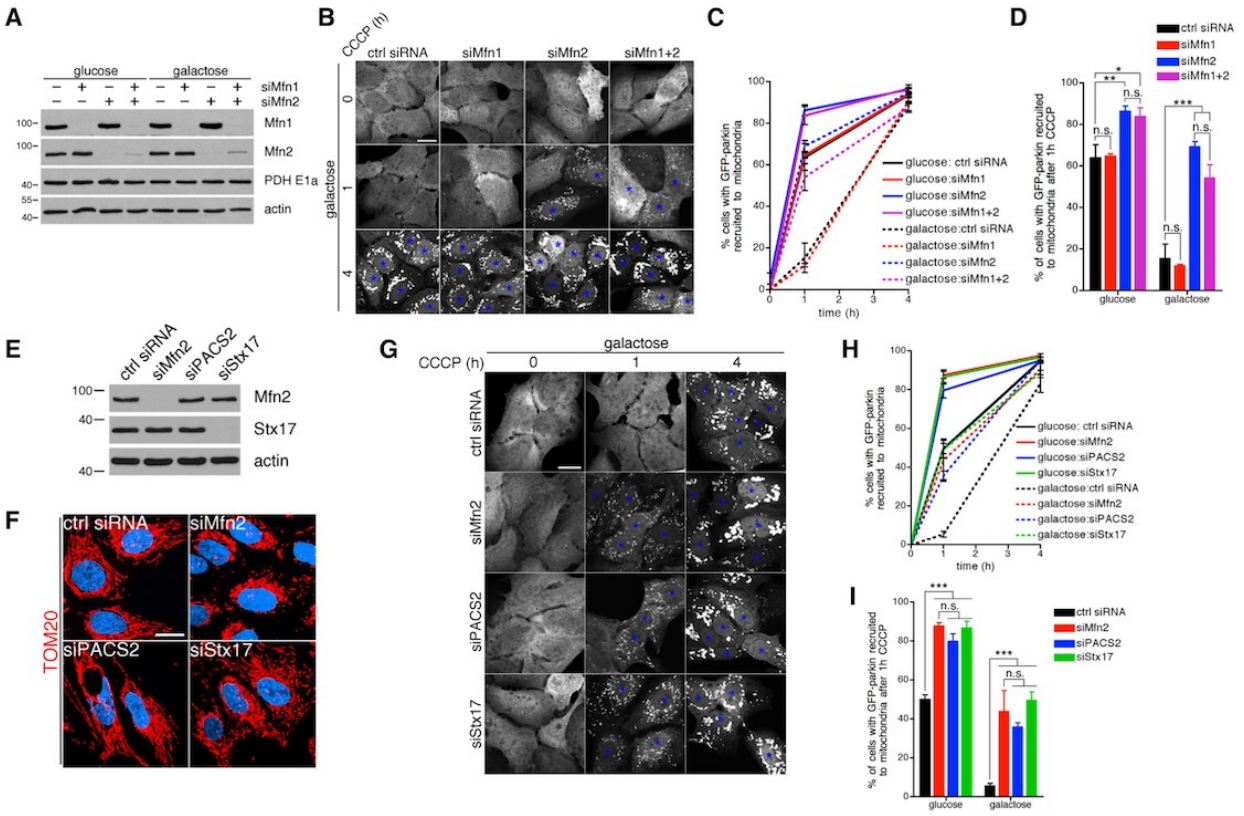


**Figure IV.S4**. *Parkin recruitment kinetics in cells lacking both Mfns and other mitochondria-ER tethering factors*. **A** Immunoblot analysis of whole-cell lysates from cells cultured in glucose or galactose transfected with control siRNA or siRNA targeting Mfn1 ( "siMfn1" ), Mfn2 ( "siMfn2" ) or both ( "siMfn1+2" ). **B** Representative confocal images of GFP-parkin recruitment to mitochondria as a function of time in U2OS:GFP-parkin cells treated with 20 μM CCCP. Blue asterisks indicate cells in which GFP-parkin has fully translocated to mitochondria. Scale bar, 20 microns. **C** Quantification of parkin recruitment in cells from **B**. Data points represent mean±SEM, n=3 replicates cells per condition, with >100 cells counted per condition for each replicate. **D** Parkin recruitment at one hour CCCP in cells from **B** arranged as a histogram. Bars represent mean±SEM. n.s., not significant; *, p<.05; **, p<.01; ***, p<.001. **E** Immunoblot analysis of whole-cell lysates from glucose-maintained U2OS:GFP-parkin cells transfected with the indicated siRNA targeting tethering-promoting proteins. **F** Mitochondrial morphology in cells from **E**, as revealed by confocal imaging of TOM20 (red) staining (Hoescht, blue). Scale bar, 20 microns. **G** Representative confocal images of GFP-parkin recruitment to mitochondria as a function of time in U2OS:GFP-parkin cells treated with 20 μM CCCP. Blue asterisks indicate cells in which GFP-parkin has fully translocated to mitochondria. Scale bar, 20 microns. **H** Quantification of parkin recruitment in cells from **G**. Data points represent mean±SEM, n=3 replicates cells per condition, with >100 cells counted per condition for each replicate. **I** Parkin recruitment at one hour CCCP in cells from **G** arranged as a histogram. Bars represent mean±SEM. n.s., not significant; **, p<.01; ***, p<.001.

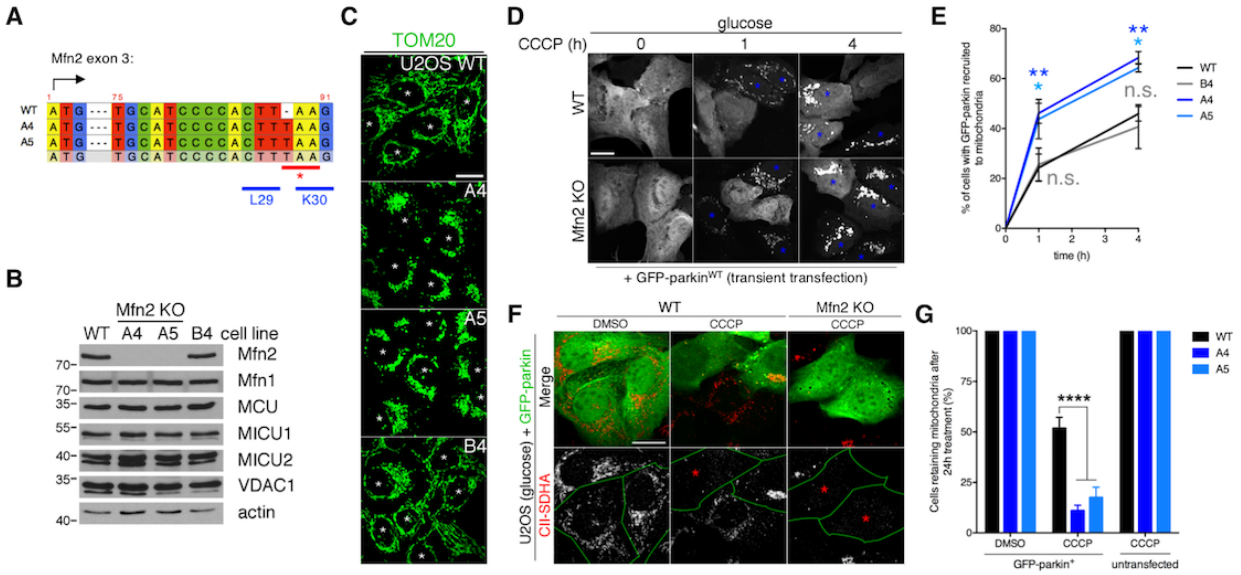


**Figure IV.S5**. *Analysis of mitophagy in Mfn2 KO U2OS cells*. **A** Genomic sequence of human Mfn2 (exon 3) that was mutated in U2OS cells using CRISPR/Cas9. The arrow indicates the codon corresponding to methionine-1; leucine-29 ( "L29" ), lysine-30 ( "K30" ) and the introduced stop codon ( "*" ) are also indicated. **B** Immunoblot analysis of whole-cell lysates from Mfn2 KO clones (A4 and A5). **C** Mitochondrial morphology in Mfn2 KO cells, as revealed by confocal imaging of TOM20 (green) staining. The asterisks indicate nuclei. Scale bar, 20 microns. **D** Representative confocal images of GFP-parkin recruitment to mitochondria as a function of time in WT or Mfn2 KO (clone A4) U2OS cells, transfected with GFP-parkin and treated with 20 μM CCCP. Blue asterisks indicate cells in which GFP-parkin has fully translocated to mitochondria. Scale bar, 20 microns. **E** Quantification of parkin recruitment in cells from **D**. Data points represent mean±SEM, n=3 replicates per condition, with >100 cells counted per condition for each replicate. n.s., not significant; *, p<.05; **, p<.01. Significance (or lack thereof) is colour-coded according to genotype. **F** Representative images of glucose-cultured WT and Mfn KO cells transfected with GFP-parkin (green) treated with 20 μM CCCP for 24 hours analyzed for their mitochondrial content (represented by SDHA, red). Green lines delineate the boarders of parkin-expressing cells, and red asterisks indicate cells devoid of SDHA signal. "Untransfected" refers to cells in the experiment lacking parkin expression. Scale bar, 20 microns. **G** Quantification of complete mitochondrial turnover in cells from **F**. Bars represent mean±SEM, n=3 replicates cells per condition, with 38 to 63 cells counted per condition for each replicate. n.s., not significant; ****, p<.0001.

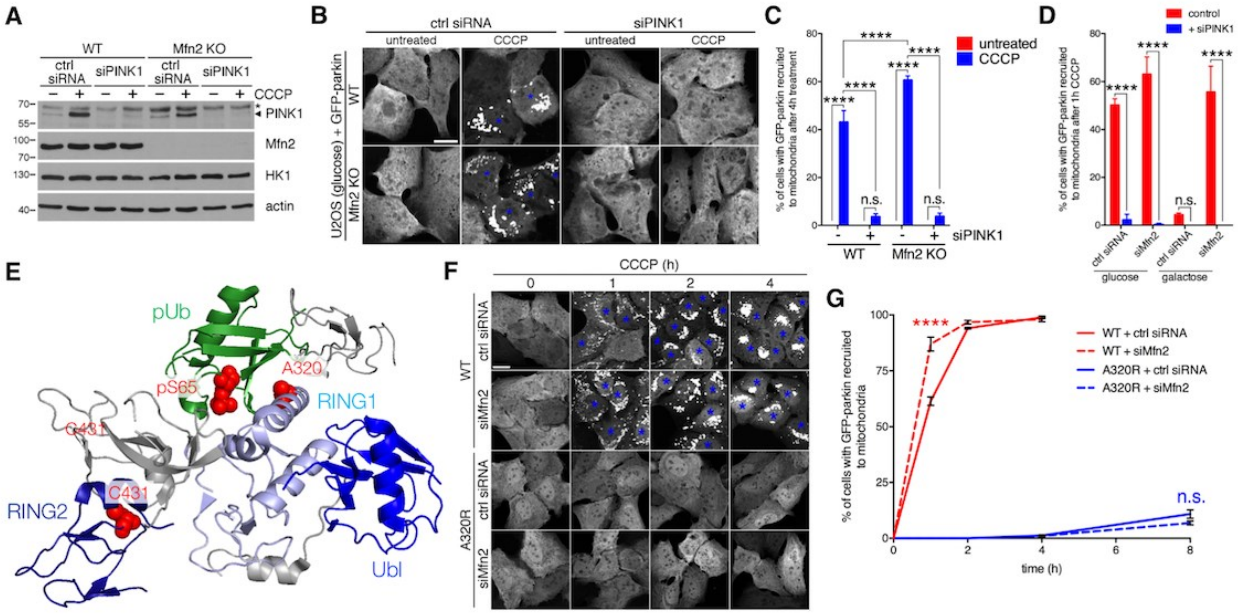


**Figure IV.S6**. *Parkin recruitment in Mfn2-depleted cells requires PINK1 and phosphoubiquitin binding*. **A** Immunoblot analysis of PINK1 depletion in WT and Mfn2 KO (clone A4) U2OS cells treated with 20 μM CCCP for four hours. The arrowhead indicates the PINK1 band, while the asterisk indicates a non-specific band. **B** U2OS cells from **A** were transfected with GFP-parkin and treated with 20 μM CCCP for four hours prior to fixation. Blue asterisks mark cells in which parkin has been recruited to mitochondria. Scale bar, 10 microns. **C** Quantification of parkin-expressing cells from **A**, left untreated (red bars) or treated with 20 μM CCCP for four hours (blue bars). Bars represent mean±SEM, n=3 replicates cells per condition, with >100 GFP-positive cells counted per condition for each replicate. n.s., not significant; ****, p<.0001. **D** Quantification of parkin recruitment in U2OS:GFP-parkin cells, grown on glucose or galactose, treated with 20 μM CCCP for one hour prior to fixation. Cells were transfected with control siRNA ( "ctrl siRNA" ) or siMfn2, and either additional ctrl siRNA (red bars) or siPINK1 (blue bars). Bars represent mean±SEM, n=3 replicates cells per condition, with >100 cells counted per condition for each replicate. n.s., not significant; ****, p<.0001. **E** Crystal structure of parkin complexed with pUb (PDB ID 5N2W, Kumar *et al.*, 2017). Sites of Ub phosphorylation (S65 in Ub), pUb binding (A320 in parkin) and catalysis (C431 in parkin) are highlighted in red, with relevant domains of parkin coloured different shades of blue, and ubiquitin in green. **F** Representative confocal images of U2OS cells stably expressing WT or A320R mutant parkin. Cells were treated with 20 μM CCCP for the indicated time prior to fixation. Blue asterisks indicate cells in which GFP-parkin has been recruited to mitochondria. Scale bar, 20 microns. **G** Quantification of parkin recruitment in cells from **F**. Data points represent mean±SEM, n=3 replicates cells per condition, with >100 cells counted per condition for each replicate. n.s., not significant; ****, p<.0001.

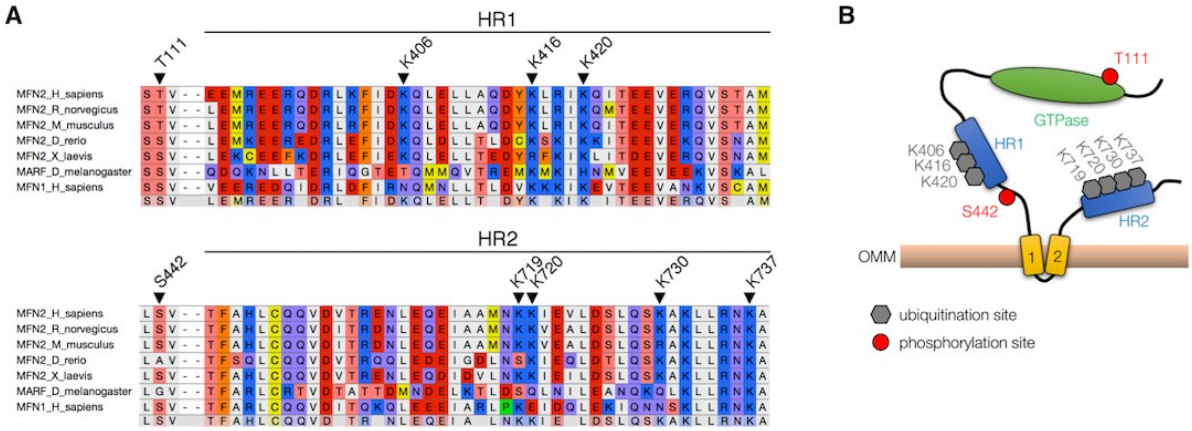


**Figure IV.S7**. *Location and conservation of ubiquitination and phosphorylation sites in Mfn2*. **A** Sequence alignment of sites of Mfn2 modification across species. Ubiquitinated lysines and phosphorylated serines and threonines are indicated by arrowheads. Residue numbering is according to the human sequence. HR, heptad repeat domain. **B** Diagram of Mfn2 post-translational modification by parkin-mediated ubiquitination (Sarraf *et al.*, 2013) and PINK1-mediated phosphorylation (Chen & Dorn, 2012). Phosphosites are denoted in red, while sites of ubiquitination.

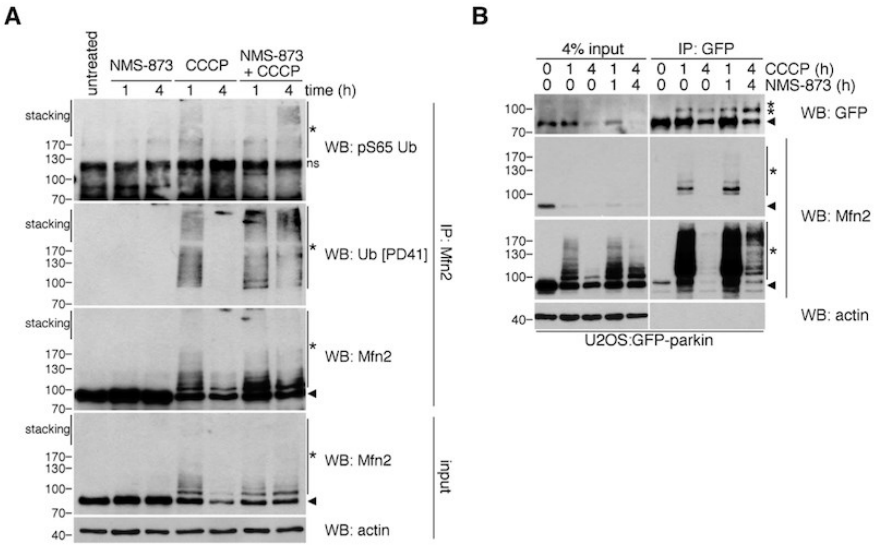


**Figure IV.S8**. *Mfn2 is a parkin receptor only under conditions of p97 inhibition*. **A** Immunoprecipitation of Mfn2 under denaturing conditions from U2OS:GFP-parkin cells treated with 20 µM CCCP and/or 25 µM NMS-873 for the indicated time, using an anti-Mfn2 antobody. Immunoprecipitates were separated by SDS-PAGE and immunoblotted for the indicated protein. The arrowhead indicates the unmodified form of the protein, while the asterisks denote ubiquitinated forms. "ns" denotes a non-specific band. **B** Co-immunoprecipitation of mitofusins with GFP-parkin U2OS:GFP-parkin cells treat with 20 µM CCCP in the presence or absence of 25 µM NMS-873 for the indicated time, using an anti-GFP antibody. Immunoprecipitates were separated, along with 4% input, by SDS-PAGE and immunoblotted for the indicated protein. The arrowhead indicates the unmodified form of the protein, while the asterisks denote ubiquitinated forms.

| | m/z | mass | MASCOT | Biotools | chromatogram integration | | ratio (CCCP/DMSO) | st. dev. |
|---|---|---|---|---|---|---|---|---|
| | | | | | DMSO | CCCP | | |
| Mfn2 | | | | | | | | |
| 87-94 | 422.746 | 843.4814 | 31.7 | 67 | 408872 | 203897 | 0.50 | |
| 136-155 | 551.767 | 2203.038 | 37 | 515 | 1248306 | 590612 | 0.47 | |
| 281-294 | 805.396 | 1608.782 | 47.4 | 38 | 366682 | 232634 | 0.63 | |
| 317-334 | 887.929 | 1773.845 | 28.7 | 138 | 320931 | 209202 | 0.65 | |
| 335-343 | 624.279 | 1246.543 | 40.5 | 260 | 622222 | 432874 | 0.70 | |
| 344-355 | 485.242 | 1452.704 | 33.4 | 122 | 543344 | 427304 | 0.79 | |
| 511-519 | 529.785 | 1057.556 | 44.5 | 129 | 674980 | 426423 | 0.63 | |
| | | | | | | | 0.62 | 0.11 |
| UB | | | | | | | | |
| 12-27 | 894.463 | 1786.912 | 20.6 | 32 | 159348 | 1448370 | 9.09 | |
| 55-72 | 533.293 | 2129.144 | | 30 | 26226 | 194939 | 7.43 | |
| Phospho-55-72 | 553.286 | 2209.113 | | 14 | 40531 | 531020 | 13.10 | |
| 30-42 | 508.598 | 1522.771 | | 21 | 25146 | 260961 | 10.38 | |
| | | | | | | | 10.00 | 2.39 |

**Supplementary Table IV.S1**. *MS quantification for the Mfn2 immunoprecipitation*. Table depicting chemical properties, peptide scores and peak integration values for Mfn2- and Ub-related species in the MS experiment corresponding to Fig. IV.2E and F.

## IV.VIII INTEGRATIVE SUMMARY

The work in Chapter IV elucidates a mechanism by which the ER represses parkin-/PINK1-dependent mitophagy through Mfn2 interorganellar bridges that span mitochondria-ER contacts, and highlights an important dynamic between Mfn2 and the p97 ATPase. This PINK1/parkin/Mfn2/p97 axis of ER/mitochondria uncoupling functions at the onset of mitophagy (i.e. likely prior to autophagosomal membrane expansion) and demonstrates that regulatory mechanisms exist at the level of pathway initiation. Perhaps more importantly, this work hints at a complexity in parkin/PINK1 signaling – that is, the architecture of substrate positioning with respect to availability to parkin and/or PINK1 – that has so far been overlooked in the field.

In the following Discussion (Chapter V), the relationship between PINK1/parkin-dependent MDV formation (Chapters II and III) and destruction of mitochondria-ER contact sites (Chapter IV) is discussed, in addition to how differential outputs (MDVs vs. mitophagy) can be triggered by a similar set of factors, as well as mechanisms of OMM curvature related to mitochondrial vesicles.

# Chapter V

# DISCUSSION

## V.I SUMMARY OF RESULTS

Here, the roles of PINK1/parkin and Stx17 in MDV biogenesis and targeting, respectively, are described, along with the role of parkin- and PINK1-dependent Mfn2 phosphoubiquitination in mitophagy. In response to mitochondrial oxidative stress, parkin is recruited to mitochondrial foci where it catalyzes the formation of mitochondrial vesicles that transport components of the mitochondrial matrix and IMM to the late endosome. Generation of this population of MDVs by parkin requires both parkin Ub ligase activity and PINK1, but is independent of canonical autophagy machinery. This pathway functions as a "first response"-type mechanism that presumably would function prior to depolarization in an effort to salvage the organelle (Fig. II.8). MDV-endolysosome fusion is achieved by a SNARE-dependent mechanism, involving Stx17 and VAMP7 on the MDV outer membrane and endolysosomal membrane, respectively. Along with SNAP29, these proteins form a ternary SNARE complex that triggers fusion in a manner that requires the HOPS tethering complex. This work, comprising Chapters II and III, demonstrate that vesicular trafficking from mitochondria to the lysosome is a quality control mechanism governed by parkin and PINK1, and that this pathway utilizes canonical cellular trafficking mechanisms. Returning to mitophagy, parkin and PINK1 additionally catalyze Mfn2 phosphoubiquitination to trigger the extraction of Mfn2 interorganellar bridges from the membrane by p97 and their proteasomal degradation. As described in Chapter IV, this acts to uncouple the ER from mitochondria and may drive mitophagy by making more substrates available to parkin and PINK1. Taken together, these studies describe early steps in parkin/PINK1 quality control at the molecular scale, and emphasize the importance of understanding these types of (sub-) organellar turnover pathways on a mechanistic level.

## V.II DISCUSSION

### V.II.i *The OMM phosphoubiquitylome as an effector of the PINK1/parkin system*

How exactly parkin and PINK1 form mitochondrial vesicles remains to be elucidated, although appropriation of certain mechanistic aspects from the mitophagy can be expected. MDV formation requires parkin ligase activity (Fig. II.2) and involves the recruitment of the ligase to the OMM (Fig. II.1), and thus a role for activation by pUb-dependent Ubl displacement and its subsequent PINK1-dependent phosphorylaion (Sauve et al., 2015) seems apparent. This mechanism has the potential to act as a switch in determining the type of damage response enacted by the parkin/PINK1 system. Fig. V.1 depicts how such a hypothetical phosphoswitch mechanism

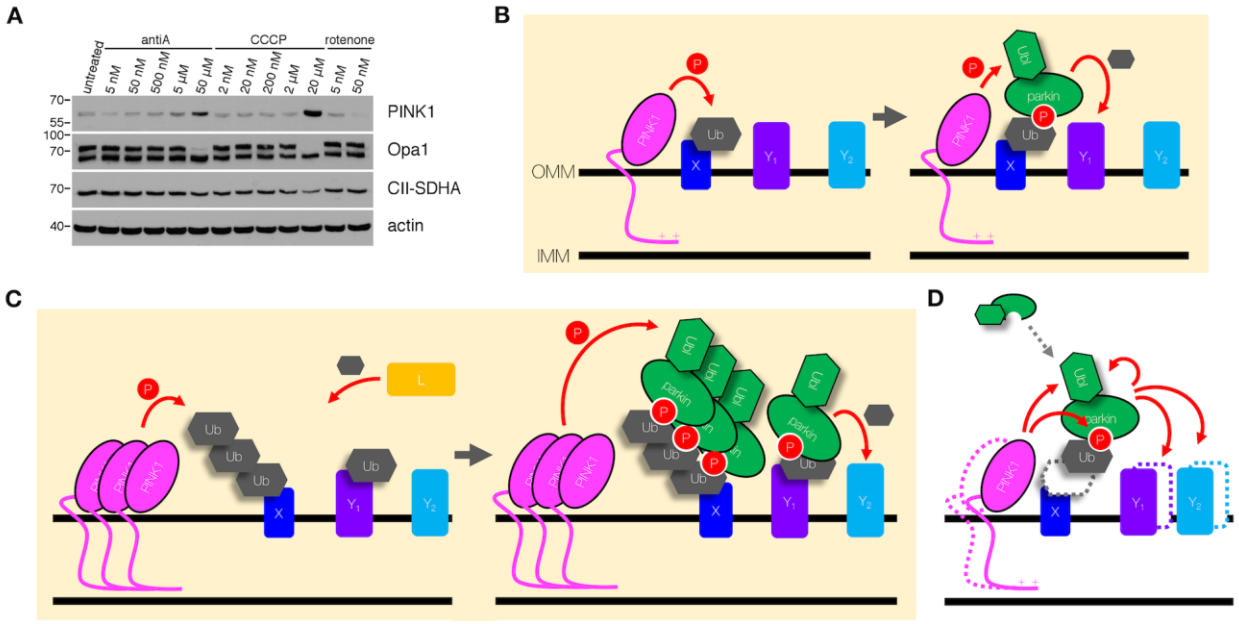


**Figure V.1**. *The kinetics of mitochondrial quality control.* **A** Immunoblot detection of full-length PINK1 in whole-cell extracts from HEK293T cells treated for one hour with the indicated concentration of antimycin A (antiA), CCCP or rotenone. **B** Model of parkin activation under weakly-depolarizing conditions. PINK1 accumulates on the OMM and phosphorylates ubiquitinated protein X (left), and in turn pUb-X acts as a parkin receptor. PINK1 phosphorylation of the Ubl domain activates parkin (right), enabling it to ubiquitinate protein $Y_1$. **C** Model of parkin activation under depolarizing conditions. Massive accumulation of PINK1 on the OMM leads to phosphorylation of ubiquinated protein X (left). Additionally, activation of Ub ligase L increases ubiquitination of OMM proteins, resulting in polyubiquitination of protein X and $Y_1$. pUb-conjugated X and $Y_1$ act as parkin receptors (right), facilitating Ubl phosphorylation and parkin-mediated ubiquitination of protein $Y_2$. **D** Diagrammatic summary of factors influencing mitochondrial ubiquitination by parkin. See text for details.

may occur, by contrasting MDV formation – which concomitantly occurs with mild depolarization (Fig. II.6A) – and depolarization-induced mitophagy. PINK1 levels on the OMM may play an important role vis-à-vis the quality control pathway triggered, as the concentration of PINK1 scales with decreasing $\Delta\Psi_m$ (Fig. V.1A). Indeed, this may explain the observation by Suen *et al*. that mitophagy occurs in cybrid cell lines harbouring only very deleterious mtDNA mutations (Suen et al., 2010), implying the existence of a $\Delta\Psi_m$ threshold beyond which mitophagy is initiated. In our hands, CCCP and antimycin A decrease $\Delta\Psi_m$ by ~80% and ~30%, respectively (Fig. II.6A), highlighting the degree of difference between these two stimuli. On the OMM of mildly depolarized mitochondria (Fig. V.1B) – i.e. those suffering from localized stress or damage – PINK1 accumulation and phosphorylation of a Ub moiety already conjugated (Tang et al., 2017) to a receptor ("protein X-Ub") would recruit parkin from the cytosol, where it is activated by PINK1 and ligation of Ub to substrate $Y_1$ in a targeted fashion occurs, triggering the downstream formation of MDVs. It is important to note that PINK1 is also capable of sensing unfolded proteins in the mitochondrial matrix independently of $\Delta\Psi_m$ (Jin and Youle, 2013) and, coupled with alternative import mechanisms (Becker et al., 2012; Okatsu et al., 2015a), this may also contribute to PINK1 accumulation during oxidative stress.

In contrast, complete depolarization of a mitochondria (Fig. V.1C) potentially changes the molecular landscape upon which parkin is activated – the OMM phosphoubiquitylome – at the time of initiation in two ways; drastically increasing the concentration of PINK1 stabilized on the OMM (Fig. V.1A) and potentially activating other Ub ligases ("ligase L"). Concerning the latter point, the mitochondrial E3 Ub ligases MAPL (a dual SUMO/Ub ligase) and MARCH5 have been reported to function in stress response-type pathways (Li et al., 2015; Xu et al., 2016), and alternatively other non-mitochondrial E3 ligases, such as glycoprotein 78, promote mitochondrial

ubiquitination during depolarization (Fu et al., 2013). Additionally, F-box only protein 7 (FBXO7) is a Ub ligase mutated in EOPD (Di Fonzo et al., 2009; Lohmann et al., 2015; Shojaee et al., 2008) that facilitates parkin-mediated mitophagy (Burchell et al., 2013). Cells lacking FBXO7 have a reduced rate of mitophagy, and the N-terminal Ubl of FBXO7 interacts with both parkin and PINK1 (Burchell et al., 2013). Interestingly, the S65 residue is conserved in the FBXO7 Ubl (Fig. V.2), and thus the possibility of a role for phosphorylation by PINK1 in the FBXO7-parkin interaction exists, allowing FBXO7 to participate in parkin recruitment to depolarized mitochondria via direct binding or by the ligation of Ub to mitochondrial substrates (followed by phosphorylation by PINK1). Finally, other Ub-like proteins may also facilitate parkin recruitment to depolarized mitochondria. For example, SUMO1 – which can be ligated to proteins at the OMM by MAPL (Braschi et al., 2009) – retains an acidic residue (aspartate) at the position equivalent to S65 in Ub (Fig. V.2). Accordingly, SUMOylated OMM proteins could facilitate parkin recruitment; indeed, SUMO1 binds parkin allosterically and increases its Ub ligase activity (Um and Chung, 2006). To summarize, how PINK1 and Ub ligases shape the mitochondrial phosphoubiquitylome may have direct consequences on how parkin responds to mitochondrial damage; compared to mild depolarization, increasing the number of parkin binding sites on mitochondria (Fig. V.1C) via the phosphorylation of Ub chains, the phosphorylation of Ub conjugated to a different array of proteins, or the

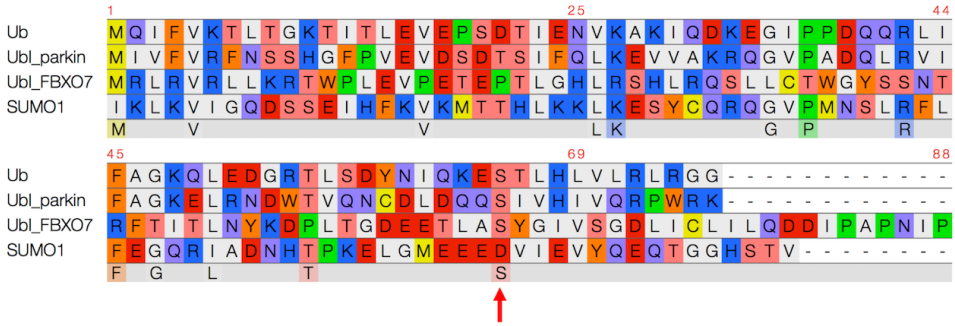


**Figure V.2**. *Conservation of S65 and acidic residues in Ub-like modules*. Primary sequence alignment of ubiquitin (Ub, mature form), the parkin and FBXO7 Ubl domains, and SUMO1 (from humans). S65 is indicated by the red arrow. Sequences were obtained from Uniprot.com and the alignment was constructed using eBioX.

recruitment of other factors that bind parkin could promote the parkin-mediated ubiquitination of substrates that would, under more polarized conditions, forego ubiquitination. For example, in Fig. V.1C (right panel) "protein $Y_2$" is ubiquitinated due to the increased concentration of parkin on the OMM and the presence of Ub already on protein $Y_1$, despite the fact that the $K_D$ for $Y_1$ ubiquitination would be much smaller than that for $Y_2$. Moreover, $Y_1$ now acts as a parkin receptor in addition to protein X and, under these conditions, what was a localized PINK1/parkin/X/$Y_1$ cascade has now expanded to include $Y_2$. Accordingly, this hypothetical example may explain how a localized response to mild damage may expand to include the entire depolarized organelle. Factors contributing to parkin activation, including protein abundance (dotted lines) and enzymatic events (red arrows), are depicted in Fig. V.1D. It is worth noting that the $K_D$ for the phosphorylation of the parkin Ubl by PINK1 is ~10-fold less than that for Ub (Rasool and Trempe, unpublished results). PINK1 may thus favour activating parkin over creating more parkin binding sites on the OMM. Additionally, parkin ubiquitinates itself in response to depolarization (even in paradigms involving endogenous parkin), and this tags the protein for proteasomal turnover (Durcan et al., 2014; Rakovic et al., 2013; Sarraf et al., 2013). Both these mechanisms could aid in restraining the breadth of parkin-mediated ubiquitination. In conclusion, which type of quality control response is orchestrated by the PINK1/parkin system may fundamentally be a question of enzyme kinetics.

### V.II.ii *Molecular mechanisms of MDV generation*

Elaborating on the hypothetical pUb-/PINK1-dependent activation mechanism in parkin-mediated MDV biogenesis described above, a role for the PINK1/parkin/p97/Mfn2 axis described in Chapter IV is possible, and would be consistent with the importance of both p97 and Mfn2 in

modifying fruit fly phenotypes of *PARKIN* and *PINK1* mutants (Yun et al., 2014; Zhang et al., 2017a). Indeed, preliminary evidence suggests that ubiquitination of both the Mfn2 HR1 and HR2 domains is critical for the generation of parkin/PINK1 MDVs in cells (McLelland and Fon, unpublished results). A selective requirement for ubiquitination in the HR2 domain in the formation of MDVs may provide a useful tool to study the pathway in isolation from mitophagy going forward. One possible mechanistic scenario where the HR2 domain becomes necessary for MDV formation is depicted in Fig. V.3A. Assuming a single-pass Mfn2 topology model proposed by Mattie *et al*. in which the HR2 is normally in the IMS (Mattie et al., in revision), localized ROS production may oxidize redox-sensitive cysteines in the C-terminus of Mfn2 (Shutt et al., 2012;

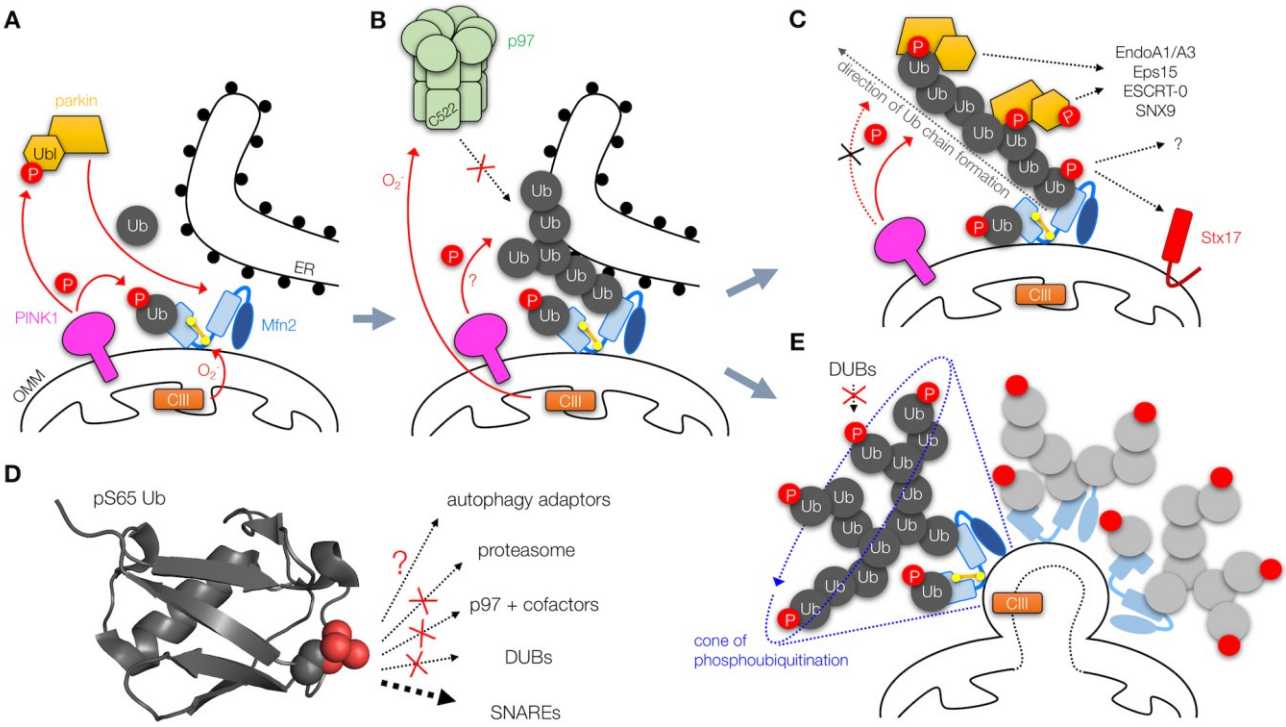


**Figure V.3**. *Hypothetical model of membrane deformation during MDV biogenesis*. **A** CIII-derived superoxide creates a disulfide bond in Mfn2 that prevents its import, allowing for recruitment of parkin via Ub phosphorylation and its activation by PINK1. In this paradigm, Mfn2 is presented as a hypothetical substrate. **B** (p)Ub chains are protected from proteasomal turnover through C522 oxidation of p97 and/or by phosphorylation of distal Ub moieties linked to Mfn2. **C** pUb chains recruit parkin, and the Ubl or pUbl (see text) recruit membrane-bending proteins. Alternatively, pUb recruits factors that may aid in membrane deformation, such as Stx17. **D** Structure (cartoon) of pS65 Ub (PDB ID 4WZP) with the phosphate labeled in red. Arrows indicate the strength of interactions with binding partners. **E** Branching of chains coupled to Ub phosphorylation by PINK1 results in a stable "cone of phosphoubiquitination" that drives membrane curvature by the geometry of its hydrodynamic radius (see text for more details).

Thaher et al., 2017), preventing the translocation of the HR2 domain across the OMM during import through the formation of a disulfide bond in *cis* as depicted in Fig. V.3A, or potentially in *trans*. This cytosolically-exposed HR2 domain could be recognized by an E3 ligase (or parkin, although this is less likely), and the concurrent stabilization of PINK1 in the presence of ubiquitinated HR2 would produce the pUb receptor required to recruit parkin from the cytosol to mediate HR1 domain ubiquitination. In mitophagy, Mfn2 is conversely already assembled into bridges and, topologically, only the HR1 domain is available to the cytosol. Here, a stress-activated ligase (i.e. "ligase L" in Fig. V.1C) catalyzes the initial ubiquitination event (Tang et al., 2017) on HR1 in order to establish the pUb receptor platform. In both paradigms, the HR1 domain is the target of parkin-mediated ubiquitination and, in the case of mitophagy, phosphoubiquitination of Mfn2 in the HR1 domain is coupled to extraction of the complex by p97 (Fig. IV.5). Extraction of the complex from the OMM would make the HR2 available to ubiquitination (Sarraf et al., 2013). Mechanistically, the reason that these HR2 lysines are ultimately dispensable for mitophagy (Fig. IV.4I and J) may be ubiquitination at these sites occurs after p97-dependent extraction, which appears to be the crucial step in regulating mitophagy through ER-OMM contact (Fig. IV.5H to J).

While p97 regulates the turnover of the mitofusins during mitophagy ((Tanaka et al., 2010) and Fig. IV.5), it is apparently dispensable for the generation of MDVs (Fig. II.S4). p97 activity may be suppressed during MDV biogenesis, as oxidation of p97 on the conserved C522 within the second ATPase domain inhibits its activity (Noguchi et al., 2005). Interestingly, the yeast p97 homologue Cdc48p has a threonine at this position, and is resistant to inactivation by oxidation (Noguchi et al., 2005), consistent with a role for Cdc48p in maintaining mitochondrial integrity during oxidative stress in this organism (Heo et al., 2010). Additional factors may destabilize p97

during MDV biogenesis or, conversely, stabilize it during mitophagy. For example, SUMOylation of p97 promotes hexamer assembly and activity (Wang et al., 2016b), and MAPL is known to SUMOylate proteins at contact sites between the ER and mitochondria (Prudent et al., 2015). MAPL may accordingly stabilize the p97 hexamer at ER-OMM contacts during mitophagy. Additionally, a screen for pUb interactors demonstrated that, unlike their unphosphorylated counterparts, pUb chains fail to bind p97 and its associated cofactors (Yi and Fon, unpublished results). To summarize, suppression of p97 activity (or lack of p97 stabilization) during oxidative stress could result in the accumulation of ubiquitinated Mfn2 (Fig. V.3B), which may act as a trigger for MDV formation and dually explain preliminary data showing that MDVs cannot form in cells lacking Mfn2 or expressing Mfn2 lacking ubiquitinatable lysines in either the HR1 or HR2 domain.

After parkin and PINK1 have established the OMM platform from which to generate a vesicle (or simultaneously), the OMM and IMM must be positively deformed (from the cytosolic perspective) in order for constriction of the vesicular neck (Fig. III.3A), which may occur by several mechanisms. Firstly, a direct recruitment of membrane-bending proteins via binding to either the (p)Ubl or pUb seems plausible (Fig. V.3C). As discussed in Chapter I, the Ubl is an interactor of EndoA1 (and EndoA3), which contains an N-BAR domain capable of inducing membrane curvature upon dimerization of the protein through the direct insertion of an α-helix into the membrane (termed hydrophobic insertion) (Cui et al., 2009; Trempe et al., 2009). Depending on the amount of penetration by the N-terminal helix (which is itself regulated by phosphorylation), EndoA1 deforms membranes to various degrees (Ambroso et al., 2014), although tubulation by EndoA1 constricts the membrane to a 20- to 30-nm diameter (Mim et al., 2012; Mizuno et al., 2010) – three- to four-folds smaller than the diameter of a budding

mitochondrial vesicle. Endophilins could therefore be recruited to initiate membrane tubulations at the OMM, ultimately forming the neck of the budding vesicle (Fig. III.3A, arrow), allowing for the observed freedom in MDV diameter, which may itself be regulated by parkin-mediated ubiquitination; in COPII vesicle formation, for example, monoubiquitination of certain factors can expand the diameter of the resulting vesicle five-fold (Jin et al., 2012). Membrane curvature by endophilins is a process driven by protein concentration (Sorre et al., 2012; Zhu et al., 2012), and would accordingly fit a model of MDV biogenesis involving a pUb cascade (Fig. V.5C). Moreover, with the highly-similar EndoA2 recently being implicated in membrane scission during clathrin-independent endocytosis (Renard et al., 2015), it is conceivable that EndoA1 or A3 could also play a similar role during MDV formation. Additionally, it is worth emphasizing again that EndoA1 controls parkin levels *in vivo* (Cao et al., 2014), and that this is phenocopied in mice carrying a mutation in the phosphatase domain of synaptojanin 1 (Cao et al., 2017a) that is a likely cause of AR-JP/EOPD (Kirola et al., 2016; Krebs et al., 2013; Olgiati et al., 2014; Quadri et al., 2013; Taghavi et al., 2017). In effect, there is a genetic precedence, in addition to the molecular interaction, for a common function between parkin and the EndoA1 system.

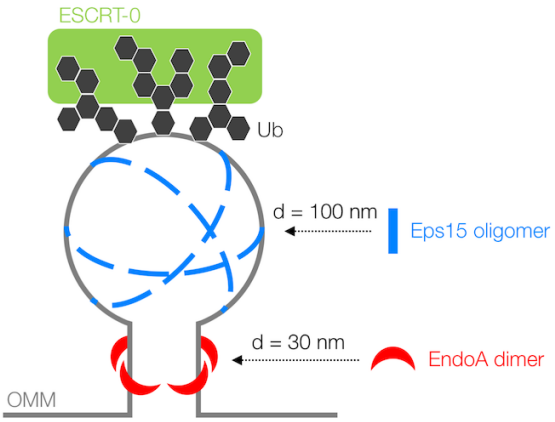


**Figure V.4**. *OMM curvature through Ubl interactors*. Hypothetical model of curvature through cooperativity of Eps15-type oligomers and EndoA-type dimers (d, diameter). ESCRT-0 clusters ubiquitinated OMM proteins on the budding mitochondrial vesicle.

The parkin Ubl also interacts with Eps15 and Hrs (Fallon et al., 2006), the latter being a component of the endosomal sorting complex required for transport complex-0 (ESCRT-0). The ESCRT system oversees the clustering of ubiquitinated, endocytosed cargo and its packaging it

into intraluminal vesicles inside the late endosome, among other functions (Hurley, 2015). ESCRT-0, through Ubl-Hrs interactions, may therefore play a similar role in clustering ubiquitinated proteins on the surface of the OMM. Eps15, a Ub-binding adaptor of the endocytic machinery, has recently been shown to bind and curve membranes through its Eps15-homology (EH) domain (Wang et al., 2016a). The isolated EH domain from the nematode Eps15 homologue, EHS-1, tubulates liposomes *in vitro* to ~100 nm (Wang et al., 2016a), similar to the diameter of MDVs. Conceivably, downstream of ESCRT-0-mediated clustering of surface cargo, the cooperativity between curvatures induced by an endophilin and Eps15 family member could produce a ~100 nm vesicle with a smaller neck amenable to scission by a dynamin-type protein (Fig. V.4) and invokes an architecture at least partially analogous to clathrin-mediated endocytosis (Sochacki et al., 2017). Here, Eps15 is recruited to clathrin-coated pits at the plasma membrane by curvature-sensing FCHo proteins to presumably act as a scaffold, and its recruitment to endocytic sites precedes that of dynamin-2 (Henne et al., 2010; Taylor et al., 2011) – a protein recently implicated in OMM fission (Lee et al., 2016). Additionally, other factors may also contribute to OMM deformation; for example, SNX9 (another classically-endocytic factor) has been reported to be a parkin substrate at the OMM during heat shock and is implicated in the biogenesis of parkin-dependent MDVs, although its C-terminal BAR domain likely only senses curvature (Matheoud et al., 2016).

It remains unclear how Ubl phosphorylation by PINK1 may affect the binding of this domain with its known interactors. An interesting limitation to consider is that PINK1 is presumably inserted in the OMM, and may not have access to a molecule of parkin bound to a pUb moiety distal to the membrane (this is illustrated in Fig. V.3C). Moreover, a recent study reported that pUb binding reveals a cryptic Ub binding site on the $R_0$RBR module, that possibly

allows for docking of a parkin-E2-Ub complex that may aid in catalytic cooperativity (Kumar et al., 2017a). Such an extended structure may prevent Ubl phosphorylation by PINK1, permitting the occurrence of Ubl binding events. Alternatively, Ubl phosphorylation may strengthen its binding to known interactors, or recruit yet-to-be-identified binding partners to the OMM.

Independently of parkin, pUb may itself recruit membrane-deforming factors (Fig. V.3C). It is worth noting that phosphorylation of S65 decreases the affinity of Ub for autophagy adaptors in the hands of this lab (Yi and Fon, unpublished results) and those of others (Heo et al., 2015), with the possible exception of OPTN, which has been reported by one group to bind pUb better than Ub (Lazarou et al., 2015; Richter et al., 2016). Interestingly, pUb apparently fails to bind many Ub-binding factors (Fig. V.3D), including proteasomal subunits and p97-associated proteins (Yi and Fon, unpublished results). Moreover, many DUBs fail to cleave phosphorylated Ub chains (Wauer et al., 2015b). The physiological role of pUb may thus simply be to recruit parkin, although other possibilities – such as Stx17 recruitment (see section III.IV) – may exist.

Alternatively, membrane curvature during MDV biogenesis may not involve the recruitment of membrane-deforming proteins at all. Formation of branched Ub chains – ligation of two more Ub residues onto different lysines of the same Ub molecule – would exponentially increase the hydrodynamic radius of the elongating chains, akin to a geometric cone of phosphoubiqutination anchored to the OMM by the initial substrate protein (Fig. V.3E). It can be assumed that the OMM substrate – in Fig. V.5E, this is presented as oxidized Mfn2 but could of course be another parkin substrate – cannot diffuse fluidly through the membrane as it is somehow restricted; for example, by intermolecular disulfide bonds, protein aggregation or recruitment into a membrane microdomain. Here, there is a conceptual similarity to intrinsically-disordered proteins (IDPs) that, in addition to their involvement in a variety of cellular process (van der Lee

et al., 2014), are also able to deform membranes. Crowding by IDPs can induce membrane curvature through the concentration of disordered regions – acting as so-called "entropic chains" with large hydrodynamic radii – on one side of the membrane (Busch et al., 2015; Stachowiak et al., 2012; van der Lee et al., 2014). Protein crowding is also sufficient to drive membrane scission *in vitro* (Snead et al., 2017). It is conceivable that clustering of branched, polyUb chains conjugated to proteins on the OMM could drive deformation of the membrane (and ultimately scission). Crowding could be driven by the stability of pUb, in that phosphorylation of distal Ub moieties by PINK1 could protect phosphorylated chains from DUBs (Fig. V.5D and E).

While the majority of this section has dealt with signaling events at the OMM, it cannot be ignored that these vesicles contain two membranes deriving from both the OMM and IMM (Fig. III.3A), and thus how the IMM is packaged into the budding MDV (Fig. V.3E, dotted line) remains an open question. PINK1 can detect misfolded proteins inside mitochondria (Jin and Youle, 2013), and aggregation of oxidized of IMM and matrix proteins may stabilize PINK1 on the adjacent OMM. Despite this inside-out signaling event, there must be an additional mechanism for the separation of these aggregates from the rest of the organelle; either a selective process driven by enzymes or a phase-separation-type event driven by entropy. Fig. V.5 depicts how oxidized

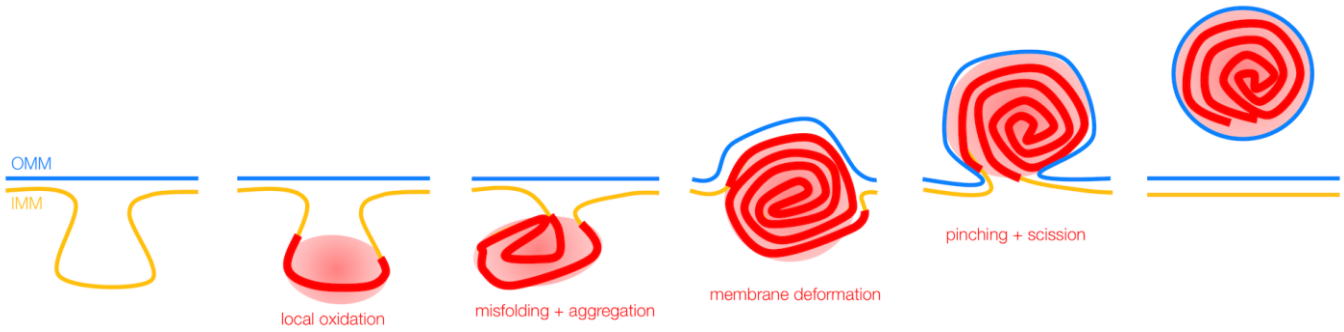


**Figure V.5**. *Aggregation-deformation model of MDV budding*. A hypothetical model of how aggregation inside the mitochondrion may drive MDV formation on its cytosolic face. The OMM and IMM are labeled in blue and orange, respectively. Oxidation of IMM proteins and surrounding, soluble factors (red) leads to the formation of a multilamellar aggregate, which is driven towards the cytosolic face of the organelle to deform the membrane. Pinching and scission occur to release the vesicle from the mitochondrion.

proteins within mitochondria may drive the pathway. The model assumes that the organelle is not structurally compromised during biogenesis of the vesicle – i.e. that its size remains the same – and, by extension, that the change in total IMM area due to extraction by the vesicle is negligible. Local oxidation of IMM membrane proteins and surrounding matrix/IMS leads to the formation of multilamellar membrane whorls driven by aggregation of membrane-anchored factors. These whorls are driven toward the exterior of the organelle by an unknown mechanism, which may contribute to membrane curvature. This process could be driven by the comparably rigid mitochondrial cristae structure, which may force the aggregate to "bulge" out of the cytoplasmic side of the organelle. This would logically be followed by further membrane bending and scission of the vesicular neck.

Undeniably, MDV biogenesis is driven by parkin-dependent ubiquitination (Fig. II.2) via its activation by PINK1 (Fig. II.5 and III.3B to D). Indeed, parkin localizes to sites of vesicle formation on the OMM (Fig. II.1C) as well as budding profiles (Fig. III.4G). Aggregation of IMM proteins (Fig. V.5), the recruitment of factors that bend membranes (Fig. V.4) and substrate ubiquitination (Fig. V.3) may all contribute to the regulation of vesicle size, curvature of the membrane, and biogenesis. Cell-free reconstitution of vesicle formation (i.e. Fig. III.1, (Soubannier et al., 2012b) and (Wang et al., 2016c)) is a powerful tool for understanding how MDVs are formed. Ideally, the identification of new machinery by mass spectrometry and, for example, the incorporation of their dominant-negative forms into assays will reveal how mitochondria shed vesicles. While assays from heart (Soubannier et al., 2012b), liver (Fig. III.1) and brain (McLelland and Fon, unpublished results) mitochondria have proved very informative, reconstituting vesicle formation from mitochondria isolated from cells – whose protein contents can be easily manipulated via transient transfection, viral transduction or genome editing – will

likely prove to be very powerful. For example, using the CRISPR/Cas9 system to insert a tag on PINK1 would allow for its visualization in MDV fractions (by immunoblot for PINK1-Flag) or in budding profiles (by electron microscopy for PINK1-APEX2) in reconstitution assays from mitochondria isolated from genome-edited cells. Moving forward, these types of assays are the most powerful tools available with which to understand how a mitochondrial vesicle is made.

V.II.iii *Bridging the mitochondrion and the endosomal system*

Does the role of Stx17 in MDV-late endosome fusion give us clues to other players in mitochondrion-to-lysosome vesicular traffic? It should be noted that, so far, Stx17 has been observed in several cellular locations, including mitochondria, ER, autophagosomes, MDVs and other endosomal structures ((Arasaki et al., 2015; Hamasaki et al., 2013); Chapter III; McLelland and Fon, unpublished observations). A common function for Stx17 in both autophagosome-lysosome and MDV-late endosome fusion may stem from its localization to contact sites between mitochondria and the ER, as well as its apparent role in their homeostasis.

At these locations, autophagosomes are generated in response to starvation, as well as infection (Hamasaki et al., 2013). Mechanistically, at mitochondria-ER contact sites, Stx17 binds SNAP29 in a binary complex that is clamped by the class-III PI3 kinase complex subunit ATG14L (Diao et al., 2015; Hamasaki et al., 2013). Stx17 is accordingly thought to recruit this complex to these locations (Hamasaki et al., 2013), and may contribute, along with PI3P, to the tethering of the lipid kinase complex to the expanding isolation membrane; as mentioned in Chapter I, the BATS domain of ATG14L additionally binds the phospholipids PI3P and PI(4,5)$P_2$ (Fan et al., 2011; Matsunaga et al., 2010; Tan et al., 2016). Conflicting reports have observed both a buildup of incomplete autophagosomes (due to a deficiency in their formation) and a buildup of mature

autophagosomes (stemming from a fusion defect) in Stx17-silenced cells (Hamasaki et al., 2013; Itakura et al., 2012b). To further complicate Stx17 function, it is clear that loss of Stx17 reduces mitochondria-ER contact (Arasaki et al., 2017; Arasaki et al., 2015). Accordingly, silencing Stx17 in our hands reduces the amount of contact visible by EM (McLelland and Fon, unpublished results) and increases the kinetics of parkin recruitment (Fig. IV.S4G to I). While it is possible that Stx17 acts as a tethering molecule – potentially through the binding of SNAREs on the opposing membrane in a half-zippered ternary complex clamped by a complexin-type molecule (Giraudo et al., 2006) – we (Fig. III.2) and others (Hamasaki et al., 2013) have shown that the SNARE is present on both ER and mitochondrial membranes, making the existence of a polarized tethering complex unlikely. A more likely scenario is one in which Stx17 supports the formation or stability of contact sites indirectly. As it acts upstream of ATG14L (Hamasaki et al., 2013), a potential function of Stx17 may include increasing mitochondria-ER contact through the recruitment of autophagic machinery in order to promote autophagy; while starvation is known to result in mitochondrial hyperfusion (Gomes et al., 2011), its effect on mitochondria-ER contact remains unknown. A consequence of a functional autophagy pathway may conversely increase mitochondria-ER contact due to increased organellar health. Indeed, the findings in Chapter IV demonstrating that depolarization results in a loss of tethering (Fig. IV.1) may be reflective of a relationship between fitness and mitochondria-ER contact. Relatedly, an alternative role for Stx17 in maintaining mitochondrial health via the MDV pathway may also promote the stability of these interorganellar junctions by the same indirect mechanism.

The association of Stx17 with ATG14L is critical for the autophagy pathway (Diao et al., 2015; Hamasaki et al., 2013). In addition to its role as a Stx17-SNAP29 clamp, ATG14L has also

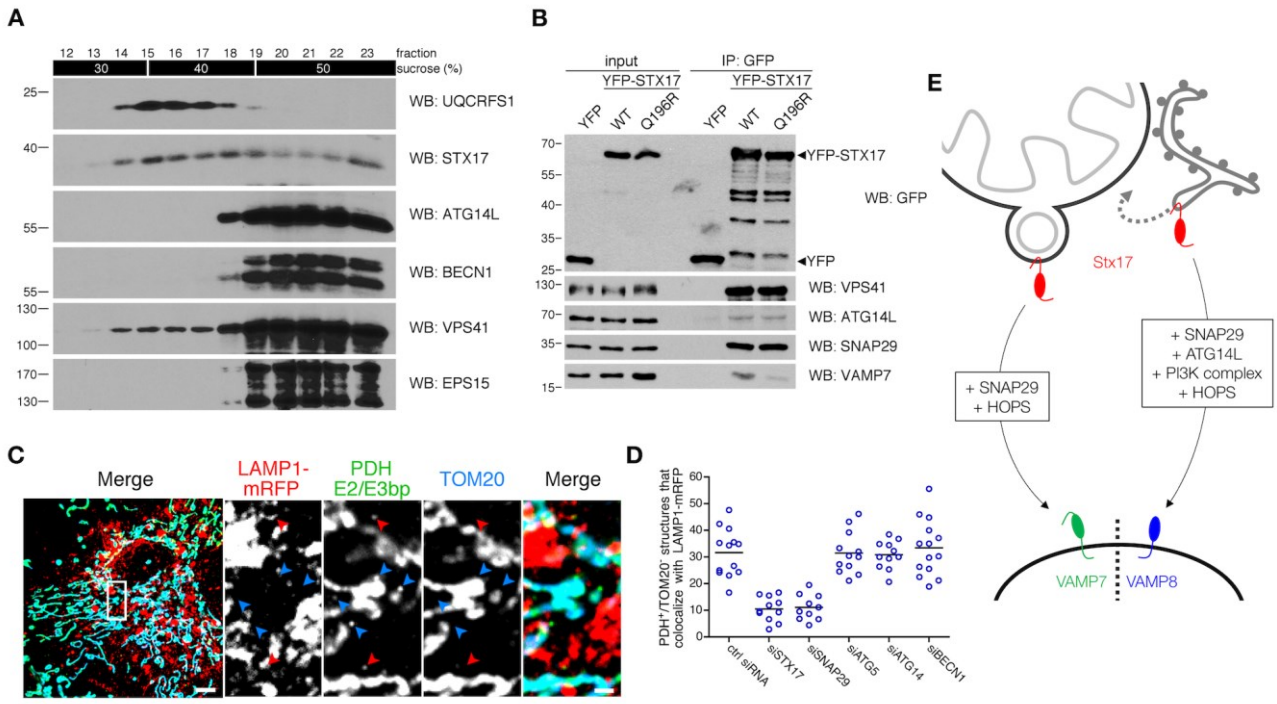


**Figure V.6**. *ATG14L is not involved in MDV-endolysosome targeting*. **A** Immunoblot detection of MDVs purified over a sucrose gradient, generated from liver mitochondria incubated with cytosol and antimycin A. This is the same experiment as the one depicted in Fig. III.1D, but reblotted for the indicated proteins. **B** Coimmunoprecipitation of Stx17 binding proteins from COS7 expressing the indicated construct. **C** COS7 cells expressing LAMP1-mRFP (red) were treated with antimycin A, then fixed and stained for PDH E2/E3bp (green) and TOM20 (blue). MDVs colocalizing with LAMP1 (red arrowheads) or not (blue arrowheads) are indicated. Scale bars, 5 and 1 microns. **D** COS7 cells were transfected with the indicated siRNA, and the percentage of MDVs colocalizing with LAMP1 (as in **C**) was quantified. **E** While Stx17 requires SNAP29 and HOPS to target MDVs to VAMP7-positive late endosomes (left pathway, see Chapter III), additional factors are recruited by Stx17 to the omegasome (right pathway), such as the ATG14L-containing class-III PI3K complex, to mediate autophagosome formation and their targeting to VAMP8-positive lysosomes.

been proposed to homo-oligomerize in order to promote the fusion of autophagosomes and endolysosomes in a membrane tethering role (Diao et al., 2015). Conversely, preliminary data suggests that ATG14L, as well as the entire lipid kinase complex, is dispensable for both MDV formation and targeting. ATG14L is not present in the MDV fraction from cell-free budding assays (Fig. V.6A), and ATG14L binds very weakly to Stx17 in the absence of starvation (Fig. V.6B) as others have reported (Hamasaki et al., 2013). Most importantly, there is no MDV targeting defect in cells lacking ATG14L (Fig. V.6C and D). Thus, MDV and autophagosome formation diverge upstream of ATG14L recruitment (Fig. V6E), an emergent observation that coincides logistically

with Stx17-positive autophagosomes and MDVs originating from the omegasome (Hayashi-Nishino et al., 2009) and the OMM (Fig. III.2), respectively. Interestingly, antimycin A selectively inhibits autophagy (Ma et al., 2011), perhaps through the prevention of Stx17 translocation to sites of autophagosome biogenesis by recruiting the SNARE to MDVs. On the OMM, Stx17 (with or without SNAP29) may be sequestered either by an OMM-specific clamp or chaperone. Ideally, IP-MS of Stx17 from a purified mitochondrial fraction could yield insight into what molecules the SNARE is binding on the OMM, using $STX17^{Q196R}$ as a control for looking at interactions involving the zero layer (Fig. III.6). As a soluble Qbc-SNARE, it is likely that SNAP29 can interact with Stx17 on the OMM. Indeed, in the context of autophagy, post-translation modification of SNAP29 via the attachment of *O*-linked β-*N*-acetylglucosamine (*O*-GlcNAc) prevents its association with Stx17 and, accordingly, starvation inhibits this type of modification to promote Stx17-SNAP29 binding (Guo et al., 2014). Nutrient-sensing via *O*-GlcNAcylation has already been implicated in mitochondrial motility (Pekkurnaz et al., 2014), and may also modulate the MDV response. Indeed, V-ATPase inhibitors trigger autophagy by interfering with amino acid release by the lysosome (Zoncu et al., 2011), and this could conceivably contribute to the increase in MDVs per cell that is seen with bafilomycin treatment (Fig. II.4A and B). Like autophagy, parkin-/PINK1-dependent MDV transport is responsive to stress and potentially other autophagy triggers, so it is not surprising that the pathway may co-opt autophagy-related proteins and mechanisms in order to deliver its cargo to the late endosome.

Contacts between the ER and mitochondria are important regulators of mitochondrial division (see Fig. I.12E) as they are sites of Drp1 stabilization (Friedman et al., 2011; Prudent et al., 2015). Stx17 interacts with at least two GTPases at mitochondria-ER contact sites; Drp1 (a large dynamin-like GTPase) in the GTP-bound state, as well as the small GTPase Rab32 (Arasaki

et al., 2015). Both Rab32 and Stx17 have been reported to be important for Drp1 recruitment to these locations (Arasaki et al., 2015; Ortiz-Sandoval et al., 2014). Rab32 is important for contact site homeostasis, as its loss affects apoptosis (potentially through Drp1), ER $Ca^{2+}$ content and lipid trafficking (Bui et al., 2010; Li et al., 2016). Rab32 is also linked to VAMP7 on the late endosome through VPS9-ankyrin-repeat protein (VARP); originally (and erroneously) thought to be a GTP exchange factor (GEF) for Rab21 (Zhang et al., 2006), VARP binds active Rab32 to act as an effector (Tamura et al., 2009). Interestingly, recruitment of VARP to endosomes has been reported to be dependent upon the retromer complex (Hesketh et al., 2014), which has already been implicated in MDV transport (Braschi et al., 2010) and is mutated in PD (Wang et al., 2016c; Zimprich et al., 2011). On the late endosome, VARP clamps VAMP7 in such a way to prevent its association with other SNAREs by keeping the SNARE domain in a folded, non-helical state (Hesketh et al., 2014; Schafer et al., 2012). It is thus conceivable that the GTP-dependent interaction between Rab32 and the first ankyrin-repeat domain of VARP (Hesketh et al., 2014; Tamura et al., 2009) links Stx17 and VAMP7 on the MDV and late endosome, respectively. This could be tested by determining if both the Stx17-VAMP7 interaction and MDV targeting are abolished in cells lacking either Rab32 or VARP. The release of VAMP7 from VARP may destabilize the non-helical fold adopted by its SNARE domain, allowing it to fold into an α-helix. This step would likely be triggered by the HOPS complex – acting not only to tether adjacent membranes but also in templating SNAREs (Baker et al., 2015; Balderhaar and Ungermann, 2013; Starai et al., 2008) – which is involved in both MDV- (Fig. III.9) and autophagosome-endolysosome fusion via Stx17 (Jiang et al., 2014; Takats et al., 2014). It is likely that templating of the R-SNARE occurs simultaneously with zippering of the four helix bundle (Baker et al.,

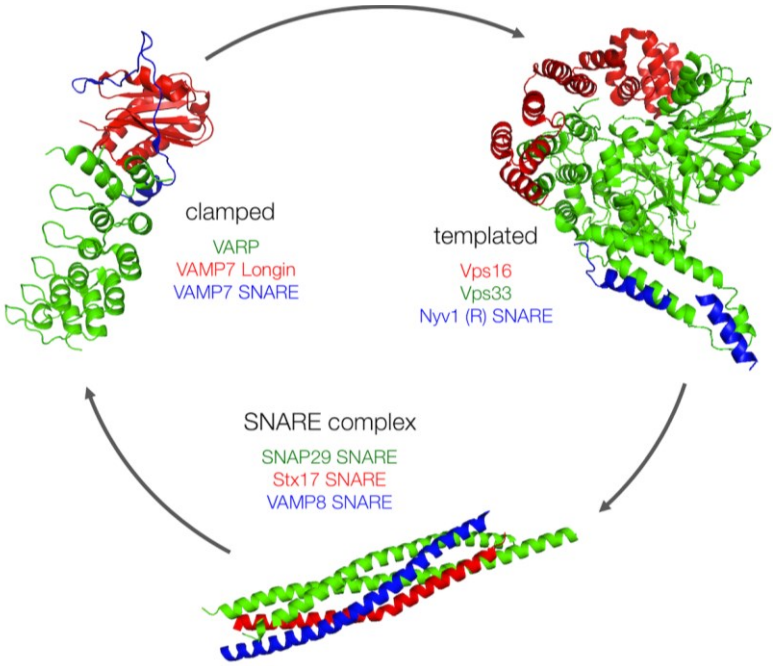


**Figure V.7**. *Conformational changes govern membrane fusion by SNAREs*. R-SNAREs adopt a variety of conformations. Top-left (PDB ID 4B93): VARP (green) clamps the VAMP7 SNARE domain (blue) into a non-fuseogenic conformation. The Longin domain of VAMP7 is depicted in red. Top-right (PDB ID 5BV0): The HOPS subunit VPS33 (green) templates the SNARE domain of the R-SNARE Nyv1 (blue). Another HOPS subunit, VPS16, is shown in red. Bottom (PDB ID 4WY4): a four-helix bundle is formed between the Q-SNAREs SNAP29 (green, two helices) and Stx17 (red, one helix) and the R-SNARE VAMP8 (blue, one helix) during membrane fusion.

2015), as this latter process is driven by protein folding (Fasshauer et al., 2002; Fiebig et al., 1999; Zorman et al., 2014). Structures of R-SNAREs cycling through several conformations – a clamped complex of VARP/VAMP7 (Hesketh et al., 2014), the R-SNARE domain of yeast Nyv1 templated by the HOPS subunits VPS33 and VPS16 (Baker et al., 2015), and the mammalian autophagic SNARE complex formed by Stx17, SNAP29 and VAMP8 (Diao et al., 2015) – are depicted in Fig. V.7.

One interesting crossover between the described MDV-endolysosome SNARE complex and PD pathways is that α-synuclein has been reported to have SNARE chaperone activity by promoting the formation of the neuronal SNARE complex (Burre et al., 2010; Chandra et al., 2005). Indeed, while pathogenic oligomers in fact block the docking of synaptic vesicle mimics *in vitro* (Choi et al., 2013), smaller multimers promote Stx1A/SNAP25/VAMP2 complex formation (Burre et al., 2014). This activity is believed to be mediated by a bridging effect, in which synuclein binds both VAMP2 (the so-called "vesicle-SNARE) and acidic phospholipids on the plasma membrane, such as phosphatidylserine (Diao et al., 2013; Lai et al., 2014; Lou et al., 2017). α-

synuclein binds to the N-terminus of VAMP2, within the 30 amino acids upstream of the R-SNARE domain (Burre et al., 2010). This sequence is rich in proline residues, as well as alanine and glycine residues, and differs in charge, as well as structurally, from the N-termini of the endolysosomal R-SNAREs VAMP7 and VAMP8 (Fig. V.8A). In lipid-bound VAMP2 (Fig. V.8B), this region adopts an extended, flexible structure (Ellena et al., 2009) – likely owing to a lack of complex R-groups in this sequence – that may become more rigid upon synuclein binding. It is thus unlikely that α-synuclein plays a direct role in MDV-endolysosome fusion, as the selectivity of its interaction with VAMP2 suggests its unique involvement in exocytosis. Indeed, a comparison of the first 30 amino acids of human R-SNAREs reveals only VAMP1 and VAMP2

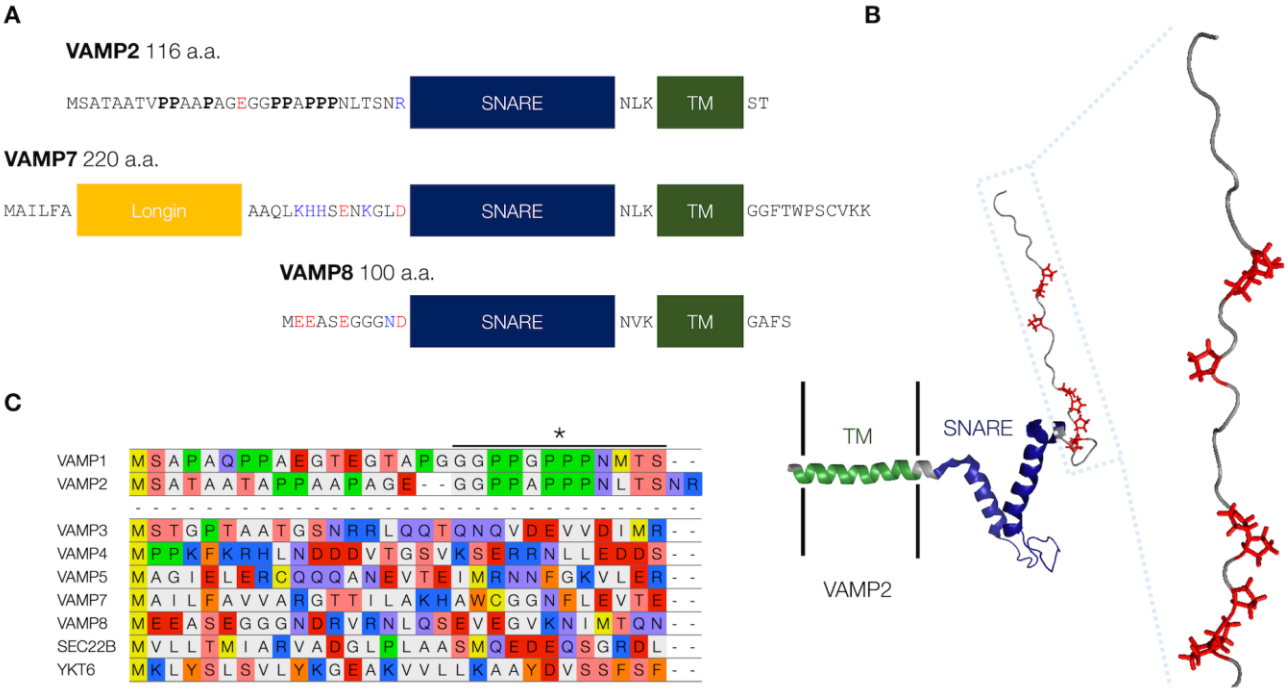


**Figure V.8**. *Comparison of the N-terminus of VAMP2 with other R-SNAREs*. **A** Sequence comparison between VAMP2, VAMP7 and VAMP8. The primary sequence of regions not contained within established domains is depicted. N-terminal proline residues are indicated by bolded text, while acidic and basic residues are in red and blue, respectively. Note that the figure is not to scale, as the Longin, SNARE and transmembrane (TM) domains contain 104, 61 and 21 amino acid residues, respectively. **B** NMR solution structure (cartoon) of rat VAMP2 in a lipid bilayer (PDB ID 2KOG). The SNARE and transmembrane (TM) domains are coloured according to the scheme in **A**. The light blue box expands the N-terminus, where proline residues are shown in red. **C** Primary sequence alignment of the first 30 amino acids of human R-SNAREs. The last 14 residues of VAMP2 are shifted so that they align with those in VAMP1 (indicated by the asterisk). The alignment was constructed using eBioX, and all sequences were obtained from Uniprot.com.

share a proline-rich, simplistic N-terminus (Fig. V.8C). Despite this, a VAMP1/synuclein interaction remains unexplored. It should be noted that a splice isoform of VAMP1, VAMP1B, contains a mitochondrial targeting sequence at its C-terminus (Isenmann et al., 1998); it is therefore possible that synuclein could be involved in an MDV-type pathway utilizing VAMP1B. Despite a perceived lack of a direct role for synuclein in MDV-endolysosome fusion via Stx17/SNAP29/VAMP7, synuclein overexpression is known to cause trafficking defects by affecting SNARE function (Cooper et al., 2006; Gitler et al., 2008; Gosavi et al., 2002; Thayanidhi et al., 2010), potentially by binding and sequestering SNAREs when present at pathophysiological concentrations. Whether synuclein overexpression or aggregation blocks MDV-endolysosome fusion remains to be investigated.

Table V.1. Descriptive Table of Observed MDV Populations

| Type | Trigger | Bilayers | Cargo | Machinery | Destination | Pathway | Selected reference |
|---|---|---|---|---|---|---|---|
| matrix carriers | ROS (mito) | 2 | matrix + IMM | parkin, PINK1, Stx17 | LE (lysosome) | QC | (McLelland et al., 2014) |
| TOM20$^+$ | ROS (cyto) | 1 | TOM20 | ? | LE (lysosome) | QC | (Soubannier et al., 2012a) |
| MAPL carriers | ? | 1 | MAPL | VPS35 | pex | pex | (Braschi et al., 2010) |
| Drp1 recyclers | fission | ? | Drp1 | VPS35 | lysosome | dynamics | (Wang et al., 2016c) |
| SNPH$^+$ | ROS (mito) | 1 | SNPH | ? | LE (lysosome) | QC? | (Lin et al., 2017) |
| MitAP vesicles | heat shock | 2 | mito antigens | SNX9, Rab9, Rab7 | Rab9$^+$ LE (PM) | immunity | (Matheoud et al., 2016) |

| | | | | | | | |
|---|---|---|---|---|---|---|---|
| mtDNA carriers | ROS | ? | oxidized mtDNA | ? | secretion | immunity | (Caielli et al., 2016) |

Abbreviations: Drp1, dynamin-related protein 1; LE, late endosome; MAPL, mitochondria-anchored protein ligase; MitAP, mitochondrial antigen presentation; pex, peroxisome; PM, plasma membrane; QC, quality control; ROS, reactive oxygen species; SNPH, syntaphilin; SNX9, sorting nexin 9; VPS35, vacuolar protein sorting 35. Notes: initial destinations are listed, while final destinations are shown in brackets.

In summary, the mechanism by which MDVs target to their intended destination likely depends on the array of factors on the MDV (outer) membrane, as well as associated proteins. In Chapter III, it was demonstrated that, at least in the case of PINK1-/parkin-dependent vesicles, the so-called "SNARE hypothesis" (Sollner et al., 1993) is applicable as Stx17 is identified as a molecule involved in the targeting of these "matrix carriers" to the late endosome (Fig. III.4B and C). Moreover, the dependence of this process on the HOPS tethering complex (Fig. III.9) implies that MDV fusion is a regulated process involving many factors. For other MDV populations (see Table V.1), the players remain unknown; although, in the case of vesicles involved in antigen presentation, factors that recruit Rab7 – which is required to present the cargo of MDVs at the cell surface but is dispensable for their formation (Matheoud et al., 2016) – can be expected to play a role. Thus, there is still much work to be done in order to understand how mitochondrial vesicles traffic to and fuse with target membranes.

### V.II.iv *Aberrant interorganellar tethering in Parkinson's Disease*

While mitochondria-ER contact sites play important roles in signaling and metabolite transfer between both organelles (see section I.IV.ii), their dysregulation in neurodegenerative disease is becoming an emerging field of intense study. As mentioned at the end of Chapter IV, recent reports have implicated both *PARKIN* and *PINK1* in the maintenance of these interorganellar junctions at the steady-state. Mitochondria-ER contact length (as measured by EM)

was reported to be increased in both *PARKIN* and *PINK1* patient fibroblasts and mutant fly brains (Celardo et al., 2016; Gautier et al., 2016), consistent with the model of parkin-/PINK1-mediated destruction of Mfn2 interorganellar bridges elucidated in Chapter IV. Somewhat paradoxically, $Ca^{2+}$ transfer between the ER and mitochondria was found to be hindered in *PARKIN* patient fibroblasts (Gautier et al., 2016). Although this may be a result of perturbed mitochondria-ER tethering as suggested by Gauthier and colleagues, it should be noted that a mass spectrometric analysis of mitochondria from *PARKIN*$^{-/-}$ and *PINK1*$^{-/-}$ rat brains revealed that MCU was downregulated in both genotypes compared to WT (Stauch et al., 2016). This could be a compensatory mechanism to deal with ER-OMM contact perturbations resulting from the loss of *PARKIN*/*PINK1*, as deletion of *MCU* rescues neurodegeneration in *PINK1*-null zebrafish (Soman et al., 2017). Stauch and colleagues additionally found that acyl-CoA:cholesterol acyltransferase 2 (ACAT2) was decreased more than five-fold in both KO genotypes, and additionally decreased in *DJ1*$^{-/-}$ rat brain mitochondria (ER-mitochondria contacts have yet to be measured in *DJ1* loss-of-function systems), representing one of the highest fold-changes across genotypes (Stauch et al., 2016). Dysregulation of ACAT2 levels in *PARKIN*$^{-/-}$ mouse brains and cell lines overexpressing parkin had been documented previously (Davison et al., 2009; Periquet et al., 2005). ACAT2 esterifies fatty acids and cholesterol (Rogers et al., 2015), and these proteins localize to membrane contact sites in yeast and mammals (Area-Gomez et al., 2012; Gulati et al., 2015). A decrease in ACAT2 levels could translate into the retention of unesterified cholesterol in membrane microdomains (Rogers et al., 2015), including the MAM (Area-Gomez et al., 2012; Hayashi and Fujimoto, 2010), and would be consistent with the increase in ER-OMM contact (Celardo et al., 2016; Gautier et al., 2016) and lipid raft-dependent functions (Cha et al., 2015) observed in *PARKIN*/*PINK1* loss-of-function systems. Indeed, a suppression of cholesterol esterification could

feed potentially pathological ER-OMM contact expansion due to a loss of parkin-/PINK1-dependent Mfn2 turnover, as Mfn2 positively regulates sterol metabolism (Duarte et al., 2012; Sandoval et al., 2014). Alternatively, the cell may shut down cholesterol modification via downregulation of ACAT2 in response to MAM dysfunction, which may tie in to defects in lipid metabolism observed in *PARKIN*$^{-/-}$ mice (Kim et al., 2011). Lipid profiling of purified MAMs from *PINK1*- and *PARKIN*-null cells or tissue would shed light on whether morphological changes observed in OMM-ER appositions are accompanied by lipid imbalances indicative of an up/downregulation of MAM function.

PINK1 appears to play an additional (and somewhat-paradoxical) role in stabilizing mitochondria-ER contact (Gelmetti et al., 2017), which was also reported in Chapter IV (Fig. IV.1H and I). Accordingly, an unbiased siRNA screen in *Drosophila* revealed a role for sterol and lipid biosynthesis in the recruitment of parkin to mitochondria; in cells lacking either sterol regulatory binding factor 1 (SREBF1), which regulates the synthesis of predominantly fatty acids, or SREBF2, which oversees sterol synthesis, inefficient PINK1 stabilization upon mitochondrial depolarization abolished parkin translocation to mitochondria, which could be rescued by exogenous fatty acids and cholesterol (Ivatt et al., 2014). Indeed, diet supplementation of octadecanoic acid ($C_{18}$ unsaturated fatty acid) also rescued mitochondrial phenotypes associated with *PARKIN* and *PINK1* mutant flies (Senyilmaz et al., 2015), and a high-throughput pharmacological screen identified statins as potent upregulators of parkin levels (Hasson et al., 2015). Finally, both *PARKIN*$^{-/-}$ mice and human individuals carrying *PINK1* single-nucleotide polymorphisms (SNPs) have abnormalities concerning the uptake of circulating fatty acids (Franks et al., 2008; Kim et al., 2011). In summary, the implications of PINK1/parkin and mitochondria-ER contact is two-fold; the localization of PINK1 to the MAM (Gelmetti et al., 2017) highlights a

reciprocal relationship in which PINK1 stabilization requires the MAM, only to signal for its destruction via parkin-dependent Mfn2 turnover (Chapter IV). Secondly, biosynthetic and signaling pathways that regulate MAM stability accordingly impinge upon parkin/PINK1 pathways.

Contacts between mitochondria and the ER are critical loci for parkin and PINK1 function. While there is an apparent dearth of direct investigation in the literature, there are several signs that this importance extends to other PD-related molecules. For example, *VPS13C* was recently shown to be mutated in several cases of EOPD across three families (Lesage et al., 2016). The four members of the VPS13 family in humans trace back to a single Vps13 gene in yeast, which localizes to membrane contact sites and, like its mammalian counterparts, is a PI3P-binding protein that regulates the metabolism of PI4P (Park et al., 2015a; Park et al., 2016; Rzepnikowska et al., 2017; Velayos-Baeza et al., 2004); in the case of *VPS13C*, it is additionally worth noting that a brain-specific isoform is the most highly-expressed variant in this tissue (Velayos-Baeza et al., 2004). Accordingly, depletion of VPS13C from cells enhances parkin-mediated mitophagy (Lesage et al., 2016), which would be consistent with it promoting ER-OMM tethering according to the findings reported in Chapter IV (see Fig. IV.S4E to I). Another example is *PLA2G6*, the causal factor at the *PARK14* locus, which supports ER $Ca^{2+}$ levels and $Ca^{2+}$ transfer to mitochondria (Strokin and Reiser, 2016; Zhou et al., 2016). The PLA2G6 protein is a stress-activated mitochondrial phospholipase and its loss leads to mitochondrial dysfunction (Kinghorn et al., 2015; Rauckhorst et al., 2015). Interestingly, there is a buildup of unacidified autophagosomes in the DAergic neurons of mice lacking the EOPD-linked isoform of *PLA2G6* (Zhou et al., 2016), which may hint at disruptions in mitochondria-ER contacts crucial for autophagosome biogenesis and maturation (Hamasaki et al., 2013; Itakura et al., 2012b).

In heterologous culture of DAergic-like cells, α-synuclein has also been reported to localize to the MAM by biochemical analyses (Guardia-Laguarta et al., 2014; Paillusson et al., 2017). Synuclein can bind the mitochondrial membrane directly in a manner that is potentially pH-dependent (Cole et al., 2008; Nakamura et al., 2011; Nakamura et al., 2008). These findings build on previous studies over the past two decades demonstrating that synuclein is associated mitochondrial dysfunction, both in cells and *in vivo* (Hsu et al., 2000; Luth et al., 2014; Martin et al., 2006; Reeve et al., 2015), and mitochondria appear to be involved in synuclein toxicity (Buttner et al., 2008; Buttner et al., 2013). Endogenous α-synuclein has been reported to support $Ca^{2+}$ transfer between both organelles (Cali et al., 2012), while overexpressed synuclein disrupts this process (Paillusson et al., 2017). Mechanistically, α-synuclein can disrupt the direct association of VAPB on the ER membrane with PTPIP51 on the OMM, a tethering complex that promotes mitochondria-ER contact (Paillusson et al., 2017; Stoica et al., 2014). In a similar manner to Mfn2 tethering complexes, the VAPB-PTPIP51 complex also positively regulates autophagy through its tethering ability (Gomez-Suaga et al., 2017; Hamasaki et al., 2013). It is therefore conceivable that synuclein-mediated toxicity is driven via disruption of the autophagy pathway downstream of mitochondria-ER uncoupling – synuclein overexpression has already been associated with autophagy defects (Winslow et al., 2010) – rather than through aberrant synuclein proteostasis; this latter hypothesis is the *status quo* for the field (Poewe et al., 2017). The importance of a healthy autophagy-lysosome pathway in preventing DAergic degeneration cannot be understated; for example, the primary phenotype of temperature-sensitive *Drosophila* mutants for *N*-ethyl-maleimide-sensitive factor (NSF), the critical ATPase responsible for SNARE complex disassembly post-fusion (Littleton et al., 2001), is neurodegeneration and locomotor defects related

to DAergic cell death (Babcock et al., 2015). This is due not to defective synaptic transmission, but to a disruption in autophagic flux and lysosomal degradation pathways (Babcock et al., 2015).

In addition to their potential implication in PD, mitochondria-ER contact dysfunction may extend to other neurodegenerative diseases; for example, it has been hypothesized that Alzheimer's disease (AD) is primarily a disease of lipid dyshomeostasis, in which lipid trafficking between mitochondria and the ER plays a role in pathogenesis (Area-Gomez and Schon, 2017). The γ-secretase complex, whose presenilin (PSEN) subunits are mutated in familial AD, localizes to and processes the amyloid precursor protein (APP) at contact sites between mitochondria and the ER (Area-Gomez et al., 2009; Del Prete et al., 2017; Puglielli et al., 2004; Puglielli et al., 2001). MAM-dependent lipid metabolism, including cholesterol esterification, and other functions are increased in i) AD patient fibroblasts, ii) MEFs lacking both PSEN1 and PSEN2, and iii) other disease paradigms (Area-Gomez et al., 2012; Hedskog et al., 2013; Tambini et al., 2016). As preliminary data indicate that mitochondria-ER contact dysfunction may also play a role in amyotrophic lateral sclerosis (Stoica et al., 2014; Stoica et al., 2016; Watanabe et al., 2016), it is possible that morphological and functional MAM abnormalities may underlie neurodegenerative disorders since, as a hub that regulates signaling and metabolism, their effects can be global and wide-ranging and, secondly, the importance of lipid transport via membrane contact sites is likely elevated in neurons as distal processes are far-removed from the *Golgi* apparatus from which ER-derived lipids are exported via vesicular trafficking pathways (Hanus and Ehlers, 2016; Palade, 1975). EM reconstruction of rodent brain tissue demonstrated that, in the case of neuronal mitochondria, ~4 to 5% of the OMM is in contact with the ER (defined as and ER-OMM distance of 30 nm or less) and – unlike ER-plasma membrane contacts, for example – this number remained remarkably constant for mitochondria in both the soma and in processes (Wu et al., 2017). It is

thus likely that MAM functions fulfill critical roles (such as lipid synthesis) in the periphery, and fit a model in which the ER dictates zones of dendritic branching (Cui-Wang et al., 2012). It is clear that understanding mitochondria-ER communication in neurons will inform our ideas regarding neurodegenerative mechanisms going forward.

### V.II.v *Integration of MDV trafficking and mitochondria-ER tethering*

It is likely that vesicle generation by the parkin/PINK1 system is related to their ability to influence mitochondria-ER contact (Chapter IV), especially given preliminary evidence implicating Mfn2 ubiquitination in the former process. An emergent question therefore becomes how the two mechanisms are related; the ER may need to be released from mitochondria in order for the latter organelle to

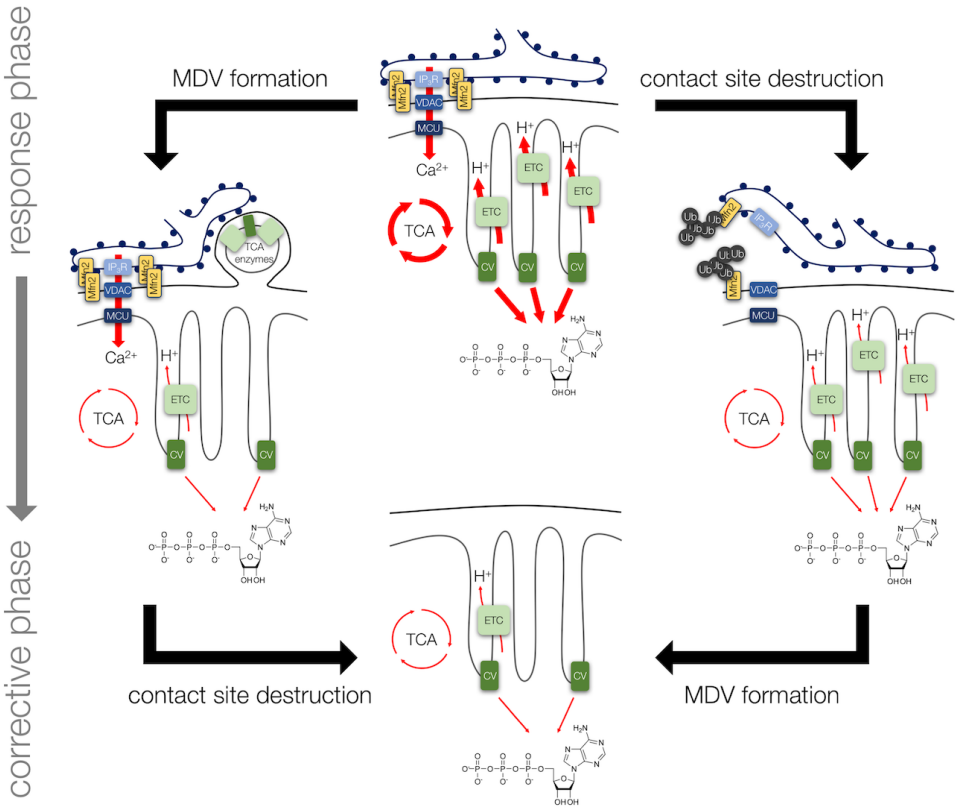


**Figure V.9**. *Parkin-/PINK1-dependent mechanisms as mitochondrial metabolic remodeling pathways*. Parkin and PINK1 maintain a balance of mitochondrial respiratory capacity in the form of ETC complexes and tricarboxylic acid (TCA) cycle enzymes. Metabolic remodeling of mitochondria occurs in two phases; a response phase is triggered by stochastic damage or signaling events, which precipitates a corrective phase that maintains a certain ratio of mitochondria-ER contact to respiratory capacity to ensure optimal functionality of the organelle. In the counter-clockwise direction, MDVs remove ETC and TCA enzymes during the response phase. Mitochondria-ER contacts are then pruned during the corrective phase to adjust for decreased respiratory capacity. In the absence of this correction, high levels of calcium may cause toxicity. In the clockwise direction, mitochondria-ER contact is destroyed in the response phase, and MDV formation subsequently matches the amount of ETC and TCA enzymes to the reduction interorganellar contact. If this correction does not occur, a large number of enzymatic complexes will remain trapped in a non-functional organelle.

generate a vesicle, or *vice versa*. One perspective from which to approach these hypotheses is to consider how the mitochondrion may balance both pathways (Fig. V.9). For example, after the extraction of OXPHOS components from mitochondria via MDVs (Fig. II.3F and G), the cell may slow TCA cycling via the uncoupling of mitochondria from the ER in order to reduce the amount of $Ca^{2+}$ – a potent TCA inducer (Llorente-Folch et al., 2015) – flowing into the matrix via the $IP_3R$/VDAC/MCU system (Fig. V.9, left side). The absence of this correction could lead to $Ca^{2+}$ mishandling and toxicity, and subsequent organellar dysfunction. Conversely, disconnection of a mitochondrion from the ER may occur first, and then MDVs would act to readjust the respiratory capacity of the organelle to the reduced capacity for ATP production (Fig. V.9, right side). Without the organelle able to adjust its respiratory capacity to decreased $Ca^{2+}$ influx, the cellular investment in ETC components would outweigh its return in energy production.

Mitochondrial biogenesis would return the mitochondrion to full functionality following this *yin*/*yang* relationship of organellar untethering and MDV production. One intriguing aspect of this entire process is that, as was mentioned in Chapter I, parkin and PINK1 have been shown to promote mitochondrial biogenesis as well. In section I.IV.i, the relationship between parkin/PINK1 and PARIS was described; parkin and PINK1 promote the ubiquitin-mediated degradation of PARIS, a suppressor of mitochondrial biogenesis through repression of PGC-1α, to ultimately drive mitochondrial gene expression (Lee et al., 2017; Shin et al., 2011; Stevens et al., 2015). Additionally, parkin and PINK1 directly support the localized translation of certain ETC components at the OMM via interactions with the ribosome (Gehrke et al., 2015). How might this happen? Clu1/CluA homologue (CLUH) binds both the ribosome and mRNAs of nDNA-encoded mitochondrial proteins, controlling their translation and metabolism (Gao et al., 2014; Schatton et al., 2017; Sen and Cox, 2016; Wakim et al., 2017). The *Drosophila* homologue of CLUH, *clueless*,

interacts genetically with *PARKIN* and suppresses *PINK1* phenotypes (Cox and Spradling, 2009; Sen et al., 2015; Wang et al., 2016d). Indeed, environment scanning in unstimulated mammalian cells using BioID revealed CLUH to be top steady-state hit for PINK1 (Hesketh and Gingras, unpublished results). Additionally, *clueless* interacts with p97, and its depletion from *Drosophila* muscles or cultured cells suppressed p97-dependent MARF degradation (Wang et al., 2016d). CLUH contains four tetratricopeptide repeat (TPR) motifs (Fig. V.10A), indicating that it likely acts as a scaffold (Passmore et al., 2005), and CLUH may thus physically couple mitochondrial biogenesis to Mfn2/MARF degradation; interactions within this system are mapped in Fig. V.10B. Fig. V.10C illustrates how the turnover of Mfn2 ER-OMM bridges may allow the ribosome access to specialized import complexes that would facilitate co-translational import (Gold et al., 2017; Williams et al., 2014) of ETC-related polypeptides and their incorporation into OXPHOS complexes at mitochondria-ER juntions. Interestingly, DJ-1 has also been shown to be associated with mRNA (van der Brug et al., 2008), although a role for DJ-1 in co-translational import of mitochondrial polypeptides remains unexplored.

How parkin and PINK1 mediate (and balance) mitochondrial turnover and biogenesis, as well as ER-OMM dissociation, takes up new meaning in the context of a polarized cell, where spatial segregation of PINK1/parkin pathways are a possibility; indeed, an analysis of *Drosophila* motor neurons found that *PARKIN* mutant animals accumulated tubular mitochondria in the cell body, with a concomitant reduction of organelles in the periphery (Sung et al., 2016). Axonal mitochondria, although reduced in number, appeared functionally unimpaired (Sung et al., 2016). DAergic neurons located in the SNpc form extensive and complex axonal arbors; in the rodent brain, the axon of a single DAergic neurons arborizes throughout ~6% of the striatum (Matsuda et al., 2009). This, combined with the inherent pacemaking activity of these neurons that renders

them sensitive to mitochondrial oxidative stress (Guzman et al., 2010), may underlie the selective vulnerability of SNpc DAergic neurons to cell death in PD (Surmeier et al., 2017). Accordingly, pUb (a surrogate for mitochondrial damage) was preferentially detected in iPSC-derived DAergic neurons challenged with an uncoupler compared to TH-negative cells (Shiba-Fukushima et al., 2017). Thus, the mechanistic and spatial relationship between various PINK1/parkin pathways and their study in disease-relevant systems likely remain unappreciated. Fig. V.11 illustrates how turnover mechanisms in the periphery could be coupled to biosynthetic pathways in the cell soma. OXPHOS in functional mitochondria in the periphery triggers successive rounds of ER-OMM

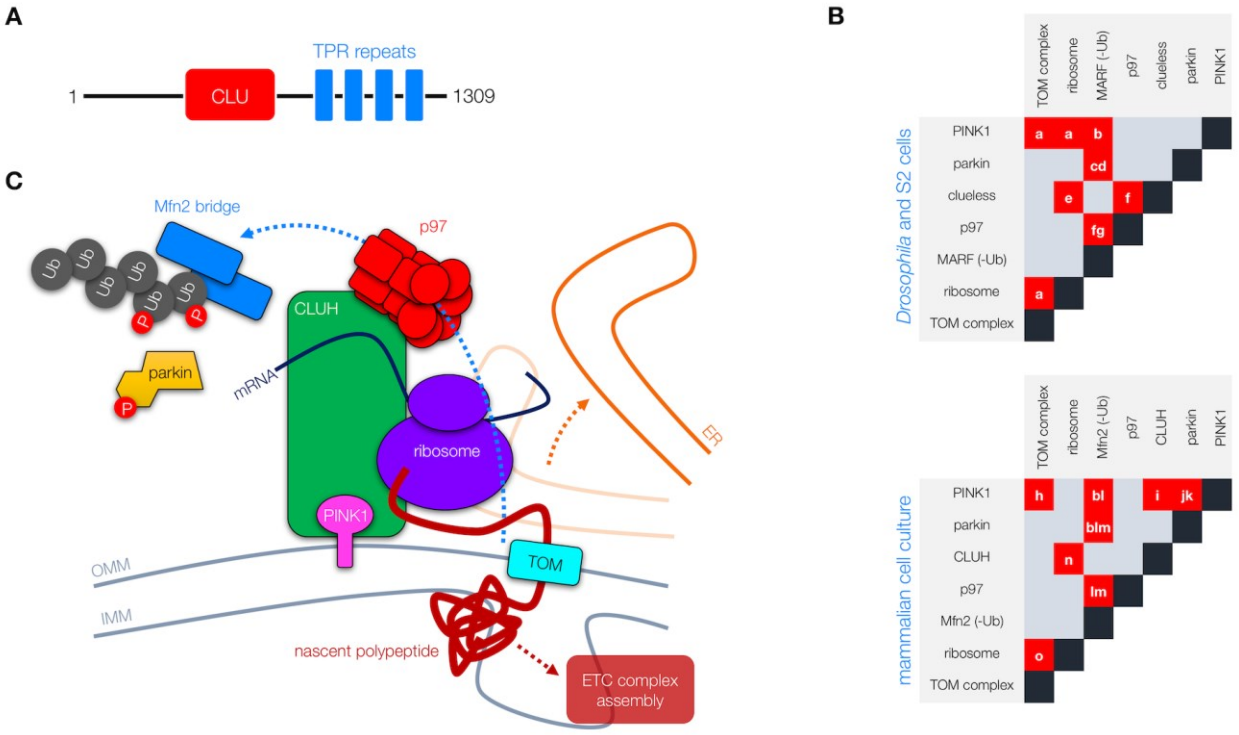


**Figure V.10**. *Does CLUH couple mitochondrial biogenesis to OMM protein turnover*? **A** Domain structure of human CLUH. The CLU domain (red) and TPR repeats (blue) are indicated. **B** Charts describing presumed physical interactions between indicated proteins in both *Drosophila* (top) and mammalian (bottom) systems. Reported interactions are denoted in red, with white letters corresponding to the following references: a, Gehrke *et al.*, 2015; b, Chen & Dorn, 2013; c, Ziviani *et al.*, 2010; d, Yun *et al.*, 2014; e, Sen & Cox, 2016; f, Wang *et al.*, 2016; g, Zhang *et al.*, 2017; h, Lazarou *et al.*, 2012; i, Hesketh & Gingras, unpublished results; j, Shiba-Fukushima *et al.*, 2012; k, Kazlauskaite *et al.*, 2014; l, Chapter IV; m, Tanaka *et al.*, 2010; n, Gao *et al.*, 2014; o, Williams *et al.*, 2014. **C** Mechanism of CLUH-dependent coupling of degradation to synthesis. PINK1/parkin ubiquitinate Mfn2, triggering its extraction by p97 and ER-OMM dissociation. This allows the ribosome access to TOM complexes that would otherwise be unavailable.

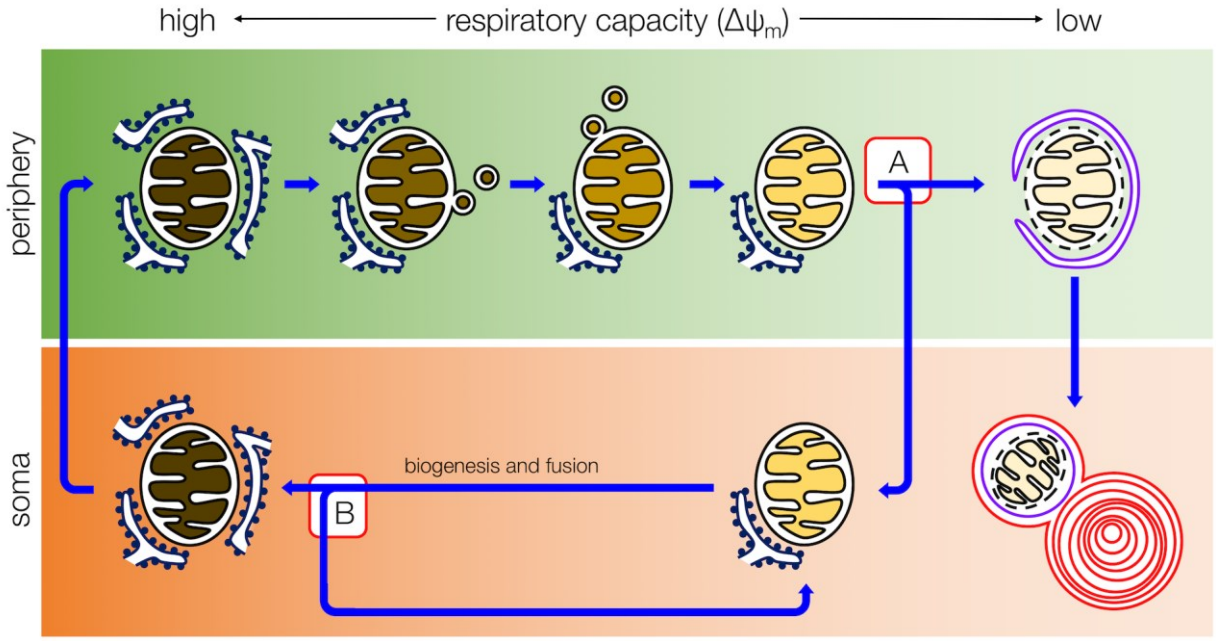


**Figure V.11**. *Mitochondrial cycling*. Healthy mitochondria in the neuronal periphery have a high "respiratory capacity", defined as their ability to generate ATP through respiration and associated with high levels of ETC complexes and TCA cycle enzymes (dark brown matrix) and ER-mitochondria contact sites which act to drive respiration. By extension, these mitochondria have a high membrane potential ($\Delta\psi_m$). ER-mitochondria contact sites are destroyed by parkin and PINK1, and as a consequence remodel their metabolic capacity by shedding mitochondrial-derived vesicles containing ETC complexes and TCA cycle enzymes (as well as other proteins). At checkpoint A, mitochondria with low respiratory capacity (pale yellow matrix) are tagged to either undergo retrograde transport to the cell soma or degradation via autophagy. In the soma, mitochondria that have avoided destruction increase their respiratory capacity through import of *de novo*-synthesized proteins, the driving of mtDNA transcription/translation, and fusion with other, healthy mitochondria. At checkpoint B, mitochondria with a high enough respiratory capacity are selected to undergo anterograde transport to the cell periphery.

dissociation and MDV formation (see also Fig. V.9), reducing the respiratory capacity (equivalent to $\Delta\Psi_m$) of the organelle. Ultimately, the organelle is trafficked back to the soma to be salvaged, or autophagocytosed and turned over by lysosomal hydrolases (Ashrafi et al., 2014; Cai et al., 2010; Lee et al., 2011). In the soma, biosynthetic pathways are activated at mitochondria depleted of their potential to produce ATP and, once these organelles surpass cut-off criteria for competency (checkpoint B in Fig. V.11), are shuttled back out to the periphery. Alternatively, while removal of OXPHOS components via MDVs would occur in the periphery, ER-OMM dissociation would be restricted to the soma where it is coupled to protein synthesis (see Fig. V.10).

## V.III CONCLUSION

The work detailed within this thesis describes core machinery governing *a*) the generation a subpopulation of mitochondrial vesicles, *b*) their turnover via fusion with the late endosome, and *c*) the destruction of contacts between mitochondria and the ER. These studies delved into basic mechanisms of membrane remodeling and architecture, as well as organelle trafficking and communication, with implications for understanding neurodegenerative disease. As discussed above (section V.II.v), it has now become critical to take the study of these molecular mechanisms, elucidated in cell cultures and cell-free assays, and transpose it into more disease-relevant systems such as iPSC-derived DAergic neurons and animal models.

Specifically, how AR-JP-related pathways interact with one another will likely inform our understanding of AR-JP pathophysiology moving forward. While *PARKIN* and *PINK1* function in a common pathway with at least some amount of conceivable crossover with *DJ1*, how these genes relate to other reported AR-JP genes *SYNJ1* (Krebs et al., 2013), a phosphatase that dephosphorylates $PI(4,5)P_2$ (McPherson et al., 1996), and *VAC14* (Taghavi et al., 2017), a scaffold that oversees the conversion of PI3P to $PI(3,5)P_2$ (Jin et al., 2008; Zhang et al., 2007), is less obvious. A recent study found that SYNJ1 was required for the maturation of autophagosomes in *Drosophila* presynaptic terminals (Vanhauwaert et al., 2017), potentially implicating SYNJ1 in mitochondria-ER contact site maintenance (Hamasaki et al., 2013). Additionally, the same study found that flies carrying the human AR-JP-linked SYNJ1 phosphatase domain mutant R258Q hindered SYNJ1-dependent dephosphorylation of PI3P and $PI(3,5)P_2$, while not affecting $PI(4,5)P_2$ levels (Vanhauwaert et al., 2017). Thus, PI3P/$PI(3,5)P_2$ homeostasis may link SYNJ1 and VAC14 functions. VAC14 interacts with TBC1D15 and members of the autophagy-lysosome pathway (Schulze et al., 2014), potentially pointing to a function of these PIPs in mitophagy

(Yamano et al., 2014) or, conversely, implicating the endolysosomal system in the maintenance of mitochondria-ER contact. The functions of multiple AR-JP genes may therefore converge on interorganellar contacts between mitochondria and the ER.

Finally, one aspect of PD that was omitted from the "cornerstones of PD" (Fig. I.2) is the involvement of immunity pathways. Inflammation occurs within the SNpc of PD patients (Mosley et al., 2012), which harbours the highest density of microglia within the mammalian brain (Kim et al., 2000). Accordingly, highly-pathogenic influenza has been shown to cause parkinsonism via the death of SNpc DAergic neurons (Henry et al., 2010; Jang et al., 2012; Jang et al., 2009), and *encephalitis lethargica* – which affects the DAergic system and is apparently treatable with levodopa (Sacks, 1983) – has been proposed to be a post-infection autoimmune disorder as, similarly to PD patients, autoantibodies against basal ganglia antigens have been detected in patient cerebral spinal fluid (Dahlstrom et al., 1990; Dale et al., 2004; Kunas et al., 1995; McRae-Degueurce et al., 1988). More recently, circulating autoantibodies against α-synuclein in PD patients were described (Sulzer et al., 2017), pointing to the idea of PD as an autoimmune disease. Indeed, DAergic neurons are capable of expressing major histocompatibility complex class I and are sensitive to cytotoxic T cells (Cebrian et al., 2014). Loss of *PARKIN* activates innate immune pathways in *Drosophila* (Greene et al., 2005), and parkin and PINK1 were recently shown to suppress mitochondrial antigen presentation (MitAP), which occurs via an MDV pathway that acts to present exogenous and autoantigens from mitochondria on the cell surface (Matheoud et al., 2016). While this was linked to parkin-dependent ubiquitination of MitAP effectors (Matheoud et al., 2016), modulation of mitochondria-ER contact through PINK1/parkin may also play a role, as this interorganellar junction has been shown to play an important role in immune responses (Horner et al., 2011; Subramanian et al., 2013; Zhou et al., 2011).

In summary, understanding the interactions between various PD pathways will likely provide the key to understanding disease pathogenesis and point to a cure. To cite two recent examples, phenotypes of iPSC-derived DAergic neurons from *PARKIN* and *PINK1* patients included both mitochondrial dysfunction and α-synuclein accumulation (Chung et al., 2016), a result replicated in neurons lacking *TMEM175* (Jinn et al., 2017), a gene associated with PD by a genome-wide association study (Nalls et al., 2014). Globally, I have made the point that these pathways may converge on communication between mitochondria and the ER, an emergent property of which is the maintenance of mitochondrial function by the parkin/PINK1 pathway. I believe the work presented within the pages of this thesis represents a small but significant advance within the fields of PD research and mitochondrial biology, and perhaps as importantly, has hopefully emphasized the extraordinary role of the cell's powerhouse.

## REFERENCES


Abbott, R.D., G.W. Ross, L.R. White, J.S. Nelson, K.H. Masaki, C.M. Tanner, J.D. Curb, P.L. Blanchette, J.S. Popper, and H. Petrovitch. 2002. Midlife adiposity and the future risk of Parkinson's disease. *Neurology*. 59:1051-1057.

Abeliovich, A., and A.D. Gitler. 2016. Defects in trafficking bridge Parkinson's disease pathology and genetics. *Nature*. 539:207-216.

Aguileta, M.A., J. Korac, T.M. Durcan, J.F. Trempe, M. Haber, K. Gehring, S. Elsasser, O. Waidmann, E.A. Fon, and K. Husnjak. 2015. The E3 ubiquitin ligase parkin is recruited to the 26 S proteasome via the proteasomal ubiquitin receptor Rpn13. *The Journal of biological chemistry*. 290:7492-7505.

Akundi, R.S., Z. Huang, J. Eason, J.D. Pandya, L. Zhi, W.A. Cass, P.G. Sullivan, and H. Bueler. 2011. Increased mitochondrial calcium sensitivity and abnormal expression of innate immunity genes precede dopaminergic defects in Pink1-deficient mice. *PloS one*. 6:e16038.

Allaman, I., M. Belanger, and P.J. Magistretti. 2015. Methylglyoxal, the dark side of glycolysis. *Front Neurosci*. 9:23.

Almeida, A., S. Moncada, and J.P. Bolanos. 2004. Nitric oxide switches on glycolysis through the AMP protein kinase and 6-phosphofructo-2-kinase pathway. *Nature cell biology*. 6:45-51.

Ambrosi, G., C. Ghezzi, S. Sepe, C. Milanese, C. Payan-Gomez, C.R. Bombardieri, M.T. Armentero, R. Zangaglia, C. Pacchetti, P.G. Mastroberardino, and F. Blandini. 2014. Bioenergetic and proteolytic defects in fibroblasts from patients with sporadic Parkinson's disease. *Biochimica et biophysica acta*. 1842:1385-1394.

Ambroso, M.R., B.G. Hegde, and R. Langen. 2014. Endophilin A1 induces different membrane shapes using a conformational switch that is regulated by phosphorylation. *Proceedings of the National Academy of Sciences of the United States of America*. 111:6982-6987.

Anderson, S., A.T. Bankier, B.G. Barrell, M.H. de Bruijn, A.R. Coulson, J. Drouin, I.C. Eperon, D.P. Nierlich, B.A. Roe, F. Sanger, P.H. Schreier, A.J. Smith, R. Staden, and I.G. Young. 1981. Sequence and organization of the human mitochondrial genome. *Nature*. 290:457-465.

Andres-Mateos, E., C. Perier, L. Zhang, B. Blanchard-Fillion, T.M. Greco, B. Thomas, H.S. Ko, M. Sasaki, H. Ischiropoulos, S. Przedborski, T.M. Dawson, and V.L. Dawson. 2007. DJ-1 gene deletion reveals that DJ-1 is an atypical peroxiredoxin-like peroxidase. *Proceedings of the National Academy of Sciences of the United States of America*. 104:14807-14812.

Anvret, A., M. Westerlund, O. Sydow, T. Willows, C. Lind, D. Galter, and A.C. Belin. 2010. Variations of the CAG trinucleotide repeat in DNA polymerase gamma (POLG1) is associated with Parkinson's disease in Sweden. *Neuroscience letters*. 485:117-120.

Arasaki, K., Y. Mikami, S.R. Shames, H. Inoue, Y. Wakana, and M. Tagaya. 2017. Legionella effector Lpg1137 shuts down ER-mitochondria communication through cleavage of syntaxin 17. *Nature communications*. 8:15406.

Arasaki, K., H. Shimizu, H. Mogari, N. Nishida, N. Hirota, A. Furuno, Y. Kudo, M. Baba, N. Baba, J. Cheng, T. Fujimoto, N. Ishihara, C. Ortiz-Sandoval, L.D. Barlow, A. Raturi, N. Dohmae, Y. Wakana, H. Inoue, K. Tani, J.B. Dacks, T. Simmen, and M. Tagaya. 2015. A role for the ancient SNARE syntaxin 17 in regulating mitochondrial division. *Developmental cell*. 32:304-317.

Area-Gomez, E., A.J. de Groof, I. Boldogh, T.D. Bird, G.E. Gibson, C.M. Koehler, W.H. Yu, K.E. Duff, M.P. Yaffe, L.A. Pon, and E.A. Schon. 2009. Presenilins are enriched in endoplasmic reticulum membranes associated with mitochondria. *The American journal of pathology*. 175:1810-1816.

Area-Gomez, E., M. Del Carmen Lara Castillo, M.D. Tambini, C. Guardia-Laguarta, A.J. de Groof, M. Madra, J. Ikenouchi, M. Umeda, T.D. Bird, S.L. Sturley, and E.A. Schon. 2012. Upregulated function of mitochondria-associated ER membranes in Alzheimer disease. *The EMBO journal*. 31:4106-4123.

Area-Gomez, E., and E.A. Schon. 2017. On the Pathogenesis of Alzheimer's Disease: The MAM Hypothesis. *FASEB J*. 31:864-867.

Arrigo, A.P., K. Tanaka, A.L. Goldberg, and W.J. Welch. 1988. Identity of the 19S 'prosome' particle with the large multifunctional protease complex of mammalian cells (the proteasome). *Nature*. 331:192-194.

Ascherio, A., and M.A. Schwarzschild. 2016. The epidemiology of Parkinson's disease: risk factors and prevention. *Lancet Neurol*. 15:1257-1272.

Ashrafi, G., J.S. Schlehe, M.J. LaVoie, and T.L. Schwarz. 2014. Mitophagy of damaged mitochondria occurs locally in distal neuronal axons and requires PINK1 and Parkin. *The Journal of cell biology*. 206:655-670.

Augustin, S., M. Nolden, S. Muller, O. Hardt, I. Arnold, and T. Langer. 2005. Characterization of peptides released from mitochondria: evidence for constant proteolysis and peptide efflux. *The Journal of biological chemistry*. 280:2691-2699.

Babcock, D.T., W. Shen, and B. Ganetzky. 2015. A neuroprotective function of NSF1 sustains autophagy and lysosomal trafficking in Drosophila. *Genetics*. 199:511-522.

Baker, R.W., P.D. Jeffrey, M. Zick, B.P. Phillips, W.T. Wickner, and F.M. Hughson. 2015. A direct role for the Sec1/Munc18-family protein Vps33 as a template for SNARE assembly. *Science*. 349:1111-1114.

Balderhaar, H.J., and C. Ungermann. 2013. CORVET and HOPS tethering complexes - coordinators of endosome and lysosome fusion. *Journal of cell science*. 126:1307-1316.

Bandyopadhyay, S., and M.R. Cookson. 2004. Evolutionary and functional relationships within the DJ1 superfamily. *BMC evolutionary biology*. 4:6.

Bankapalli, K., S. Saladi, S.S. Awadia, A.V. Goswami, M. Samaddar, and P. D'Silva. 2015. Robust glyoxalase activity of Hsp31, a ThiJ/DJ-1/PfpI family member protein, is critical for oxidative stress resistance in Saccharomyces cerevisiae. *The Journal of biological chemistry*. 290:26491-26507.

Bar-Peled, L., L.D. Schweitzer, R. Zoncu, and D.M. Sabatini. 2012. Ragulator is a GEF for the rag GTPases that signal amino acid levels to mTORC1. *Cell*. 150:1196-1208.

Barnham, K.J., and A.I. Bush. 2008. Metals in Alzheimer's and Parkinson's diseases. *Current opinion in chemical biology*. 12:222-228.

Baskaran, S., L.A. Carlson, G. Stjepanovic, L.N. Young, D.J. Kim, P. Grob, R.E. Stanley, E. Nogales, and J.H. Hurley. 2014. Architecture and dynamics of the autophagic phosphatidylinositol 3-kinase complex. *eLife*. 3.

Baughman, J.M., F. Perocchi, H.S. Girgis, M. Plovanich, C.A. Belcher-Timme, Y. Sancak, X.R. Bao, L. Strittmatter, O. Goldberger, R.L. Bogorad, V. Koteliansky, and V.K. Mootha. 2011. Integrative genomics identifies MCU as an essential component of the mitochondrial calcium uniporter. *Nature*. 476:341-345.

Beal, R., Q. Deveraux, G. Xia, M. Rechsteiner, and C. Pickart. 1996. Surface hydrophobic residues of multiubiquitin chains essential for proteolytic targeting. *Proceedings of the National Academy of Sciences of the United States of America*. 93:861-866.

Beal, R.E., D. Toscano-Cantaffa, P. Young, M. Rechsteiner, and C.M. Pickart. 1998. The hydrophobic effect contributes to polyubiquitin chain recognition. *Biochemistry*. 37:2925-2934.

Beasley, S.A., V.A. Hristova, and G.S. Shaw. 2007. Structure of the Parkin in-between-ring domain provides insights for E3-ligase dysfunction in autosomal recessive Parkinson's disease. *Proceedings of the National Academy of Sciences of the United States of America*. 104:3095-3100.

Beck, S., A. Michalski, O. Raether, M. Lubeck, S. Kaspar, N. Goedecke, C. Baessmann, D. Hornburg, F. Meier, I. Paron, N.A. Kulak, J. Cox, and M. Mann. 2015. The Impact II, a Very High-Resolution Quadrupole Time-of-Flight Instrument (QTOF) for Deep Shotgun Proteomics. *Molecular & cellular proteomics : MCP*. 14:2014-2029.

Becker, D., J. Richter, M.A. Tocilescu, S. Przedborski, and W. Voos. 2012. Pink1 kinase and its membrane potential (Deltapsi)-dependent cleavage product both localize to outer mitochondrial membrane by unique targeting mode. *The Journal of biological chemistry*. 287:22969-22987.

Beilina, A., M. Van Der Brug, R. Ahmad, S. Kesavapany, D.W. Miller, G.A. Petsko, and M.R. Cookson. 2005. Mutations in PTEN-induced putative kinase 1 associated with recessive parkinsonism have differential effects on protein stability. *Proceedings of the National Academy of Sciences of the United States of America*. 102:5703-5708.

Bender, A., K.J. Krishnan, C.M. Morris, G.A. Taylor, A.K. Reeve, R.H. Perry, E. Jaros, J.S. Hersheson, J. Betts, T. Klopstock, R.W. Taylor, and D.M. Turnbull. 2006. High levels of mitochondrial DNA deletions in substantia nigra neurons in aging and Parkinson disease. *Nature genetics*. 38:515-517.

Berg, O.G., and C.G. Kurland. 2000. Why mitochondrial genes are most often found in nuclei. *Molecular biology and evolution*. 17:951-961.

Besche, H.C., A. Peth, and A.L. Goldberg. 2009. Getting to first base in proteasome assembly. *Cell*. 138:25-28.

Betz, C., D. Stracka, C. Prescianotto-Baschong, M. Frieden, N. Demaurex, and M.N. Hall. 2013. Feature Article: mTOR complex 2-Akt signaling at mitochondria-associated endoplasmic reticulum membranes (MAM) regulates mitochondrial physiology. *Proceedings of the National Academy of Sciences of the United States of America*. 110:12526-12534.

Bindoff, L.A., M. Birch-Machin, N.E. Cartlidge, W.D. Parker, Jr., and D.M. Turnbull. 1989. Mitochondrial function in Parkinson's disease. *Lancet*. 2:49.

Bingol, B., J.S. Tea, L. Phu, M. Reichelt, C.E. Bakalarski, Q. Song, O. Foreman, D.S. Kirkpatrick, and M. Sheng. 2014. The mitochondrial deubiquitinase USP30 opposes parkin-mediated mitophagy. *Nature*. 510:370-375.

Bleazard, W., J.M. McCaffery, E.J. King, S. Bale, A. Mozdy, Q. Tieu, J. Nunnari, and J.M. Shaw. 1999. The dynamin-related GTPase Dnm1 regulates mitochondrial fission in yeast. *Nature cell biology*. 1:298-304.

Bockler, S., and B. Westermann. 2014. Mitochondrial ER contacts are crucial for mitophagy in yeast. *Developmental cell*. 28:450-458.

Boland, B., A. Kumar, S. Lee, F.M. Platt, J. Wegiel, W.H. Yu, and R.A. Nixon. 2008. Autophagy induction and autophagosome clearance in neurons: relationship to autophagic pathology

in Alzheimer's disease. *The Journal of neuroscience : the official journal of the Society for Neuroscience*. 28:6926-6937.
Bonifacino, J.S., and J.H. Hurley. 2008. Retromer. *Current opinion in cell biology*. 20:427-436.
Bonifati, V., P. Rizzu, M.J. van Baren, O. Schaap, G.J. Breedveld, E. Krieger, M.C. Dekker, F. Squitieri, P. Ibanez, M. Joosse, J.W. van Dongen, N. Vanacore, J.C. van Swieten, A. Brice, G. Meco, C.M. van Duijn, B.A. Oostra, and P. Heutink. 2003. Mutations in the DJ-1 gene associated with autosomal recessive early-onset parkinsonism. *Science*. 299:256-259.
Brady, N.R., S.P. Elmore, J.J. van Beek, K. Krab, P.J. Courtoy, L. Hue, and H.V. Westerhoff. 2004. Coordinated behavior of mitochondria in both space and time: a reactive oxygen species-activated wave of mitochondrial depolarization. *Biophys J*. 87:2022-2034.
Brandt, T., L. Cavellini, W. Kuhlbrandt, and M.M. Cohen. 2016. A mitofusin-dependent docking ring complex triggers mitochondrial fusion in vitro. *eLife*. 5.
Braschi, E., V. Goyon, R. Zunino, A. Mohanty, L. Xu, and H.M. McBride. 2010. Vps35 mediates vesicle transport between the mitochondria and peroxisomes. *Current biology : CB*. 20:1310-1315.
Braschi, E., R. Zunino, and H.M. McBride. 2009. MAPL is a new mitochondrial SUMO E3 ligase that regulates mitochondrial fission. *EMBO reports*. 10:748-754.
Brice, A. 2005. Genetics of Parkinson's disease: LRRK2 on the rise. *Brain : a journal of neurology*. 128:2760-2762.
Bui, M., S.Y. Gilady, R.E. Fitzsimmons, M.D. Benson, E.M. Lynes, K. Gesson, N.M. Alto, S. Strack, J.D. Scott, and T. Simmen. 2010. Rab32 modulates apoptosis onset and mitochondria-associated membrane (MAM) properties. *The Journal of biological chemistry*. 285:31590-31602.
Burchell, L., V.K. Chaugule, and H. Walden. 2012. Small, N-terminal tags activate Parkin E3 ubiquitin ligase activity by disrupting its autoinhibited conformation. *PloS one*. 7:e34748.
Burchell, V.S., D.E. Nelson, A. Sanchez-Martinez, M. Delgado-Camprubi, R.M. Ivatt, J.H. Pogson, S.J. Randle, S. Wray, P.A. Lewis, H. Houlden, A.Y. Abramov, J. Hardy, N.W. Wood, A.J. Whitworth, H. Laman, and H. Plun-Favreau. 2013. The Parkinson's disease-linked proteins Fbxo7 and Parkin interact to mediate mitophagy. *Nature neuroscience*. 16:1257-1265.
Burre, J., M. Sharma, and T.C. Sudhof. 2014. alpha-Synuclein assembles into higher-order multimers upon membrane binding to promote SNARE complex formation. *Proceedings of the National Academy of Sciences of the United States of America*. 111:E4274-4283.
Burre, J., M. Sharma, T. Tsetsenis, V. Buchman, M.R. Etherton, and T.C. Sudhof. 2010. Alpha-synuclein promotes SNARE-complex assembly in vivo and in vitro. *Science*. 329:1663-1667.
Busch, D.J., J.R. Houser, C.C. Hayden, M.B. Sherman, E.M. Lafer, and J.C. Stachowiak. 2015. Intrinsically disordered proteins drive membrane curvature. *Nature communications*. 6:7875.
Bustamante, E., and P.L. Pedersen. 1977. High aerobic glycolysis of rat hepatoma cells in culture: role of mitochondrial hexokinase. *Proceedings of the National Academy of Sciences of the United States of America*. 74:3735-3739.
Buttner, S., A. Bitto, J. Ring, M. Augsten, P. Zabrocki, T. Eisenberg, H. Jungwirth, S. Hutter, D. Carmona-Gutierrez, G. Kroemer, J. Winderickx, and F. Madeo. 2008. Functional mitochondria are required for alpha-synuclein toxicity in aging yeast. *The Journal of biological chemistry*. 283:7554-7560.

Buttner, S., L. Habernig, F. Broeskamp, D. Ruli, F.N. Vogtle, M. Vlachos, F. Macchi, V. Kuttner, D. Carmona-Gutierrez, T. Eisenberg, J. Ring, M. Markaki, A.A. Taskin, S. Benke, C. Ruckenstuhl, R. Braun, C. Van den Haute, T. Bammens, A. van der Perren, K.U. Frohlich, J. Winderickx, G. Kroemer, V. Baekelandt, N. Tavernarakis, G.G. Kovacs, J. Dengjel, C. Meisinger, S.J. Sigrist, and F. Madeo. 2013. Endonuclease G mediates alpha-synuclein cytotoxicity during Parkinson's disease. *The EMBO journal*. 32:3041-3054.

Byrnes, L.J., A. Singh, K. Szeto, N.M. Benvin, J.P. O'Donnell, W.R. Zipfel, and H. Sondermann. 2013. Structural basis for conformational switching and GTP loading of the large G protein atlastin. *The EMBO journal*. 32:369-384.

Cai, Q., L. Lu, J.H. Tian, Y.B. Zhu, H. Qiao, and Z.H. Sheng. 2010. Snapin-regulated late endosomal transport is critical for efficient autophagy-lysosomal function in neurons. *Neuron*. 68:73-86.

Caielli, S., S. Athale, B. Domic, E. Murat, M. Chandra, R. Banchereau, J. Baisch, K. Phelps, S. Clayton, M. Gong, T. Wright, M. Punaro, K. Palucka, C. Guiducci, J. Banchereau, and V. Pascual. 2016. Oxidized mitochondrial nucleoids released by neutrophils drive type I interferon production in human lupus. *The Journal of experimental medicine*. 213:697-713.

Cali, T., D. Ottolini, A. Negro, and M. Brini. 2012. alpha-Synuclein controls mitochondrial calcium homeostasis by enhancing endoplasmic reticulum-mitochondria interactions. *The Journal of biological chemistry*. 287:17914-17929.

Callegari, S., S. Oeljeklaus, B. Warscheid, S. Dennerlein, M. Thumm, P. Rehling, and J. Dudek. 2016. Phospho-ubiquitin-PARK2 complex as a marker for mitophagy defects. *Autophagy*:1-11.

Campanella, M., E. Casswell, S. Chong, Z. Farah, M.R. Wieckowski, A.Y. Abramov, A. Tinker, and M.R. Duchen. 2008. Regulation of mitochondrial structure and function by the F1Fo-ATPase inhibitor protein, IF1. *Cell metabolism*. 8:13-25.

Canet-Aviles, R.M., M.A. Wilson, D.W. Miller, R. Ahmad, C. McLendon, S. Bandyopadhyay, M.J. Baptista, D. Ringe, G.A. Petsko, and M.R. Cookson. 2004. The Parkinson's disease protein DJ-1 is neuroprotective due to cysteine-sulfinic acid-driven mitochondrial localization. *Proceedings of the National Academy of Sciences of the United States of America*. 101:9103-9108.

Cao, M., I. Milosevic, S. Giovedi, and P. De Camilli. 2014. Upregulation of Parkin in endophilin mutant mice. *The Journal of neuroscience : the official journal of the Society for Neuroscience*. 34:16544-16549.

Cao, M., Y. Wu, G. Ashrafi, A.J. McCartney, H. Wheeler, E.A. Bushong, D. Boassa, M.H. Ellisman, T.A. Ryan, and P. De Camilli. 2017a. Parkinson Sac Domain Mutation in Synaptojanin 1 Impairs Clathrin Uncoating at Synapses and Triggers Dystrophic Changes in Dopaminergic Axons. *Neuron*. 93:882-896 e885.

Cao, Y.L., S. Meng, Y. Chen, J.X. Feng, D.D. Gu, B. Yu, Y.J. Li, J.Y. Yang, S. Liao, D.C. Chan, and S. Gao. 2017b. MFN1 structures reveal nucleotide-triggered dimerization critical for mitochondrial fusion. *Nature*.

Cardona, F., J.V. Sanchez-Mut, H. Dopazo, and J. Perez-Tur. 2011. Phylogenetic and in silico structural analysis of the Parkinson disease-related kinase PINK1. *Hum Mutat*. 32:369-378.

Carlsson, A., M. Lindqvist, and T. Magnusson. 1957. 3,4-Dihydroxyphenylalanine and 5-hydroxytryptophan as reserpine antagonists. *Nature*. 180:1200.

Carlsson, A., M. Lindqvist, T. Magnusson, and B. Waldeck. 1958. On the presence of 3-hydroxytyramine in brain. *Science*. 127:471.

Cebrian, C., F.A. Zucca, P. Mauri, J.A. Steinbeck, L. Studer, C.R. Scherzer, E. Kanter, S. Budhu, J. Mandelbaum, J.P. Vonsattel, L. Zecca, J.D. Loike, and D. Sulzer. 2014. MHC-I expression renders catecholaminergic neurons susceptible to T-cell-mediated degeneration. *Nature communications*. 5:3633.

Celardo, I., A.C. Costa, S. Lehmann, C. Jones, N. Wood, N.E. Mencacci, G.R. Mallucci, S.H. Loh, and L.M. Martins. 2016. Mitofusin-mediated ER stress triggers neurodegeneration in pink1/parkin models of Parkinson's disease. *Cell Death Dis*. 7:e2271.

Cha, S.H., Y.R. Choi, C.H. Heo, S.J. Kang, E.H. Joe, I. Jou, H.M. Kim, and S.M. Park. 2015. Loss of parkin promotes lipid rafts-dependent endocytosis through accumulating caveolin-1: implications for Parkinson's disease. *Mol Neurodegener*. 10:63.

Chan, C.S., J.N. Guzman, E. Ilijic, J.N. Mercer, C. Rick, T. Tkatch, G.E. Meredith, and D.J. Surmeier. 2007. 'Rejuvenation' protects neurons in mouse models of Parkinson's disease. *Nature*. 447:1081-1086.

Chan, N.C., A.M. Salazar, A.H. Pham, M.J. Sweredoski, N.J. Kolawa, R.L. Graham, S. Hess, and D.C. Chan. 2011. Broad activation of the ubiquitin-proteasome system by Parkin is critical for mitophagy. *Human molecular genetics*. 20:1726-1737.

Chandra, S., G. Gallardo, R. Fernandez-Chacon, O.M. Schluter, and T.C. Sudhof. 2005. Alpha-synuclein cooperates with CSPalpha in preventing neurodegeneration. *Cell*. 123:383-396.

Chantranupong, L., S.M. Scaria, R.A. Saxton, M.P. Gygi, K. Shen, G.A. Wyant, T. Wang, J.W. Harper, S.P. Gygi, and D.M. Sabatini. 2016. The CASTOR Proteins Are Arginine Sensors for the mTORC1 Pathway. *Cell*. 165:153-164.

Chartier-Harlin, M.C., J. Kachergus, C. Roumier, V. Mouroux, X. Douay, S. Lincoln, C. Levecque, L. Larvor, J. Andrieux, M. Hulihan, N. Waucquier, L. Defebvre, P. Amouyel, M. Farrer, and A. Destee. 2004. Alpha-synuclein locus duplication as a cause of familial Parkinson's disease. *Lancet*. 364:1167-1169.

Chaudhuri, D., D.J. Artiga, S.A. Abiria, and D.E. Clapham. 2016. Mitochondrial calcium uniporter regulator 1 (MCUR1) regulates the calcium threshold for the mitochondrial permeability transition. *Proceedings of the National Academy of Sciences of the United States of America*. 113:E1872-1880.

Chaudhuri, D., Y. Sancak, V.K. Mootha, and D.E. Clapham. 2013. MCU encodes the pore conducting mitochondrial calcium currents. *eLife*. 2:e00704.

Chaugule, V.K., L. Burchell, K.R. Barber, A. Sidhu, S.J. Leslie, G.S. Shaw, and H. Walden. 2011. Autoregulation of Parkin activity through its ubiquitin-like domain. *The EMBO journal*. 30:2853-2867.

Chazotte, B. 2011. Labeling mitochondria with TMRM or TMRE. *Cold Spring Harb Protoc*. 2011:895-897.

Chen, H., S.A. Detmer, A.J. Ewald, E.E. Griffin, S.E. Fraser, and D.C. Chan. 2003. Mitofusins Mfn1 and Mfn2 coordinately regulate mitochondrial fusion and are essential for embryonic development. *The Journal of cell biology*. 160:189-200.

Chen, H., S.M. Zhang, M.A. Schwarzschild, M.A. Hernan, W.C. Willett, and A. Ascherio. 2004. Obesity and the risk of Parkinson's disease. *Am J Epidemiol*. 159:547-555.

Chen, Y., and G.W. Dorn, 2nd. 2013. PINK1-phosphorylated mitofusin 2 is a Parkin receptor for culling damaged mitochondria. *Science*. 340:471-475.

Chen, Y., E. McMillan-Ward, J. Kong, S.J. Israels, and S.B. Gibson. 2007. Mitochondrial electron-transport-chain inhibitors of complexes I and II induce autophagic cell death mediated by reactive oxygen species. *Journal of cell science*. 120:4155-4166.

Cheng, X.T., B. Zhou, M.Y. Lin, Q. Cai, and Z.H. Sheng. 2015. Axonal autophagosomes recruit dynein for retrograde transport through fusion with late endosomes. *The Journal of cell biology*. 209:377-386.

Choi, B.K., M.G. Choi, J.Y. Kim, Y. Yang, Y. Lai, D.H. Kweon, N.K. Lee, and Y.K. Shin. 2013. Large alpha-synuclein oligomers inhibit neuronal SNARE-mediated vesicle docking. *Proceedings of the National Academy of Sciences of the United States of America*. 110:4087-4092.

Chung, K.K., B. Thomas, X. Li, O. Pletnikova, J.C. Troncoso, L. Marsh, V.L. Dawson, and T.M. Dawson. 2004. S-nitrosylation of parkin regulates ubiquitination and compromises parkin's protective function. *Science*. 304:1328-1331.

Chung, S.Y., S. Kishinevsky, J.R. Mazzulli, J. Graziotto, A. Mrejeru, E.V. Mosharov, L. Puspita, P. Valiulahi, D. Sulzer, T.A. Milner, T. Taldone, D. Krainc, L. Studer, and J.W. Shim. 2016. Parkin and PINK1 Patient iPSC-Derived Midbrain Dopamine Neurons Exhibit Mitochondrial Dysfunction and alpha-Synuclein Accumulation. *Stem Cell Reports*. 7:664-677.

Cipolat, S., O. Martins de Brito, B. Dal Zilio, and L. Scorrano. 2004. OPA1 requires mitofusin 1 to promote mitochondrial fusion. *Proceedings of the National Academy of Sciences of the United States of America*. 101:15927-15932.

Clark, I.E., M.W. Dodson, C. Jiang, J.H. Cao, J.R. Huh, J.H. Seol, S.J. Yoo, B.A. Hay, and M. Guo. 2006. Drosophila pink1 is required for mitochondrial function and interacts genetically with parkin. *Nature*. 441:1162-1166.

Cole, N.B., D. Dieuliis, P. Leo, D.C. Mitchell, and R.L. Nussbaum. 2008. Mitochondrial translocation of alpha-synuclein is promoted by intracellular acidification. *Experimental cell research*. 314:2076-2089.

Constantinescu, R., J. Elm, P. Auinger, S. Sharma, E.F. Augustine, L. Khadim, K. Kieburtz, and N.-P. Investigators. 2014. Malignant melanoma in early-treated Parkinson's disease: the NET-PD trial. *Movement disorders : official journal of the Movement Disorder Society*. 29:263-265.

Constantinescu, R., M. Romer, K. Kieburtz, and D.I.o.t.P.S. Group. 2007. Malignant melanoma in early Parkinson's disease: the DATATOP trial. *Movement disorders : official journal of the Movement Disorder Society*. 22:720-722.

Cooper, A.A., A.D. Gitler, A. Cashikar, C.M. Haynes, K.J. Hill, B. Bhullar, K. Liu, K. Xu, K.E. Strathearn, F. Liu, S. Cao, K.A. Caldwell, G.A. Caldwell, G. Marsischky, R.D. Kolodner, J. Labaer, J.C. Rochet, N.M. Bonini, and S. Lindquist. 2006. Alpha-synuclein blocks ER-Golgi traffic and Rab1 rescues neuron loss in Parkinson's models. *Science*. 313:324-328.

Cornelissen, T., D. Haddad, F. Wauters, C. Van Humbeeck, W. Mandemakers, B. Koentjoro, C. Sue, K. Gevaert, B. De Strooper, P. Verstreken, and W. Vandenberghe. 2014. The deubiquitinase USP15 antagonizes Parkin-mediated mitochondrial ubiquitination and mitophagy. *Human molecular genetics*. 23:5227-5242.

Cortese, G.P., M. Zhu, D. Williams, S. Heath, and C.L. Waites. 2016. Parkin Deficiency Reduces Hippocampal Glutamatergic Neurotransmission by Impairing AMPA Receptor Endocytosis. *The Journal of neuroscience : the official journal of the Society for Neuroscience*. 36:12243-12258.

Cox, R.T., and A.C. Spradling. 2009. Clueless, a conserved Drosophila gene required for mitochondrial subcellular localization, interacts genetically with parkin. *Dis Model Mech*. 2:490-499.

Csordas, G., C. Renken, P. Varnai, L. Walter, D. Weaver, K.F. Buttle, T. Balla, C.A. Mannella, and G. Hajnoczky. 2006. Structural and functional features and significance of the physical linkage between ER and mitochondria. *The Journal of cell biology*. 174:915-921.

Cui, H., G.S. Ayton, and G.A. Voth. 2009. Membrane binding by the endophilin N-BAR domain. *Biophys J*. 97:2746-2753.

Cui-Wang, T., C. Hanus, T. Cui, T. Helton, J. Bourne, D. Watson, K.M. Harris, and M.D. Ehlers. 2012. Local zones of endoplasmic reticulum complexity confine cargo in neuronal dendrites. *Cell*. 148:309-321.

Cullen, P.J., and H.C. Korswagen. 2012. Sorting nexins provide diversity for retromer-dependent trafficking events. *Nature cell biology*. 14:29-37.

Cunningham, C.N., J.M. Baughman, L. Phu, J.S. Tea, C. Yu, M. Coons, D.S. Kirkpatrick, B. Bingol, and J.E. Corn. 2015. USP30 and parkin homeostatically regulate atypical ubiquitin chains on mitochondria. *Nature cell biology*. 17:160-169.

d'Azzo, A., A. Bongiovanni, and T. Nastasi. 2005. E3 ubiquitin ligases as regulators of membrane protein trafficking and degradation. *Traffic*. 6:429-441.

Dahlstrom, A., A. Wigander, K. Lundmark, C.G. Gottfries, P.M. Carvey, and A. McRae. 1990. Investigations on auto-antibodies in Alzheimer's and Parkinson's diseases, using defined neuronal cultures. *Journal of neural transmission. Supplementum*. 29:195-206.

Dale, R.C., A.J. Church, R.A. Surtees, A.J. Lees, J.E. Adcock, B. Harding, B.G. Neville, and G. Giovannoni. 2004. Encephalitis lethargica syndrome: 20 new cases and evidence of basal ganglia autoimmunity. *Brain : a journal of neurology*. 127:21-33.

Dall'Armi, C., K.A. Devereaux, and G. Di Paolo. 2013. The role of lipids in the control of autophagy. *Current biology : CB*. 23:R33-45.

Darios, F., O. Corti, C.B. Lucking, C. Hampe, M.P. Muriel, N. Abbas, W.J. Gu, E.C. Hirsch, T. Rooney, M. Ruberg, and A. Brice. 2003. Parkin prevents mitochondrial swelling and cytochrome c release in mitochondria-dependent cell death. *Human molecular genetics*. 12:517-526.

Daumke, O., and G.J. Praefcke. 2011. Structural insights into membrane fusion at the endoplasmic reticulum. *Proceedings of the National Academy of Sciences of the United States of America*. 108:2175-2176.

Davidzon, G., P. Greene, M. Mancuso, K.J. Klos, J.E. Ahlskog, M. Hirano, and S. DiMauro. 2006. Early-onset familial parkinsonism due to POLG mutations. *Annals of neurology*. 59:859-862.

Davison, E.J., K. Pennington, C.C. Hung, J. Peng, R. Rafiq, A. Ostareck-Lederer, D.H. Ostareck, H.C. Ardley, R.E. Banks, and P.A. Robinson. 2009. Proteomic analysis of increased Parkin expression and its interactants provides evidence for a role in modulation of mitochondrial function. *Proteomics*. 9:4284-4297.

Dawson, T.M., H.S. Ko, and V.L. Dawson. 2010. Genetic animal models of Parkinson's disease. *Neuron*. 66:646-661.

de Brito, O.M., and L. Scorrano. 2008. Mitofusin 2 tethers endoplasmic reticulum to mitochondria. *Nature*. 456:605-610.

De Stefani, D., A. Raffaello, E. Teardo, I. Szabo, and R. Rizzuto. 2011. A forty-kilodalton protein of the inner membrane is the mitochondrial calcium uniporter. *Nature*. 476:336-340.

Deas, E., H. Plun-Favreau, S. Gandhi, H. Desmond, S. Kjaer, S.H. Loh, A.E. Renton, R.J. Harvey, A.J. Whitworth, L.M. Martins, A.Y. Abramov, and N.W. Wood. 2011. PINK1 cleavage at

position A103 by the mitochondrial protease PARL. *Human molecular genetics*. 20:867-879.

Deatherage, B.L., and B.T. Cookson. 2012. Membrane vesicle release in bacteria, eukaryotes, and archaea: a conserved yet underappreciated aspect of microbial life. *Infection and immunity*. 80:1948-1957.

Dehay, B., A. Ramirez, M. Martinez-Vicente, C. Perier, M.H. Canron, E. Doudnikoff, A. Vital, M. Vila, C. Klein, and E. Bezard. 2012. Loss of P-type ATPase ATP13A2/PARK9 function induces general lysosomal deficiency and leads to Parkinson disease neurodegeneration. *Proceedings of the National Academy of Sciences of the United States of America*. 109:9611-9616.

Del Prete, D., J.M. Suski, B. Oules, D. Debayle, A.S. Gay, S. Lacas-Gervais, R. Bussiere, C. Bauer, P. Pinton, P. Paterlini-Brechot, M.R. Wieckowski, F. Checler, and M. Chami. 2017. Localization and Processing of the Amyloid-beta Protein Precursor in Mitochondria-Associated Membranes. *Journal of Alzheimer's disease : JAD*. 55:1549-1570.

Deng, H., M.W. Dodson, H. Huang, and M. Guo. 2008. The Parkinson's disease genes pink1 and parkin promote mitochondrial fission and/or inhibit fusion in Drosophila. *Proceedings of the National Academy of Sciences of the United States of America*. 105:14503-14508.

Denison, S.R., F. Wang, N.A. Becker, B. Schule, N. Kock, L.A. Phillips, C. Klein, and D.I. Smith. 2003. Alterations in the common fragile site gene Parkin in ovarian and other cancers. *Oncogene*. 22:8370-8378.

Deter, R.L., P. Baudhuin, and C. De Duve. 1967. Participation of lysosomes in cellular autophagy induced in rat liver by glucagon. *The Journal of cell biology*. 35:C11-16.

Dexter, D.T., P. Jenner, A.H. Schapira, and C.D. Marsden. 1992. Alterations in levels of iron, ferritin, and other trace metals in neurodegenerative diseases affecting the basal ganglia. The Royal Kings and Queens Parkinson's Disease Research Group. *Annals of neurology*. 32 Suppl:S94-100.

Di Fonzo, A., M.C. Dekker, P. Montagna, A. Baruzzi, E.H. Yonova, L. Correia Guedes, A. Szczerbinska, T. Zhao, L.O. Dubbel-Hulsman, C.H. Wouters, E. de Graaff, W.J. Oyen, E.J. Simons, G.J. Breedveld, B.A. Oostra, M.W. Horstink, and V. Bonifati. 2009. FBXO7 mutations cause autosomal recessive, early-onset parkinsonian-pyramidal syndrome. *Neurology*. 72:240-245.

Diao, J., J. Burre, S. Vivona, D.J. Cipriano, M. Sharma, M. Kyoung, T.C. Sudhof, and A.T. Brunger. 2013. Native alpha-synuclein induces clustering of synaptic-vesicle mimics via binding to phospholipids and synaptobrevin-2/VAMP2. *eLife*. 2:e00592.

Diao, J., R. Liu, Y. Rong, M. Zhao, J. Zhang, Y. Lai, Q. Zhou, L.M. Wilz, J. Li, S. Vivona, R.A. Pfuetzner, A.T. Brunger, and Q. Zhong. 2015. ATG14 promotes membrane tethering and fusion of autophagosomes to endolysosomes. *Nature*. 520:563-566.

Duarte, A., C. Poderoso, M. Cooke, G. Soria, F. Cornejo Maciel, V. Gottifredi, and E.J. Podesta. 2012. Mitochondrial fusion is essential for steroid biosynthesis. *PloS one*. 7:e45829.

Duchen, M.R., A. Leyssens, and M. Crompton. 1998. Transient mitochondrial depolarizations reflect focal sarcoplasmic reticular calcium release in single rat cardiomyocytes. *The Journal of cell biology*. 142:975-988.

Durcan, T.M., M. Kontogiannea, T. Thorarinsdottir, L. Fallon, A.J. Williams, A. Djarmati, T. Fantaneanu, H.L. Paulson, and E.A. Fon. 2011. The Machado-Joseph disease-associated mutant form of ataxin-3 regulates parkin ubiquitination and stability. *Human molecular genetics*. 20:141-154.

Durcan, T.M., M.Y. Tang, J.R. Perusse, E.A. Dashti, M.A. Aguileta, G.L. McLelland, P. Gros, T.A. Shaler, D. Faubert, B. Coulombe, and E.A. Fon. 2014. USP8 regulates mitophagy by removing K6-linked ubiquitin conjugates from parkin. *The EMBO journal*. 33:2473-2491.

Eerola, J., P.T. Luoma, T. Peuralinna, S. Scholz, C. Paisan-Ruiz, A. Suomalainen, A.B. Singleton, and P.J. Tienari. 2010. POLG1 polyglutamine tract variants associated with Parkinson's disease. *Neuroscience letters*. 477:1-5.

Eid, S., S. Turk, A. Volkamer, F. Rippmann, and S. Fulle. 2017. KinMap: a web-based tool for interactive navigation through human kinome data. *BMC Bioinformatics*. 18:16.

Ellena, J.F., B. Liang, M. Wiktor, A. Stein, D.S. Cafiso, R. Jahn, and L.K. Tamm. 2009. Dynamic structure of lipid-bound synaptobrevin suggests a nucleation-propagation mechanism for trans-SNARE complex formation. *Proceedings of the National Academy of Sciences of the United States of America*. 106:20306-20311.

Espay, A.J., P.A. LeWitt, and H. Kaufmann. 2014. Norepinephrine deficiency in Parkinson's disease: the case for noradrenergic enhancement. *Movement disorders : official journal of the Movement Disorder Society*. 29:1710-1719.

Exner, N., B. Treske, D. Paquet, K. Holmstrom, C. Schiesling, S. Gispert, I. Carballo-Carbajal, D. Berg, H.H. Hoepken, T. Gasser, R. Kruger, K.F. Winklhofer, F. Vogel, A.S. Reichert, G. Auburger, P.J. Kahle, B. Schmid, and C. Haass. 2007. Loss-of-function of human PINK1 results in mitochondrial pathology and can be rescued by parkin. *The Journal of neuroscience : the official journal of the Society for Neuroscience*. 27:12413-12418.

Fallon, L., C.M. Belanger, A.T. Corera, M. Kontogiannea, E. Regan-Klapisz, F. Moreau, J. Voortman, M. Haber, G. Rouleau, T. Thorarinsdottir, A. Brice, P.M. van Bergen En Henegouwen, and E.A. Fon. 2006. A regulated interaction with the UIM protein Eps15 implicates parkin in EGF receptor trafficking and PI(3)K-Akt signalling. *Nature cell biology*. 8:834-842.

Fallon, L., F. Moreau, B.G. Croft, N. Labib, W.J. Gu, and E.A. Fon. 2002. Parkin and CASK/LIN-2 associate via a PDZ-mediated interaction and are co-localized in lipid rafts and postsynaptic densities in brain. *The Journal of biological chemistry*. 277:486-491.

Fan, W., A. Nassiri, and Q. Zhong. 2011. Autophagosome targeting and membrane curvature sensing by Barkor/Atg14(L). *Proceedings of the National Academy of Sciences of the United States of America*. 108:7769-7774.

Fasshauer, D., W. Antonin, V. Subramaniam, and R. Jahn. 2002. SNARE assembly and disassembly exhibit a pronounced hysteresis. *Nat Struct Biol*. 9:144-151.

Fasshauer, D., R.B. Sutton, A.T. Brunger, and R. Jahn. 1998. Conserved structural features of the synaptic fusion complex: SNARE proteins reclassified as Q- and R-SNAREs. *Proceedings of the National Academy of Sciences of the United States of America*. 95:15781-15786.

Felsenstein, J. 1974. The evolutionary advantage of recombination. *Genetics*. 78:737-756.

Fiebig, K.M., L.M. Rice, E. Pollock, and A.T. Brunger. 1999. Folding intermediates of SNARE complex assembly. *Nat Struct Biol*. 6:117-123.

Filadi, R., E. Greotti, G. Turacchio, A. Luini, T. Pozzan, and P. Pizzo. 2015. Mitofusin 2 ablation increases endoplasmic reticulum-mitochondria coupling. *Proceedings of the National Academy of Sciences of the United States of America*. 112:E2174-2181.

Finck, B.N., and D.P. Kelly. 2006. PGC-1 coactivators: inducible regulators of energy metabolism in health and disease. *The Journal of clinical investigation*. 116:615-622.

Finney, N., F. Walther, P.Y. Mantel, D. Stauffer, G. Rovelli, and K.K. Dev. 2003. The cellular protein level of parkin is regulated by its ubiquitin-like domain. *The Journal of biological chemistry*. 278:16054-16058.

Fiorese, C.J., A.M. Schulz, Y.F. Lin, N. Rosin, M.W. Pellegrino, and C.M. Haynes. 2016. The Transcription Factor ATF5 Mediates a Mammalian Mitochondrial UPR. *Current biology : CB*. 26:2037-2043.

Franks, P.W., C. Scheele, R.J. Loos, A.R. Nielsen, F.M. Finucane, C. Wahlestedt, B.K. Pedersen, N.J. Wareham, and J.A. Timmons. 2008. Genomic variants at the PINK1 locus are associated with transcript abundance and plasma nonesterified fatty acid concentrations in European whites. *FASEB J*. 22:3135-3145.

Fratti, R.A., K.M. Collins, C.M. Hickey, and W. Wickner. 2007. Stringent 3Q.1R composition of the SNARE 0-layer can be bypassed for fusion by compensatory SNARE mutation or by lipid bilayer modification. *The Journal of biological chemistry*. 282:14861-14867.

Frezza, C., S. Cipolat, O. Martins de Brito, M. Micaroni, G.V. Beznoussenko, T. Rudka, D. Bartoli, R.S. Polishuck, N.N. Danial, B. De Strooper, and L. Scorrano. 2006. OPA1 controls apoptotic cristae remodeling independently from mitochondrial fusion. *Cell*. 126:177-189.

Frezza, C., S. Cipolat, and L. Scorrano. 2007. Organelle isolation: functional mitochondria from mouse liver, muscle and cultured fibroblasts. *Nature protocols*. 2:287-295.

Friedman, J.R., L.L. Lackner, M. West, J.R. DiBenedetto, J. Nunnari, and G.K. Voeltz. 2011. ER tubules mark sites of mitochondrial division. *Science*. 334:358-362.

Friedman, J.R., and J. Nunnari. 2014. Mitochondrial form and function. *Nature*. 505:335-343.

Fu, M., P. St-Pierre, J. Shankar, P.T. Wang, B. Joshi, and I.R. Nabi. 2013. Regulation of mitophagy by the Gp78 E3 ubiquitin ligase. *Molecular biology of the cell*. 24:1153-1162.

Furuno, K., T. Ishikawa, K. Akasaki, S. Lee, Y. Nishimura, H. Tsuji, M. Himeno, and K. Kato. 1990. Immunocytochemical study of the surrounding envelope of autophagic vacuoles in cultured rat hepatocytes. *Experimental cell research*. 189:261-268.

Gandhi, S., A. Wood-Kaczmar, Z. Yao, H. Plun-Favreau, E. Deas, K. Klupsch, J. Downward, D.S. Latchman, S.J. Tabrizi, N.W. Wood, M.R. Duchen, and A.Y. Abramov. 2009. PINK1-associated Parkinson's disease is caused by neuronal vulnerability to calcium-induced cell death. *Molecular cell*. 33:627-638.

Ganley, I.G., K. Carroll, L. Bittova, and S. Pfeffer. 2004. Rab9 GTPase regulates late endosome size and requires effector interaction for its stability. *Molecular biology of the cell*. 15:5420-5430.

Ganley, I.G., P.M. Wong, N. Gammoh, and X. Jiang. 2011. Distinct autophagosomal-lysosomal fusion mechanism revealed by thapsigargin-induced autophagy arrest. *Molecular cell*. 42:731-743.

Gao, J., D. Schatton, P. Martinelli, H. Hansen, D. Pla-Martin, E. Barth, C. Becker, J. Altmueller, P. Frommolt, M. Sardiello, and E.I. Rugarli. 2014. CLUH regulates mitochondrial biogenesis by binding mRNAs of nuclear-encoded mitochondrial proteins. *The Journal of cell biology*. 207:213-223.

Gao, Y., S. Zorman, G. Gundersen, Z. Xi, L. Ma, G. Sirinakis, J.E. Rothman, and Y. Zhang. 2012. Single reconstituted neuronal SNARE complexes zipper in three distinct stages. *Science*. 337:1340-1343.

Gautier, C.A., Z. Erpapazoglou, F. Mouton-Liger, M.P. Muriel, F. Cormier, S. Bigou, S. Duffaure, M. Girard, B. Foret, A. Iannielli, V. Broccoli, C. Dalle, D. Bohl, P.P. Michel, J.C. Corvol, A. Brice, and O. Corti. 2016. The endoplasmic reticulum-mitochondria interface is

perturbed in PARK2 knockout mice and patients with PARK2 mutations. *Human molecular genetics*.

Gautier, C.A., T. Kitada, and J. Shen. 2008. Loss of PINK1 causes mitochondrial functional defects and increased sensitivity to oxidative stress. *Proceedings of the National Academy of Sciences of the United States of America*. 105:11364-11369.

Ge, L., D. Melville, M. Zhang, and R. Schekman. 2013. The ER-Golgi intermediate compartment is a key membrane source for the LC3 lipidation step of autophagosome biogenesis. *eLife*. 2:e00947.

Gehrke, S., Z. Wu, M. Klinkenberg, Y. Sun, G. Auburger, S. Guo, and B. Lu. 2015. PINK1 and Parkin control localized translation of respiratory chain component mRNAs on mitochondria outer membrane. *Cell metabolism*. 21:95-108.

Geisler, S., K.M. Holmstrom, D. Skujat, F.C. Fiesel, O.C. Rothfuss, P.J. Kahle, and W. Springer. 2010. PINK1/Parkin-mediated mitophagy is dependent on VDAC1 and p62/SQSTM1. *Nature cell biology*. 12:119-131.

Gelmetti, V., P. De Rosa, L. Torosantucci, E.S. Marini, A. Romagnoli, M. Di Rienzo, G. Arena, D. Vignone, G.M. Fimia, and E.M. Valente. 2017. PINK1 and BECN1 relocalize at mitochondria-associated membranes during mitophagy and promote ER-mitochondria tethering and autophagosome formation. *Autophagy*. 13:654-669.

Gil, A., L.M. Gutierrez, C. Carrasco-Serrano, M.T. Alonso, S. Viniegra, and M. Criado. 2002. Modifications in the C terminus of the synaptosome-associated protein of 25 kDa (SNAP-25) and in the complementary region of synaptobrevin affect the final steps of exocytosis. *The Journal of biological chemistry*. 277:9904-9910.

Giraudo, C.G., W.S. Eng, T.J. Melia, and J.E. Rothman. 2006. A clamping mechanism involved in SNARE-dependent exocytosis. *Science*. 313:676-680.

Gispert, S., F. Ricciardi, A. Kurz, M. Azizov, H.H. Hoepken, D. Becker, W. Voos, K. Leuner, W.E. Muller, A.P. Kudin, W.S. Kunz, A. Zimmermann, J. Roeper, D. Wenzel, M. Jendrach, M. Garcia-Arencibia, J. Fernandez-Ruiz, L. Huber, H. Rohrer, M. Barrera, A.S. Reichert, U. Rub, A. Chen, R.L. Nussbaum, and G. Auburger. 2009. Parkinson phenotype in aged PINK1-deficient mice is accompanied by progressive mitochondrial dysfunction in absence of neurodegeneration. *PloS one*. 4:e5777.

Gitler, A.D., B.J. Bevis, J. Shorter, K.E. Strathearn, S. Hamamichi, L.J. Su, K.A. Caldwell, G.A. Caldwell, J.C. Rochet, J.M. McCaffery, C. Barlowe, and S. Lindquist. 2008. The Parkinson's disease protein alpha-synuclein disrupts cellular Rab homeostasis. *Proceedings of the National Academy of Sciences of the United States of America*. 105:145-150.

Gold, V.A., P. Chroscicki, P. Bragoszewski, and A. Chacinska. 2017. Visualization of cytosolic ribosomes on the surface of mitochondria by electron cryo-tomography. *EMBO reports*. 18:1786-1800.

Goldberg, A.L. 2007. Functions of the proteasome: from protein degradation and immune surveillance to cancer therapy. *Biochemical Society transactions*. 35:12-17.

Gomes, L.C., G. Di Benedetto, and L. Scorrano. 2011. During autophagy mitochondria elongate, are spared from degradation and sustain cell viability. *Nature cell biology*. 13:589-598.

Gomez-Suaga, P., S. Paillusson, R. Stoica, W. Noble, D.P. Hanger, and C.C. Miller. 2017. The ER-Mitochondria Tethering Complex VAPB-PTPIP51 Regulates Autophagy. *Current biology : CB*. 27:371-385.

Gong, G., M. Song, G. Csordas, D.P. Kelly, S.J. Matkovich, and G.W. Dorn, 2nd. 2015. Parkin-mediated mitophagy directs perinatal cardiac metabolic maturation in mice. *Science*. 350:aad2459.

Gosavi, N., H.J. Lee, J.S. Lee, S. Patel, and S.J. Lee. 2002. Golgi fragmentation occurs in the cells with prefibrillar alpha-synuclein aggregates and precedes the formation of fibrillar inclusion. *The Journal of biological chemistry*. 277:48984-48992.

Gould, S.B., S.G. Garg, and W.F. Martin. 2016. Bacterial Vesicle Secretion and the Evolutionary Origin of the Eukaryotic Endomembrane System. *Trends Microbiol*. 24:525-534.

Graham, M.E., P. Washbourne, M.C. Wilson, and R.D. Burgoyne. 2001. SNAP-25 with mutations in the zero layer supports normal membrane fusion kinetics. *Journal of cell science*. 114:4397-4405.

Greene, A.W., K. Grenier, M.A. Aguileta, S. Muise, R. Farazifard, M.E. Haque, H.M. McBride, D.S. Park, and E.A. Fon. 2012. Mitochondrial processing peptidase regulates PINK1 processing, import and Parkin recruitment. *EMBO reports*. 13:378-385.

Greene, J.C., A.J. Whitworth, L.A. Andrews, T.J. Parker, and L.J. Pallanck. 2005. Genetic and genomic studies of Drosophila parkin mutants implicate oxidative stress and innate immune responses in pathogenesis. *Human molecular genetics*. 14:799-811.

Greene, J.C., A.J. Whitworth, I. Kuo, L.A. Andrews, M.B. Feany, and L.J. Pallanck. 2003. Mitochondrial pathology and apoptotic muscle degeneration in Drosophila parkin mutants. *Proceedings of the National Academy of Sciences of the United States of America*. 100:4078-4083.

Grimsley, G.R., J.M. Scholtz, and C.N. Pace. 2009. A summary of the measured pK values of the ionizable groups in folded proteins. *Protein Sci*. 18:247-251.

Grunewald, A., M.E. Gegg, J.W. Taanman, R.H. King, N. Kock, C. Klein, and A.H. Schapira. 2009. Differential effects of PINK1 nonsense and missense mutations on mitochondrial function and morphology. *Exp Neurol*. 219:266-273.

Grunewald, A., K.A. Rygiel, P.D. Hepplewhite, C.M. Morris, M. Picard, and D.M. Turnbull. 2016. Mitochondrial DNA Depletion in Respiratory Chain-Deficient Parkinson Disease Neurons. *Annals of neurology*. 79:366-378.

Grunewald, A., L. Voges, A. Rakovic, M. Kasten, H. Vandebona, C. Hemmelmann, K. Lohmann, S. Orolicki, A. Ramirez, A.H. Schapira, P.P. Pramstaller, C.M. Sue, and C. Klein. 2010. Mutant Parkin impairs mitochondrial function and morphology in human fibroblasts. *PloS one*. 5:e12962.

Gu, J., M. Wu, R. Guo, K. Yan, J. Lei, N. Gao, and M. Yang. 2016. The architecture of the mammalian respirasome. *Nature*. 537:639-643.

Gu, W.J., O. Corti, F. Araujo, C. Hampe, S. Jacquier, C.B. Lucking, N. Abbas, C. Duyckaerts, T. Rooney, L. Pradier, M. Ruberg, and A. Brice. 2003. The C289G and C418R missense mutations cause rapid sequestration of human Parkin into insoluble aggregates. *Neurobiology of disease*. 14:357-364.

Guardia-Laguarta, C., E. Area-Gomez, C. Rub, Y. Liu, J. Magrane, D. Becker, W. Voos, E.A. Schon, and S. Przedborski. 2014. alpha-Synuclein Is Localized to Mitochondria-Associated ER Membranes. *The Journal of neuroscience : the official journal of the Society for Neuroscience*. 34:249-259.

Gui, Y.X., Z.P. Xu, W. Lv, H.M. Liu, J.J. Zhao, and X.Y. Hu. 2012. Association of mitochondrial DNA polymerase gamma gene POLG1 polymorphisms with parkinsonism in Chinese populations. *PloS one*. 7:e50086.

Gulati, S., D. Balderes, C. Kim, Z.A. Guo, L. Wilcox, E. Area-Gomez, J. Snider, H. Wolinski, I. Stagljar, J.T. Granato, K.V. Ruggles, J.A. DeGiorgis, S.D. Kohlwein, E.A. Schon, and S.L. Sturley. 2015. ATP-binding cassette transporters and sterol O-acyltransferases interact at membrane microdomains to modulate sterol uptake and esterification. *FASEB J*. 29:4682-4694.

Guo, B., Q. Liang, L. Li, Z. Hu, F. Wu, P. Zhang, Y. Ma, B. Zhao, A.L. Kovacs, Z. Zhang, D. Feng, S. Chen, and H. Zhang. 2014. O-GlcNAc-modification of SNAP-29 regulates autophagosome maturation. *Nature cell biology*. 16:1215-1226.

Gutierrez, M.G., D.B. Munafo, W. Beron, and M.I. Colombo. 2004. Rab7 is required for the normal progression of the autophagic pathway in mammalian cells. *Journal of cell science*. 117:2687-2697.

Guzman, J.N., J. Sanchez-Padilla, D. Wokosin, J. Kondapalli, E. Ilijic, P.T. Schumacker, and D.J. Surmeier. 2010. Oxidant stress evoked by pacemaking in dopaminergic neurons is attenuated by DJ-1. *Nature*. 468:696-700.

Haglund, K., P.P. Di Fiore, and I. Dikic. 2003. Distinct monoubiquitin signals in receptor endocytosis. *Trends in biochemical sciences*. 28:598-603.

Hailey, D.W., A.S. Rambold, P. Satpute-Krishnan, K. Mitra, R. Sougrat, P.K. Kim, and J. Lippincott-Schwartz. 2010. Mitochondria supply membranes for autophagosome biogenesis during starvation. *Cell*. 141:656-667.

Hamasaki, M., N. Furuta, A. Matsuda, A. Nezu, A. Yamamoto, N. Fujita, H. Oomori, T. Noda, T. Haraguchi, Y. Hiraoka, A. Amano, and T. Yoshimori. 2013. Autophagosomes form at ER-mitochondria contact sites. *Nature*. 495:389-393.

Hampe, C., H. Ardila-Osorio, M. Fournier, A. Brice, and O. Corti. 2006. Biochemical analysis of Parkinson's disease-causing variants of Parkin, an E3 ubiquitin-protein ligase with monoubiquitylation capacity. *Human molecular genetics*. 15:2059-2075.

Hanson, P.I., R. Roth, H. Morisaki, R. Jahn, and J.E. Heuser. 1997. Structure and conformational changes in NSF and its membrane receptor complexes visualized by quick-freeze/deep-etch electron microscopy. *Cell*. 90:523-535.

Hanus, C., and M.D. Ehlers. 2016. Specialization of biosynthetic membrane trafficking for neuronal form and function. *Curr Opin Neurobiol*. 39:8-16.

Hao, L.Y., B.I. Giasson, and N.M. Bonini. 2010. DJ-1 is critical for mitochondrial function and rescues PINK1 loss of function. *Proceedings of the National Academy of Sciences of the United States of America*. 107:9747-9752.

Hao, Q., S. Jiao, Z. Shi, C. Li, X. Meng, Z. Zhang, Y. Wang, X. Song, W. Wang, R. Zhang, Y. Zhao, C.C. Wong, and Z. Zhou. 2015. A non-canonical role of the p97 complex in RIG-I antiviral signaling. *The EMBO journal*. 34:2903-2920.

Haque, M.E., K.J. Thomas, C. D'Souza, S. Callaghan, T. Kitada, R.S. Slack, P. Fraser, M.R. Cookson, A. Tandon, and D.S. Park. 2008. Cytoplasmic Pink1 activity protects neurons from dopaminergic neurotoxin MPTP. *Proceedings of the National Academy of Sciences of the United States of America*. 105:1716-1721.

Harbauer, A.B., R.P. Zahedi, A. Sickmann, N. Pfanner, and C. Meisinger. 2014. The Protein Import Machinery of Mitochondria-A Regulatory Hub in Metabolism, Stress, and Disease. *Cell metabolism*.

Harder, Z., R. Zunino, and H. McBride. 2004. Sumo1 conjugates mitochondrial substrates and participates in mitochondrial fission. *Current biology : CB*. 14:340-345.

Hasim, S., N.A. Hussin, F. Alomar, K.R. Bidasee, K.W. Nickerson, and M.A. Wilson. 2014. A glutathione-independent glyoxalase of the DJ-1 superfamily plays an important role in managing metabolically generated methylglyoxal in Candida albicans. *The Journal of biological chemistry*. 289:1662-1674.

Hasson, S.A., A.I. Fogel, C. Wang, R. MacArthur, R. Guha, S. Heman-Ackah, S. Martin, R.J. Youle, and J. Inglese. 2015. Chemogenomic profiling of endogenous PARK2 expression using a genome-edited coincidence reporter. *ACS Chem Biol*. 10:1188-1197.

Hasson, S.A., L.A. Kane, K. Yamano, C.H. Huang, D.A. Sliter, E. Buehler, C. Wang, S.M. Heman-Ackah, T. Hessa, R. Guha, S.E. Martin, and R.J. Youle. 2013. High-content genome-wide RNAi screens identify regulators of parkin upstream of mitophagy. *Nature*. 504:291-295.

Hatefi, Y. 1985. The mitochondrial electron transport and oxidative phosphorylation system. *Annu Rev Biochem*. 54:1015-1069.

Hattori, T., K. Watanabe, Y. Uechi, H. Yoshioka, and Y. Ohta. 2005. Repetitive transient depolarizations of the inner mitochondrial membrane induced by proton pumping. *Biophys J*. 88:2340-2349.

Hayashi, T., and M. Fujimoto. 2010. Detergent-resistant microdomains determine the localization of sigma-1 receptors to the endoplasmic reticulum-mitochondria junction. *Mol Pharmacol*. 77:517-528.

Hayashi-Nishino, M., N. Fujita, T. Noda, A. Yamaguchi, T. Yoshimori, and A. Yamamoto. 2009. A subdomain of the endoplasmic reticulum forms a cradle for autophagosome formation. *Nature cell biology*. 11:1433-1437.

Healy, D.G., M. Falchi, S.S. O'Sullivan, V. Bonifati, A. Durr, S. Bressman, A. Brice, J. Aasly, C.P. Zabetian, S. Goldwurm, J.J. Ferreira, E. Tolosa, D.M. Kay, C. Klein, D.R. Williams, C. Marras, A.E. Lang, Z.K. Wszolek, J. Berciano, A.H. Schapira, T. Lynch, K.P. Bhatia, T. Gasser, A.J. Lees, N.W. Wood, and L.C. International. 2008. Phenotype, genotype, and worldwide genetic penetrance of LRRK2-associated Parkinson's disease: a case-control study. *Lancet Neurol*. 7:583-590.

Hedskog, L., C.M. Pinho, R. Filadi, A. Ronnback, L. Hertwig, B. Wiehager, P. Larssen, S. Gellhaar, A. Sandebring, M. Westerlund, C. Graff, B. Winblad, D. Galter, H. Behbahani, P. Pizzo, E. Glaser, and M. Ankarcrona. 2013. Modulation of the endoplasmic reticulum-mitochondria interface in Alzheimer's disease and related models. *Proceedings of the National Academy of Sciences of the United States of America*. 110:7916-7921.

Heeman, B., C. Van den Haute, S.A. Aelvoet, F. Valsecchi, R.J. Rodenburg, V. Reumers, Z. Debyser, G. Callewaert, W.J. Koopman, P.H. Willems, and V. Baekelandt. 2011. Depletion of PINK1 affects mitochondrial metabolism, calcium homeostasis and energy maintenance. *Journal of cell science*. 124:1115-1125.

Henne, W.M., E. Boucrot, M. Meinecke, E. Evergren, Y. Vallis, R. Mittal, and H.T. McMahon. 2010. FCHo proteins are nucleators of clathrin-mediated endocytosis. *Science*. 328:1281-1284.

Henry, J., R.J. Smeyne, H. Jang, B. Miller, and M.S. Okun. 2010. Parkinsonism and neurological manifestations of influenza throughout the 20th and 21st centuries. *Parkinsonism Relat Disord*. 16:566-571.

Heo, J.M., N. Livnat-Levanon, E.B. Taylor, K.T. Jones, N. Dephoure, J. Ring, J. Xie, J.L. Brodsky, F. Madeo, S.P. Gygi, K. Ashrafi, M.H. Glickman, and J. Rutter. 2010. A stress-responsive system for mitochondrial protein degradation. *Molecular cell*. 40:465-480.

Heo, J.M., A. Ordureau, J.A. Paulo, J. Rinehart, and J.W. Harper. 2015. The PINK1-PARKIN Mitochondrial Ubiquitylation Pathway Drives a Program of OPTN/NDP52 Recruitment and TBK1 Activation to Promote Mitophagy. *Molecular cell*. 60:7-20.

Hershko, A., A. Ciechanover, H. Heller, A.L. Haas, and I.A. Rose. 1980. Proposed role of ATP in protein breakdown: conjugation of protein with multiple chains of the polypeptide of ATP-dependent proteolysis. *Proceedings of the National Academy of Sciences of the United States of America*. 77:1783-1786.

Hesketh, G.G., I. Perez-Dorado, L.P. Jackson, L. Wartosch, I.B. Schafer, S.R. Gray, A.J. McCoy, O.B. Zeldin, E.F. Garman, M.E. Harbour, P.R. Evans, M.N. Seaman, J.P. Luzio, and D.J. Owen. 2014. VARP is recruited on to endosomes by direct interaction with retromer, where together they function in export to the cell surface. *Developmental cell*. 29:591-606.

Hirsch, L., N. Jette, A. Frolkis, T. Steeves, and T. Pringsheim. 2016. The Incidence of Parkinson's Disease: A Systematic Review and Meta-Analysis. *Neuroepidemiology*. 46:292-300.

Horner, S.M., H.M. Liu, H.S. Park, J. Briley, and M. Gale, Jr. 2011. Mitochondrial-associated endoplasmic reticulum membranes (MAM) form innate immune synapses and are targeted by hepatitis C virus. *Proceedings of the National Academy of Sciences of the United States of America*. 108:14590-14595.

Hornykiewicz, O. 2010. A brief history of levodopa. *J Neurol*. 257:S249-252.

Hoyer-Hansen, M., L. Bastholm, I.S. Mathiasen, F. Elling, and M. Jaattela. 2005. Vitamin D analog EB1089 triggers dramatic lysosomal changes and Beclin 1-mediated autophagic cell death. *Cell death and differentiation*. 12:1297-1309.

Hristova, V.A., S.A. Beasley, R.J. Rylett, and G.S. Shaw. 2009. Identification of a novel Zn2+-binding domain in the autosomal recessive juvenile Parkinson-related E3 ligase parkin. *The Journal of biological chemistry*. 284:14978-14986.

Hsu, L.J., Y. Sagara, A. Arroyo, E. Rockenstein, A. Sisk, M. Mallory, J. Wong, T. Takenouchi, M. Hashimoto, and E. Masliah. 2000. alpha-synuclein promotes mitochondrial deficit and oxidative stress. *The American journal of pathology*. 157:401-410.

Hu, J., Y. Shibata, P.P. Zhu, C. Voss, N. Rismanchi, W.A. Prinz, T.A. Rapoport, and C. Blackstone. 2009. A class of dynamin-like GTPases involved in the generation of the tubular ER network. *Cell*. 138:549-561.

Hughes, A.L., and D.E. Gottschling. 2012. An early age increase in vacuolar pH limits mitochondrial function and lifespan in yeast. *Nature*. 492:261-265.

Hung, V., P. Zou, H.W. Rhee, N.D. Udeshi, V. Cracan, T. Svinkina, S.A. Carr, V.K. Mootha, and A.Y. Ting. 2014. Proteomic mapping of the human mitochondrial intermembrane space in live cells via ratiometric APEX tagging. *Molecular cell*. 55:332-341.

Hurley, J.H. 2015. ESCRTs are everywhere. *The EMBO journal*. 34:2398-2407.

Husnjak, K., S. Elsasser, N. Zhang, X. Chen, L. Randles, Y. Shi, K. Hofmann, K.J. Walters, D. Finley, and I. Dikic. 2008. Proteasome subunit Rpn13 is a novel ubiquitin receptor. *Nature*. 453:481-488.

Iguchi, M., Y. Kujuro, K. Okatsu, F. Koyano, H. Kosako, M. Kimura, N. Suzuki, S. Uchiyama, K. Tanaka, and N. Matsuda. 2013. Parkin-catalyzed ubiquitin-ester transfer is triggered by PINK1-dependent phosphorylation. *The Journal of biological chemistry*. 288:22019-22032.

Imai, K., F. Hao, N. Fujita, Y. Tsuji, Y. Oe, Y. Araki, M. Hamasaki, T. Noda, and T. Yoshimori. 2016. Atg9A trafficking through the recycling endosomes is required for autophagosome formation. *Journal of cell science*. 129:3781-3791.

Imai, Y., M. Soda, and R. Takahashi. 2000. Parkin suppresses unfolded protein stress-induced cell death through its E3 ubiquitin-protein ligase activity. *The Journal of biological chemistry*. 275:35661-35664.

Ingerman, E., E.M. Perkins, M. Marino, J.A. Mears, J.M. McCaffery, J.E. Hinshaw, and J. Nunnari. 2005. Dnm1 forms spirals that are structurally tailored to fit mitochondria. *The Journal of cell biology*. 170:1021-1027.

Isenmann, S., Y. Khew-Goodall, J. Gamble, M. Vadas, and B.W. Wattenberg. 1998. A splice-isoform of vesicle-associated membrane protein-1 (VAMP-1) contains a mitochondrial targeting signal. *Molecular biology of the cell*. 9:1649-1660.

Ishihara, N., Y. Eura, and K. Mihara. 2004. Mitofusin 1 and 2 play distinct roles in mitochondrial fusion reactions via GTPase activity. *Journal of cell science*. 117:6535-6546.

Ishihara, N., Y. Fujita, T. Oka, and K. Mihara. 2006. Regulation of mitochondrial morphology through proteolytic cleavage of OPA1. *The EMBO journal*. 25:2966-2977.

Itakura, E., C. Kishi, K. Inoue, and N. Mizushima. 2008. Beclin 1 forms two distinct phosphatidylinositol 3-kinase complexes with mammalian Atg14 and UVRAG. *Molecular biology of the cell*. 19:5360-5372.

Itakura, E., C. Kishi-Itakura, I. Koyama-Honda, and N. Mizushima. 2012a. Structures containing Atg9A and the ULK1 complex independently target depolarized mitochondria at initial stages of Parkin-mediated mitophagy. *Journal of cell science*. 125:1488-1499.

Itakura, E., C. Kishi-Itakura, and N. Mizushima. 2012b. The hairpin-type tail-anchored SNARE syntaxin 17 targets to autophagosomes for fusion with endosomes/lysosomes. *Cell*. 151:1256-1269.

Ivankovic, D., K.Y. Chau, A.H. Schapira, and M.E. Gegg. 2016. Mitochondrial and lysosomal biogenesis are activated following PINK1/parkin-mediated mitophagy. *Journal of neurochemistry*. 136:388-402.

Ivatt, R.M., A. Sanchez-Martinez, V.K. Godena, S. Brown, E. Ziviani, and A.J. Whitworth. 2014. Genome-wide RNAi screen identifies the Parkinson disease GWAS risk locus SREBF1 as a regulator of mitophagy. *Proceedings of the National Academy of Sciences of the United States of America*. 111:8494-8499.

Jager, S., C. Bucci, I. Tanida, T. Ueno, E. Kominami, P. Saftig, and E.L. Eskelinen. 2004. Role for Rab7 in maturation of late autophagic vacuoles. *Journal of cell science*. 117:4837-4848.

Janer, A., J. Prudent, V. Paupe, S. Fahiminiya, J. Majewski, N. Sgarioto, C. Des Rosiers, A. Forest, Z.Y. Lin, A.C. Gingras, G. Mitchell, H.M. McBride, and E.A. Shoubridge. 2016. SLC25A46 is required for mitochondrial lipid homeostasis and cristae maintenance and is responsible for Leigh syndrome. *EMBO Mol Med*. 8:1019-1038.

Jang, H., D. Boltz, J. McClaren, A.K. Pani, M. Smeyne, A. Korff, R. Webster, and R.J. Smeyne. 2012. Inflammatory effects of highly pathogenic H5N1 influenza virus infection in the CNS of mice. *The Journal of neuroscience : the official journal of the Society for Neuroscience*. 32:1545-1559.

Jang, H., D. Boltz, K. Sturm-Ramirez, K.R. Shepherd, Y. Jiao, R. Webster, and R.J. Smeyne. 2009. Highly pathogenic H5N1 influenza virus can enter the central nervous system and induce neuroinflammation and neurodegeneration. *Proceedings of the National Academy of Sciences of the United States of America*. 106:14063-14068.

Ji, W.K., A.L. Hatch, R.A. Merrill, S. Strack, and H.N. Higgs. 2015. Actin filaments target the oligomeric maturation of the dynamin GTPase Drp1 to mitochondrial fission sites. *eLife*. 4:e11553.

Jiang, H., Y. Ren, E.Y. Yuen, P. Zhong, M. Ghaedi, Z. Hu, G. Azabdaftari, K. Nakaso, Z. Yan, and J. Feng. 2012. Parkin controls dopamine utilization in human midbrain dopaminergic neurons derived from induced pluripotent stem cells. *Nature communications*. 3:668.

Jiang, P., T. Nishimura, Y. Sakamaki, E. Itakura, T. Hatta, T. Natsume, and N. Mizushima. 2014. The HOPS complex mediates autophagosome-lysosome fusion through interaction with syntaxin 17. *Molecular biology of the cell*. 25:1327-1337.

Jin, L., K.B. Pahuja, K.E. Wickliffe, A. Gorur, C. Baumgartel, R. Schekman, and M. Rape. 2012. Ubiquitin-dependent regulation of COPII coat size and function. *Nature*. 482:495-500.

Jin, N., C.Y. Chow, L. Liu, S.N. Zolov, R. Bronson, M. Davisson, J.L. Petersen, Y. Zhang, S. Park, J.E. Duex, D. Goldowitz, M.H. Meisler, and L.S. Weisman. 2008. VAC14 nucleates a protein complex essential for the acute interconversion of PI3P and PI(3,5)P(2) in yeast and mouse. *The EMBO journal*. 27:3221-3234.

Jin, S.M., M. Lazarou, C. Wang, L.A. Kane, D.P. Narendra, and R.J. Youle. 2010. Mitochondrial membrane potential regulates PINK1 import and proteolytic destabilization by PARL. *The Journal of cell biology*. 191:933-942.

Jin, S.M., and R.J. Youle. 2013. The accumulation of misfolded proteins in the mitochondrial matrix is sensed by PINK1 to induce PARK2/Parkin-mediated mitophagy of polarized mitochondria. *Autophagy*. 9:1750-1757.

Jinn, S., R.E. Drolet, P.E. Cramer, A.H. Wong, D.M. Toolan, C.A. Gretzula, B. Voleti, G. Vassileva, J. Disa, M. Tadin-Strapps, and D.J. Stone. 2017. TMEM175 deficiency impairs lysosomal and mitochondrial function and increases alpha-synuclein aggregation. *Proceedings of the National Academy of Sciences of the United States of America*. 114:2389-2394.

Joch, M., A.R. Ase, C.X. Chen, P.A. MacDonald, M. Kontogiannea, A.T. Corera, A. Brice, P. Seguela, and E.A. Fon. 2007. Parkin-mediated monoubiquitination of the PDZ protein PICK1 regulates the activity of acid-sensing ion channels. *Molecular biology of the cell*. 18:3105-3118.

Kabeya, Y., N. Mizushima, T. Ueno, A. Yamamoto, T. Kirisako, T. Noda, E. Kominami, Y. Ohsumi, and T. Yoshimori. 2000. LC3, a mammalian homologue of yeast Apg8p, is localized in autophagosome membranes after processing. *The EMBO journal*. 19:5720-5728.

Kahns, S., S. Lykkebo, L.D. Jakobsen, M.S. Nielsen, and P.H. Jensen. 2002. Caspase-mediated parkin cleavage in apoptotic cell death. *The Journal of biological chemistry*. 277:15303-15308.

Kamer, K.J., and V.K. Mootha. 2015. The molecular era of the mitochondrial calcium uniporter. *Nature reviews. Molecular cell biology*. 16:545-553.

Kane, L.A., M. Lazarou, A.I. Fogel, Y. Li, K. Yamano, S.A. Sarraf, S. Banerjee, and R.J. Youle. 2014. PINK1 phosphorylates ubiquitin to activate Parkin E3 ubiquitin ligase activity. *The Journal of cell biology*. 205:143-153.

Kannan, M., S. Lahiri, L.K. Liu, V. Choudhary, and W.A. Prinz. 2017. Phosphatidylserine synthesis at membrane contact sites promotes its transport out of the ER. *J Lipid Res*. 58:553-562.

Karanasios, E., S.A. Walker, H. Okkenhaug, M. Manifava, E. Hummel, H. Zimmermann, Q. Ahmed, M.C. Domart, L. Collinson, and N.T. Ktistakis. 2016. Autophagy initiation by ULK complex assembly on ER tubulovesicular regions marked by ATG9 vesicles. *Nature communications*. 7:12420.

Karbowski, M., K.L. Norris, M.M. Cleland, S.Y. Jeong, and R.J. Youle. 2006. Role of Bax and Bak in mitochondrial morphogenesis. *Nature*. 443:658-662.

Katayama, H., T. Kogure, N. Mizushima, T. Yoshimori, and A. Miyawaki. 2011. A sensitive and quantitative technique for detecting autophagic events based on lysosomal delivery. *Chemistry & biology*. 18:1042-1052.

Katz, L., and P. Brennwald. 2000. Testing the 3Q:1R "rule": mutational analysis of the ionic "zero" layer in the yeast exocytic SNARE complex reveals no requirement for arginine. *Molecular biology of the cell*. 11:3849-3858.

Kazlauskaite, A., V. Kelly, C. Johnson, C. Baillie, C.J. Hastie, M. Peggie, T. Macartney, H.I. Woodroof, D.R. Alessi, P.G. Pedrioli, and M.M. Muqit. 2014a. Phosphorylation of Parkin at Serine65 is essential for activation: elaboration of a Miro1 substrate-based assay of Parkin E3 ligase activity. *Open biology*. 4:130213.

Kazlauskaite, A., C. Kondapalli, R. Gourlay, D.G. Campbell, M.S. Ritorto, K. Hofmann, D.R. Alessi, A. Knebel, M. Trost, and M.M. Muqit. 2014b. Parkin is activated by PINK1-dependent phosphorylation of ubiquitin at Ser65. *The Biochemical journal*. 460:127-139.

Kazlauskaite, A., R.J. Martinez-Torres, S. Wilkie, A. Kumar, J. Peltier, A. Gonzalez, C. Johnson, J. Zhang, A.G. Hope, M. Peggie, M. Trost, D.M. van Aalten, D.R. Alessi, A.R. Prescott, A. Knebel, H. Walden, and M.M. Muqit. 2015. Binding to serine 65-phosphorylated ubiquitin primes Parkin for optimal PINK1-dependent phosphorylation and activation. *EMBO reports*. 16:939-954.

Khaminets, A., C. Behl, and I. Dikic. 2016. Ubiquitin-Dependent And Independent Signals In Selective Autophagy. *Trends in cell biology*. 26:6-16.

Khan, M., G.H. Syed, S.J. Kim, and A. Siddiqui. 2016. Hepatitis B Virus-Induced Parkin-Dependent Recruitment of Linear Ubiquitin Assembly Complex (LUBAC) to Mitochondria and Attenuation of Innate Immunity. *PLoS Pathog*. 12:e1005693.

Kihara, A., T. Noda, N. Ishihara, and Y. Ohsumi. 2001. Two distinct Vps34 phosphatidylinositol 3-kinase complexes function in autophagy and carboxypeptidase Y sorting in Saccharomyces cerevisiae. *The Journal of cell biology*. 152:519-530.

Kim, J., Y.C. Kim, C. Fang, R.C. Russell, J.H. Kim, W. Fan, R. Liu, Q. Zhong, and K.L. Guan. 2013a. Differential regulation of distinct Vps34 complexes by AMPK in nutrient stress and autophagy. *Cell*. 152:290-303.

Kim, K.Y., M.V. Stevens, M.H. Akter, S.E. Rusk, R.J. Huang, A. Cohen, A. Noguchi, D. Springer, A.V. Bocharov, T.L. Eggerman, D.F. Suen, R.J. Youle, M. Amar, A.T. Remaley, and M.N. Sack. 2011. Parkin is a lipid-responsive regulator of fat uptake in mice and mutant human cells. *The Journal of clinical investigation*. 121:3701-3712.

Kim, N.C., E. Tresse, R.M. Kolaitis, A. Molliex, R.E. Thomas, N.H. Alami, B. Wang, A. Joshi, R.B. Smith, G.P. Ritson, B.J. Winborn, J. Moore, J.Y. Lee, T.P. Yao, L. Pallanck, M. Kundu, and J.P. Taylor. 2013b. VCP is essential for mitochondrial quality control by PINK1/Parkin and this function is impaired by VCP mutations. *Neuron*. 78:65-80.

Kim, W.G., R.P. Mohney, B. Wilson, G.H. Jeohn, B. Liu, and J.S. Hong. 2000. Regional difference in susceptibility to lipopolysaccharide-induced neurotoxicity in the rat brain: role of microglia. *The Journal of neuroscience : the official journal of the Society for Neuroscience*. 20:6309-6316.

Kimura, Y., J. Fukushi, S. Hori, N. Matsuda, K. Okatsu, Y. Kakiyama, J. Kawawaki, A. Kakizuka, and K. Tanaka. 2013. Different dynamic movements of wild-type and pathogenic VCPs and their cofactors to damaged mitochondria in a Parkin-mediated mitochondrial quality

control system. *Genes to cells : devoted to molecular & cellular mechanisms*. 18:1131-1143.

Kinghorn, K.J., J.I. Castillo-Quan, F. Bartolome, P.R. Angelova, L. Li, S. Pope, H.M. Cocheme, S. Khan, S. Asghari, K.P. Bhatia, J. Hardy, A.Y. Abramov, and L. Partridge. 2015. Loss of PLA2G6 leads to elevated mitochondrial lipid peroxidation and mitochondrial dysfunction. *Brain : a journal of neurology*. 138:1801-1816.

Kirichok, Y., G. Krapivinsky, and D.E. Clapham. 2004. The mitochondrial calcium uniporter is a highly selective ion channel. *Nature*. 427:360-364.

Kirola, L., M. Behari, C. Shishir, and B.K. Thelma. 2016. Identification of a novel homozygous mutation Arg459Pro in SYNJ1 gene of an Indian family with autosomal recessive juvenile Parkinsonism. *Parkinsonism Relat Disord*. 31:124-128.

Kishi-Itakura, C., I. Koyama-Honda, E. Itakura, and N. Mizushima. 2014. Ultrastructural analysis of autophagosome organization using mammalian autophagy-deficient cells. *Journal of cell science*. 127:4089-4102.

Kitada, T., S. Asakawa, N. Hattori, H. Matsumine, Y. Yamamura, S. Minoshima, M. Yokochi, Y. Mizuno, and N. Shimizu. 1998. Mutations in the parkin gene cause autosomal recessive juvenile parkinsonism. *Nature*. 392:605-608.

Klecker, T., S. Bockler, and B. Westermann. 2014. Making connections: interorganelle contacts orchestrate mitochondrial behavior. *Trends in cell biology*.

Klionsky, D.J., F.C. Abdalla, H. Abeliovich, R.T. Abraham, A. Acevedo-Arozena, K. Adeli, L. Agholme, M. Agnello, P. Agostinis, J.A. Aguirre-Ghiso, H.J. Ahn, O. Ait-Mohamed, S. Ait-Si-Ali, T. Akematsu, S. Akira, H.M. Al-Younes, M.A. Al-Zeer, M.L. Albert, R.L. Albin, J. Alegre-Abarrategui, M.F. Aleo, M. Alirezaei, A. Almasan, M. Almonte-Becerril, A. Amano, R. Amaravadi, S. Amarnath, A.O. Amer, N. Andrieu-Abadie, V. Anantharam, D.K. Ann, S. Anoopkumar-Dukie, H. Aoki, N. Apostolova, G. Arancia, J.P. Aris, K. Asanuma, N.Y. Asare, H. Ashida, V. Askanas, D.S. Askew, P. Auberger, M. Baba, S.K. Backues, E.H. Baehrecke, B.A. Bahr, X.Y. Bai, Y. Bailly, R. Baiocchi, G. Baldini, W. Balduini, A. Ballabio, B.A. Bamber, E.T. Bampton, G. Banhegyi, C.R. Bartholomew, D.C. Bassham, R.C. Bast, Jr., H. Batoko, B.H. Bay, I. Beau, D.M. Bechet, T.J. Begley, C. Behl, C. Behrends, S. Bekri, B. Bellaire, L.J. Bendall, L. Benetti, L. Berliocchi, H. Bernardi, F. Bernassola, S. Besteiro, I. Bhatia-Kissova, X. Bi, M. Biard-Piechaczyk, J.S. Blum, L.H. Boise, P. Bonaldo, D.L. Boone, B.C. Bornhauser, K.R. Bortoluci, I. Bossis, F. Bost, J.P. Bourquin, P. Boya, M. Boyer-Guittaut, P.V. Bozhkov, N.R. Brady, C. Brancolini, A. Brech, J.E. Brenman, A. Brennand, E.H. Bresnick, P. Brest, D. Bridges, M.L. Bristol, P.S. Brookes, E.J. Brown, J.H. Brumell, et al. 2012. Guidelines for the use and interpretation of assays for monitoring autophagy. *Autophagy*. 8:445-544.

Kloepper, T.H., C.N. Kienle, and D. Fasshauer. 2008. SNAREing the basis of multicellularity: consequences of protein family expansion during evolution. *Molecular biology and evolution*. 25:2055-2068.

Komander, D., and M. Rape. 2012. The ubiquitin code. *Annu Rev Biochem*. 81:203-229.

Kondapalli, C., A. Kazlauskaite, N. Zhang, H.I. Woodroof, D.G. Campbell, R. Gourlay, L. Burchell, H. Walden, T.J. Macartney, M. Deak, A. Knebel, D.R. Alessi, and M.M. Muqit. 2012. PINK1 is activated by mitochondrial membrane potential depolarization and stimulates Parkin E3 ligase activity by phosphorylating Serine 65. *Open biology*. 2:120080.

Kopek, B.G., G. Perkins, D.J. Miller, M.H. Ellisman, and P. Ahlquist. 2007. Three-dimensional analysis of a viral RNA replication complex reveals a virus-induced mini-organelle. *PLoS biology*. 5:e220.

Kordower, J.H., C.W. Olanow, H.B. Dodiya, Y. Chu, T.G. Beach, C.H. Adler, G.M. Halliday, and R.T. Bartus. 2013. Disease duration and the integrity of the nigrostriatal system in Parkinson's disease. *Brain : a journal of neurology*. 136:2419-2431.

Korobova, F., V. Ramabhadran, and H.N. Higgs. 2013. An actin-dependent step in mitochondrial fission mediated by the ER-associated formin INF2. *Science*. 339:464-467.

Koshiba, T., S.A. Detmer, J.T. Kaiser, H. Chen, J.M. McCaffery, and D.C. Chan. 2004. Structural basis of mitochondrial tethering by mitofusin complexes. *Science*. 305:858-862.

Kostic, M., M.H. Ludtmann, H. Bading, M. Hershfinkel, E. Steer, C.T. Chu, A.Y. Abramov, and I. Sekler. 2015. PKA Phosphorylation of NCLX Reverses Mitochondrial Calcium Overload and Depolarization, Promoting Survival of PINK1-Deficient Dopaminergic Neurons. *Cell reports*. 13:376-386.

Koumandou, V.L., B. Wickstead, M.L. Ginger, M. van der Giezen, J.B. Dacks, and M.C. Field. 2013. Molecular paleontology and complexity in the last eukaryotic common ancestor. *Critical reviews in biochemistry and molecular biology*. 48:373-396.

Kovacs-Bogdan, E., Y. Sancak, K.J. Kamer, M. Plovanich, A. Jambhekar, R.J. Huber, M.A. Myre, M.D. Blower, and V.K. Mootha. 2014. Reconstitution of the mitochondrial calcium uniporter in yeast. *Proceedings of the National Academy of Sciences of the United States of America*. 111:8985-8990.

Koyano, F., K. Okatsu, H. Kosako, Y. Tamura, E. Go, M. Kimura, Y. Kimura, H. Tsuchiya, H. Yoshihara, T. Hirokawa, T. Endo, E.A. Fon, J.F. Trempe, Y. Saeki, K. Tanaka, and N. Matsuda. 2014. Ubiquitin is phosphorylated by PINK1 to activate parkin. *Nature*. 510:162-166.

Kravtsova-Ivantsiv, Y., and A. Ciechanover. 2012. Non-canonical ubiquitin-based signals for proteasomal degradation. *Journal of cell science*. 125:539-548.

Krebs, C.E., S. Karkheiran, J.C. Powell, M. Cao, V. Makarov, H. Darvish, G. Di Paolo, R.H. Walker, G.A. Shahidi, J.D. Buxbaum, P. De Camilli, Z. Yue, and C. Paisan-Ruiz. 2013. The Sac1 domain of SYNJ1 identified mutated in a family with early-onset progressive Parkinsonism with generalized seizures. *Hum Mutat*. 34:1200-1207.

Kumar, A., V.K. Chaugule, T.E.C. Condos, K.R. Barber, C. Johnson, R. Toth, R. Sundaramoorthy, A. Knebel, G.S. Shaw, and H. Walden. 2017a. Parkin-phosphoubiquitin complex reveals cryptic ubiquitin-binding site required for RBR ligase activity. *Nature structural & molecular biology*. 24:475-483.

Kumar, A., J. Tamjar, A.D. Waddell, H.I. Woodroof, O.G. Raimi, A.M. Shaw, M. Peggie, M.M. Muqit, and D.M. van Aalten. 2017b. Structure of PINK1 and mechanisms of Parkinson's disease associated mutations. *eLife*. 6.

Kumar, K.R., A. Djarmati-Westenberger, and A. Grunewald. 2011. Genetics of Parkinson's disease. *Semin Neurol*. 31:433-440.

Kunas, R.C., A. McRae, J. Kesselring, and P.M. Villiger. 1995. Antidopaminergic antibodies in a patient with a complex autoimmune disorder and rapidly progressing Parkinson's disease. *J Allergy Clin Immunol*. 96:688-690.

Kwon, K., D. Choi, J.K. Hyun, H.S. Jung, K. Baek, and C. Park. 2013. Novel glyoxalases from Arabidopsis thaliana. *The FEBS journal*. 280:3328-3339.

Lackner, L.L., J.S. Horner, and J. Nunnari. 2009. Mechanistic analysis of a dynamin effector. *Science*. 325:874-877.

Lahiri, S., J.T. Chao, S. Tavassoli, A.K. Wong, V. Choudhary, B.P. Young, C.J. Loewen, and W.A. Prinz. 2014. A conserved endoplasmic reticulum membrane protein complex (EMC) facilitates phospholipid transfer from the ER to mitochondria. *PLoS biology*. 12:e1001969.

Lai, Y., S. Kim, J. Varkey, X. Lou, J.K. Song, J. Diao, R. Langen, and Y.K. Shin. 2014. Nonaggregated alpha-synuclein influences SNARE-dependent vesicle docking via membrane binding. *Biochemistry*. 53:3889-3896.

Lamb, C.A., T. Yoshimori, and S.A. Tooze. 2013. The autophagosome: origins unknown, biogenesis complex. *Nature reviews. Molecular cell biology*. 14:759-774.

Laplante, M., and D.M. Sabatini. 2012. mTOR signaling in growth control and disease. *Cell*. 149:274-293.

Lauer, J.M., S. Dalal, K.E. Marz, M.L. Nonet, and P.I. Hanson. 2006. SNARE complex zero layer residues are not critical for N-ethylmaleimide-sensitive factor-mediated disassembly. *The Journal of biological chemistry*. 281:14823-14832.

Lawrence, G.W., and J.O. Dolly. 2002a. Ca2+-induced changes in SNAREs and synaptotagmin I correlate with triggered exocytosis from chromaffin cells: insights gleaned into the signal transduction using trypsin and botulinum toxins. *Journal of cell science*. 115:2791-2800.

Lawrence, G.W., and J.O. Dolly. 2002b. Multiple forms of SNARE complexes in exocytosis from chromaffin cells: effects of Ca(2+), MgATP and botulinum toxin type A. *Journal of cell science*. 115:667-673.

Lazarou, M., S.M. Jin, L.A. Kane, and R.J. Youle. 2012. Role of PINK1 binding to the TOM complex and alternate intracellular membranes in recruitment and activation of the E3 ligase Parkin. *Developmental cell*. 22:320-333.

Lazarou, M., D.P. Narendra, S.M. Jin, E. Tekle, S. Banerjee, and R.J. Youle. 2013. PINK1 drives Parkin self-association and HECT-like E3 activity upstream of mitochondrial binding. *The Journal of cell biology*. 200:163-172.

Lazarou, M., D.A. Sliter, L.A. Kane, S.A. Sarraf, C. Wang, J.L. Burman, D.P. Sideris, A.I. Fogel, and R.J. Youle. 2015. The ubiquitin kinase PINK1 recruits autophagy receptors to induce mitophagy. *Nature*. 524:309-314.

Lee, J.E., L.M. Westrate, H. Wu, C. Page, and G.K. Voeltz. 2016. Multiple dynamin family members collaborate to drive mitochondrial division. *Nature*. 540:139-143.

Lee, J.Y., J. Song, K. Kwon, S. Jang, C. Kim, K. Baek, J. Kim, and C. Park. 2012. Human DJ-1 and its homologs are novel glyoxalases. *Human molecular genetics*. 21:3215-3225.

Lee, S., Y. Sato, and R.A. Nixon. 2011. Lysosomal proteolysis inhibition selectively disrupts axonal transport of degradative organelles and causes an Alzheimer's-like axonal dystrophy. *The Journal of neuroscience : the official journal of the Society for Neuroscience*. 31:7817-7830.

Lee, S., C. Zhang, and X. Liu. 2015. Role of glucose metabolism and ATP in maintaining PINK1 levels during Parkin-mediated mitochondrial damage responses. *The Journal of biological chemistry*. 290:904-917.

Lee, Y., D.A. Stevens, S.U. Kang, H. Jiang, Y.I. Lee, H.S. Ko, L.A. Scarffe, G.E. Umanah, H. Kang, S. Ham, T.I. Kam, K. Allen, S. Brahmachari, J.W. Kim, S. Neifert, S.P. Yun, F.C. Fiesel, W. Springer, V.L. Dawson, J.H. Shin, and T.M. Dawson. 2017. PINK1 Primes Parkin-Mediated Ubiquitination of PARIS in Dopaminergic Neuronal Survival. *Cell reports*. 18:918-932.

Lefebvre, V., Q. Du, S. Baird, A.C. Ng, M. Nascimento, M. Campanella, H.M. McBride, and R.A. Screaton. 2013. Genome-wide RNAi screen identifies ATPase inhibitory factor 1 (ATPIF1) as essential for PARK2 recruitment and mitophagy. *Autophagy*. 9:1770-1779.

Lesage, S., V. Drouet, E. Majounie, V. Deramecourt, M. Jacoupy, A. Nicolas, F. Cormier-Dequaire, S.M. Hassoun, C. Pujol, S. Ciura, Z. Erpapazoglou, T. Usenko, C.A. Maurage, M. Sahbatou, S. Liebau, J. Ding, B. Bilgic, M. Emre, N. Erginel-Unaltuna, G. Guven, F. Tison, C. Tranchant, M. Vidailhet, J.C. Corvol, P. Krack, A.L. Leutenegger, M.A. Nalls, D.G. Hernandez, P. Heutink, J.R. Gibbs, J. Hardy, N.W. Wood, T. Gasser, A. Durr, J.F. Deleuze, M. Tazir, A. Destee, E. Lohmann, E. Kabashi, A. Singleton, O. Corti, A. Brice, S. French Parkinson's Disease Genetics, C. International Parkinson's Disease Genomics, and I. International Parkinson's Disease Genomics Consortium. 2016. Loss of VPS13C Function in Autosomal-Recessive Parkinsonism Causes Mitochondrial Dysfunction and Increases PINK1/Parkin-Dependent Mitophagy. *American journal of human genetics*. 98:500-513.

Li, F., D. Kummel, J. Coleman, K.M. Reinisch, J.E. Rothman, and F. Pincet. 2014. A half-zippered SNARE complex represents a functional intermediate in membrane fusion. *Journal of the American Chemical Society*. 136:3456-3464.

Li, J., W. Qi, G. Chen, D. Feng, J.H. Liu, B. Ma, C.Q. Zhou, C.L. Mu, W.L. Zhang, Q. Chen, and Y.S. Zhu. 2015. Mitochondrial outer-membrane E3 ligase MUL1 ubiquitinates ULK1 and regulates selenite-induced mitophagy. *Autophagy*. 11:1216-1229.

Li, K., W. Zhang, H. Fang, W. Xie, J. Liu, M. Zheng, X. Wang, W. Wang, W. Tan, and H. Cheng. 2012. Superoxide flashes reveal novel properties of mitochondrial reactive oxygen species excitability in cardiomyocytes. *Biophys J*. 102:1011-1021.

Li, Q., J. Wang, Y. Wan, and D. Chen. 2016. Depletion of Rab32 decreases intracellular lipid accumulation and induces lipolysis through enhancing ATGL expression in hepatocytes. *Biochemical and biophysical research communications*. 471:492-496.

Lim, C.Y., and R. Zoncu. 2016. The lysosome as a command-and-control center for cellular metabolism. *The Journal of cell biology*. 214:653-664.

Lin, M.Y., X.T. Cheng, P. Tammineni, Y. Xie, B. Zhou, Q. Cai, and Z.H. Sheng. 2017. Releasing Syntaphilin Removes Stressed Mitochondria from Axons Independent of Mitophagy under Pathophysiological Conditions. *Neuron*. 94:595-610 e596.

Lin, W., and U.J. Kang. 2008. Characterization of PINK1 processing, stability, and subcellular localization. *Journal of neurochemistry*. 106:464-474.

Lin, Y., X. Hou, W.J. Shen, R. Hanssen, V.K. Khor, Y. Cortez, A.N. Roseman, S. Azhar, and F.B. Kraemer. 2016. SNARE-Mediated Cholesterol Movement to Mitochondria Supports Steroidogenesis in Rodent Cells. *Molecular endocrinology*. 30:234-247.

Lin, Y.F., and C.M. Haynes. 2016. Metabolism and the UPR(mt). *Molecular cell*. 61:677-682.

Littleton, J.T., R.J. Barnard, S.A. Titus, J. Slind, E.R. Chapman, and B. Ganetzky. 2001. SNARE-complex disassembly by NSF follows synaptic-vesicle fusion. *Proceedings of the National Academy of Sciences of the United States of America*. 98:12233-12238.

Liu, L., D. Feng, G. Chen, M. Chen, Q. Zheng, P. Song, Q. Ma, C. Zhu, R. Wang, W. Qi, L. Huang, P. Xue, B. Li, X. Wang, H. Jin, J. Wang, F. Yang, P. Liu, Y. Zhu, S. Sui, and Q. Chen. 2012. Mitochondrial outer-membrane protein FUNDC1 mediates hypoxia-induced mitophagy in mammalian cells. *Nature cell biology*. 14:177-185.

Liu, R., X. Gao, Y. Lu, and H. Chen. 2011. Meta-analysis of the relationship between Parkinson disease and melanoma. *Neurology*. 76:2002-2009.

Llorente-Folch, I., C.B. Rueda, B. Pardo, G. Szabadkai, M.R. Duchen, and J. Satrustegui. 2015. The regulation of neuronal mitochondrial metabolism by calcium. *J Physiol*. 593:3447-3462.

Lobasso, S., P. Tanzarella, D. Vergara, M. Maffia, T. Cocco, and A. Corcelli. 2017. Lipid profiling of parkin-mutant human skin fibroblasts. *J Cell Physiol*.

Lohmann, E., A.S. Coquel, A. Honore, H. Gurvit, H. Hanagasi, M. Emre, A.L. Leutenegger, V. Drouet, M. Sahbatou, G. Guven, N. Erginel-Unaltuna, J.F. Deleuze, S. Lesage, and A. Brice. 2015. A new F-box protein 7 gene mutation causing typical Parkinson's disease. *Movement disorders : official journal of the Movement Disorder Society*. 30:1130-1133.

Loson, O.C., Z. Song, H. Chen, and D.C. Chan. 2013. Fis1, Mff, MiD49, and MiD51 mediate Drp1 recruitment in mitochondrial fission. *Molecular biology of the cell*. 24:659-667.

Lou, X., J. Kim, B.J. Hawk, and Y.K. Shin. 2017. alpha-Synuclein may cross-bridge v-SNARE and acidic phospholipids to facilitate SNARE-dependent vesicle docking. *The Biochemical journal*. 474:2039-2049.

Lucking, C.B., A. Durr, V. Bonifati, J. Vaughan, G. De Michele, T. Gasser, B.S. Harhangi, G. Meco, P. Denefle, N.W. Wood, Y. Agid, A. Brice, G. French Parkinson's Disease Genetics Study, and D. European Consortium on Genetic Susceptibility in Parkinson's. 2000. Association between early-onset Parkinson's disease and mutations in the parkin gene. *N Engl J Med*. 342:1560-1567.

Luoma, P.T., J. Eerola, S. Ahola, A.H. Hakonen, O. Hellstrom, K.T. Kivisto, P.J. Tienari, and A. Suomalainen. 2007. Mitochondrial DNA polymerase gamma variants in idiopathic sporadic Parkinson disease. *Neurology*. 69:1152-1159.

Luth, E.S., I.G. Stavrovskaya, T. Bartels, B.S. Kristal, and D.J. Selkoe. 2014. Soluble, prefibrillar alpha-synuclein oligomers promote complex I-dependent, Ca2+-induced mitochondrial dysfunction. *The Journal of biological chemistry*. 289:21490-21507.

Lutz, A.K., N. Exner, M.E. Fett, J.S. Schlehe, K. Kloos, K. Lammermann, B. Brunner, A. Kurz-Drexler, F. Vogel, A.S. Reichert, L. Bouman, D. Vogt-Weisenhorn, W. Wurst, J. Tatzelt, C. Haass, and K.F. Winklhofer. 2009. Loss of parkin or PINK1 function increases Drp1-dependent mitochondrial fragmentation. *The Journal of biological chemistry*. 284:22938-22951.

Ma, X., M. Jin, Y. Cai, H. Xia, K. Long, J. Liu, Q. Yu, and J. Yuan. 2011. Mitochondrial electron transport chain complex III is required for antimycin A to inhibit autophagy. *Chemistry & biology*. 18:1474-1481.

Magnaghi, P., R. D'Alessio, B. Valsasina, N. Avanzi, S. Rizzi, D. Asa, F. Gasparri, L. Cozzi, U. Cucchi, C. Orrenius, P. Polucci, D. Ballinari, C. Perrera, A. Leone, G. Cervi, E. Casale, Y. Xiao, C. Wong, D.J. Anderson, A. Galvani, D. Donati, T. O'Brien, P.K. Jackson, and A. Isacchi. 2013. Covalent and allosteric inhibitors of the ATPase VCP/p97 induce cancer cell death. *Nature chemical biology*. 9:548-556.

Malek, N., D.M. Swallow, K.A. Grosset, M.A. Lawton, C.R. Smith, N.P. Bajaj, R.A. Barker, Y. Ben-Shlomo, C. Bresner, D.J. Burn, T. Foltynie, H.R. Morris, N. Williams, N.W. Wood, D.G. Grosset, and P.R. Investigators. 2016. Olfaction in Parkin single and compound heterozygotes in a cohort of young onset Parkinson's disease patients. *Acta Neurol Scand*. 134:271-276.

Malik, B.R., V.K. Godena, and A.J. Whitworth. 2015. VPS35 pathogenic mutations confer no dominant toxicity but partial loss of function in Drosophila and genetically interact with parkin. *Human molecular genetics*. 24:6106-6117.

Mann, V.M., J.M. Cooper, D. Krige, S.E. Daniel, A.H. Schapira, and C.D. Marsden. 1992. Brain, skeletal muscle and platelet homogenate mitochondrial function in Parkinson's disease. *Brain : a journal of neurology*. 115 ( Pt 2):333-342.

Mari, M., J. Griffith, E. Rieter, L. Krishnappa, D.J. Klionsky, and F. Reggiori. 2010. An Atg9-containing compartment that functions in the early steps of autophagosome biogenesis. *The Journal of cell biology*. 190:1005-1022.

Marin, I., and A. Ferrus. 2002. Comparative genomics of the RBR family, including the Parkinson's disease-related gene parkin and the genes of the ariadne subfamily. *Molecular biology and evolution*. 19:2039-2050.

Martin, L.J., Y. Pan, A.C. Price, W. Sterling, N.G. Copeland, N.A. Jenkins, D.L. Price, and M.K. Lee. 2006. Parkinson's disease alpha-synuclein transgenic mice develop neuronal mitochondrial degeneration and cell death. *The Journal of neuroscience : the official journal of the Society for Neuroscience*. 26:41-50.

Matheoud, D., A. Sugiura, A. Bellemare-Pelletier, A. Laplante, C. Rondeau, M. Chemali, A. Fazel, J.J. Bergeron, L.E. Trudeau, Y. Burelle, E. Gagnon, H.M. McBride, and M. Desjardins. 2016. Parkinson's Disease-Related Proteins PINK1 and Parkin Repress Mitochondrial Antigen Presentation. *Cell*. 166:314-327.

Matsuda, N., S. Sato, K. Shiba, K. Okatsu, K. Saisho, C.A. Gautier, Y.S. Sou, S. Saiki, S. Kawajiri, F. Sato, M. Kimura, M. Komatsu, N. Hattori, and K. Tanaka. 2010. PINK1 stabilized by mitochondrial depolarization recruits Parkin to damaged mitochondria and activates latent Parkin for mitophagy. *The Journal of cell biology*. 189:211-221.

Matsuda, W., T. Furuta, K.C. Nakamura, H. Hioki, F. Fujiyama, R. Arai, and T. Kaneko. 2009. Single nigrostriatal dopaminergic neurons form widely spread and highly dense axonal arborizations in the neostriatum. *The Journal of neuroscience : the official journal of the Society for Neuroscience*. 29:444-453.

Matsunaga, K., E. Morita, T. Saitoh, S. Akira, N.T. Ktistakis, T. Izumi, T. Noda, and T. Yoshimori. 2010. Autophagy requires endoplasmic reticulum targeting of the PI3-kinase complex via Atg14L. *The Journal of cell biology*. 190:511-521.

Mattie, S., J. Riemer, J.G. Wideman, and H.M. McBride. in revision. Redox-regulated C-terminus of Mitofusin-2 residues within the mitochondrial intermembrane space.

McCormack, A., N. Chegeni, F. Chegini, A. Colella, J. Power, D. Keating, and T. Chataway. 2016. Purification of alpha-synuclein containing inclusions from human post mortem brain tissue. *J Neurosci Methods*. 266:141-150.

McCormick, A.L., V.L. Smith, D. Chow, and E.S. Mocarski. 2003. Disruption of mitochondrial networks by the human cytomegalovirus UL37 gene product viral mitochondrion-localized inhibitor of apoptosis. *Journal of virology*. 77:631-641.

McCoy, M.K., A. Kaganovich, I.N. Rudenko, J. Ding, and M.R. Cookson. 2014. Hexokinase activity is required for recruitment of parkin to depolarized mitochondria. *Human molecular genetics*. 23:145-156.

McDowell, E.N., A.E. Kisielewski, J.W. Pike, H.L. Franco, H.H. Yao, and K.J. Johnson. 2012. A transcriptome-wide screen for mRNAs enriched in fetal Leydig cells: CRHR1 agonism stimulates rat and mouse fetal testis steroidogenesis. *PloS one*. 7:e47359.

McEwan, D.G., D. Popovic, A. Gubas, S. Terawaki, H. Suzuki, D. Stadel, F.P. Coxon, D. Miranda de Stegmann, S. Bhogaraju, K. Maddi, A. Kirchof, E. Gatti, M.H. Helfrich, S. Wakatsuki, C. Behrends, P. Pierre, and I. Dikic. 2015. PLEKHM1 regulates autophagosome-lysosome fusion through HOPS complex and LC3/GABARAP proteins. *Molecular cell*. 57:39-54.

McLelland, G.L., S.A. Lee, H.M. McBride, and E.A. Fon. 2016. Syntaxin-17 delivers PINK1/parkin-dependent mitochondrial vesicles to the endolysosomal system. *The Journal of cell biology*.

McLelland, G.L., V. Soubannier, C.X. Chen, H.M. McBride, and E.A. Fon. 2014. Parkin and PINK1 function in a vesicular trafficking pathway regulating mitochondrial quality control. *The EMBO journal*. 33:282-295.

McPherson, P.S., E.P. Garcia, V.I. Slepnev, C. David, X. Zhang, D. Grabs, W.S. Sossin, R. Bauerfeind, Y. Nemoto, and P. De Camilli. 1996. A presynaptic inositol-5-phosphatase. *Nature*. 379:353-357.

McRae-Degueurce, A., L. Rosengren, K. Haglid, S. Booj, C.G. Gottfries, A.C. Granerus, and A. Dahlstrom. 1988. Immunocytochemical investigations on the presence of neuron-specific antibodies in the CSF of Parkinson's disease cases. *Neurochem Res*. 13:679-684.

Medina, D.L., S. Di Paola, I. Peluso, A. Armani, D. De Stefani, R. Venditti, S. Montefusco, A. Scotto-Rosato, C. Prezioso, A. Forrester, C. Settembre, W. Wang, Q. Gao, H. Xu, M. Sandri, R. Rizzuto, M.A. De Matteis, and A. Ballabio. 2015. Lysosomal calcium signalling regulates autophagy through calcineurin and TFEB. *Nature cell biology*. 17:288-299.

Meerang, M., D. Ritz, S. Paliwal, Z. Garajova, M. Bosshard, N. Mailand, P. Janscak, U. Hubscher, H. Meyer, and K. Ramadan. 2011. The ubiquitin-selective segregase VCP/p97 orchestrates the response to DNA double-strand breaks. *Nature cell biology*. 13:1376-1382.

Meiser, J., S. Delcambre, A. Wegner, C. Jager, J. Ghelfi, A.F. d'Herouel, X. Dong, D. Weindl, C. Stautner, Y. Nonnenmacher, A. Michelucci, O. Popp, F. Giesert, S. Schildknecht, L. Kramer, J.G. Schneider, D. Woitalla, W. Wurst, A. Skupin, D.M. Weisenhorn, R. Kruger, M. Leist, and K. Hiller. 2016. Loss of DJ-1 impairs antioxidant response by altered glutamine and serine metabolism. *Neurobiology of disease*. 89:112-125.

Meissner, C., H. Lorenz, A. Weihofen, D.J. Selkoe, and M.K. Lemberg. 2011. The mitochondrial intramembrane protease PARL cleaves human Pink1 to regulate Pink1 trafficking. *Journal of neurochemistry*. 117:856-867.

Metzger, M.B., V.A. Hristova, and A.M. Weissman. 2012. HECT and RING finger families of E3 ubiquitin ligases at a glance. *Journal of cell science*. 125:531-537.

Meulener, M.C., K. Xu, L. Thomson, H. Ischiropoulos, and N.M. Bonini. 2006. Mutational analysis of DJ-1 in Drosophila implicates functional inactivation by oxidative damage and aging. *Proceedings of the National Academy of Sciences of the United States of America*. 103:12517-12522.

Mim, C., H. Cui, J.A. Gawronski-Salerno, A. Frost, E. Lyman, G.A. Voth, and V.M. Unger. 2012. Structural basis of membrane bending by the N-BAR protein endophilin. *Cell*. 149:137-145.

Mironova, G.D., M. Baumann, O. Kolomytkin, Z. Krasichkova, A. Berdimuratov, T. Sirota, I. Virtanen, and N.E. Saris. 1994. Purification of the channel component of the mitochondrial calcium uniporter and its reconstitution into planar lipid bilayers. *J Bioenerg Biomembr*. 26:231-238.

Mishra, P., V. Carelli, G. Manfredi, and D.C. Chan. 2014. Proteolytic cleavage of Opa1 stimulates mitochondrial inner membrane fusion and couples fusion to oxidative phosphorylation. *Cell metabolism*. 19:630-641.

Mishra, P., and D.C. Chan. 2016. Metabolic regulation of mitochondrial dynamics. *The Journal of cell biology*. 212:379-387.

Mizuno, N., C.C. Jao, R. Langen, and A.C. Steven. 2010. Multiple modes of endophilin-mediated conversion of lipid vesicles into coated tubes: implications for synaptic endocytosis. *The Journal of biological chemistry*. 285:23351-23358.

Mizushima, N., T. Yoshimori, and B. Levine. 2010. Methods in mammalian autophagy research. *Cell*. 140:313-326.

Mohan, M., and G.D. Mellick. 2016. Role of the VPS35 D620N mutation in Parkinson's disease. *Parkinsonism Relat Disord*.

Moore, A.S., and E.L. Holzbaur. 2016. Dynamic recruitment and activation of ALS-associated TBK1 with its target optineurin are required for efficient mitophagy. *Proceedings of the National Academy of Sciences of the United States of America*. 113:E3349-3358.

Morais, V.A., D. Haddad, K. Craessaerts, P.J. De Bock, J. Swerts, S. Vilain, L. Aerts, L. Overbergh, A. Grunewald, P. Seibler, C. Klein, K. Gevaert, P. Verstreken, and B. De Strooper. 2014. PINK1 loss-of-function mutations affect mitochondrial complex I activity via NdufA10 ubiquinone uncoupling. *Science*. 344:203-207.

Morais, V.A., P. Verstreken, A. Roethig, J. Smet, A. Snellinx, M. Vanbrabant, D. Haddad, C. Frezza, W. Mandemakers, D. Vogt-Weisenhorn, R. Van Coster, W. Wurst, L. Scorrano, and B. De Strooper. 2009. Parkinson's disease mutations in PINK1 result in decreased Complex I activity and deficient synaptic function. *EMBO Mol Med*. 1:99-111.

Mori, H., T. Kondo, M. Yokochi, H. Matsumine, Y. Nakagawa-Hattori, T. Miyake, K. Suda, and Y. Mizuno. 1998. Pathologic and biochemical studies of juvenile parkinsonism linked to chromosome 6q. *Neurology*. 51:890-892.

Mortiboys, H., K.K. Johansen, J.O. Aasly, and O. Bandmann. 2010. Mitochondrial impairment in patients with Parkinson disease with the G2019S mutation in LRRK2. *Neurology*. 75:2017-2020.

Mortiboys, H., K.J. Thomas, W.J. Koopman, S. Klaffke, P. Abou-Sleiman, S. Olpin, N.W. Wood, P.H. Willems, J.A. Smeitink, M.R. Cookson, and O. Bandmann. 2008. Mitochondrial function and morphology are impaired in parkin-mutant fibroblasts. *Annals of neurology*. 64:555-565.

Mosley, R.L., J.A. Hutter-Saunders, D.K. Stone, and H.E. Gendelman. 2012. Inflammation and adaptive immunity in Parkinson's disease. *Cold Spring Harbor perspectives in medicine*. 2:a009381.

Mozdy, A.D., J.M. McCaffery, and J.M. Shaw. 2000. Dnm1p GTPase-mediated mitochondrial fission is a multi-step process requiring the novel integral membrane component Fis1p. *The Journal of cell biology*. 151:367-380.

Muftuoglu, M., B. Elibol, O. Dalmizrak, A. Ercan, G. Kulaksiz, H. Ogus, T. Dalkara, and N. Ozer. 2004. Mitochondrial complex I and IV activities in leukocytes from patients with parkin mutations. *Movement disorders : official journal of the Movement Disorder Society*. 19:544-548.

Muller, H.J. 1964. The Relation of Recombination to Mutational Advance. *Mutat Res*. 106:2-9.

Murakami, Y., S. Matsufuji, T. Kameji, S. Hayashi, K. Igarashi, T. Tamura, K. Tanaka, and A. Ichihara. 1992. Ornithine decarboxylase is degraded by the 26S proteasome without ubiquitination. *Nature*. 360:597-599.

Murakawa, T., O. Yamaguchi, A. Hashimoto, S. Hikoso, T. Takeda, T. Oka, H. Yasui, H. Ueda, Y. Akazawa, H. Nakayama, M. Taneike, T. Misaka, S. Omiya, A.M. Shah, A. Yamamoto, K. Nishida, Y. Ohsumi, K. Okamoto, Y. Sakata, and K. Otsu. 2015. Bcl-2-like protein 13

is a mammalian Atg32 homologue that mediates mitophagy and mitochondrial fragmentation. *Nature communications*. 6:7527.

Murley, A., R.D. Sarsam, A. Toulmay, J. Yamada, W.A. Prinz, and J. Nunnari. 2015. Ltc1 is an ER-localized sterol transporter and a component of ER-mitochondria and ER-vacuole contacts. *The Journal of cell biology*. 209:539-548.

Nagatsua, T., and M. Sawadab. 2009. L-dopa therapy for Parkinson's disease: past, present, and future. *Parkinsonism Relat Disord*. 15 Suppl 1:S3-8.

Nakamura, K., V.M. Nemani, F. Azarbal, G. Skibinski, J.M. Levy, K. Egami, L. Munishkina, J. Zhang, B. Gardner, J. Wakabayashi, H. Sesaki, Y. Cheng, S. Finkbeiner, R.L. Nussbaum, E. Masliah, and R.H. Edwards. 2011. Direct membrane association drives mitochondrial fission by the Parkinson disease-associated protein alpha-synuclein. *The Journal of biological chemistry*. 286:20710-20726.

Nakamura, K., V.M. Nemani, E.K. Wallender, K. Kaehlcke, M. Ott, and R.H. Edwards. 2008. Optical reporters for the conformation of alpha-synuclein reveal a specific interaction with mitochondria. *The Journal of neuroscience : the official journal of the Society for Neuroscience*. 28:12305-12317.

Nalls, M.A., N. Pankratz, C.M. Lill, C.B. Do, D.G. Hernandez, M. Saad, A.L. DeStefano, E. Kara, J. Bras, M. Sharma, C. Schulte, M.F. Keller, S. Arepalli, C. Letson, C. Edsall, H. Stefansson, X. Liu, H. Pliner, J.H. Lee, R. Cheng, C. International Parkinson's Disease Genomics, G.I. Parkinson's Study Group Parkinson's Research: The Organized, andMe, GenePd, C. NeuroGenetics Research, G. Hussman Institute of Human, I. Ashkenazi Jewish Dataset, H. Cohorts for, E. Aging Research in Genetic, C. North American Brain Expression, C. United Kingdom Brain Expression, C. Greek Parkinson's Disease, G. Alzheimer Genetic Analysis, M.A. Ikram, J.P. Ioannidis, G.M. Hadjigeorgiou, J.C. Bis, M. Martinez, J.S. Perlmutter, A. Goate, K. Marder, B. Fiske, M. Sutherland, G. Xiromerisiou, R.H. Myers, L.N. Clark, K. Stefansson, J.A. Hardy, P. Heutink, H. Chen, N.W. Wood, H. Houlden, H. Payami, A. Brice, W.K. Scott, T. Gasser, L. Bertram, N. Eriksson, T. Foroud, and A.B. Singleton. 2014. Large-scale meta-analysis of genome-wide association data identifies six new risk loci for Parkinson's disease. *Nature genetics*. 46:989-993.

Naon, D., and L. Scorrano. 2014. At the right distance: ER-mitochondria juxtaposition in cell life and death. *Biochimica et biophysica acta*. 1843:2184-2194.

Naon, D., M. Zaninello, M. Giacomello, T. Varanita, F. Grespi, S. Lakshminaranayan, A. Serafini, M. Semenzato, S. Herkenne, M.I. Hernandez-Alvarez, A. Zorzano, D. De Stefani, G.W. Dorn, 2nd, and L. Scorrano. 2016. Critical reappraisal confirms that Mitofusin 2 is an endoplasmic reticulum-mitochondria tether. *Proceedings of the National Academy of Sciences of the United States of America*.

Narendra, D., L.A. Kane, D.N. Hauser, I.M. Fearnley, and R.J. Youle. 2010a. p62/SQSTM1 is required for Parkin-induced mitochondrial clustering but not mitophagy; VDAC1 is dispensable for both. *Autophagy*. 6:1090-1106.

Narendra, D., A. Tanaka, D.F. Suen, and R.J. Youle. 2008. Parkin is recruited selectively to impaired mitochondria and promotes their autophagy. *The Journal of cell biology*. 183:795-803.

Narendra, D.P., S.M. Jin, A. Tanaka, D.F. Suen, C.A. Gautier, J. Shen, M.R. Cookson, and R.J. Youle. 2010b. PINK1 is selectively stabilized on impaired mitochondria to activate Parkin. *PLoS biology*. 8:e1000298.

Nargund, A.M., C.J. Fiorese, M.W. Pellegrino, P. Deng, and C.M. Haynes. 2015. Mitochondrial and nuclear accumulation of the transcription factor ATFS-1 promotes OXPHOS recovery during the UPR(mt). *Molecular cell*. 58:123-133.

Nargund, A.M., M.W. Pellegrino, C.J. Fiorese, B.M. Baker, and C.M. Haynes. 2012. Mitochondrial import efficiency of ATFS-1 regulates mitochondrial UPR activation. *Science*. 337:587-590.

Neuspiel, M., A.C. Schauss, E. Braschi, R. Zunino, P. Rippstein, R.A. Rachubinski, M.A. Andrade-Navarro, and H.M. McBride. 2008. Cargo-selected transport from the mitochondria to peroxisomes is mediated by vesicular carriers. *Current biology : CB*. 18:102-108.

Neuspiel, M., R. Zunino, S. Gangaraju, P. Rippstein, and H. McBride. 2005. Activated mitofusin 2 signals mitochondrial fusion, interferes with Bax activation, and reduces susceptibility to radical induced depolarization. *Journal of Biological Chemistry*. 280:25060-25070.

Newmeyer, D.D., and S. Ferguson-Miller. 2003. Mitochondria: releasing power for life and unleashing the machineries of death. *Cell*. 112:481-490.

Nezich, C.L., C. Wang, A.I. Fogel, and R.J. Youle. 2015. MiT/TFE transcription factors are activated during mitophagy downstream of Parkin and Atg5. *The Journal of cell biology*. 210:435-450.

Nguyen, T.N., B.S. Padman, J. Usher, V. Oorschot, G. Ramm, and M. Lazarou. 2016. Atg8 family LC3/GABARAP proteins are crucial for autophagosome-lysosome fusion but not autophagosome formation during PINK1/Parkin mitophagy and starvation. *The Journal of cell biology*. 215:857-874.

Nishida, Y., S. Arakawa, K. Fujitani, H. Yamaguchi, T. Mizuta, T. Kanaseki, M. Komatsu, K. Otsu, Y. Tsujimoto, and S. Shimizu. 2009. Discovery of Atg5/Atg7-independent alternative macroautophagy. *Nature*. 461:654-658.

Nishioka, K., S. Hayashi, M.J. Farrer, A.B. Singleton, H. Yoshino, H. Imai, T. Kitami, K. Sato, R. Kuroda, H. Tomiyama, K. Mizoguchi, M. Murata, T. Toda, I. Imoto, J. Inazawa, Y. Mizuno, and N. Hattori. 2006. Clinical heterogeneity of alpha-synuclein gene duplication in Parkinson's disease. *Annals of neurology*. 59:298-309.

Noguchi, M., T. Takata, Y. Kimura, A. Manno, K. Murakami, M. Koike, H. Ohizumi, S. Hori, and A. Kakizuka. 2005. ATPase activity of p97/valosin-containing protein is regulated by oxidative modification of the evolutionally conserved cysteine 522 residue in walker a motif. *Journal of Biological Chemistry*. 280:41332-41341.

Nunnari, J., W.F. Marshall, A. Straight, A. Murray, J.W. Sedat, and P. Walter. 1997. Mitochondrial transmission during mating in Saccharomyces cerevisiae is determined by mitochondrial fusion and fission and the intramitochondrial segregation of mitochondrial DNA. *Molecular biology of the cell*. 8:1233-1242.

Okatsu, K., M. Kimura, T. Oka, K. Tanaka, and N. Matsuda. 2015a. Unconventional PINK1 localization to the outer membrane of depolarized mitochondria drives Parkin recruitment. *Journal of cell science*. 128:964-978.

Okatsu, K., F. Koyano, M. Kimura, H. Kosako, Y. Saeki, K. Tanaka, and N. Matsuda. 2015b. Phosphorylated ubiquitin chain is the genuine Parkin receptor. *The Journal of cell biology*. 209:111-128.

Okatsu, K., T. Oka, M. Iguchi, K. Imamura, H. Kosako, N. Tani, M. Kimura, E. Go, F. Koyano, M. Funayama, K. Shiba-Fukushima, S. Sato, H. Shimizu, Y. Fukunaga, H. Taniguchi, M. Komatsu, N. Hattori, K. Mihara, K. Tanaka, and N. Matsuda. 2012. PINK1

autophosphorylation upon membrane potential dissipation is essential for Parkin recruitment to damaged mitochondria. *Nature communications*. 3:1016.

Okatsu, K., M. Uno, F. Koyano, E. Go, M. Kimura, T. Oka, K. Tanaka, and N. Matsuda. 2013. A dimeric PINK1-containing complex on depolarized mitochondria stimulates Parkin recruitment. *The Journal of biological chemistry*. 288:36372-36384.

Olgiati, S., A. De Rosa, M. Quadri, C. Criscuolo, G.J. Breedveld, M. Picillo, S. Pappata, M. Quarantelli, P. Barone, G. De Michele, and V. Bonifati. 2014. PARK20 caused by SYNJ1 homozygous Arg258Gln mutation in a new Italian family. *Neurogenetics*. 15:183-188.

Olsen, J.H., S. Friis, and K. Frederiksen. 2006. Malignant melanoma and other types of cancer preceding Parkinson disease. *Epidemiology*. 17:582-587.

Ordureau, A., J.M. Heo, D.M. Duda, J.A. Paulo, J.L. Olszewski, D. Yanishevski, J. Rinehart, B.A. Schulman, and J.W. Harper. 2015. Defining roles of PARKIN and ubiquitin phosphorylation by PINK1 in mitochondrial quality control using a ubiquitin replacement strategy. *Proceedings of the National Academy of Sciences of the United States of America*. 112:6637-6642.

Ordureau, A., S.A. Sarraf, D.M. Duda, J.M. Heo, M.P. Jedrychowski, V.O. Sviderskiy, J.L. Olszewski, J.T. Koerber, T. Xie, S.A. Beausoleil, J.A. Wells, S.P. Gygi, B.A. Schulman, and J.W. Harper. 2014. Quantitative proteomics reveal a feedforward mechanism for mitochondrial PARKIN translocation and ubiquitin chain synthesis. *Molecular cell*. 56:360-375.

Ortiz-Sandoval, C.G., S.C. Hughes, J.B. Dacks, and T. Simmen. 2014. Interaction with the effector dynamin-related protein 1 (Drp1) is an ancient function of Rab32 subfamily proteins. *Cell Logist*. 4:e986399.

Osellame, L.D., A.P. Singh, D.A. Stroud, C.S. Palmer, D. Stojanovski, R. Ramachandran, and M.T. Ryan. 2016. Cooperative and independent roles of the Drp1 adaptors Mff, MiD49 and MiD51 in mitochondrial fission. *Journal of cell science*. 129:2170-2181.

Ossig, R., H.D. Schmitt, B. de Groot, D. Riedel, S. Keranen, H. Ronne, H. Grubmuller, and R. Jahn. 2000. Exocytosis requires asymmetry in the central layer of the SNARE complex. *The EMBO journal*. 19:6000-6010.

Otsuga, D., B.R. Keegan, E. Brisch, J.W. Thatcher, G.J. Hermann, W. Bleazard, and J.M. Shaw. 1998. The dynamin-related GTPase, Dnm1p, controls mitochondrial morphology in yeast. *The Journal of cell biology*. 143:333-349.

Oxenoid, K., Y. Dong, C. Cao, T. Cui, Y. Sancak, A.L. Markhard, Z. Grabarek, L. Kong, Z. Liu, B. Ouyang, Y. Cong, V.K. Mootha, and J.J. Chou. 2016. Architecture of the mitochondrial calcium uniporter. *Nature*. 533:269-273.

Paillusson, S., P. Gomez-Suaga, R. Stoica, D. Little, P. Gissen, M.J. Devine, W. Noble, D.P. Hanger, and C.C.J. Miller. 2017. alpha-Synuclein binds to the ER-mitochondria tethering protein VAPB to disrupt Ca2+ homeostasis and mitochondrial ATP production. *Acta neuropathologica*. 134:129-149.

Paisan-Ruiz, C., S. Jain, E.W. Evans, W.P. Gilks, J. Simon, M. van der Brug, A. Lopez de Munain, S. Aparicio, A.M. Gil, N. Khan, J. Johnson, J.R. Martinez, D. Nicholl, I.M. Carrera, A.S. Pena, R. de Silva, A. Lees, J.F. Marti-Masso, J. Perez-Tur, N.W. Wood, and A.B. Singleton. 2004. Cloning of the gene containing mutations that cause PARK8-linked Parkinson's disease. *Neuron*. 44:595-600.

Palacino, J.J., D. Sagi, M.S. Goldberg, S. Krauss, C. Motz, M. Wacker, J. Klose, and J. Shen. 2004. Mitochondrial dysfunction and oxidative damage in parkin-deficient mice. *The Journal of biological chemistry*. 279:18614-18622.

Palade, G. 1975. Intracellular aspects of the process of protein synthesis. *Science*. 189:867.

Palade, G.E. 1952. The fine structure of mitochondria. *Anat Rec*. 114:427-451.

Palade, G.E. 1953. An electron microscope study of the mitochondrial structure. *J Histochem Cytochem*. 1:188-211.

Palmieri, M., S. Impey, H. Kang, A. di Ronza, C. Pelz, M. Sardiello, and A. Ballabio. 2011. Characterization of the CLEAR network reveals an integrated control of cellular clearance pathways. *Human molecular genetics*. 20:3852-3866.

Papinski, D., M. Schuschnig, W. Reiter, L. Wilhelm, C.A. Barnes, A. Maiolica, I. Hansmann, T. Pfaffenwimmer, M. Kijanska, I. Stoffel, S.S. Lee, A. Brezovich, J.H. Lou, B.E. Turk, R. Aebersold, G. Ammerer, M. Peter, and C. Kraft. 2014. Early steps in autophagy depend on direct phosphorylation of Atg9 by the Atg1 kinase. *Molecular cell*. 53:471-483.

Park, J., S.B. Lee, S. Lee, Y. Kim, S. Song, S. Kim, E. Bae, J. Kim, M. Shong, J.M. Kim, and J. Chung. 2006. Mitochondrial dysfunction in Drosophila PINK1 mutants is complemented by parkin. *Nature*. 441:1157-1161.

Park, J.S., S. Halegoua, S. Kishida, and A.M. Neiman. 2015a. A conserved function in phosphatidylinositol metabolism for mammalian Vps13 family proteins. *PloS one*. 10:e0124836.

Park, J.S., M.K. Thorsness, R. Policastro, L.L. McGoldrick, N.M. Hollingsworth, P.E. Thorsness, and A.M. Neiman. 2016. Yeast Vps13 promotes mitochondrial function and is localized at membrane contact sites. *Molecular biology of the cell*. 27:2435-2449.

Park, S., S.G. Choi, S.M. Yoo, J. Nah, E. Jeong, H. Kim, and Y.K. Jung. 2015b. Pyruvate stimulates mitophagy via PINK1 stabilization. *Cell Signal*. 27:1824-1830.

Parkinson, J. 1817. Essay on the Shaking Palsy. Sherwood, Neely and Jones, London. 88 pp.

Passmore, L.A., C.R. Booth, C. Venien-Bryan, S.J. Ludtke, C. Fioretto, L.N. Johnson, W. Chiu, and D. Barford. 2005. Structural analysis of the anaphase-promoting complex reveals multiple active sites and insights into polyubiquitylation. *Molecular cell*. 20:855-866.

Paupe, V., J. Prudent, E.P. Dassa, O.Z. Rendon, and E.A. Shoubridge. 2015. CCDC90A (MCUR1) is a cytochrome c oxidase assembly factor and not a regulator of the mitochondrial calcium uniporter. *Cell metabolism*. 21:109-116.

Pekkurnaz, G., J.C. Trinidad, X. Wang, D. Kong, and T.L. Schwarz. 2014. Glucose regulates mitochondrial motility via Milton modification by O-GlcNAc transferase. *Cell*. 158:54-68.

Pena-Llopis, S., S. Vega-Rubin-de-Celis, J.C. Schwartz, N.C. Wolff, T.A. Tran, L. Zou, X.J. Xie, D.R. Corey, and J. Brugarolas. 2011. Regulation of TFEB and V-ATPases by mTORC1. *The EMBO journal*. 30:3242-3258.

Perez, F.A., and R.D. Palmiter. 2005. Parkin-deficient mice are not a robust model of parkinsonism. *Proceedings of the National Academy of Sciences of the United States of America*. 102:2174-2179.

Perier, C., A. Bender, E. Garcia-Arumi, M.J. Melia, J. Bove, C. Laub, T. Klopstock, M. Elstner, R.B. Mounsey, P. Teismann, T. Prolla, A.L. Andreu, and M. Vila. 2013. Accumulation of mitochondrial DNA deletions within dopaminergic neurons triggers neuroprotective mechanisms. *Brain : a journal of neurology*. 136:2369-2378.

Periquet, M., O. Corti, S. Jacquier, and A. Brice. 2005. Proteomic analysis of parkin knockout mice: alterations in energy metabolism, protein handling and synaptic function. *Journal of neurochemistry*. 95:1259-1276.

Petit, A., T. Kawarai, E. Paitel, N. Sanjo, M. Maj, M. Scheid, F. Chen, Y. Gu, H. Hasegawa, S. Salehi-Rad, L. Wang, E. Rogaeva, P. Fraser, B. Robinson, P. St George-Hyslop, and A. Tandon. 2005. Wild-type PINK1 prevents basal and induced neuronal apoptosis, a protective effect abrogated by Parkinson disease-related mutations. *The Journal of biological chemistry*. 280:34025-34032.

Phillips, M.J., and G.K. Voeltz. 2016. Structure and function of ER membrane contact sites with other organelles. *Nature reviews. Molecular cell biology*. 17:69-82.

Pickrell, A.M., C.H. Huang, S.R. Kennedy, A. Ordureau, D.P. Sideris, J.G. Hoekstra, J.W. Harper, and R.J. Youle. 2015. Endogenous Parkin Preserves Dopaminergic Substantia Nigral Neurons following Mitochondrial DNA Mutagenic Stress. *Neuron*. 87:371-381.

Pitts, K.R., Y. Yoon, E.W. Krueger, and M.A. McNiven. 1999. The dynamin-like protein DLP1 is essential for normal distribution and morphology of the endoplasmic reticulum and mitochondria in mammalian cells. *Molecular biology of the cell*. 10:4403-4417.

Poewe, W., K. Seppi, C.M. Tanner, G.M. Halliday, P. Brundin, J. Volkmann, A.E. Schrag, and A.E. Lang. 2017. Parkinson disease. *Nat Rev Dis Primers*. 3:17013.

Pogson, J.H., R.M. Ivatt, A. Sanchez-Martinez, R. Tufi, E. Wilson, H. Mortiboys, and A.J. Whitworth. 2014. The complex I subunit NDUFA10 selectively rescues Drosophila pink1 mutants through a mechanism independent of mitophagy. *PLoS genetics*. 10:e1004815.

Poirier, M.A., J.C. Hao, P.N. Malkus, C. Chan, M.F. Moore, D.S. King, and M.K. Bennett. 1998. Protease resistance of syntaxin.SNAP-25.VAMP complexes. Implications for assembly and structure. *The Journal of biological chemistry*. 273:11370-11377.

Polson, H.E., J. de Lartigue, D.J. Rigden, M. Reedijk, S. Urbe, M.J. Clague, and S.A. Tooze. 2010. Mammalian Atg18 (WIPI2) localizes to omegasome-anchored phagophores and positively regulates LC3 lipidation. *Autophagy*. 6:506-522.

Polymeropoulos, M.H., C. Lavedan, E. Leroy, S.E. Ide, A. Dehejia, A. Dutra, B. Pike, H. Root, J. Rubenstein, R. Boyer, E.S. Stenroos, S. Chandrasekharappa, A. Athanassiadou, T. Papapetropoulos, W.G. Johnson, A.M. Lazzarini, R.C. Duvoisin, G. Di Iorio, L.I. Golbe, and R.L. Nussbaum. 1997. Mutation in the alpha-synuclein gene identified in families with Parkinson's disease. *Science*. 276:2045-2047.

Poole, A.C., R.E. Thomas, L.A. Andrews, H.M. McBride, A.J. Whitworth, and L.J. Pallanck. 2008. The PINK1/Parkin pathway regulates mitochondrial morphology. *Proceedings of the National Academy of Sciences of the United States of America*. 105:1638-1643.

Poole, A.C., R.E. Thomas, S. Yu, E.S. Vincow, and L. Pallanck. 2010. The mitochondrial fusion-promoting factor mitofusin is a substrate of the PINK1/parkin pathway. *PloS one*. 5:e10054.

Popovic, D., and I. Dikic. 2014. TBC1D5 and the AP2 complex regulate ATG9 trafficking and initiation of autophagy. *EMBO reports*. 15:392-401.

Praefcke, G.J., and H.T. McMahon. 2004. The dynamin superfamily: universal membrane tubulation and fission molecules? *Nature reviews. Molecular cell biology*. 5:133-147.

Pridgeon, J.W., J.A. Olzmann, L.S. Chin, and L. Li. 2007. PINK1 protects against oxidative stress by phosphorylating mitochondrial chaperone TRAP1. *PLoS biology*. 5:e172.

Prudent, J., R. Zunino, A. Sugiura, S. Mattie, G.C. Shore, and H.M. McBride. 2015. MAPL SUMOylation of Drp1 Stabilizes an ER/Mitochondrial Platform Required for Cell Death. *Molecular cell*. 59:941-955.

Puglielli, L., B.C. Ellis, L.A. Ingano, and D.M. Kovacs. 2004. Role of acyl-coenzyme a: cholesterol acyltransferase activity in the processing of the amyloid precursor protein. *J Mol Neurosci*. 24:93-96.

Puglielli, L., G. Konopka, E. Pack-Chung, L.A. Ingano, O. Berezovska, B.T. Hyman, T.Y. Chang, R.E. Tanzi, and D.M. Kovacs. 2001. Acyl-coenzyme A: cholesterol acyltransferase modulates the generation of the amyloid beta-peptide. *Nature cell biology*. 3:905-912.

Puri, C., M. Renna, C.F. Bento, K. Moreau, and D.C. Rubinsztein. 2013. Diverse autophagosome membrane sources coalesce in recycling endosomes. *Cell*. 154:1285-1299.

Pyle, A., H. Anugrha, M. Kurzawa-Akanbi, A. Yarnall, D. Burn, and G. Hudson. 2016. Reduced mitochondrial DNA copy number is a biomarker of Parkinson's disease. *Neurobiology of aging*. 38:216 e217-210.

Qi, Y., L. Yan, C. Yu, X. Guo, X. Zhou, X. Hu, X. Huang, Z. Rao, Z. Lou, and J. Hu. 2016. Structures of human mitofusin 1 provide insight into mitochondrial tethering. *The Journal of cell biology*. 215:621-629.

Quadri, M., M. Fang, M. Picillo, S. Olgiati, G.J. Breedveld, J. Graafland, B. Wu, F. Xu, R. Erro, M. Amboni, S. Pappata, M. Quarantelli, G. Annesi, A. Quattrone, H.F. Chien, E.R. Barbosa, N. International Parkinsonism Genetics, B.A. Oostra, P. Barone, J. Wang, and V. Bonifati. 2013. Mutation in the SYNJ1 gene associated with autosomal recessive, early-onset Parkinsonism. *Hum Mutat*. 34:1208-1215.

Ragusa, M.J., R.E. Stanley, and J.H. Hurley. 2012. Architecture of the Atg17 complex as a scaffold for autophagosome biogenesis. *Cell*. 151:1501-1512.

Rakovic, A., A. Grunewald, J. Kottwitz, N. Bruggemann, P.P. Pramstaller, K. Lohmann, and C. Klein. 2011. Mutations in PINK1 and Parkin impair ubiquitination of Mitofusins in human fibroblasts. *PloS one*. 6:e16746.

Rakovic, A., K. Shurkewitsch, P. Seibler, A. Grunewald, A. Zanon, J. Hagenah, D. Krainc, and C. Klein. 2013. Phosphatase and tensin homolog (PTEN)-induced putative kinase 1 (PINK1)-dependent ubiquitination of endogenous Parkin attenuates mitophagy: study in human primary fibroblasts and induced pluripotent stem cell-derived neurons. *The Journal of biological chemistry*. 288:2223-2237.

Ramirez, A., A. Heimbach, J. Grundemann, B. Stiller, D. Hampshire, L.P. Cid, I. Goebel, A.F. Mubaidin, A.L. Wriekat, J. Roeper, A. Al-Din, A.M. Hillmer, M. Karsak, B. Liss, C.G. Woods, M.I. Behrens, and C. Kubisch. 2006. Hereditary parkinsonism with dementia is caused by mutations in ATP13A2, encoding a lysosomal type 5 P-type ATPase. *Nature genetics*. 38:1184-1191.

Raturi, A., T. Gutierrez, C. Ortiz-Sandoval, A. Ruangkittisakul, M.S. Herrera-Cruz, J.P. Rockley, K. Gesson, D. Ourdev, P.H. Lou, E. Lucchinetti, N. Tahbaz, M. Zaugg, S. Baksh, K. Ballanyi, and T. Simmen. 2016. TMX1 determines cancer cell metabolism as a thiol-based modulator of ER-mitochondria Ca2+ flux. *The Journal of cell biology*. 214:433-444.

Rauckhorst, A.J., D.R. Pfeiffer, and K.M. Broekemeier. 2015. The iPLA(2)gamma is identified as the membrane potential sensitive phospholipase in liver mitochondria. *FEBS letters*. 589:2367-2371.

Reeve, A.K., M.H. Ludtmann, P.R. Angelova, E.M. Simcox, M.H. Horrocks, D. Klenerman, S. Gandhi, D.M. Turnbull, and A.Y. Abramov. 2015. Aggregated alpha-synuclein and

complex I deficiency: exploration of their relationship in differentiated neurons. *Cell Death Dis*. 6:e1820.

Reggiori, F., and D.J. Klionsky. 2013. Autophagic processes in yeast: mechanism, machinery and regulation. *Genetics*. 194:341-361.

Reggiori, F., and C. Ungermann. 2017. Autophagosome Maturation and Fusion. *Journal of molecular biology*. 429:486-496.

Reitzer, L.J., B.M. Wice, and D. Kennell. 1979. Evidence that glutamine, not sugar, is the major energy source for cultured HeLa cells. *The Journal of biological chemistry*. 254:2669-2676.

Renard, H.F., M. Simunovic, J. Lemiere, E. Boucrot, M.D. Garcia-Castillo, S. Arumugam, V. Chambon, C. Lamaze, C. Wunder, A.K. Kenworthy, A.A. Schmidt, H.T. McMahon, C. Sykes, P. Bassereau, and L. Johannes. 2015. Endophilin-A2 functions in membrane scission in clathrin-independent endocytosis. *Nature*. 517:493-496.

Richardson, L.G., E.A. Clendening, H. Sheen, S.K. Gidda, K.A. White, and R.T. Mullen. 2014. A unique N-terminal sequence in the Carnation Italian ringspot virus p36 replicase-associated protein interacts with the host cell ESCRT-I component Vps23. *Journal of virology*. 88:6329-6344.

Richter, B., D.A. Sliter, L. Herhaus, A. Stolz, C. Wang, P. Beli, G. Zaffagnini, P. Wild, S. Martens, S.A. Wagner, R.J. Youle, and I. Dikic. 2016. Phosphorylation of OPTN by TBK1 enhances its binding to Ub chains and promotes selective autophagy of damaged mitochondria. *Proceedings of the National Academy of Sciences of the United States of America*. 113:4039-4044.

Riley, B.E., J.C. Lougheed, K. Callaway, M. Velasquez, E. Brecht, L. Nguyen, T. Shaler, D. Walker, Y. Yang, K. Regnstrom, L. Diep, Z. Zhang, S. Chiou, M. Bova, D.R. Artis, N. Yao, J. Baker, T. Yednock, and J.A. Johnston. 2013. Structure and function of Parkin E3 ubiquitin ligase reveals aspects of RING and HECT ligases. *Nature communications*. 4:1982.

Rogers, M.A., J. Liu, B.L. Song, B.L. Li, C.C. Chang, and T.Y. Chang. 2015. Acyl-CoA:cholesterol acyltransferases (ACATs/SOATs): Enzymes with multiple sterols as substrates and as activators. *J Steroid Biochem Mol Biol*. 151:102-107.

Rogov, V., V. Dotsch, T. Johansen, and V. Kirkin. 2014. Interactions between autophagy receptors and ubiquitin-like proteins form the molecular basis for selective autophagy. *Molecular cell*. 53:167-178.

Rosenbloom, A.B., S.H. Lee, M. To, A. Lee, J.Y. Shin, and C. Bustamante. 2014. Optimized two-color super resolution imaging of Drp1 during mitochondrial fission with a slow-switching Dronpa variant. *Proceedings of the National Academy of Sciences of the United States of America*. 111:13093-13098.

Rosenbloom, K.R., J. Armstrong, G.P. Barber, J. Casper, H. Clawson, M. Diekhans, T.R. Dreszer, P.A. Fujita, L. Guruvadoo, M. Haeussler, R.A. Harte, S. Heitner, G. Hickey, A.S. Hinrichs, R. Hubley, D. Karolchik, K. Learned, B.T. Lee, C.H. Li, K.H. Miga, N. Nguyen, B. Paten, B.J. Raney, A.F. Smit, M.L. Speir, A.S. Zweig, D. Haussler, R.M. Kuhn, and W.J. Kent. 2015. The UCSC Genome Browser database: 2015 update. *Nucleic Acids Res*. 43:D670-681.

Ross, O.A., A.T. Braithwaite, L.M. Skipper, J. Kachergus, M.M. Hulihan, F.A. Middleton, K. Nishioka, J. Fuchs, T. Gasser, D.M. Maraganore, C.H. Adler, L. Larvor, M.C. Chartier-Harlin, C. Nilsson, J.W. Langston, K. Gwinn, N. Hattori, and M.J. Farrer. 2008. Genomic

investigation of alpha-synuclein multiplication and parkinsonism. *Annals of neurology*. 63:743-750.

Rostovtseva, T.K., H. Boukari, A. Antignani, B. Shiu, S. Banerjee, A. Neutzner, and R.J. Youle. 2009. Bax activates endophilin B1 oligomerization and lipid membrane vesiculation. *The Journal of biological chemistry*. 284:34390-34399.

Rothman, J.E. 2014. The principle of membrane fusion in the cell (Nobel lecture). *Angewandte Chemie*. 53:12676-12694.

Rugarli, E.I., and T. Langer. 2012. Mitochondrial quality control: a matter of life and death for neurons. *The EMBO journal*. 31:1336-1349.

Russell, R.C., Y. Tian, H. Yuan, H.W. Park, Y.Y. Chang, J. Kim, H. Kim, T.P. Neufeld, A. Dillin, and K.L. Guan. 2013. ULK1 induces autophagy by phosphorylating Beclin-1 and activating VPS34 lipid kinase. *Nature cell biology*. 15:741-750.

Ryan, B.J., S. Hoek, E.A. Fon, and R. Wade-Martins. 2015. Mitochondrial dysfunction and mitophagy in Parkinson's: from familial to sporadic disease. *Trends in biochemical sciences*. 40:200-210.

Rzepnikowska, W., K. Flis, J. Kaminska, M. Grynberg, A. Urbanek, K.R. Ayscough, and T. Zoladek. 2017. Amino acid substitution equivalent to human chorea-acanthocytosis I2771R in yeast Vps13 protein affects its binding to phosphatidylinositol 3-phosphate. *Human molecular genetics*. 26:1497-1510.

Sacks, O. 1983. The origin of "Awakenings". *Br Med J (Clin Res Ed)*. 287:1968-1969.

Safadi, S.S., and G.S. Shaw. 2007. A disease state mutation unfolds the parkin ubiquitin-like domain. *Biochemistry*. 46:14162-14169.

Safadi, S.S., and G.S. Shaw. 2010. Differential interaction of the E3 ligase parkin with the proteasomal subunit S5a and the endocytic protein Eps15. *The Journal of biological chemistry*. 285:1424-1434.

Sakata, E., Y. Yamaguchi, E. Kurimoto, J. Kikuchi, S. Yokoyama, S. Yamada, H. Kawahara, H. Yokosawa, N. Hattori, Y. Mizuno, K. Tanaka, and K. Kato. 2003. Parkin binds the Rpn10 subunit of 26S proteasomes through its ubiquitin-like domain. *EMBO reports*. 4:301-306.

Sancak, Y., L. Bar-Peled, R. Zoncu, A.L. Markhard, S. Nada, and D.M. Sabatini. 2010. Ragulator-Rag complex targets mTORC1 to the lysosomal surface and is necessary for its activation by amino acids. *Cell*. 141:290-303.

Sandebring, A., N. Dehvari, M. Perez-Manso, K.J. Thomas, E. Karpilovski, M.R. Cookson, R.F. Cowburn, and A. Cedazo-Minguez. 2009. Parkin deficiency disrupts calcium homeostasis by modulating phospholipase C signalling. *The FEBS journal*. 276:5041-5052.

Sandoval, H., C.K. Yao, K. Chen, M. Jaiswal, T. Donti, Y.Q. Lin, V. Bayat, B. Xiong, K. Zhang, G. David, W.L. Charng, S. Yamamoto, L. Duraine, B.H. Graham, and H.J. Bellen. 2014. Mitochondrial fusion but not fission regulates larval growth and synaptic development through steroid hormone production. *eLife*. 3.

Sardiello, M., and A. Ballabio. 2009. Lysosomal enhancement: a CLEAR answer to cellular degradative needs. *Cell Cycle*. 8:4021-4022.

Sarraf, S.A., M. Raman, V. Guarani-Pereira, M.E. Sowa, E.L. Huttlin, S.P. Gygi, and J.W. Harper. 2013. Landscape of the PARKIN-dependent ubiquitylome in response to mitochondrial depolarization. *Nature*. 496:372-376.

Sauve, V., A. Lilov, M. Seirafi, M. Vranas, S. Rasool, G. Kozlov, T. Sprules, J. Wang, J.F. Trempe, and K. Gehring. 2015. A Ubl/ubiquitin switch in the activation of Parkin. *The EMBO journal*. 34:2492-2505.

Sazanov, L.A. 2015. A giant molecular proton pump: structure and mechanism of respiratory complex I. *Nature reviews. Molecular cell biology*. 16:375-388.

Schafer, I.B., G.G. Hesketh, N.A. Bright, S.R. Gray, P.R. Pryor, P.R. Evans, J.P. Luzio, and D.J. Owen. 2012. The binding of Varp to VAMP7 traps VAMP7 in a closed, fusogenically inactive conformation. *Nature structural & molecular biology*. 19:1300-1309.

Schapira, A.H., J.M. Cooper, D. Dexter, P. Jenner, J.B. Clark, and C.D. Marsden. 1989. Mitochondrial complex I deficiency in Parkinson's disease. *Lancet*. 1:1269.

Schatton, D., D. Pla-Martin, M.C. Marx, H. Hansen, A. Mourier, I. Nemazanyy, A. Pessia, P. Zentis, T. Corona, V. Kondylis, E. Barth, A.C. Schauss, V. Velagapudi, and E.I. Rugarli. 2017. CLUH regulates mitochondrial metabolism by controlling translation and decay of target mRNAs. *The Journal of cell biology*.

Schink, K.O., C. Raiborg, and H. Stenmark. 2013. Phosphatidylinositol 3-phosphate, a lipid that regulates membrane dynamics, protein sorting and cell signalling. *Bioessays*. 35:900-912.

Schneider, W.C., and G.H. Hogeboom. 1951. Cytochemical studies of mammalian tissues; the isolation of cell components by differential centrifugation: a review. *Cancer Res*. 11:1-22.

Schon, E.A., and S. Przedborski. 2011. Mitochondria: the next (neurode)generation. *Neuron*. 70:1033-1053.

Schreiner, P., X. Chen, K. Husnjak, L. Randles, N. Zhang, S. Elsasser, D. Finley, I. Dikic, K.J. Walters, and M. Groll. 2008. Ubiquitin docking at the proteasome through a novel pleckstrin-homology domain interaction. *Nature*. 453:548-552.

Schu, P.V., K. Takegawa, M.J. Fry, J.H. Stack, M.D. Waterfield, and S.D. Emr. 1993. Phosphatidylinositol 3-kinase encoded by yeast VPS34 gene essential for protein sorting. *Science*. 260:88-91.

Schulze, U., B. Vollenbroker, D.A. Braun, T. Van Le, D. Granado, J. Kremerskothen, B. Franzel, R. Klosowski, J. Barth, C. Fufezan, D.A. Wolters, H. Pavenstadt, and T. Weide. 2014. The Vac14-interaction network is linked to regulators of the endolysosomal and autophagic pathway. *Molecular & cellular proteomics : MCP*. 13:1397-1411.

Schwid, S.R., J. Bausch, D. Oakes, L. Schuchter, C. Tanner, M. Forrest, A.E. Lang, I. Shoulson, P.P. Investigators, I. Shoulson, C. Hyson, D. Oakes, E. Flagg, A. Rudolph, K. Kieburtz, A. Lang, S. Fahn, L. Gauger, and C. Goetz. 2010. Cancer incidence in a trial of an antiapoptotic agent for Parkinson's disease. *Movement disorders : official journal of the Movement Disorder Society*. 25:1801-1808.

Scialo, F., A. Sriram, D. Fernandez-Ayala, N. Gubina, M. Lohmus, G. Nelson, A. Logan, H.M. Cooper, P. Navas, J.A. Enriquez, M.P. Murphy, and A. Sanz. 2016. Mitochondrial ROS Produced via Reverse Electron Transport Extend Animal Lifespan. *Cell metabolism*. 23:725-734.

Scorrano, L. 2013. Keeping mitochondria in shape: a matter of life and death. *European journal of clinical investigation*. 43:886-893.

Scott, C.C., F. Vacca, and J. Gruenberg. 2014. Endosome maturation, transport and functions. *Semin Cell Dev Biol*. 31:2-10.

Sen, A., and R.T. Cox. 2016. Clueless is a conserved ribonucleoprotein that binds the ribosome at the mitochondrial outer membrane. *Biol Open*. 5:195-203.

Sen, A., S. Kalvakuri, R. Bodmer, and R.T. Cox. 2015. Clueless, a protein required for mitochondrial function, interacts with the PINK1-Parkin complex in Drosophila. *Dis Model Mech*. 8:577-589.

Senior, A.E. 1988. ATP synthesis by oxidative phosphorylation. *Physiol Rev*. 68:177-231.

Senyilmaz, D., S. Virtue, X. Xu, C.Y. Tan, J.L. Griffin, A.K. Miller, A. Vidal-Puig, and A.A. Teleman. 2015. Regulation of mitochondrial morphology and function by stearoylation of TFR1. *Nature*. 525:124-128.

Settembre, C., C. Di Malta, V.A. Polito, M. Garcia Arencibia, F. Vetrini, S. Erdin, S.U. Erdin, T. Huynh, D. Medina, P. Colella, M. Sardiello, D.C. Rubinsztein, and A. Ballabio. 2011. TFEB links autophagy to lysosomal biogenesis. *Science*. 332:1429-1433.

Settembre, C., R. Zoncu, D.L. Medina, F. Vetrini, S. Erdin, S. Erdin, T. Huynh, M. Ferron, G. Karsenty, M.C. Vellard, V. Facchinetti, D.M. Sabatini, and A. Ballabio. 2012. A lysosome-to-nucleus signalling mechanism senses and regulates the lysosome via mTOR and TFEB. *The EMBO journal*. 31:1095-1108.

Shaltouki, A., R. Sivapatham, Y. Pei, A.A. Gerencser, O. Momcilovic, M.S. Rao, and X. Zeng. 2015. Mitochondrial alterations by PARKIN in dopaminergic neurons using PARK2 patient-specific and PARK2 knockout isogenic iPSC lines. *Stem Cell Reports*. 4:847-859.

Shen, Q., K. Yamano, B.P. Head, S. Kawajiri, J.T. Cheung, C. Wang, J.H. Cho, N. Hattori, R.J. Youle, and A.M. van der Bliek. 2014. Mutations in Fis1 disrupt orderly disposal of defective mitochondria. *Molecular biology of the cell*. 25:145-159.

Sherer, N.M., M.J. Lehmann, L.F. Jimenez-Soto, A. Ingmundson, S.M. Horner, G. Cicchetti, P.G. Allen, M. Pypaert, J.M. Cunningham, and W. Mothes. 2003. Visualization of retroviral replication in living cells reveals budding into multivesicular bodies. *Traffic*. 4:785-801.

Shi, G., and G.A. McQuibban. 2017. The Mitochondrial Rhomboid Protease PARL Is Regulated by PDK2 to Integrate Mitochondrial Quality Control and Metabolism. *Cell reports*. 18:1458-1472.

Shi, S.Y., S.Y. Lu, T. Sivasubramaniyam, X.S. Revelo, E.P. Cai, C.T. Luk, S.A. Schroer, P. Patel, R.H. Kim, E. Bombardier, J. Quadrilatero, A.R. Tupling, T.W. Mak, D.A. Winer, and M. Woo. 2015. DJ-1 links muscle ROS production with metabolic reprogramming and systemic energy homeostasis in mice. *Nature communications*. 6:7415.

Shiba-Fukushima, K., Y. Imai, S. Yoshida, Y. Ishihama, T. Kanao, S. Sato, and N. Hattori. 2012. PINK1-mediated phosphorylation of the Parkin ubiquitin-like domain primes mitochondrial translocation of Parkin and regulates mitophagy. *Scientific reports*. 2:1002.

Shiba-Fukushima, K., K.I. Ishikawa, T. Inoshita, N. Izawa, M. Takanashi, S. Sato, O. Onodera, W. Akamatsu, H. Okano, Y. Imai, and N. Hattori. 2017. Evidence that phosphorylated ubiquitin signaling is involved in the etiology of Parkinson's disease. *Human molecular genetics*.

Shimura, H., N. Hattori, S. Kubo, Y. Mizuno, S. Asakawa, S. Minoshima, N. Shimizu, K. Iwai, T. Chiba, K. Tanaka, and T. Suzuki. 2000. Familial Parkinson disease gene product, parkin, is a ubiquitin-protein ligase. *Nature genetics*. 25:302-305.

Shin, J.H., H.S. Ko, H. Kang, Y. Lee, Y.I. Lee, O. Pletinkova, J.C. Troconso, V.L. Dawson, and T.M. Dawson. 2011. PARIS (ZNF746) repression of PGC-1alpha contributes to neurodegeneration in Parkinson's disease. *Cell*. 144:689-702.

Shojaee, S., F. Sina, S.S. Banihosseini, M.H. Kazemi, R. Kalhor, G.A. Shahidi, H. Fakhrai-Rad, M. Ronaghi, and E. Elahi. 2008. Genome-wide linkage analysis of a Parkinsonian-pyramidal syndrome pedigree by 500 K SNP arrays. *American journal of human genetics*. 82:1375-1384.

Shutt, T., M. Geoffrion, R. Milne, and H.M. McBride. 2012. The intracellular redox state is a core determinant of mitochondrial fusion. *EMBO reports*. 13:909-915.

Siekevitz, P. 1957. Powerhouse of the cell. *Scientific American*. 197:131-140.

Silvestri, L., V. Caputo, E. Bellacchio, L. Atorino, B. Dallapiccola, E.M. Valente, and G. Casari. 2005. Mitochondrial import and enzymatic activity of PINK1 mutants associated to recessive parkinsonism. *Human molecular genetics*. 14:3477-3492.

Simmen, T., J.E. Aslan, A.D. Blagoveshchenskaya, L. Thomas, L. Wan, Y. Xiang, S.F. Feliciangeli, C.H. Hung, C.M. Crump, and G. Thomas. 2005. PACS-2 controls endoplasmic reticulum-mitochondria communication and Bid-mediated apoptosis. *The EMBO journal*. 24:717-729.

Smirnova, E., D.L. Shurland, S.N. Ryazantsev, and A.M. van der Bliek. 1998. A human dynamin-related protein controls the distribution of mitochondria. *The Journal of cell biology*. 143:351-358.

Smit, J.J., and T.K. Sixma. 2014. RBR E3-ligases at work. *EMBO reports*. 15:142-154.

Snead, W.T., C.C. Hayden, A.K. Gadok, C. Zhao, E.M. Lafer, P. Rangamani, and J.C. Stachowiak. 2017. Membrane fission by protein crowding. *Proceedings of the National Academy of Sciences of the United States of America*. 114:E3258-E3267.

Sochacki, K.A., A.M. Dickey, M.P. Strub, and J.W. Taraska. 2017. Endocytic proteins are partitioned at the edge of the clathrin lattice in mammalian cells. *Nature cell biology*. 19:352-361.

Soleimanpour, S.A., A. Gupta, M. Bakay, A.M. Ferrari, D.N. Groff, J. Fadista, L.A. Spruce, J.A. Kushner, L. Groop, S.H. Seeholzer, B.A. Kaufman, H. Hakonarson, and D.A. Stoffers. 2014. The diabetes susceptibility gene Clec16a regulates mitophagy. *Cell*. 157:1577-1590.

Sollner, T., S.W. Whiteheart, M. Brunner, H. Erdjument-Bromage, S. Geromanos, P. Tempst, and J.E. Rothman. 1993. SNAP receptors implicated in vesicle targeting and fusion. *Nature*. 362:318-324.

Soman, S., M. Keatinge, M. Moein, M. Da Costa, H. Mortiboys, A. Skupin, S. Sugunan, M. Bazala, J. Kuznicki, and O. Bandmann. 2017. Inhibition of the mitochondrial calcium uniporter rescues dopaminergic neurons in pink1-/- zebrafish. *Eur J Neurosci*. 45:528-535.

Song, P., K. Trajkovic, T. Tsunemi, and D. Krainc. 2016. Parkin Modulates Endosomal Organization and Function of the Endo-Lysosomal Pathway. *The Journal of neuroscience : the official journal of the Society for Neuroscience*. 36:2425-2437.

Song, Z., M. Ghochani, J.M. McCaffery, T.G. Frey, and D.C. Chan. 2009. Mitofusins and OPA1 mediate sequential steps in mitochondrial membrane fusion. *Molecular biology of the cell*. 20:3525-3532.

Sorre, B., A. Callan-Jones, J. Manzi, B. Goud, J. Prost, P. Bassereau, and A. Roux. 2012. Nature of curvature coupling of amphiphysin with membranes depends on its bound density. *Proceedings of the National Academy of Sciences of the United States of America*. 109:173-178.

Soubannier, V., G.L. McLelland, R. Zunino, E. Braschi, P. Rippstein, E.A. Fon, and H.M. McBride. 2012a. A vesicular transport pathway shuttles cargo from mitochondria to lysosomes. *Current biology : CB*. 22:135-141.

Soubannier, V., P. Rippstein, B.A. Kaufman, E.A. Shoubridge, and H.M. McBride. 2012b. Reconstitution of mitochondria derived vesicle formation demonstrates selective enrichment of oxidized cargo. *PloS one*. 7:e52830.

Soukup, S.F., S. Kuenen, R. Vanhauwaert, J. Manetsberger, S. Hernandez-Diaz, J. Swerts, N. Schoovaerts, S. Vilain, N.V. Gounko, K. Vints, A. Geens, B. De Strooper, and P. Verstreken. 2016. A LRRK2-Dependent EndophilinA Phosphoswitch Is Critical for Macroautophagy at Presynaptic Terminals. *Neuron*. 92:829-844.

Spillantini, M.G., M.L. Schmidt, V.M. Lee, J.Q. Trojanowski, R. Jakes, and M. Goedert. 1997. Alpha-synuclein in Lewy bodies. *Nature*. 388:839-840.

Spratt, D.E., R.J. Martinez-Torres, Y.J. Noh, P. Mercier, N. Manczyk, K.R. Barber, J.D. Aguirre, L. Burchell, A. Purkiss, H. Walden, and G.S. Shaw. 2013. A molecular explanation for the recessive nature of parkin-linked Parkinson's disease. *Nature communications*. 4:1983.

Stachowiak, J.C., E.M. Schmid, C.J. Ryan, H.S. Ann, D.Y. Sasaki, M.B. Sherman, P.L. Geissler, D.A. Fletcher, and C.C. Hayden. 2012. Membrane bending by protein-protein crowding. *Nature cell biology*. 14:944-949.

Starai, V.J., C.M. Hickey, and W. Wickner. 2008. HOPS proofreads the trans-SNARE complex for yeast vacuole fusion. *Molecular biology of the cell*. 19:2500-2508.

Stauch, K.L., L.M. Villeneuve, P.R. Purnell, S. Pandey, C. Guda, and H.S. Fox. 2016. SWATH-MS proteome profiling data comparison of DJ-1, Parkin, and PINK1 knockout rat striatal mitochondria. *Data Brief*. 9:589-593.

Stavru, F., A.E. Palmer, C. Wang, R.J. Youle, and P. Cossart. 2013. Atypical mitochondrial fission upon bacterial infection. *Proceedings of the National Academy of Sciences of the United States of America*. 110:16003-16008.

Stevens, D.A., Y. Lee, H.C. Kang, B.D. Lee, Y.I. Lee, A. Bower, H. Jiang, S.U. Kang, S.A. Andrabi, V.L. Dawson, J.H. Shin, and T.M. Dawson. 2015. Parkin loss leads to PARIS-dependent declines in mitochondrial mass and respiration. *Proceedings of the National Academy of Sciences of the United States of America*. 112:11696-11701.

Stichel, C.C., X.R. Zhu, V. Bader, B. Linnartz, S. Schmidt, and H. Lubbert. 2007. Mono- and double-mutant mouse models of Parkinson's disease display severe mitochondrial damage. *Human molecular genetics*. 16:2377-2393.

Stoica, R., K.J. De Vos, S. Paillusson, S. Mueller, R.M. Sancho, K.F. Lau, G. Vizcay-Barrena, W.L. Lin, Y.F. Xu, J. Lewis, D.W. Dickson, L. Petrucelli, J.C. Mitchell, C.E. Shaw, and C.C. Miller. 2014. ER-mitochondria associations are regulated by the VAPB-PTPIP51 interaction and are disrupted by ALS/FTD-associated TDP-43. *Nature communications*. 5:3996.

Stoica, R., S. Paillusson, P. Gomez-Suaga, J.C. Mitchell, D.H. Lau, E.H. Gray, R.M. Sancho, G. Vizcay-Barrena, K.J. De Vos, C.E. Shaw, D.P. Hanger, W. Noble, and C.C. Miller. 2016. ALS/FTD-associated FUS activates GSK-3beta to disrupt the VAPB-PTPIP51 interaction and ER-mitochondria associations. *EMBO reports*. 17:1326-1342.

Strokin, M., and G. Reiser. 2016. Mitochondria from a mouse model of the human infantile neuroaxonal dystrophy (INAD) with genetic defects in VIA iPLA2 have disturbed Ca(2+) regulation with reduction in Ca(2+) capacity. *Neurochem Int*. 99:187-193.

Subramanian, N., K. Natarajan, M.R. Clatworthy, Z. Wang, and R.N. Germain. 2013. The adaptor MAVS promotes NLRP3 mitochondrial localization and inflammasome activation. *Cell*. 153:348-361.

Suen, D.F., D.P. Narendra, A. Tanaka, G. Manfredi, and R.J. Youle. 2010. Parkin overexpression selects against a deleterious mtDNA mutation in heteroplasmic cybrid cells. *Proceedings of the National Academy of Sciences of the United States of America*. 107:11835-11840.

Sugiura, A., S. Mattie, J. Prudent, and H.M. McBride. 2017. Newly born peroxisomes are a hybrid of mitochondrial and ER-derived pre-peroxisomes. *Nature*. 542:251-254.

Sugiura, A., G.L. McLelland, E.A. Fon, and H.M. McBride. 2014. A new pathway for mitochondrial quality control: mitochondrial-derived vesicles. *The EMBO journal*. 33:2142-2156.

Sugiura, A., S. Nagashima, T. Tokuyama, T. Amo, Y. Matsuki, S. Ishido, Y. Kudo, H.M. McBride, T. Fukuda, N. Matsushita, R. Inatome, and S. Yanagi. 2013. MITOL regulates endoplasmic reticulum-mitochondria contacts via Mitofusin2. *Molecular cell*. 51:20-34.

Sulzer, D., R.N. Alcalay, F. Garretti, L. Cote, E. Kanter, J. Agin-Liebes, C. Liong, C. McMurtrey, W.H. Hildebrand, X. Mao, V.L. Dawson, T.M. Dawson, C. Oseroff, J. Pham, J. Sidney, M.B. Dillon, C. Carpenter, D. Weiskopf, E. Phillips, S. Mallal, B. Peters, A. Frazier, C.S. Lindestam Arlehamn, and A. Sette. 2017. T cells from patients with Parkinson's disease recognize alpha-synuclein peptides. *Nature*. 546:656-661.

Sun, Q., W. Fan, K. Chen, X. Ding, S. Chen, and Q. Zhong. 2008. Identification of Barkor as a mammalian autophagy-specific factor for Beclin 1 and class III phosphatidylinositol 3-kinase. *Proceedings of the National Academy of Sciences of the United States of America*. 105:19211-19216.

Sun, Y., A.A. Vashisht, J. Tchieu, J.A. Wohlschlegel, and L. Dreier. 2012. Voltage-dependent anion channels (VDACs) recruit Parkin to defective mitochondria to promote mitochondrial autophagy. *The Journal of biological chemistry*. 287:40652-40660.

Sung, H., L.C. Tandarich, K. Nguyen, and P.J. Hollenbeck. 2016. Compartmentalized Regulation of Parkin-Mediated Mitochondrial Quality Control in the Drosophila Nervous System In Vivo. *The Journal of neuroscience : the official journal of the Society for Neuroscience*. 36:7375-7391.

Surmeier, D.J., J.A. Obeso, and G.M. Halliday. 2017. Selective neuronal vulnerability in Parkinson disease. *Nat Rev Neurosci*. 18:101-113.

Sutton, R.B., D. Fasshauer, R. Jahn, and A.T. Brunger. 1998. Crystal structure of a SNARE complex involved in synaptic exocytosis at 2.4 A resolution. *Nature*. 395:347-353.

Swaney, D.L., R.A. Rodriguez-Mias, and J. Villen. 2015. Phosphorylation of ubiquitin at Ser65 affects its polymerization, targets, and proteome-wide turnover. *EMBO reports*. 16:1131-1144.

Szabadkai, G., K. Bianchi, P. Varnai, D. De Stefani, M.R. Wieckowski, D. Cavagna, A.I. Nagy, T. Balla, and R. Rizzuto. 2006. Chaperone-mediated coupling of endoplasmic reticulum and mitochondrial Ca2+ channels. *The Journal of cell biology*. 175:901-911.

Taghavi, S., R. Chaouni, A. Tafakhori, L.J. Azcona, S.G. Firouzabadi, M.D. Omrani, J. Jamshidi, B. Emamalizadeh, G.A. Shahidi, M. Ahmadi, S.A.H. Habibi, A. Ahmadifard, A. Fazeli, M. Motallebi, P. Petramfar, S. Askarpour, S. Askarpour, H.A. Shahmohammadibeni, N. Shahmohammadibeni, H. Eftekhari, A.E. Shafiei Zarneh, S. Mohammadihosseinabad, M. Khorrami, S. Najmi, A. Chitsaz, P. Shokraeian, H. Ehsanbakhsh, J. Rezaeidian, R. Ebrahimi Rad, F. Madadi, M. Andarva, E. Alehabib, M. Atakhorrami, S.E. Mortazavi, Z. Azimzadeh, M. Bayat, A.M. Besharati, M.A. Harati-Ghavi, S. Omidvari, Z. Dehghani-Tafti, F. Mohammadi, B. Mohammad Hossein Pour, H. Noorollahi Moghaddam, E. Esmaili Shandiz, A. Habibi, Z. Taherian-Esfahani, H. Darvish, and C. Paisan-Ruiz. 2017. A Clinical and Molecular Genetic Study of 50 Families with Autosomal Recessive Parkinsonism Revealed Known and Novel Gene Mutations. *Mol Neurobiol*.

Taguchi, N., N. Ishihara, A. Jofuku, T. Oka, and K. Mihara. 2007. Mitotic phosphorylation of dynamin-related GTPase Drp1 participates in mitochondrial fission. *The Journal of biological chemistry*. 282:11521-11529.

Takats, S., P. Nagy, A. Varga, K. Pircs, M. Karpati, K. Varga, A.L. Kovacs, K. Hegedus, and G. Juhasz. 2013. Autophagosomal Syntaxin17-dependent lysosomal degradation maintains neuronal function in Drosophila. *The Journal of cell biology*. 201:531-539.

Takats, S., K. Pircs, P. Nagy, A. Varga, M. Karpati, K. Hegedus, H. Kramer, A.L. Kovacs, M. Sass, and G. Juhasz. 2014. Interaction of the HOPS complex with Syntaxin 17 mediates autophagosome clearance in Drosophila. *Molecular biology of the cell*. 25:1338-1354.

Tambini, M.D., M. Pera, E. Kanter, H. Yang, C. Guardia-Laguarta, D. Holtzman, D. Sulzer, E. Area-Gomez, and E.A. Schon. 2016. ApoE4 upregulates the activity of mitochondria-associated ER membranes. *EMBO reports*. 17:27-36.

Tamura, K., N. Ohbayashi, Y. Maruta, E. Kanno, T. Itoh, and M. Fukuda. 2009. Varp is a novel Rab32/38-binding protein that regulates Tyrp1 trafficking in melanocytes. *Molecular biology of the cell*. 20:2900-2908.

Tan, X., N. Thapa, Y. Liao, S. Choi, and R.A. Anderson. 2016. PtdIns(4,5)P2 signaling regulates ATG14 and autophagy. *Proceedings of the National Academy of Sciences of the United States of America*. 113:10896-10901.

Tanaka, A., M.M. Cleland, S. Xu, D.P. Narendra, D.F. Suen, M. Karbowski, and R.J. Youle. 2010. Proteasome and p97 mediate mitophagy and degradation of mitofusins induced by Parkin. *The Journal of cell biology*. 191:1367-1380.

Tang, M.Y., M. Vranas, A.I. Krahn, S. Pundlik, J.F. Trempe, and E.A. Fon. 2017. Structure-guided mutagenesis reveals a hierarchical mechanism of Parkin activation. *Nature communications*. 8:14697.

Tatsuta, T., and T. Langer. 2008. Quality control of mitochondria: protection against neurodegeneration and ageing. *The EMBO journal*. 27:306-314.

Taylor, M.J., D. Perrais, and C.J. Merrifield. 2011. A high precision survey of the molecular dynamics of mammalian clathrin-mediated endocytosis. *PLoS biology*. 9:e1000604.

Terreni, L., E. Calabrese, A.M. Calella, G. Forloni, and C. Mariani. 2001. New mutation (R42P) of the parkin gene in the ubiquitinlike domain associated with parkinsonism. *Neurology*. 56:463-466.

Terrones, O., B. Antonsson, H. Yamaguchi, H.G. Wang, J. Liu, R.M. Lee, A. Herrmann, and G. Basanez. 2004. Lipidic pore formation by the concerted action of proapoptotic BAX and tBID. *The Journal of biological chemistry*. 279:30081-30091.

Thaher, O., C. Wolf, P.N. Dey, A. Pouya, V. Wullner, S. Tenzer, and A. Methner. 2017. The thiol switch C684 in Mitofusin-2 mediates redox-induced alterations of mitochondrial shape and respiration. *Neurochem Int*.

Thayanidhi, N., J.R. Helm, D.C. Nycz, M. Bentley, Y. Liang, and J.C. Hay. 2010. Alpha-synuclein delays endoplasmic reticulum (ER)-to-Golgi transport in mammalian cells by antagonizing ER/Golgi SNAREs. *Molecular biology of the cell*. 21:1850-1863.

Thomas, K.J., M.K. McCoy, J. Blackinton, A. Beilina, M. van der Brug, A. Sandebring, D. Miller, D. Maric, A. Cedazo-Minguez, and M.R. Cookson. 2011. DJ-1 acts in parallel to the PINK1/parkin pathway to control mitochondrial function and autophagy. *Human molecular genetics*. 20:40-50.

Thrash, J.C., A. Boyd, M.J. Huggett, J. Grote, P. Carini, R.J. Yoder, B. Robbertse, J.W. Spatafora, M.S. Rappe, and S.J. Giovannoni. 2011. Phylogenomic evidence for a common ancestor of mitochondria and the SAR11 clade. *Scientific reports*. 1:13.

Tomoo, K., Y. Mukai, Y. In, H. Miyagawa, K. Kitamura, A. Yamano, H. Shindo, and T. Ishida. 2008. Crystal structure and molecular dynamics simulation of ubiquitin-like domain of murine parkin. *Biochimica et biophysica acta*. 1784:1059-1067.

Toyama, E.Q., S. Herzig, J. Courchet, T.L. Lewis, Jr., O.C. Loson, K. Hellberg, N.P. Young, H. Chen, F. Polleux, D.C. Chan, and R.J. Shaw. 2016. Metabolism. AMP-activated protein kinase mediates mitochondrial fission in response to energy stress. *Science*. 351:275-281.

Trempe, J.F. 2011. Reading the ubiquitin postal code. *Current opinion in structural biology*. 21:792-801.

Trempe, J.F., C.X. Chen, K. Grenier, E.M. Camacho, G. Kozlov, P.S. McPherson, K. Gehring, and E.A. Fon. 2009. SH3 domains from a subset of BAR proteins define a Ubl-binding domain and implicate parkin in synaptic ubiquitination. *Molecular cell*. 36:1034-1047.

Trempe, J.F., V. Sauve, K. Grenier, M. Seirafi, M.Y. Tang, M. Menade, S. Al-Abdul-Wahid, J. Krett, K. Wong, G. Kozlov, B. Nagar, E.A. Fon, and K. Gehring. 2013. Structure of parkin reveals mechanisms for ubiquitin ligase activation. *Science*. 340:1451-1455.

Trinh, K., K. Moore, P.D. Wes, P.J. Muchowski, J. Dey, L. Andrews, and L.J. Pallanck. 2008. Induction of the phase II detoxification pathway suppresses neuron loss in Drosophila models of Parkinson's disease. *The Journal of neuroscience : the official journal of the Society for Neuroscience*. 28:465-472.

Tsuboyama, K., I. Koyama-Honda, Y. Sakamaki, M. Koike, H. Morishita, and N. Mizushima. 2016. The ATG conjugation systems are important for degradation of the inner autophagosomal membrane. *Science*. 354:1036-1041.

Twig, G., A. Elorza, A.J. Molina, H. Mohamed, J.D. Wikstrom, G. Walzer, L. Stiles, S.E. Haigh, S. Katz, G. Las, J. Alroy, M. Wu, B.F. Py, J. Yuan, J.T. Deeney, B.E. Corkey, and O.S. Shirihai. 2008. Fission and selective fusion govern mitochondrial segregation and elimination by autophagy. *The EMBO journal*. 27:433-446.

Uemura, T., M. Yamamoto, A. Kametaka, Y.S. Sou, A. Yabashi, A. Yamada, H. Annoh, S. Kametaka, M. Komatsu, and S. Waguri. 2014. A cluster of thin tubular structures mediates transformation of the endoplasmic reticulum to autophagic isolation membrane. *Molecular and cellular biology*. 34:1695-1706.

Um, J.W., and K.C. Chung. 2006. Functional modulation of parkin through physical interaction with SUMO-1. *J Neurosci Res*. 84:1543-1554.

Vais, H., J.E. Tanis, M. Muller, R. Payne, K. Mallilankaraman, and J.K. Foskett. 2015. MCUR1, CCDC90A, Is a Regulator of the Mitochondrial Calcium Uniporter. *Cell metabolism*. 22:533-535.

Valente, E.M., P.M. Abou-Sleiman, V. Caputo, M.M. Muqit, K. Harvey, S. Gispert, Z. Ali, D. Del Turco, A.R. Bentivoglio, D.G. Healy, A. Albanese, R. Nussbaum, R. Gonzalez-Maldonado, T. Deller, S. Salvi, P. Cortelli, W.P. Gilks, D.S. Latchman, R.J. Harvey, B. Dallapiccola, G. Auburger, and N.W. Wood. 2004. Hereditary early-onset Parkinson's disease caused by mutations in PINK1. *Science*. 304:1158-1160.

van der Brug, M.P., J. Blackinton, J. Chandran, L.Y. Hao, A. Lal, K. Mazan-Mamczarz, J. Martindale, C. Xie, R. Ahmad, K.J. Thomas, A. Beilina, J.R. Gibbs, J. Ding, A.J. Myers, M. Zhan, H. Cai, N.M. Bonini, M. Gorospe, and M.R. Cookson. 2008. RNA binding activity of the recessive parkinsonism protein DJ-1 supports involvement in multiple cellular pathways. *Proceedings of the National Academy of Sciences of the United States of America*. 105:10244-10249.

van der Lee, R., M. Buljan, B. Lang, R.J. Weatheritt, G.W. Daughdrill, A.K. Dunker, M. Fuxreiter, J. Gough, J. Gsponer, D.T. Jones, P.M. Kim, R.W. Kriwacki, C.J. Oldfield, R.V. Pappu, P. Tompa, V.N. Uversky, P.E. Wright, and M.M. Babu. 2014. Classification of intrinsically disordered regions and proteins. *Chem Rev*. 114:6589-6631.

van der Merwe, C., B. Loos, C. Swart, C. Kinnear, F. Henning, L. van der Merwe, K. Pillay, N. Muller, D. Zaharie, L. Engelbrecht, J. Carr, and S. Bardien. 2014. Mitochondrial impairment observed in fibroblasts from South African Parkinson's disease patients with parkin mutations. *Biochemical and biophysical research communications*. 447:334-340.

Van Laar, V.S., B. Arnold, S.J. Cassady, C.T. Chu, E.A. Burton, and S.B. Berman. 2011. Bioenergetics of neurons inhibit the translocation response of Parkin following rapid mitochondrial depolarization. *Human molecular genetics*. 20:927-940.

Vanhauwaert, R., S. Kuenen, R. Masius, A. Bademosi, J. Manetsberger, N. Schoovaerts, L. Bounti, S. Gontcharenko, J. Swerts, S. Vilain, M. Picillo, P. Barone, S.T. Munshi, F.M. de Vrij, S.A. Kushner, N.V. Gounko, W. Mandemakers, V. Bonifati, F.A. Meunier, S.F. Soukup, and P. Verstreken. 2017. The SAC1 domain in synaptojanin is required for autophagosome maturation at presynaptic terminals. *The EMBO journal*. 36:1392-1411.

Velayos-Baeza, A., A. Vettori, R.R. Copley, C. Dobson-Stone, and A.P. Monaco. 2004. Analysis of the human VPS13 gene family. *Genomics*. 84:536-549.

Venderova, K., and D.S. Park. 2012. Programmed cell death in Parkinson's disease. *Cold Spring Harbor perspectives in medicine*. 2.

Vijay-Kumar, S., C.E. Bugg, and W.J. Cook. 1987. Structure of ubiquitin refined at 1.8 A resolution. *Journal of molecular biology*. 194:531-544.

Vilain, S., G. Esposito, D. Haddad, O. Schaap, M.P. Dobreva, M. Vos, S. Van Meensel, V.A. Morais, B. De Strooper, and P. Verstreken. 2012. The yeast complex I equivalent NADH dehydrogenase rescues pink1 mutants. *PLoS genetics*. 8:e1002456.

Vilarino-Guell, C., C. Wider, O.A. Ross, J.C. Dachsel, J.M. Kachergus, S.J. Lincoln, A.I. Soto-Ortolaza, S.A. Cobb, G.J. Wilhoite, J.A. Bacon, B. Behrouz, H.L. Melrose, E. Hentati, A. Puschmann, D.M. Evans, E. Conibear, W.W. Wasserman, J.O. Aasly, P.R. Burkhard, R. Djaldetti, J. Ghika, F. Hentati, A. Krygowska-Wajs, T. Lynch, E. Melamed, A. Rajput, A.H. Rajput, A. Solida, R.M. Wu, R.J. Uitti, Z.K. Wszolek, F. Vingerhoets, and M.J. Farrer. 2011. VPS35 mutations in Parkinson disease. *American journal of human genetics*. 89:162-167.

Vincow, E.S., G. Merrihew, R.E. Thomas, N.J. Shulman, R.P. Beyer, M.J. MacCoss, and L.J. Pallanck. 2013. The PINK1-Parkin pathway promotes both mitophagy and selective respiratory chain turnover in vivo. *Proceedings of the National Academy of Sciences of the United States of America*. 110:6400-6405.

Vives-Bauza, C., C. Zhou, Y. Huang, M. Cui, R.L. de Vries, J. Kim, J. May, M.A. Tocilescu, W. Liu, H.S. Ko, J. Magrane, D.J. Moore, V.L. Dawson, R. Grailhe, T.M. Dawson, C. Li, K. Tieu, and S. Przedborski. 2010. PINK1-dependent recruitment of Parkin to mitochondria in mitophagy. *Proceedings of the National Academy of Sciences of the United States of America*. 107:378-383.

Vos, M., G. Esposito, J.N. Edirisinghe, S. Vilain, D.M. Haddad, J.R. Slabbaert, S. Van Meensel, O. Schaap, B. De Strooper, R. Meganathan, V.A. Morais, and P. Verstreken. 2012. Vitamin K2 is a mitochondrial electron carrier that rescues pink1 deficiency. *Science*. 336:1306-1310.

Vos, M., A. Geens, C. Bohm, L. Deaulmerie, J. Swerts, M. Rossi, K. Craessaerts, E.P. Leites, P. Seibler, A. Rakovic, T. Lohnau, B. De Strooper, S.M. Fendt, V.A. Morais, C. Klein, and P. Verstreken. 2017. Cardiolipin promotes electron transport between ubiquinone and complex I to rescue PINK1 deficiency. *The Journal of cell biology*.

Wai, T., S. Saita, H. Nolte, S. Muller, T. Konig, R. Richter-Dennerlein, H.G. Sprenger, J. Madrenas, M. Muhlmeister, U. Brandt, M. Kruger, and T. Langer. 2016. The membrane scaffold SLP2 anchors a proteolytic hub in mitochondria containing PARL and the i-AAA protease YME1L. *EMBO reports*. 17:1844-1856.

Wakim, J., D. Goudenege, R. Perrot, N. Gueguen, V. Desquiret-Dumas, J.M. Chao de la Barca, I. Dalla Rosa, F. Manero, M. Le Mao, S. Chupin, A. Chevrollier, V. Procaccio, D. Bonneau, D.C. Logan, P. Reynier, G. Lenaers, and S. Khiati. 2017. CLUH couples mitochondrial distribution to the energetic and metabolic status. *Journal of cell science*. 130:1940-1951.

Wang, D., L. Qian, H. Xiong, J. Liu, W.S. Neckameyer, S. Oldham, K. Xia, J. Wang, R. Bodmer, and Z. Zhang. 2006. Antioxidants protect PINK1-dependent dopaminergic neurons in Drosophila. *Proceedings of the National Academy of Sciences of the United States of America*. 103:13520-13525.

Wang, H., H.Q. Sun, X. Zhu, L. Zhang, J. Albanesi, B. Levine, and H. Yin. 2015a. GABARAPs regulate PI4P-dependent autophagosome:lysosome fusion. *Proceedings of the National Academy of Sciences of the United States of America*. 112:7015-7020.

Wang, L., A. Johnson, M. Hanna, and A. Audhya. 2016a. Eps15 membrane-binding and -bending activity acts redundantly with Fcho1 during clathrin-mediated endocytosis. *Molecular biology of the cell*. 27:2675-2687.

Wang, L., X. Yang, S. Li, Z. Wang, Y. Liu, J. Feng, Y. Zhu, and Y. Shen. 2014. Structural and mechanistic insights into MICU1 regulation of mitochondrial calcium uptake. *The EMBO journal*. 33:594-604.

Wang, T., W.C. Xu, M.L. Qin, Y. Yang, P.H. Bao, F.X. Shen, Z.L. Zhang, and J. Xu. 2016b. Pathogenic Mutations in the Valosin-containing Protein/p97(VCP) N-domain Inhibit the SUMOylation of VCP and Lead to Impaired Stress Response. *Journal of Biological Chemistry*. 291:14373-14384.

Wang, W., X. Wang, H. Fujioka, C. Hoppel, A.L. Whone, M.A. Caldwell, P.J. Cullen, J. Liu, and X. Zhu. 2016c. Parkinson's disease-associated mutant VPS35 causes mitochondrial dysfunction by recycling DLP1 complexes. *Nature medicine*. 22:54-63.

Wang, X., D. Winter, G. Ashrafi, J. Schlehe, Y.L. Wong, D. Selkoe, S. Rice, J. Steen, M.J. LaVoie, and T.L. Schwarz. 2011. PINK1 and Parkin target Miro for phosphorylation and degradation to arrest mitochondrial motility. *Cell*. 147:893-906.

Wang, Y., M. Serricchio, M. Jauregui, R. Shanbhag, T. Stoltz, C.T. Di Paolo, P.K. Kim, and G.A. McQuibban. 2015b. Deubiquitinating enzymes regulate PARK2-mediated mitophagy. *Autophagy*. 11:595-606.

Wang, Z.H., C. Clark, and E.R. Geisbrecht. 2016d. Drosophila clueless is involved in Parkin-dependent mitophagy by promoting VCP-mediated Marf degradation. *Human molecular genetics*. 25:1946-1964.

Watanabe, S., H. Ilieva, H. Tamada, H. Nomura, O. Komine, F. Endo, S. Jin, P. Mancias, H. Kiyama, and K. Yamanaka. 2016. Mitochondria-associated membrane collapse is a common pathomechanism in SIGMAR1- and SOD1-linked ALS. *EMBO Mol Med*. 8:1421-1437.

Watanabe, Y., N. Katayama, K. Takeuchi, T. Togano, R. Itoh, M. Sato, M. Yamazaki, M. Abe, T. Sato, K. Oda, M. Yokoyama, K. Takao, M. Fukaya, T. Miyakawa, M. Watanabe, K. Sakimura, T. Manabe, and M. Igarashi. 2013. Point mutation in syntaxin-1A causes abnormal vesicle recycling, behaviors, and short term plasticity. *The Journal of biological chemistry*. 288:34906-34919.

Wauer, T., and D. Komander. 2013. Structure of the human Parkin ligase domain in an autoinhibited state. *The EMBO journal*. 32:2099-2112.

Wauer, T., M. Simicek, A. Schubert, and D. Komander. 2015a. Mechanism of phospho-ubiquitin-induced PARKIN activation. *Nature*. 524:370-374.

Wauer, T., K.N. Swatek, J.L. Wagstaff, C. Gladkova, J.N. Pruneda, M.A. Michel, M. Gersch, C.M. Johnson, S.M. Freund, and D. Komander. 2015b. Ubiquitin Ser65 phosphorylation affects ubiquitin structure, chain assembly and hydrolysis. *The EMBO journal*. 34:307-325.

Wenzel, D.M., A. Lissounov, P.S. Brzovic, and R.E. Klevit. 2011. UBCH7 reactivity profile reveals parkin and HHARI to be RING/HECT hybrids. *Nature*. 474:105-108.

West, A.B., and N.T. Maidment. 2004. Genetics of parkin-linked disease. *Human genetics*. 114:327-336.

Whitworth, A.J., J.R. Lee, V.M. Ho, R. Flick, R. Chowdhury, and G.A. McQuibban. 2008. Rhomboid-7 and HtrA2/Omi act in a common pathway with the Parkinson's disease factors Pink1 and Parkin. *Dis Model Mech*. 1:168-174; discussion 173.

Whitworth, A.J., D.A. Theodore, J.C. Greene, H. Benes, P.D. Wes, and L.J. Pallanck. 2005. Increased glutathione S-transferase activity rescues dopaminergic neuron loss in a Drosophila model of Parkinson's disease. *Proceedings of the National Academy of Sciences of the United States of America*. 102:8024-8029.

Wild, P., H. Farhan, D.G. McEwan, S. Wagner, V.V. Rogov, N.R. Brady, B. Richter, J. Korac, O. Waidmann, C. Choudhary, V. Dotsch, D. Bumann, and I. Dikic. 2011. Phosphorylation of the autophagy receptor optineurin restricts Salmonella growth. *Science*. 333:228-233.

Williams, C.C., C.H. Jan, and J.S. Weissman. 2014. Targeting and plasticity of mitochondrial proteins revealed by proximity-specific ribosome profiling. *Science*. 346:748-751.

Williams, D.R., A. Hadeed, A.S. al-Din, A.L. Wreikat, and A.J. Lees. 2005. Kufor Rakeb disease: autosomal recessive, levodopa-responsive parkinsonism with pyramidal degeneration, supranuclear gaze palsy, and dementia. *Movement disorders : official journal of the Movement Disorder Society*. 20:1264-1271.

Winslow, A.R., C.W. Chen, S. Corrochano, A. Acevedo-Arozena, D.E. Gordon, A.A. Peden, M. Lichtenberg, F.M. Menzies, B. Ravikumar, S. Imarisio, S. Brown, C.J. O'Kane, and D.C. Rubinsztein. 2010. alpha-Synuclein impairs macroautophagy: implications for Parkinson's disease. *The Journal of cell biology*. 190:1023-1037.

Wirdefeldt, K., C.E. Weibull, H. Chen, F. Kamel, C. Lundholm, F. Fang, and W. Ye. 2014. Parkinson's disease and cancer: A register-based family study. *Am J Epidemiol*. 179:85-94.

Wong, E.S., J.M. Tan, C. Wang, Z. Zhang, S.P. Tay, N. Zaiden, H.S. Ko, V.L. Dawson, T.M. Dawson, and K.L. Lim. 2007. Relative sensitivity of parkin and other cysteine-containing enzymes to stress-induced solubility alterations. *The Journal of biological chemistry*. 282:12310-12318.

Wong, Y.C., and E.L. Holzbaur. 2014. Optineurin is an autophagy receptor for damaged mitochondria in parkin-mediated mitophagy that is disrupted by an ALS-linked mutation. *Proceedings of the National Academy of Sciences of the United States of America*. 111:E4439-4448.

Woodroof, H.I., J.H. Pogson, M. Begley, L.C. Cantley, M. Deak, D.G. Campbell, D.M. van Aalten, A.J. Whitworth, D.R. Alessi, and M.M. Muqit. 2011. Discovery of catalytically active orthologues of the Parkinson's disease kinase PINK1: analysis of substrate specificity and impact of mutations. *Open biology*. 1:110012.

Wu, Y., C. Whiteus, C.S. Xu, K.J. Hayworth, R.J. Weinberg, H.F. Hess, and P. De Camilli. 2017. Contacts between the endoplasmic reticulum and other membranes in neurons. *Proceedings of the National Academy of Sciences of the United States of America*. 114:E4859-E4867.

Xi, J., Y. Liu, H. Liu, H. Chen, M.E. Emborg, and S.C. Zhang. 2012. Specification of midbrain dopamine neurons from primate pluripotent stem cells. *Stem Cells*. 30:1655-1663.

Xia, Q., L. Liao, D. Cheng, D.M. Duong, M. Gearing, J.J. Lah, A.I. Levey, and J. Peng. 2008. Proteomic identification of novel proteins associated with Lewy bodies. *Front Biosci*. 13:3850-3856.

Xie, Z., and D.J. Klionsky. 2007. Autophagosome formation: core machinery and adaptations. *Nature cell biology*. 9:1102-1109.

Xu, S., E. Cherok, S. Das, S.A. Li, B.A. Roelofs, S.X. Ge, B.M. Polster, L. Boyman, W.J. Lederer, C.X. Wang, and M. Karbowski. 2016. Mitochondrial E3 ubiquitin ligase MARCH5 controls mitochondrial fission and cell sensitivity to stress-induced apoptosis through regulation of MiD49 protein. *Molecular biology of the cell*. 27:349-359.

Yamamoto, H., S. Kakuta, T.M. Watanabe, A. Kitamura, T. Sekito, C. Kondo-Kakuta, R. Ichikawa, M. Kinjo, and Y. Ohsumi. 2012. Atg9 vesicles are an important membrane source during early steps of autophagosome formation. *The Journal of cell biology*. 198:219-233.

Yamano, K., A.I. Fogel, C. Wang, A.M. van der Bliek, and R.J. Youle. 2014. Mitochondrial Rab GAPs govern autophagosome biogenesis during mitophagy. *eLife*. 3:e01612.

Yamano, K., N. Matsuda, and K. Tanaka. 2016. The ubiquitin signal and autophagy: an orchestrated dance leading to mitochondrial degradation. *EMBO reports*.

Yamano, K., B.B. Queliconi, F. Koyano, Y. Saeki, T. Hirokawa, K. Tanaka, and N. Matsuda. 2015. Site-specific Interaction Mapping of Phosphorylated Ubiquitin to Uncover Parkin Activation. *The Journal of biological chemistry*. 290:25199-25211.

Yamano, K., and R.J. Youle. 2013. PINK1 is degraded through the N-end rule pathway. *Autophagy*. 9:1758-1769.

Yang, Y., S. Gehrke, Y. Imai, Z. Huang, Y. Ouyang, J.W. Wang, L. Yang, M.F. Beal, H. Vogel, and B. Lu. 2006. Mitochondrial pathology and muscle and dopaminergic neuron degeneration caused by inactivation of Drosophila Pink1 is rescued by Parkin. *Proceedings of the National Academy of Sciences of the United States of America*. 103:10793-10798.

Yang, Y., Y. Ouyang, L. Yang, M.F. Beal, A. McQuibban, H. Vogel, and B. Lu. 2008. Pink1 regulates mitochondrial dynamics through interaction with the fission/fusion machinery. *Proceedings of the National Academy of Sciences of the United States of America*. 105:7070-7075.

Yang, Z., and D.J. Klionsky. 2010. Mammalian autophagy: core molecular machinery and signaling regulation. *Current opinion in cell biology*. 22:124-131.

Yao, D., Z. Gu, T. Nakamura, Z.Q. Shi, Y. Ma, B. Gaston, L.A. Palmer, E.M. Rockenstein, Z. Zhang, E. Masliah, T. Uehara, and S.A. Lipton. 2004. Nitrosative stress linked to sporadic Parkinson's disease: S-nitrosylation of parkin regulates its E3 ubiquitin ligase activity. *Proceedings of the National Academy of Sciences of the United States of America*. 101:10810-10814.

Yao, Z., S. Gandhi, V.S. Burchell, H. Plun-Favreau, N.W. Wood, and A.Y. Abramov. 2011. Cell metabolism affects selective vulnerability in PINK1-associated Parkinson's disease. *Journal of cell science*. 124:4194-4202.

Yoshii, S.R., C. Kishi, N. Ishihara, and N. Mizushima. 2011. Parkin mediates proteasome-dependent protein degradation and rupture of the outer mitochondrial membrane. *The Journal of biological chemistry*. 286:19630-19640.

Yoshii, S.R., and N. Mizushima. 2015. Autophagy machinery in the context of mammalian mitophagy. *Biochimica et biophysica acta*. 1853:2797-2801.

Youle, R.J., and D.P. Narendra. 2011. Mechanisms of mitophagy. *Nature reviews. Molecular cell biology*. 12:9-14.

Youle, R.J., and A.M. van der Bliek. 2012. Mitochondrial fission, fusion, and stress. *Science*. 337:1062-1065.

Yu, W., Y. Sun, S. Guo, and B. Lu. 2011. The PINK1/Parkin pathway regulates mitochondrial dynamics and function in mammalian hippocampal and dopaminergic neurons. *Human molecular genetics*. 20:3227-3240.

Yun, J., R. Puri, H. Yang, M.A. Lizzio, C. Wu, Z.H. Sheng, and M. Guo. 2014. MUL1 acts in parallel to the PINK1/parkin pathway in regulating mitofusin and compensates for loss of PINK1/parkin. *eLife*. 3:e01958.

Zanellati, M.C., V. Monti, C. Barzaghi, C. Reale, N. Nardocci, A. Albanese, E.M. Valente, D. Ghezzi, and B. Garavaglia. 2015. Mitochondrial dysfunction in Parkinson disease: evidence in mutant PARK2 fibroblasts. *Front Genet*. 6:78.

Zhang, T., P. Mishra, B.A. Hay, D. Chan, and M. Guo. 2017a. Valosin-containing protein (VCP/p97) inhibitors relieve Mitofusin-dependent mitochondrial defects due to VCP disease mutants. *eLife*. 6.

Zhang, X., X. He, X.Y. Fu, and Z. Chang. 2006. Varp is a Rab21 guanine nucleotide exchange factor and regulates endosome dynamics. *Journal of cell science*. 119:1053-1062.

Zhang, Y. 2017. Energetics, kinetics, and pathway of SNARE folding and assembly revealed by optical tweezers. *Protein Sci*.

Zhang, Y., J. Gao, K.K. Chung, H. Huang, V.L. Dawson, and T.M. Dawson. 2000. Parkin functions as an E2-dependent ubiquitin- protein ligase and promotes the degradation of the synaptic vesicle-associated protein, CDCrel-1. *Proceedings of the National Academy of Sciences of the United States of America*. 97:13354-13359.

Zhang, Y., D.T. Nguyen, E.M. Olzomer, G.P. Poon, N.J. Cole, A. Puvanendran, B.R. Phillips, and D. Hesselson. 2017b. Rescue of Pink1 Deficiency by Stress-Dependent Activation of Autophagy. *Cell Chem Biol*.

Zhang, Y., S.N. Zolov, C.Y. Chow, S.G. Slutsky, S.C. Richardson, R.C. Piper, B. Yang, J.J. Nau, R.J. Westrick, S.J. Morrison, M.H. Meisler, and L.S. Weisman. 2007. Loss of Vac14, a regulator of the signaling lipid phosphatidylinositol 3,5-bisphosphate, results in neurodegeneration in mice. *Proceedings of the National Academy of Sciences of the United States of America*. 104:17518-17523.

Zhao, J., J. Zhang, M. Yu, Y. Xie, Y. Huang, D.W. Wolff, P.W. Abel, and Y. Tu. 2013. Mitochondrial dynamics regulates migration and invasion of breast cancer cells. *Oncogene*. 32:4814-4824.

Zheng, X., and T. Hunter. 2013. Parkin mitochondrial translocation is achieved through a novel catalytic activity coupled mechanism. *Cell research*. 23:886-897.

Zhong, Y., Q.J. Wang, X. Li, Y. Yan, J.M. Backer, B.T. Chait, N. Heintz, and Z. Yue. 2009. Distinct regulation of autophagic activity by Atg14L and Rubicon associated with Beclin 1-phosphatidylinositol-3-kinase complex. *Nature cell biology*. 11:468-476.

Zhou, C., Y. Huang, Y. Shao, J. May, D. Prou, C. Perier, W. Dauer, E.A. Schon, and S. Przedborski. 2008. The kinase domain of mitochondrial PINK1 faces the cytoplasm. *Proceedings of the National Academy of Sciences of the United States of America*. 105:12022-12027.

Zhou, Q., A. Yen, G. Rymarczyk, H. Asai, C. Trengrove, N. Aziz, M.T. Kirber, G. Mostoslavsky, T. Ikezu, B. Wolozin, and V.M. Bolotina. 2016. Impairment of PARK14-dependent Ca(2+) signalling is a novel determinant of Parkinson's disease. *Nature communications*. 7:10332.

Zhou, R., A.S. Yazdi, P. Menu, and J. Tschopp. 2011. A role for mitochondria in NLRP3 inflammasome activation. *Nature*. 469:221-225.

Zhu, C., S.L. Das, and T. Baumgart. 2012. Nonlinear sorting, curvature generation, and crowding of endophilin N-BAR on tubular membranes. *Biophys J*. 102:1837-1845.

Zimprich, A., A. Benet-Pages, W. Struhal, E. Graf, S.H. Eck, M.N. Offman, D. Haubenberger, S. Spielberger, E.C. Schulte, P. Lichtner, S.C. Rossle, N. Klopp, E. Wolf, K. Seppi, W. Pirker, S. Presslauer, B. Mollenhauer, R. Katzenschlager, T. Foki, C. Hotzy, E. Reinthaler, A. Harutyunyan, R. Kralovics, A. Peters, F. Zimprich, T. Brucke, W. Poewe, E. Auff, C. Trenkwalder, B. Rost, G. Ransmayr, J. Winkelmann, T. Meitinger, and T.M. Strom. 2011. A mutation in VPS35, encoding a subunit of the retromer complex, causes late-onset Parkinson disease. *American journal of human genetics*. 89:168-175.

Ziviani, E., R.N. Tao, and A.J. Whitworth. 2010. Drosophila parkin requires PINK1 for mitochondrial translocation and ubiquitinates mitofusin. *Proceedings of the National Academy of Sciences of the United States of America*. 107:5018-5023.

Zoncu, R., L. Bar-Peled, A. Efeyan, S. Wang, Y. Sancak, and D.M. Sabatini. 2011. mTORC1 senses lysosomal amino acids through an inside-out mechanism that requires the vacuolar H(+)-ATPase. *Science*. 334:678-683.

Zorman, S., A.A. Rebane, L. Ma, G. Yang, M.A. Molski, J. Coleman, F. Pincet, J.E. Rothman, and Y. Zhang. 2014. Common intermediates and kinetics, but different energetics, in the assembly of SNARE proteins. *eLife*. 3:e03348.